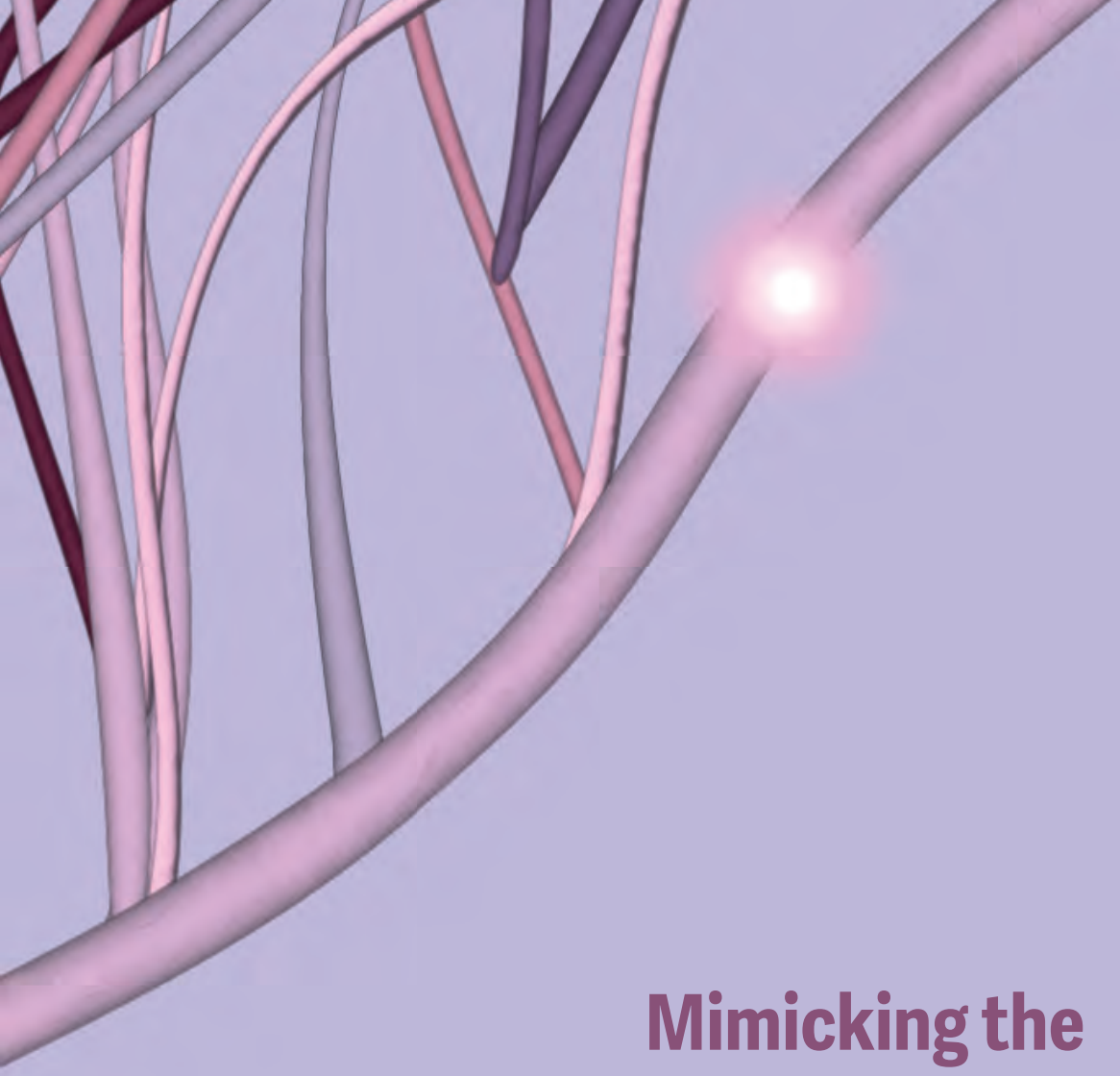

Mimicking the Regenerative Matrix:

Bioactive Scaffolds to Improve Skin Repair

Nancy Avila Martinez

RADBOUD UNIVERSITY PRESS

Radboud Dissertation Series

Mimicking the Regenerative Matrix:

Bioactive Scaffolds to Improve Skin Repair

Nancy Margarita Avila Martinez

This publication has been made possible by the funding from the European Union's Horizon 2020 research and innovation programme under the Marie Skłodowska-Curie grant agreement No 955722.

Mimicking the Regenerative Matrix: Bioactive Scaffolds to Improve Skin Repair
Nancy Margarita Avila Martinez

Radboud Dissertation Series
ISSN: 2950-2772 (Online); 2950-2780 (Print)

Published by RADBOUD UNIVERSITY PRESS
Postbus 9100, 6500 HA Nijmegen, The Netherlands
www.radbouduniversitypress.nl

Design: Proefschrift AIO | Guus Gijben
Cover: Proefschrift AIO | Guntra Laivacuma
Printing: DPN Rikken/Pumbo

ISBN: 9789465151564
DOI: 10.54195/9789465151564
Free download at: https://doi.org/10.54195/9789465151564

RADBOUD
UNIVERSITY
PRESS

Mimicking the Regenerative Matrix:

Bioactive Scaffolds to Improve Skin Repair

Proefschrift ter verkrijging van de graad van doctor
aan de Radboud Universiteit Nijmegen
op gezag van de rector magnificus prof. dr. J.M. Sanders,
volgens besluit van het college voor promoties
in het openbaar te verdedigen op

maandag 27 oktober 2025
om 16.30 uur precies

door

Nancy Margarita Avila Martinez
geboren op 28 januari 1994
te Soledad de Graciano Sanchez (Mexico)

Promotor:
Dr. ir. W.F. Daamen

Copromotoren:
Dr. A.H.M.S.M. van Kuppevelt
Dr. ir. B.K.H.L. Boekema (Vereniging Samenwerkende Brandwondencentra)

Manuscriptcommissie:
Dr. X.F. Walboomers
Dr. A.E.L. El Ghalbzouri (Leids Universitair Medisch Centrum)
Prof. dr. A. Cambi

Mimicking the Regenerative Matrix:

Bioactive Scaffolds to Improve Skin Repair

Dissertation to obtain the degree of doctor
from Radboud University Nijmegen
on the authority of the Rector Magnificus prof. dr. J.M. Sanders,
according to the decision of the Doctorate Board
to be defended in public on

Monday, October 27, 2025
at 4.30 pm

by

Nancy Margarita Avila Martinez
born on January 28, 1994
in Soledad de Graciano Sanchez (Mexico)

Supervisor:
Dr. ir. W.F. Daamen

Co-supervisors:
Dr. A.H.M.S.M. van Kuppevelt
Dr. ir. B.K.H.L. Boekema (Vereniging Samenwerkende Brandwondencentra)

Manuscript Committee:
Dr. X.F. Walboomers
Dr. A.E.L. El Ghalbzouri (Leiden University Medical Center)
Prof. dr. A. Cambi

Table of contents

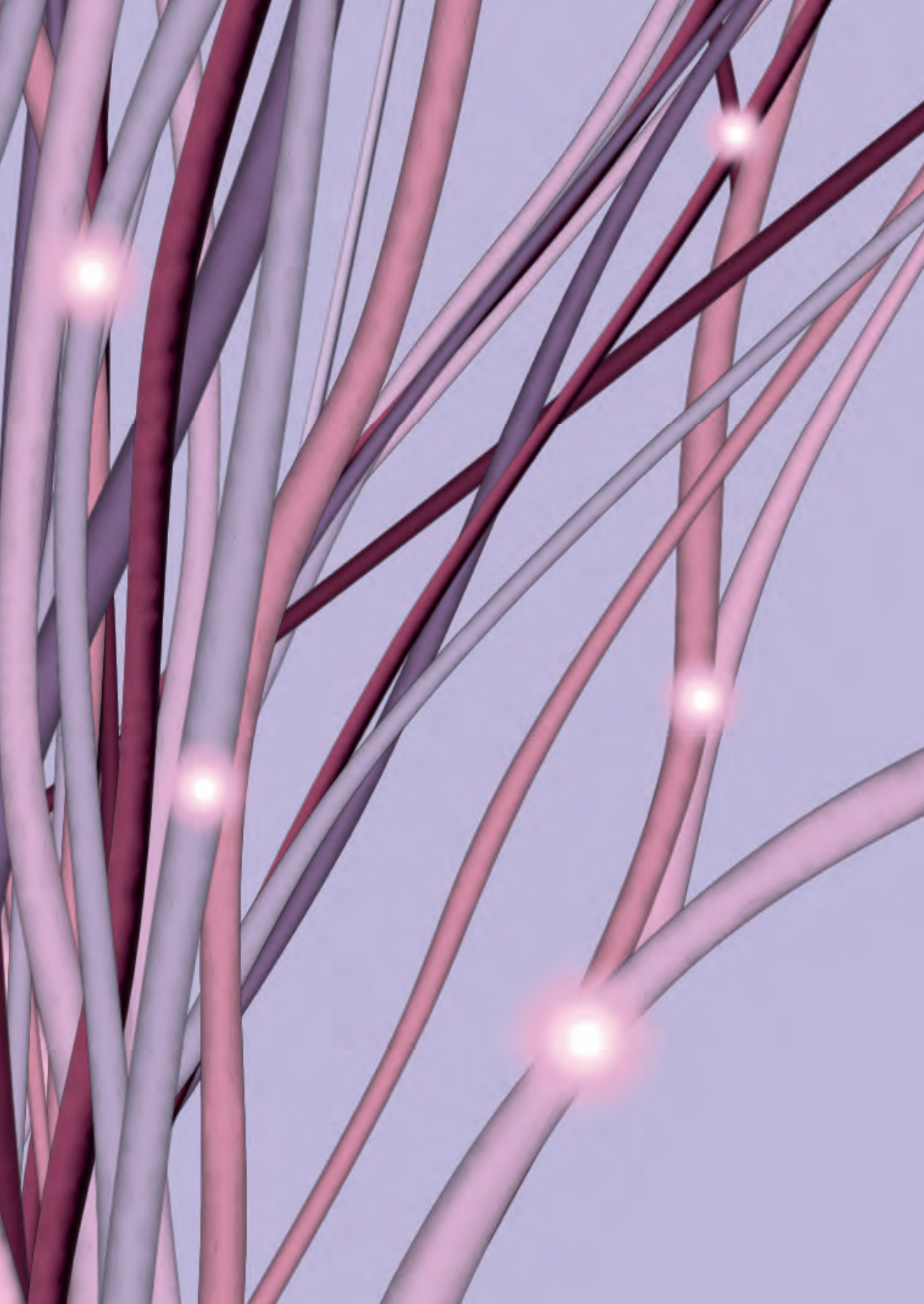

Chapter 1

General introduction

General introduction

Biomaterials play a central role in skin tissue engineering**,** a rapidly evolving field focused on developing functional skin substitutes for wound healing, reconstructive surgery, and disease modeling [1]. While many strategies involve the incorporation of cells and bioactive molecules to restore skin integrity in cases such as severe burns, chronic wounds, or genetic disorders [2, 3], this thesis centers on acellular dermal templates with a focus on molecules associated with scarless healing. It explores how specific biomaterial components, particularly extracellular matrix molecules, can enhance skin regeneration, offering promising avenues for clinical applications. To understand their full potential, it is important to first consider the structure and function of the skin.

Skin morphology

The skin is the largest organ of the human body with an approximate surface between 1.6-2 m^2 and performs important functions such as thermoregulation, immunity, repair and protection [4]. Morphologically, three layers can be appreciated in the human skin. These are, from the inside to the outside: hypodermis, dermis and, epidermis. The hypodermis, also known as subcutaneous tissue, primarily stores fat for insulation and is composed mainly of adipocytes [5].

The dermis is the thickest layer of the skin and provides structural support, nutrients and mechanical stability [6]. This layer is vascularized and contains appendages such as hair follicles, sweat glands and sebaceous glands. In the dermis, the extracellular matrix (ECM) predominates over the cellular components formed by connective tissue cells. The deepest dermal layer is known as reticular dermis with thick collagen fibers, while the papillary dermis, a thin layer located under the epidermis, is composed of loose connective tissue. The dermis is composed of ~30% collagen dry weight (mainly types I and III), followed by elastin, fibronectin, proteoglycans and glycosaminoglycans (GAGs) [7]. The primary cellular components of the dermis are fibroblasts, which produce protein fibers, along with immune cells such as dendritic cells, macrophages and mast cells [8]. The epidermis and upper part of the dermis are connected through the dermo-epidermal junction that includes not only the basement membrane but also hemidesmosomes of keratinocytes and anchoring fibrils produced by fibroblasts. This area contains types IV and VII collagen, laminin, fibronectin and heparan sulfate that support binding between laminins and integrins to hemidesmosomes [9, 10].

The epidermis is the outer layer of the skin, covering the dermis. This layer is further divided into four or five strata depending on the location in the body, where the innermost is the stratum basale, followed by the stratum spinosum and stratum granulosum until the stratum corneum. In the case of thick skin such as palm and soles, a stratum lucidum is positioned on the stratum granulosum [11]. The keratinocytes are the predominant cell type in the epidermis, comprising ~80% of the epithelial tissue. They form a robust barrier that protects the body from the external environment. Melanocytes, which produce melanin to protect against UV radiation, and Merkel cells, involved in touch sensation, are located in the basal layer of the epidermis. In contrast, Langerhans cells, which play a key role in the immune response to pathogens and foreign substances, reside in the stratum spinosum [11].

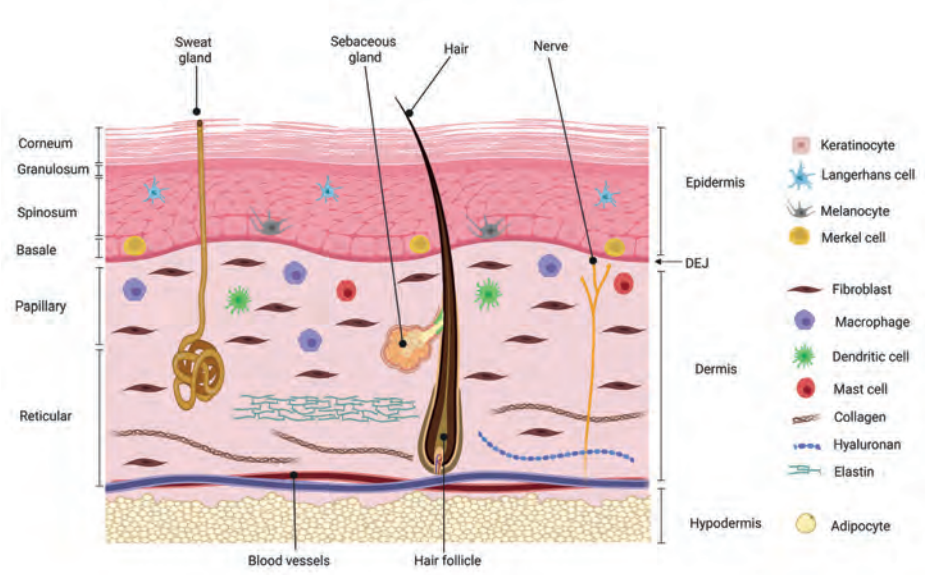

Figure 1. Schematic representation of the skin and its appendages. The skin is composed of three main layers: the epidermis, featuring stratified and basal keratinocytes and basal layer cells such as melanocytes and Merkel cells; the dermis, subdivided into the papillary (cell-rich) and reticular (ECM-rich) regions, containing fibroblasts, immune cells, blood vessels, nerves, sweat glands, and hair follicles; and the hypodermis, a subcutaneous layer primarily composed of adipocytes. Skin appendages like hair follicles and glands are present in the dermis or adipose tissue and extend through the epidermis. Note: layer proportions in epidermis and papillary dermis are enlarged for illustrative purposes and do not reflect actual thickness. Created in BioRender. Avila, N. (2025) https://BioRender.com/ce9r0s8.

Skin lesions

Despite its resilience and flexibility, the skin remains vulnerable to both external trauma and intrinsic defects, such as genetic disorders (e.g., Ehlers-Danlos syndrome), physical injuries (e.g., cuts), and thermal damage (e.g., burns) [12, 13]. This thesis focuses on developing skin substitutes for full-thickness wounds resulting after scar reconstructions or burns. According to the depth and extension, burns can be classified in different degrees. Superficial burns are limited to the epidermis and typically heal quickly through re-epithelialization. Partial thickness burns affect the upper part of the dermis, while deep burns reach the reticular region. Superficial and partial-thickness burns are typically painful, whereas deeper burns may be less painful due to nerve damage [14]. Full-thickness burns destroy the dermis, including appendages and nerves, and reach the hypodermis, significantly impairing tissue repair. Burn depth is difficult to estimate and is often mixed within wounds. Extensive injuries require medical and often surgical intervention to cover the wound, prevent complications, and promote healing [15].

Full-thickness injuries often result in incomplete repair and scar formation [16]. Conversely, in early fetal development, the skin is capable of scarless healing [17]. This difference is thought to stem from variations in skin structure and the cellular and molecular mechanisms activated at different developmental stages. Burn wounds, in particular, involve a more complex healing process characterized by delayed repair, persistent inflammation, excessive fibrosis, and functional impairment [18]. Although the mechanisms underlying these distinct healing outcomes are not fully elucidated, the wound healing process offers valuable insights into how regeneration may be enhanced.

Wound healing

During healing of a skin wound, two processes in the human body can occur, regeneration or repair. Regeneration is the complete replacement of different tissues and cell types in damaged organs, including its appendages such as hair follicles, nerves, blood vessels and glands. This process prevails during embryonic development [19]. On the other hand, repair rather than regeneration is common in adult mammals and its main purpose is a rapid wound closure to prevent dehydration and the entry of infectious agents, finally resulting in some form of scar [20].

Repair in adults

Wound healing takes place in multiple overlapping stages involving hemostasis, inflammation, proliferation and remodeling. During hemostasis, platelets bind to exposed collagen and aggregate, triggering clot formation through a fibrin

mesh that halts bleeding. In the inflammatory phase, neutrophils and resident macrophages eliminate pathogens and clear debris, followed by circulating monocytes that exit the blood stream and differentiate into M0 macrophages [21, 22]. These later polarize into M1 macrophages, which release pro-inflammatory cytokines and growth factors such as transforming growth factor beta 1 (TGF-β1) to recruit fibroblasts and initiate tissue formation [23]. As healing progresses into the proliferation stage, M0 and M1 macrophages transition into the M2 phenotype, promoting angiogenesis and tissue repair [24]. Under the influence of TGF-β1, fibroblasts transform into myofibroblasts, characterized by the incorporation of α-smooth muscle actin (α-SMA) stress fibers in the cytoskeleton, allowing them to contract the ECM [25]. Myofibroblasts also produce provisional ECM, composed mostly of type III collagen (Col III). Meanwhile, re-epithelization takes place by keratinocytes covering the granular tissue [26]. In the remodeling stage, matrix metalloproteinases degrade early ECM components such as Col III, which are replaced with type I collagen (Col I), produced by (myo)fibroblasts, forming a stiffer matrix. Fibroblasts are involved in self-amplifying loops where increased ECM and tissue stiffness activate mechanosensitive TGF-β1 pathways leading to myofibroblast differentiation, which further leads to ECM accumulation and continued contraction driving scar formation [27, 28]. Unlike native skin, scar tissue lacks appendages such as hair follicles and sweat glands, resulting in functional and structural deficits at the wound site [29].

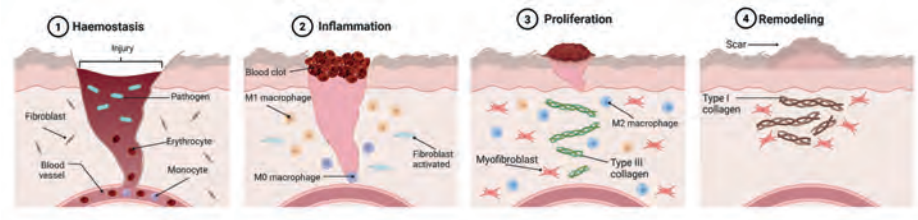

Figure 2. Global overview of the wound healing process described in the text above. Following injury, a blood clot forms to seal the wound and initiate healing. The inflammatory phase begins with M0 macrophages (derived from circulatory monocytes) polarizing into the M1 subtype, recruiting immune and stromal cells such as fibroblasts. During the proliferative phase, macrophages polarize to M2 phenotype, and fibroblasts differentiate into myofibroblasts that deposit granulation tissue rich in type III collagen. In the final remodeling phase, type III collagen is gradually replaced by type I collagen, typically resulting in scar formation. An extensive description of the wound healing process can be found in **Chapter 2**. Created in BioRender. Avila, N. (2025) https://BioRender.com/9yb67wo.

Regeneration during fetal wound healing

Fetal wound healing is distinct from adult healing, and is characterized by minimal inflammation, rapid regeneration and scarless outcomes. Several factors

contribute to this unique process such as a different skin microenvironment as more extensively described by Martin [30]. The fetal immune system is immature and relies heavily on maternal support via the fetal-maternal interface, composed of the placenta and decidua, which facilitates immune tolerance and nutrient exchange [31]. Following injury, decidual and maternal macrophages act as first responders, while fetal macrophage activity remains low, correlating with a significantly shortened inflammatory phase [32]. Studies have shown that inducing inflammation in fetal wounds can trigger scarring, suggesting inflammation is a key driver of fibrosis [33, 34]. Moreover, elevated protein levels of TGF-β3 in early fetal wounds with downregulation of TGF-β1 [35, 36], have associated TGF-β3 with an antifibrotic function. Fetal fibroblasts migrate faster than adult ones and deposit higher amounts of Col III [37] and hyaluronan (HA) [38], supporting a hydrated, permissive environment for regeneration. Notably, fetal keratinocytes close wounds through a contractile actin purse-string mechanism, enabling fast and coordinated closure [39]. In contrast, adult keratinocytes migrate individually using lamellipodia, resulting in a slower healing [40].

Burn wounds in adults

Burn wounds, particularly in the case of deep burns, are marked by extensive tissue destruction, including vascular damage, loss of skin appendages and a disrupted healing process [18]. Necrotic avascular tissue forms over the wound, known as eschar, covering the surface and acting as a barrier that hinders cell migration and delays closure [41]. Fibroblasts present in this eschar are often dysfunctional, showing altered responses to growth factors and contributing to disorganized collagen deposition [42, 43]. Prolonged inflammation, driven by sustained M1 macrophage activity and elevated TGF-β1 levels, promotes fibrosis in burn wound healing [44, 45]. In addition, impaired vascularization and reduced M2 macrophage transition hinder proper resolution of inflammation and tissue repair [46], resulting in imbalanced collagen deposition, with increased and disorganized Col I and reduced Col III contributing to (hypertrophic) scars [47].

Current therapies for burn wound care

Extensive, large full-thickness skin injuries, e.g., affecting more than >25% of the total body surface area, require immediate clinical intervention [48] to restore the skin barrier and prevent fluid loss, infection, and systemic complications [49]. The primary treatment strategy for severe burns is skin transplantation, which can be supplemented with dermal substitutes like Matriderm, Integra or Novosorb.

Skin transplants can be categorized into autologous (from the patient), allogeneic (from a different donor), and xenogeneic (from a different species) sources. Autologous grafts remain the gold standard due to their biocompatibility and retention of native skin structures such as appendages and vasculature [50]. However, in large area burns, donor site availability becomes a limiting factor, and harvesting healthy skin can itself lead to additional trauma and delayed healing. Allografts provide temporary cover and are limited by tissue bank availability with a risk of immune rejection. Xenogeneic matrix, while more accessible, requires intensive decellularization to remove antigenic components, which can damage the extracellular matrix (ECM) and reduce bioactivity [51].

Tissue engineering and regenerative medicine offer alternative solutions by combining biomaterials, cell cultures, and bioactive molecules to mimic the structure and function of native skin. Engineered skin constructs aim to provide protective coverage, promote faster and more organized tissue regeneration, minimize scarring, and be safe, reproducible, and cost-effective [52]. Among these, cultured epidermal autografts have shown promise but are fragile, show blistering after closure and require extended culture times and high cellular viability, limiting their use in acute cases where immediate treatment is essential [53].

Dermal substitutes can be either cellular or acellular. Cellular constructs, like Dermagraft®, incorporate e.g., neonatal fibroblasts that support ECM production but face logistical challenges with preparation and storage constraints [54]. In contrast, acellular dermal templates offer off-the-shelf availability and avoid immune complications while serving as a scaffold that mimics the original dermal ECM. The constructs are typically fabricated from natural biomaterials, known for their biocompatibility, or synthetic polymers which offer durability and handling advantages [55]. Note that these approaches still require complementary split-thickness skin transplantation.

Towards smarter skin substitutes: Aims and outline of this thesis

Most commercially available skin substitutes for burn treatment rely on animal-derived Col I, the primary structural protein in human skin, as highlighted by the product list made by Yildirimer *et al.* [56]. While these products provide a biodegradable support for healing, they often result in imperfect skin repair and scarring, emphasizing the need for biomaterials that better promote true regeneration.

Regenerative models

Unlike humans, certain species exhibit remarkable regenerative capabilities, offering insight into pro-regenerative ECM profiles. The axolotl, for example, is well known for its ability to regenerate limbs and internal organs [57], while Acomys carihinus (or spiny mouse) is one of the few mammals capable of regenerating skin in adults without scarring [58]. Identifying key ECM components (the matrisome) expressed during their wound healing offers inspiration for developing biomaterials that mimic these regenerative environments. **Chapter 2** provides a comparative analysis of their transcriptomic and proteomic profiles, highlighting ECM molecules with potential for application in biomaterial design [59].

Mimicking fetal skin

Interestingly, human fetal skin (before 24 weeks of gestation) can heal without scarring [60], and a review by Gomes *et al.* [61] cataloged distinct ECM molecules present during this stage. Among these**,** HA and Col III have received particular attention for its abundance in fetal skin [62], while both components decline with age, showing an association with reduced healing capacity in adults. HA, a major ECM glycosaminoglycan during early gestation (particularly in the first 6 weeks) [63], contributes to skin hydration and supports cellular processes. Its concentration in fetal skin ranges from 0.12-0.53 µg/mg dry weight in sheep and rabbits [64-66]. While HA has been widely explored in hydrogel formulations for skin repair [67], its application in scaffolds for dermal templates, particularly relevant for treating burn wounds, remains underdeveloped. This topic is addressed in detail in **Chapter 3** by the development of Col I scaffolds incorporating HA, where their influence on fibrotic markers is examined *in vitro*. In addition, the Col I/III ratio shifts with age from fetal (2:1) to newborn (1:1) to adult stage (3:1) [68-70], increasing the stiffness of the dermal matrix and impacting healing outcomes as observed in fetal skin [69, 71]. Since many wound-healing cells are mechanosensitive, a softer ECM, e.g., such as one naturally enriched in Col III, has been associated with improved regenerative outcomes [72, 73]. To mimic some of these properties, **Chapter 4** explores scaffolds based on fibrillar Col I combined with atelocollagen with removed telopeptides that is inherently softer than native fibrillar collagen and further enriched with extracted human Col III. This chapter focuses on the extraction of Col III from human placenta and the creation of Col I/III scaffolds with varying ratios, followed by *in vitro* and *in vivo* evaluation.

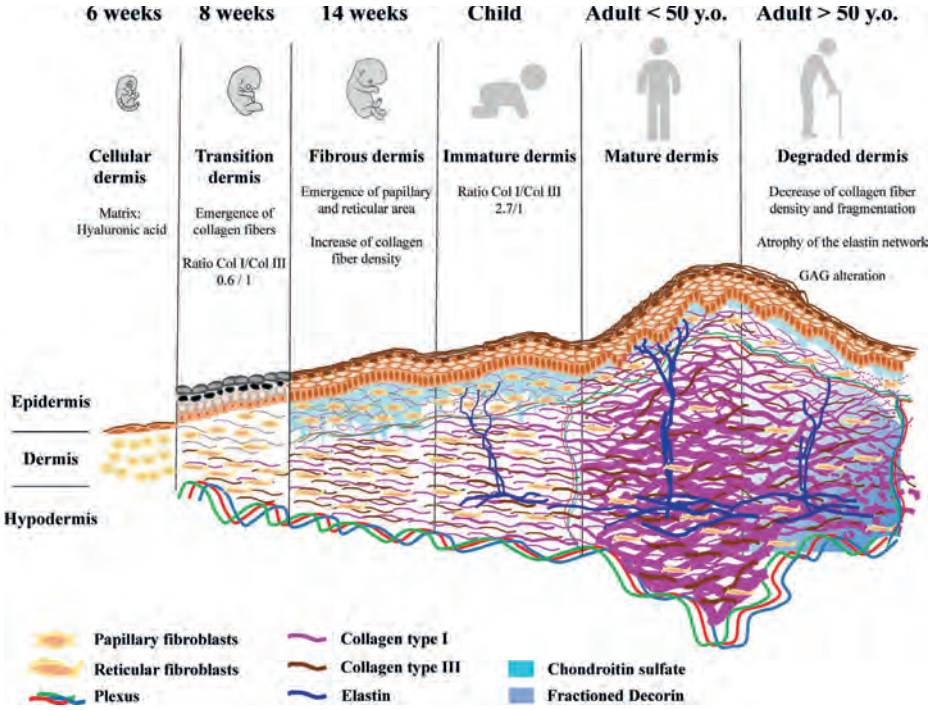

Figure 3. Schematic representation of dermal composition during human development and aging. In the prenatal stage, the dermis is rich in hyaluronic acid (HA) and type III collagen (Col III). As aging progresses, Col III decreases while Col I becomes more predominant. Figure reproduced from Haydont *et al.* (2019), DOI: 10.1016/j.mad.2018.03.006 licensed under CC-BY-NC-ND [62].

Regenerative studies in prenatal mice have identified upregulated effector molecules during early skin development [74]. One promising but underexplored candidate is sonic hedgehog (SHH), a crucial morphogen involved in embryogenesis and tissue patterning. SHH contains a heparin-binding domain, making it suitable for incorporation into biomaterials functionalized with heparin or heparan sulfate (HS) [75]. Our research group has developed collagen-heparin scaffolds that improved *in utero* wound healing in a sheep model [76]. However, heparan sulfate is susceptible to enzymatic degradation, particularly in an inflammatory environment (e.g., burns) rich in glycosidases [77], which limits its capacity to stabilize growth factors. To overcome this, the company OTR3 created heparan sulfate mimetics, known as Regenerating Agents (RGTA). One variant, OTR4120, has demonstrated promising results in promoting wound healing when used in topical formulations [78]. In this thesis, **Chapter 5** explores the integration of OTR4120 into biomaterial scaffolds, evaluates its potential to bind SHH, and assesses the effect of Col I-OTR4120 scaffolds on macrophage polarization and wound healing in rats.

Wound healing models

Before clinical application, skin substitutes must undergo rigorous testing to assess safety, biocompatibility, and efficacy. This includes both *in vitro* (cell-based) and *in vivo* (animal) studies that aim to mimic human wound healing responses [79]. Cell lines are often used because of their reproducibility, but they lack fidelity compared to primary human cells, used in this thesis, which offer superior physiological relevance [80]. Fibroblasts, being the principal cellular component of the dermis, are commonly employed to assess the efficacy of skin substitutes [78]. Therefore, in **Chapters 3 and 4**, fibroblasts were used to evaluate the biocompatibility of the developed scaffolds and their potential to modulate fibrotic responses in the presence of additional components such as HA and Col III. Given that fibroblast behavior can vary significantly depending on their source and developmental stage [43, 81], fetal and eschar fibroblasts (derived from burnt tissue) were also incorporated in **Chapter 3**. Fetal fibroblasts, known for their regenerative, scarless healing properties [37], and eschar fibroblasts, characterized by their pro-fibrotic phenotype [82], were selected to determine whether their distinct gene expression profiles would be maintained or modulated in the presence of HA. This approach aimed to elucidate whether our scaffolds could eventually be used alongside regenerative cell therapies to enhance healing outcomes. Macrophages represent another cell type that plays a central role in wound healing, especially in modulating inflammation and tissue regeneration [24]. Since immune responses during wound healing vary between fetal and adult wounds, this thesis investigates macrophage polarization in response to different biomaterial formulations incorporating components abundant in fetal skin, as explored in **Chapters 3, 4, and 5**. Finally, animal testing is required in the validation process and for approval of medical devices as it provides a more comprehensive assessment of skin wound healing than *in vitro* testing alone, especially including systemic responses [83]. Therefore, the wound healing response, including contraction, is studied after the application of biofunctionalized skin substitutes in a full thickness wound in Wistar rats in **Chapters 4 and 5**.

Overall, this thesis focuses on identifying ECM components that may enhance skin regeneration and studies the integration of these components into bioengineered Col I-based dermal substitutes along with their pre-clinical evaluation. **Chapter 6** encompasses the general discussion of the results of the thesis and provides perspectives on the optimization of future skin substitutes. A summary of the thesis is presented in **Chapter 7**.

References

1. Yu, J.R., et al., *Current and Future Perspectives on Skin Tissue Engineering: Key Features of Biomedical Research, Translational Assessment, and Clinical Application.* Advanced Healthcare Materials, 2019. **8**(5): p. 1801471.
2. Dutra Alves, N.S., et al., *Advances in regenerative medicine-based approaches for skin regeneration and rejuvenation.* Frontiers in Bioengineering and Biotechnology, 2025. **13**.
3. Qin, J., et al., *Recent Advances in Bioengineered Scaffolds for Cutaneous Wound Healing.* Frontiers in Bioengineering and Biotechnology, 2022. **10**.
4. Gallo, R.L., *Human Skin Is the Largest Epithelial Surface for Interaction with Microbes.* J Invest Dermatol, 2017. **137**(6): p. 1213-4.
5. Liu, M., F. Lu, and J. Feng, *Aging and homeostasis of the hypodermis in the age-related deterioration of skin function.* Cell Death & Disease, 2024. **15**(6): p. 443.
6. Nafisi, S. and H.I. Maibach, *Skin penetration of nanoparticles.* Emerging Nanotechnologies in Immunology: the Design, Applications and Toxicology of Nanopharmaceuticals and Nanovaccines, 2018: p. 47-88.
7. Tarnutzer, K., et al., *Collagen constitutes about 12% in females and 17% in males of the total protein in mice.* Scientific Reports, 2023. **13**(1): p. 4490.
8. Saladin, K.S., *Anatomia & fisiologia*. 2013: Piccin-Nuova Libraria.
9. Shimizu, H., *Shimizu's dermatology*. Second edition. ed. Dermatology. 2017, Chichester, West Sussex ; Hoboken, NJ: Chichester, West Sussex ; Hoboken, NJ : John Wiley and Sons, Incorporated, 2017.
10. Villone, D., et al., *Supramolecular Interactions in the Dermo-epidermal Junction Zone: ANCHORING FIBRIL-COLLAGEN VII TIGHTLY BINDS TO BANDED COLLAGEN FIBRILS**, in *J Biol Chem*. 2008. p. 24506-13.
11. Yousef, H., M. Alhajj, and S. Sharma, *Anatomy, Skin (Integument), Epidermis.* 2019.
12. Richmond, J.M. and J.E. Harris, *Immunology and Skin in Health and Disease*, in *Cold Spring Harb Perspect Med*. 2014.
13. Norris, C.M., *CHAPTER 1 - Healing*, in *Managing Sports Injuries (Fourth Edition)*, C.M. Norris, Editor. 2011, Churchill Livingstone: Oxford. p. 1-27.
14. Paprottka, F., et al., *German, European or American burn guidelines – Is one superior to another?* Ann Burns Fire Disasters, 2016. **29**(1): p. 30-6.
15. Wolf, M.G.J.L.-P.K.F.S.S.E., *Handbook of Burns Volume 1 - Acute Burn Care*. 1 ed. Vol. 1. 2012: Springer-Verlag Wien.
16. Than, P.A., C.R. Davis, and G.C. Gurtner, *Chapter 4 - Clinical Management of Wound Healing and Hypertrophic Scarring*, in *Skin Tissue Engineering and Regenerative Medicine*, M.Z. Albanna and J.H. Holmes Iv, Editors. 2016, Academic Press: Boston. p. 61-81.
17. Larson, B.J., M.T. Longaker, and H.P. Lorenz, *Scarless Fetal Wound Healing: A Basic Science Review.* Plastic and Reconstructive Surgery, 2010. **126**(4): p. 1172-1180.
18. Brusselaers, N., et al., *Severe burn injury in europe: a systematic review of the incidence, etiology, morbidity, and mortality*, in *Crit Care*. 2010. p. R188.
19. Nguyen, D.T., D.P. Orgill, and G.F. Murphy, *The pathophysiologic basis for wound healing and cutaneous regeneration.* Biomaterials for Treating Skin Loss, 2009: p. 25-57.
20. Gonzalez, A.O., et al., *Wound healing - A literature review.* An Bras Dermatol, 2016. **91**(5): p. 614-20.

21. Potter, D.A., D. Veitch, and G.A. Johnston, *Scarring and wound healing.* British Journal of Hospital Medicine, 2019. **80**(11): p. C166-C171.
22. Su, Y., et al., *Neutrophils and Macrophages as Targets for Development of Nanotherapeutics in Inflammatory Diseases.* Pharmaceutics, 2020. **12**(12).
23. Silva, M.T., *Macrophage phagocytosis of neutrophils at inflammatory/infectious foci: a cooperative mechanism in the control of infection and infectious inflammation.* J Leukoc Biol, 2011. **89**(5): p. 675-83.
24. Zheng, H., et al., *Recent advances in strategies to target the behavior of macrophages in wound healing.* Biomedicine & pharmacotherapy, 2023. **165**.
25. Tai, Y., et al., *Myofibroblasts: Function, Formation, and Scope of Molecular Therapies for Skin Fibrosis.* Biomolecules, 2021. **11**(8): p. 1095.
26. Alhajj, M. and A. Goyal, *Physiology, Granulation Tissue*, in *StatPearls*. 2025, StatPearls Publishing. Copyright © 2025, StatPearls Publishing LLC.: Treasure Island (FL).
27. Walker, M., M. Godin, and A.E. Pelling, *Mechanical stretch sustains myofibroblast phenotype and function in microtissues through latent TGF-β1 activation.* Integrative Biology, 2020. **12**(8): p. 199-210.
28. Leong, E., M. Bezuhly, and J.S. Marshall, *Distinct Metalloproteinase Expression and Functions in Systemic Sclerosis and Fibrosis: What We Know and the Potential for Intervention.* Frontiers in Physiology, 2021. **Volume 12 - 2021**.
29. Monstrey, S., et al., *Updated Scar Management Practical Guidelines: Non-invasive and invasive measures.* Journal of Plastic, Reconstructive & Aesthetic Surgery, 2014. **67**(8): p. 1017-1025.
30. Martin, P., *Wound healing--aiming for perfect skin regeneration.* Science, 1997. **276**(5309): p. 75-81.
31. Andreescu, M., *Correlation Between Maternal-Fetus Interface and Placenta-Mediated Complications.* Cureus, 2024. **16**(6): p. e62457.
32. DiPietro, L.A., T.A. Wilgus, and T.J. Koh, *Macrophages in Healing Wounds: Paradoxes and Paradigms.* Int J Mol Sci, 2021. **22**(2).
33. Hu, M.S., et al., *Embryonic skin development and repair.* Organogenesis, 2018. **14**(1): p. 46-63.
34. Wilgus, T.A., et al., *The impact of cyclooxygenase-2 mediated inflammation on scarless fetal wound healing.* Am J Pathol, 2004. **165**(3): p. 753-61.
35. Kathju, S., P.H. Gallo, and L. Satish, *Scarless integumentary wound healing in the mammalian fetus: molecular basis and therapeutic implications.* Birth Defects Res C Embryo Today, 2012. **96**(3): p. 223-36.
36. Chen, W., et al., *Ontogeny of expression of transforming growth factor-beta and its receptors and their possible relationship with scarless healing in human fetal skin.* Wound Repair Regen, 2005. **13**(1): p. 68-75.
37. Carter, R., et al., *Differential expression of procollagen genes between mid-and late-gestational fetal fibroblasts.* Journal of Surgical Research, 2009. **156**(1): p. 90-94.
38. Longaker, M.T., et al., *Studies in fetal wound healing. V. A prolonged presence of hyaluronic acid characterizes fetal wound fluid.* Annals of surgery, 1991. **213**(4): p. 292.
39. Martin, P. and J. Lewis, *Actin cables and epidermal movement in embryonic wound healing.* Nature, 1992. **360**(6400): p. 179-183.
40. Fenteany, G., P.A. Janmey, and T.P. Stossel, *Signaling pathways and cell mechanics involved in wound closure by epithelial cell sheets.* Curr Biol, 2000. **10**(14): p. 831-8.
41. Branski, L.K., et al., *A porcine model of full-thickness burn, excision and skin autografting.* Burns, 2008. **34**(8): p. 1119-27.

42. Wang, X.Q., et al., *The correlation of in vivo burn scar contraction with the level of a-smooth muscle actin expression.* Burns, 2011. **37**(8): p. 1367-77.
43. Kutluoğlu, G.C., et al., *Comparison of dermal and eschar fibroblasts in full skin equivalents.* Wound Repair Regen, 2025. **33**(1): p. e70001.
44. Mulder, P.P.G., et al., *Burn-injured skin is marked by a prolonged local acute inflammatory response of innate immune cells and pro-inflammatory cytokines.* Frontiers in Immunology, 2022. **13**.
45. Finnerty, C.C., et al., *Hypertrophic scarring: the greatest unmet challenge after burn injury.* Lancet, 2016. **388**(10052): p. 1427-1436.
46. Pi, L., et al., *LncRNA XIST accelerates burn wound healing by promoting M2 macrophage polarization through targeting IL-33 via miR-19b.* Cell Death Discovery, 2022. **8**(1): p. 220.
47. Faour, S., et al., *Fibrosis in burns: an overview of mechanisms and therapies.* American Journal of Physiology-Cell Physiology, 2023. **325**(6): p. C1545-C1557.
48. Vivó, C., R. Galeiras, and M.D.P. del Caz, *Initial evaluation and management of the critical burn patient.* Medicina Intensiva (English Edition), 2016. **40**(1): p. 49-59.
49. Voigt, C.D., et al., *14 - The Skin Bank*, in *Total Burn Care (Fifth Edition)*, D.N. Herndon, Editor. 2018, Elsevier. p. 158-166.e2.
50. Blume, P.A., *Chapter 19 - Skin grafts*, in *Lower Extremity Soft Tissue & Cutaneous Plastic Surgery (Second Edition)*, G.D. Dockery and M.E. Crawford, Editors. 2012, W.B. Saunders: Oxford. p. 207-224.
51. Cui, H.M., Y.M. Chai, and Y.L. Yu, *Progress in developing decellularized bioscaffolds for enhancing skin construction.* Journal of Biomedical Materials Research Part A, 2019. **107**(8): p. 1849-1859.
52. Dearman, B.L., S.T. Boyce, and J.E. Greenwood, *Advances in Skin Tissue Bioengineering and the Challenges of Clinical Translation.* Frontiers in Surgery, 2021. **Volume 8 - 2021**.
53. Rheinwald, J.G. and H. Green, *Serial cultivation of strains of human epidermal keratinocytes: the formation of keratinizing colonies from single cells.* Cell, 1975. **6**(3): p. 331-43.
54. Criswell, T., et al., *Shipping and Logistics Considerations for Regenerative Medicine Therapies.* Stem Cells Transl Med, 2022. **11**(2): p. 107-113.
55. Zeng, Q., et al., *5.534 - Skin Tissue Engineering*, in *Comprehensive Biomaterials*, P. Ducheyne, Editor. 2011, Elsevier: Oxford. p. 467-499.
56. Yildirimer, L., N.T. Thanh, and A.M. Seifalian, *Skin regeneration scaffolds: a multimodal bottom-up approach*. Trends Biotechnol, 2012. **30**(12): p. 638-48.
57. Voss, S.R., et al., *Ambystoma mexicanum, the Axolotl: A Versatile Amphibian Model for Regeneration, Development, and Evolution Studies.* Emerging Model Organisms: Laboratory Manual, Vol 2, 2010: p. 397-419.
58. Seifert, A.W. and K. Muneoka, *The blastema and epimorphic regeneration in mammals.* Dev Biol, 2018. **433**(2): p. 190-199.
59. Avila-Martinez, N., et al., *Matrisomal components involved in regenerative wound healing in axolotl and Acomys: implications for biomaterial development.* Biomater Sci, 2023. **11**(18): p. 6060-6081.
60. Lorenz, H.P., et al., *The fetal fibroblast - the effector cell of scarless fetal skin repair.* Plastic and Reconstructive Surgery, 1995. **96**(6): p. 1251-1259.
61. Gomes, M., et al., *Fetal Skin Wound Healing: Key Extracellular Matrix Components and Regulators in Scarless Healing.* J Invest Dermatol, 2025. **145**(2): p. 280-302.
62. Haydont, V., B.A. Bernard, and N.O. Fortunel, *Age-related evolutions of the dermis: Clinical signs, fibroblast and extracellular matrix dynamics.* Mechanisms of Ageing and Development, 2019. **177**: p. 150-156.

63. Caplan, A.I., M.Y. Fiszman, and H.M. Eppenberger, *Molecular and cell isoforms during development.* Science, 1983. **221**(4614): p. 921-927.
64. Freund, R.M., et al., *Serial quantitation of hyaluronan and sulfated glycosaminoglycans in fetal sheep skin.* Biochem Mol Biol Int, 1993. **29**(4): p. 773-83.
65. Longaker, M.T., et al., *Studies in fetal wound healing. V. A prolonged presence of hyaluronic acid characterizes fetal wound fluid.* Ann Surg, 1991. **213**(4): p. 292-6.
66. Mast, B.A., et al., *Hyaluronic acid is a major component of the matrix of fetal rabbit skin and wounds: implications for healing by regeneration.* Matrix, 1991. **11**(1): p. 63-8.
67. Zhang, M., et al., *Hyaluronic acid hydrogels with excellent self-healing capacity and photo-enhanced mechanical properties for wound healing.* Int J Biol Macromol, 2024. **267**(Pt 1): p. 131235.
68. Epstein, E.H., *[a1(III)]3 Human Skin Collagen: RELEASE BY PEPSIN DIGESTION AND PREPONDERANCE IN FETAL LIFE.* Journal of Biological Chemistry, 1974. **249**(10): p. 3225-3231.
69. Cheng, W., et al., *The content and ratio of type I and III collagen in skin differ with age and injury.* African Journal of Biotechnology, 2011. **10**(13): p. 2524-2529.
70. Sykes, B., et al., *The estimation of two collagens from human dermis by interrupted gel electrophoresis.* Biochemical and Biophysical Research Communications, 1976. **72**(4): p. 1472-1480.
71. Gao, J., et al., *Age-related changes in the ratio of Type I/III collagen and fibril diameter in mouse skin.* Regen Biomater, 2023. **10**: p. rbac110.
72. Singh, D., V. Rai, and D.K. Agrawal, *Regulation of Collagen I and Collagen III in Tissue Injury and Regeneration.* Cardiol Cardiovasc Med, 2023. **7**(1): p. 5-16.
73. Tronci, G., et al., *Protease-sensitive atelocollagen hydrogels promote healing in a diabetic wound model.* Journal of Materials Chemistry B, 2016. **4**(45): p. 7249-7258.
74. Uijtdewilligen, P.J.E., et al., *Towards embryonic-like scaffolds for skin tissue engineering: identification of effector molecules and construction of scaffolds.* Journal of Tissue Engineering and Regenerative Medicine, 2016. **10**(1): p. E34-E44.
75. Whalen, D.M., et al., *Structural insights into proteoglycan-shaped Hedgehog signaling.* Proc Natl Acad Sci U S A, 2013. **110**(41): p. 16420-5.
76. Oostendorp, C., et al., *Sustained Postnatal Skin Regeneration Upon Prenatal Application of Functionalized Collagen Scaffolds.* Tissue Engineering Part A, 2021. **27**(1-2): p. 10-25.
77. Olczyk, P., L. Mencner, and K. Komosinska-Vassev, *Diverse Roles of Heparan Sulfate and Heparin in Wound Repair.* Biomed Research International, 2015. **2015**.
78. Barritault, D., *Overview of 10 years of practice with CACIPLIQ20® matrix therapy as a healing agent for hard to heal wounds: Efficacy, cost-effectiveness and future perspectives.* Wound Medicine, 2020. **28**: p. 100180.
79. Sarian, M.N., et al., *A review with updated perspectives on in vitro and in vivo wound healing models.* Turk J Biol, 2023. **47**(4): p. 236-246.
80. Drucker, Daniel J., *Never Waste a Good Crisis: Confronting Reproducibility in Translational Research.* Cell Metabolism, 2016. **24**(3): p. 348-360.
81. Alaish, S.M., et al., *Biology of fetal wound healing: Hyaluronate receptor expression in fetal fibroblasts.* Journal of Pediatric Surgery, 1994. **29**(8): p. 1040-1043.
82. van den Bogaerdt, A.J., et al., *The suitability of cells from different tissues for use in tissue-engineered skin substitutes.* Arch Dermatol Res, 2002. **294**(3): p. 135-42.
83. Saeed, S. and M. Martins-Green, *Animal models for the study of acute cutaneous wound healing.* Wound Repair and Regeneration, 2023. **31**(1): p. 6-16.

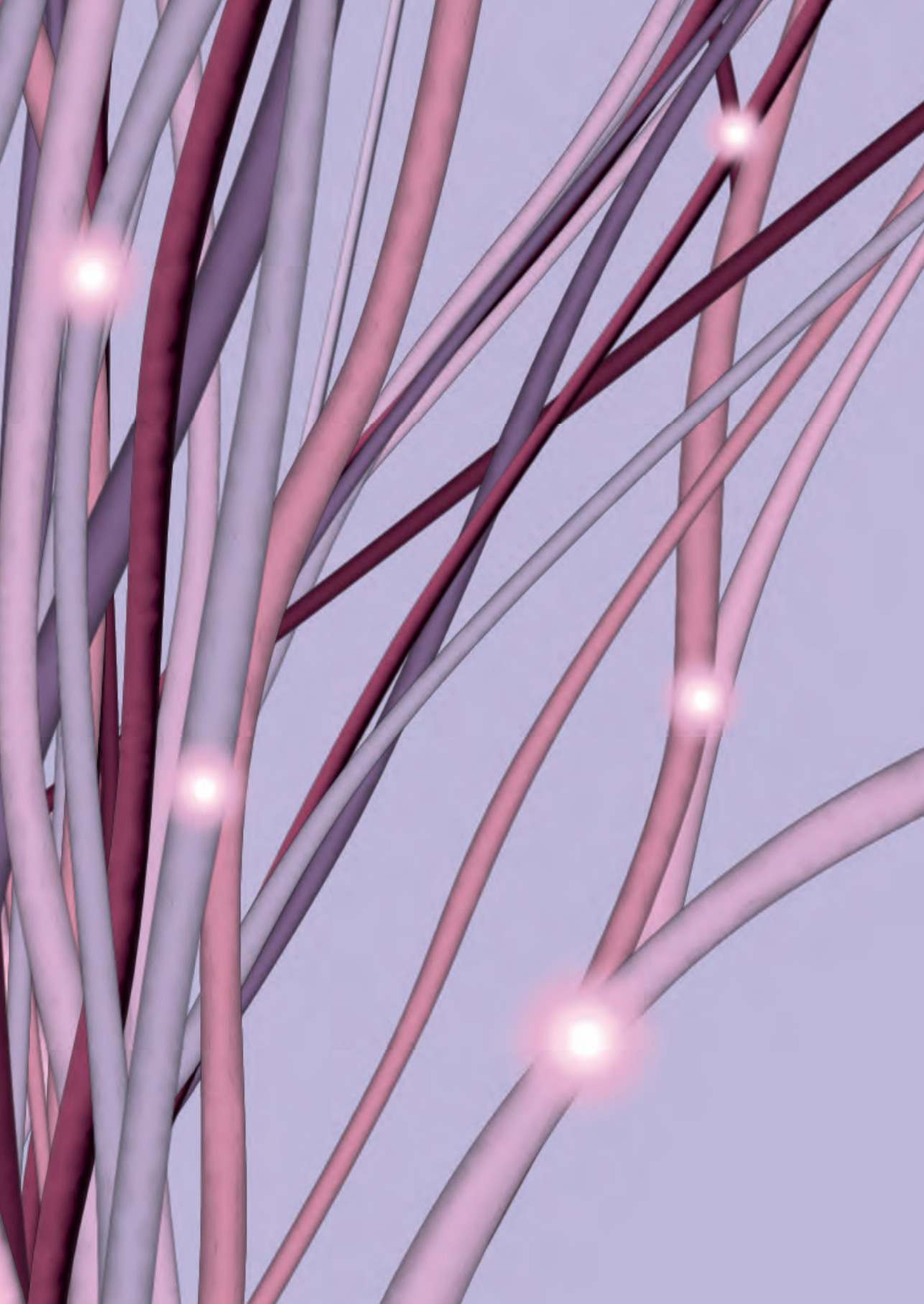

Chapter 2

Matrisomal components involved in regenerative wound healing in axolotl and *Acomys*: Implications for biomaterial development

Nancy Avila-Martinez [a,†], Merel Gansevoort [a,†], Juul Verbakel [a,b], Haarshaadri Jayaprakash [c,d], Ines Maria Araujo [d,f], Marta Vitorino [c,d,f], Gustavo Tiscornia[c,e], Toin H. van Kuppevelt [a], Willeke F. Daamen [a]

a. Department of Medical BioSciences, Radboud Research Institute, Radboud university medical center, PO Box 9101, 6500 HB Nijmegen, The Netherlands

b. Current address: Biointerface Science, Department of Biomedical Engineering, Eindhoven University of Technology, PO Box 513, 5600 MB Eindhoven, The Netherlands

c. Centre of Marine Sciences (CCMAR), University of Algarve, 8005-139, Faro, Portugal

d. Faculty of Medicine and Biomedical Sciences (FMCB), University of Algarve, 8005-139, Faro, Portugal

e. Eugin Barcelona, Balmes, 236, 08006 Barcelona, Spain

f. Algarve Biomedical Center Research Institute (ABC-RI), University of Algarve, 8005-139, Faro, Portugal

† Both authors contributed equally to this work.

Biomater Sci. 2023;11:6060-6081. Doi: 10.1039/d3bm00835e

Abstract

Achieving regeneration in humans has been a long-standing goal of many researchers. Whereas amphibians like the axolotl (*Ambystoma mexicanum*) are capable of regenerating whole organs and even limbs, most mammals heal their wounds via fibrotic scarring. Recently, the African spiny mouse (*Acomys* sp.) has been shown to be injury resistant and capable of regenerating several tissue types. A major focal point of research with *Acomys* has been the identification of drivers of regeneration. In this search, the matrisome components related to the extracellular matrix (ECM) are often overlooked. In this review, we compare *Acomys* and axolotl skin wound healing and blastema-mediated regeneration by examining their wound healing responses and comparing the expression pattern of matrisome genes, including glycosaminoglycan (GAG) related genes. The goal of this review is to identify matrisome genes that are upregulated during regeneration and could be potential candidates for inclusion in pro-regenerative biomaterials. Research papers describing transcriptomic or proteomic coverage of either skin regeneration or blastema formation in *Acomys* and axolotl were selected. Matrisome and GAG related genes were extracted from each dataset and the resulting lists of genes were compared. In our analysis, we found several genes that were consistently upregulated, suggesting possible involvement in regenerative processes. Most of the components have been implicated in regulation of cell behavior, extracellular matrix remodeling and wound healing. Incorporation of such pro-regenerative factors into biomaterials may help to shift pro-fibrotic processes to regenerative responses in treated wounds.

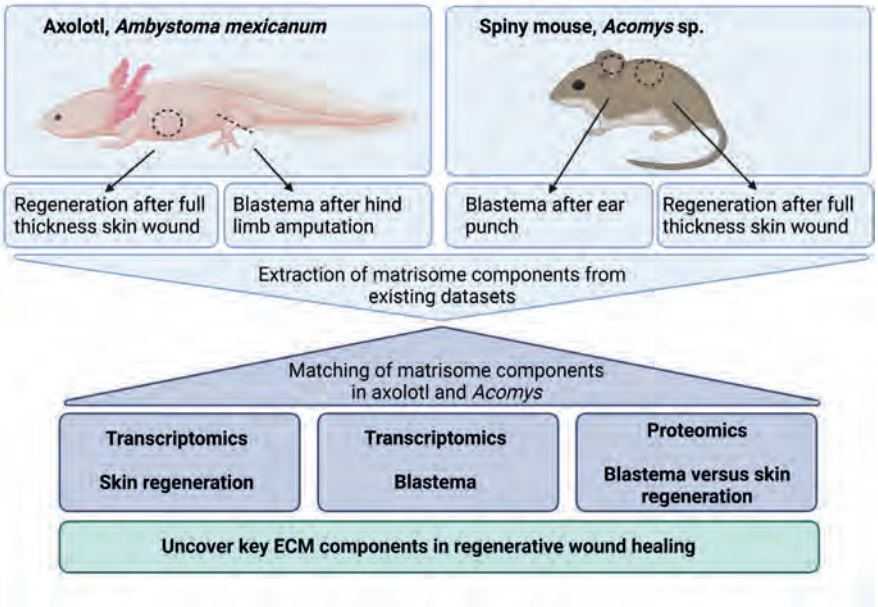

Introduction

Throughout the animal kingdom, adult skin wounding can be resolved either by fibrotic scarring or tissue regeneration. With some exceptions such as ear punch closure in rabbits [1, 2], antler regrowth in deer [3, 4], digit tip regeneration in children and mice [5, 6], most adult mammals repair their wounds by fibrotic scarring [7, 8]. In humans, fibrosis in response to the destruction of both the epidermis and dermis (full-thickness skin wounds), such as third degree burns and traumas, results in scars that can have a severe impact on the patients' quality of life. Often, follow-up procedures, treatments, and medication are required to alleviate the functional impairment and discomfort caused by these scars [9]. In contrast, some species of vertebrates (fish, amphibians, salamanders) are capable of skin regeneration. Why are some organisms capable of regeneration while others are not? Why is scarless regeneration in humans, with some notable exceptions, lost after early development? Both cell intrinsic and cell extrinsic factors are believed to play a role in the fibrosis vs. regeneration outcome, but the cellular and molecular mechanisms underlying fibrosis compared to regeneration remain poorly understood. Understanding the drivers of fibrotic scarring vs. regeneration will aid in developing approaches and therapies to induce skin wound regeneration in humans. These novel therapies would meet an important medical need. In this context the discovery of *Acomys* as an adult mammal capable of skin regeneration becomes significant.

Fibrotic wound repair is a (patho)physiological mechanism where an exacerbated healing response occurs and a fibrous tissue is formed. In contrast, regeneration involves complete structural and functional reconstruction of a tissue or organ after wounding and is traditionally understood as a specialized re-enactment of development [10, 11]. Research into the underlying molecular and cellular mechanisms of both fibrosis and regeneration in the skin have often focused on cell-intrinsic behavior and underlying genetic pathways or molecular players. In contrast, the role and contribution of the extracellular matrix (ECM) and its components during both fibrosis and regeneration is still poorly understood. Initially regarded as a somewhat inert structural scaffold, it is now accepted that the ECM is a major determinant of cell behavior in all tissues, mediated by its structure, composition and modifications. For example, increasing the stiffness of 3D collagen hydrogels by introducing intra- and interfibrillar crosslinks activated the expression of pro-fibrotic genes by adipocytes [12]. The ECM can regulate the capture and activity of growth factors, which in turn influences local cellular processes, as is seen in the maintenance of stem cell niches [13, 14]. It stands to reason that the ECM plays a role during skin

regeneration and that the "regenerative matrix" is a highly specialized environment unique to regenerative species. The ECM and all its associated (glyco)proteins are collectively known as the matrisome. The Matrisome Project has assembled lists of all ECM-related genes, divided into two groups; core matrisome genes, (composed of collagens, glycoproteins and proteoglycans), and matrisome associated genes, including regulators, secreted factors and ECM-affiliated proteins [15, 16]. In particular, proteoglycans are underrepresented in the Matrisome Project. Proteoglycans consist of a core protein with glycosaminoglycan (GAG) side chains, the latter of which convey important biological properties. Proteoglycans are an important component of the ECM, but the high variability of the GAG side chains makes it difficult to assess their involvement. Proteoglycans (and thus GAGs) may play a significant role during regeneration. The metabolism and regulation of proteoglycans, in particular the subset of genes pertaining to GAG metabolism, are a focus of this review.

While many publications have focused on comparing regeneration competent to regeneration incompetent animals, two exceptional models of regeneration provide unique opportunities to explore the phenomenon of scarless regeneration: the axolotl (*Ambystoma mexicanum*) and the African spiny mouse (*Acomys* sp.). We will refer to *Ambystoma mexicanum* simply as 'axolotl'. This is in line with other scientific reports and the *Ambystoma* genus also encompasses other salamanders that are not investigated here. On the other hand, we will address the African spiny mouse by its genus name '*Acomys*'. Various species of *Acomys* are investigated in this review and the genus name is most commonly in relevant scientific literature. *Acomys* is unique since it is a remarkable exception to the rule that adult mammals cannot regenerate their tissues, with individuals displaying remarkable wound healing responses throughout all life stages. Some mouse strains have acquired regenerative characteristics through selective breeding or genetic manipulation (MRL mouse, p21-/- mouse), but the natural regenerative potential of *Acomys* is far superior [17]. Every species of the Acomys genus examined so far has shown the ability to regenerate various tissues. The regenerative capacities of the axolotl are unparalleled, with individuals being able to regrow entire limbs. In contrast, frogs (*Xenopus* sp.) complete regeneration of amputated limbs with the formation of a cartilaginous spike [18]. Zebrafish, another well characterized model for regeneration, shows limitations to fin regeneration based on the amputation plane and adult zebrafish are unable to regenerate skin [19, 20]. These limitations prompted us to focus our comparison on axolotl and *Acomys*. In this review, we investigate the role of matrisome components during wound healing in two regeneration competent animals by analyzing existing datasets from previous publications. We aim to

compare the healing responses in terms of the ECM-related gene and protein profiles, with a focus on skin wound healing. We postulate that identification of matrisome-related targets involved in the regenerative process may lead to novel approaches in human wound healing, especially with regards to biomaterial development for skin wound healing. It is not our intention to compare or relate *Acomys* to humans. Instead, by comparing a regenerative competent amphibian (axolotl) and a regenerative competent mammal (*Acomys*) we may identify drivers of regeneration that transcend species. We will first briefly touch upon the process of regular wound healing ending in fibrosis and the process of regeneration via blastema as seen in some vertebrates.

Wound healing responses

The mammalian skin wound healing response, culminating in scar formation, can be divided into three distinct phases: inflammation, proliferation and remodeling [21] (Figure 1A). The inflammatory phase occurs directly after wounding and is characterized by blood clot formation (hemostasis) and the invasion of neutrophils and monocytes[22]. Macrophages play an important role by phagocytizing cell debris and bacteria, as well as secreting various growth factors and chemo-attractants. The proliferation phase, also known as the granulation tissue formation phase, encompasses both wound re-epithelialization and the formation of a dense network consisting of fibroblasts and neovasculature in a collagen and fibronectin rich matrix[23]. This is a temporary matrix that is often highly disorganized compared to the original tissue and prone to rupturing. During the remodeling stage, the granulation tissue is remodeled into a smooth textured scar: rich in type I collagen fibers and lacking secondary skin appendages, such as hair follicles and sebaceous glands [24].

Some species resolve complete limb amputation through blastema-mediated regeneration. A blastema, also known as a regeneration bud, is an autonomous structure composed of a heterogeneous mass of dedifferentiated stem/progenitor cells that goes through morphogenesis, thereby creating a multitude of cell types to replace the missing organ or limb [25, 26] (Figure 1B). The blastema is located under a layer of immature wound epithelium and it is created after the initial inflammatory response is resolved. Histolysis, re-innervation and ECM production will induce the migration and accumulation of cells under the wound epithelium that will differentiate into mesenchymal and ectodermal cell types [27]. A requirement for blastema formation is the molecular and cellular interaction between the wound epithelium, nerves, dermal cells and the ECM at the wound site [28]. In the final stage,

cells inside the blastema differentiate and eventually form the missing organ, tissue or appendage [27]. Blastema formation has been identified in different species, such as zebrafish [29], flatworms [30], urodeles [26] and even some mammals (*Acomys* full-thickness ear wounds [31] and mouse digit tip [5]). Intriguingly, under the right circumstances the fingertips of children up to 10 years of age heal similarly to the mouse digit tip [6].

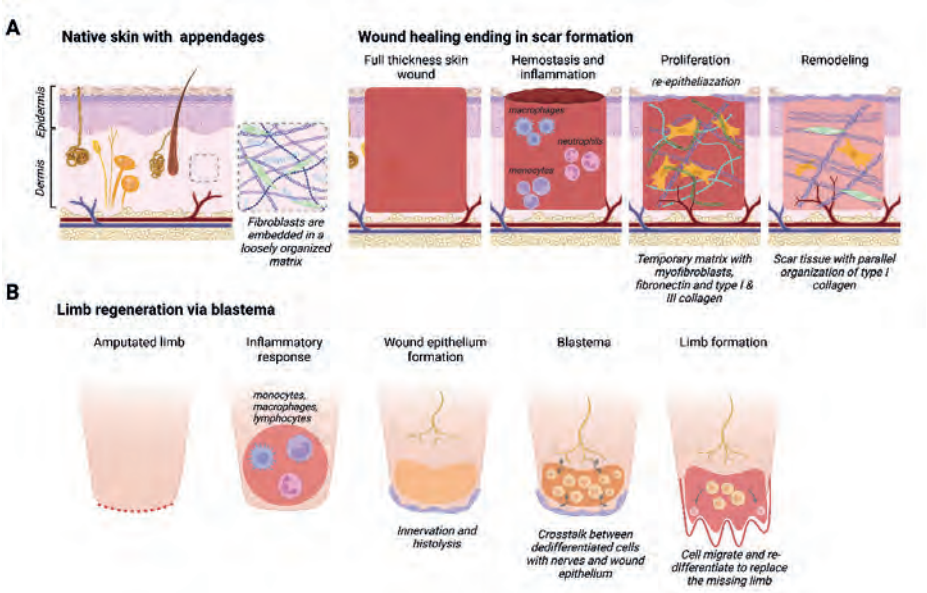

Figure 1. Wound healing responses. Schematic representations of A) native mammalian skin consisting of the epidermis and dermis with skin appendages and different phases of full-thickness skin wound healing ending in scar formation, and B) Phases in limb regeneration via a blastema in amphibians. Created with BioRender.com.

While the fibrotic response is the norm in most mammals, some exceptions exist as seen in the regeneration capacity of fetal wounds and digit tip regeneration in mice and children. Human skin wounds regenerate without scarring up to 24 weeks of gestation, thereafter the healing response will gravitate towards scar tissue formation [32]. Research in fetal sheep indicated that, aside from gestational age, wound size also affects the regenerative capacity; with wounds exceeding 4 mm in diameter demonstrating an increased tendency to scar [33]. A unique feature in fetal wounds is the 'cable' of actin filaments that develops around the wound edge. Wound closure through contraction of this actin ring has been compared to a drawstring closure [34-36]. Recently, it has been postulated that myofibroblast-mediated wound contraction in adult mammals inhibits regeneration and drives

scar formation [37]. In addition, a distinct immune response has been recorded in fetal wound regeneration that contributes to a non-inflammatory ECM environment [32, 38]. The composition of fetal ECM, with an abundance of type III collagen and hyaluronan, is important in this aspect [32]. Children up to ~10 years of age are even able to fully regenerate a digit tip, as long as the wound is distal to the upper interphalangeal joint with sufficient nail bed [39, 40] and little to no intervention [41, 42]. Storer *et al.* showed that the ECM determines the blastema state and plasticity of mesenchymal cells in non-regenerative fingertip amputations [43], suggesting the importance of focusing further on the role of the matrix in regeneration.

Acomys, African spiny mouse, a mammal capable of regeneration

Recently, the African spiny mouse (*Acomys*) has emerged as a remarkable exception to the rule that adult mammals are incapable of regeneration [44]. This rodent genus is found throughout Africa and the Middle East. Belonging to the subfamily Deomyinae, they are part of the Muroidea family and share a common ancestor with the Muridae, diverging about 23 million years ago [45]. The genus comprises over 20 different species, but most studies have focused on *A. cahirinus*.

Following up anecdotal reports of 'skin jumping' in *Acomys*, Seifert and colleagues reported *A. kempi* and *A. percivali* [46] exhibited remarkable wound healing properties after extensive skin damage caused by mild handling of wild-caught animals. Following this initial report several groups have found that depending on type of organ and injury, *Acomys* shows remarkable responses to injury: extensive regeneration has been observed in skin, ear, muscle, digit tip and spinal cord [47] (Figure 2). Acute ischemia wound models of heart and kidney do not seem to regenerate but show resistance to wounding and diminished fibrosis [48]. In contrast, *Mus musculus* shows extensive fibrotic scarring to similar injuries. Evolutionarily separated by only 23 million years, *Acomys* and *Mus* provide a powerful comparative framework to identify the cellular and molecular differences between regeneration and fibrotic scarring.

In all regenerative systems, the immune system is thought to play an important role through its ability to modulate inflammation, as severe inflammation can be detrimental to the healing process. Several groups have extensively described the immune response observed in *Acomys* [48-52]. In general, *Acomys* wounds demonstrated a distinct role for macrophage activity when compared to *Mus* [50].

Mature macrophages (F4/80+) were absent in *Acomys* full-thickness skin wound beds, along with a distinct lack of pro-inflammatory cytokines [51]. In *Acomys* ear wounds, CD86+ macrophages (classically activated M1) were absent from the blastema, being confined to the wound edges in the connective tissue distal to cartilage. CD206+ macrophages (M2, pro-regenerative) were restricted to the region beneath the wound epidermis and practically absent from the rest of the blastema [48]. On the other hand, in *Mus*, both M1 and M2 macrophages are present throughout all connective tissues of the injured area [53]. Interestingly, the depletion of macrophages through clodronate liposome injections severely delayed ear hole closure in *Acomys* [50]. The neutrophil response in *Acomys* is delayed compared to *Mus* and differences were found in the number of neutrophils in various compartments, such as blood and bone marrow, when comparing several species of *Acomys* to *Mus* [52].

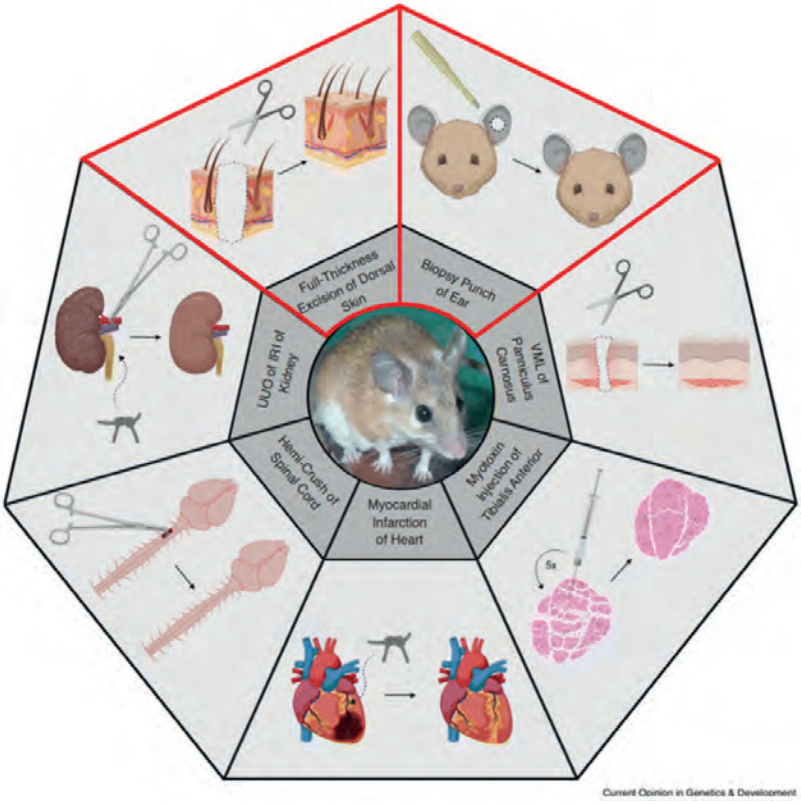

Figure 2. Overview of tissues/organs with a remarkable healing response in *Acomys*. This review aims to elucidate the involvement of the matrisome during regeneration of the skin and ear (lined in red). VML = volumetric tissue loss, UUO = unilateral obstruction, IRI = ischemia reperfusion injury. Reproduced from Sandoval & Maden (2020) [48] with permission from Elsevier, 2020, under the STM permissions guidelines.

A second factor of particular significance for skin regeneration is the skin biology of *Acomys*. *Acomys* dorsal skin is weak and tears easily when subjected to a mean tensile strength of 0.11 MPa, a force approximately 20 times weaker than that required to tear skin of *Mus* [46]. Using atomic force microscopy to measure spatial tissue stiffness, intact *Acomys* skin did not exceed 15 kPa and wound centers measured no more than 5 kPa. Putting these findings into context, skin of C57Bl/6 mice measures 28 kPa, with wound beds of 10.5 kPa, further demonstrating the unique biomechanical properties of *Acomys* skin [54]. Following fast re-epithelialization after skin injury, *Acomys* granulation matrix was loosely organized with less collagenous deposition and increased gene expression of the matrix metalloproteinases *Mmp2* and *Mmp9* compared to *Mus* [51, 55]. Overall, *Acomys* showed a distinct profile for protein remodeling and protein synthesis [56, 57]. Upon completion of regeneration, *Acomys* skin developed hair follicles, sebaceous glands and an intact panniculus carnosus [46, 51]. After wounding, enriched proteins belonged to pathways related to tight junction formation, endocytosis, ribosomes, proteasomes, Wnt signaling, MAPK signaling and vasopressin-regulated water reabsorption. Components of the ubiquitin-proteasome degradation pathway were strongly upregulated in *Acomys* and proteins in the ribosome related pathways were also implicated [56, 57]. Overall, enhanced protein turnover seems an important characteristic of skin wound healing in Acomys. The unique characteristics of *Acomys'* skin may benefit wound healing, but the fact that *Acomys* is capable of regenerating other organs indicates that its skin biology may not be the only factor contributing to its regenerative potential.

Full-thickness skin wounds in *Acomys* regenerate without the presence of a blastema whereas ear punch wound closure in *Acomys* has been reported to occur through the formation of a blastema [27, 31, 46]. Research using an ear hole punch model in *A. cahirinus* was reported by Matias Santos and colleagues [58], in response to the initial ear punch study [46]. In these studies, reports on muscle regeneration were inconsistent, with the original study (Seifert 2012) mentioning the absence of muscle fibers in contrast to the study of Matias Santos (2016), who reported presence of muscle fibers within the regenerating region. Additionally, all regular skin appendages, such as hair follicles and sebaceous glands, had regenerated and nerve fibers were present [58]. Gawriluk and colleagues demonstrated that the wound matrix of *A. cahirinus* exhibits several hallmarks of blastema-mediated regeneration [31]. The *Acomys* ear wound beds showed several signs of the blastema-like wound epidermis, such as restriction of proliferating cells to the wound borders, lack of basal-apical polarity in basal keratinocytes and presence of keratin 17 in the wound matrix. Evidence of reinnervation, an essential process in epimorphic regeneration, was obtained as enrichment of genes involved in axon guidance, neuroactivity and

growth was observed. Re-entry of mesenchymal cells into the cell cycle, another defining characteristic of the blastema, was also observed. Taken together these observations provide strong evidence for the formation of blastema in *Acomys* ear punch wounds and cements the importance of *Acomys* as a model system capable of tissue regeneration. In this review, we compare its wound healing responses to those of the axolotl, an animal well known for its regenerative abilities.

Axolotl, salamanders capable of full organ regeneration

The axolotl (*Ambystoma mexicanum*) is a paedomorphic (or 'neotenic') salamander belonging to the Urodele order of the *Amphibia*. The axolotl grows through a process of juvenilization, meaning it delays somatic development and retains physiologically juvenile features during its development to sexual maturity [59]. Therefore, the axolotl is an animal that reaches sexual maturity without going through metamorphosis. Metamorphosis occurs only when they are in contact with an external and artificial stimulus, which is uncommon in the wild [60]. The axolotl represents an important model organism in the field of regenerative medicine due to its highly efficient regeneration capacity. Regeneration has been observed in limbs and several organs such as the skin, heart, brain, lungs, and eyes [61, 62] (Figure 3).

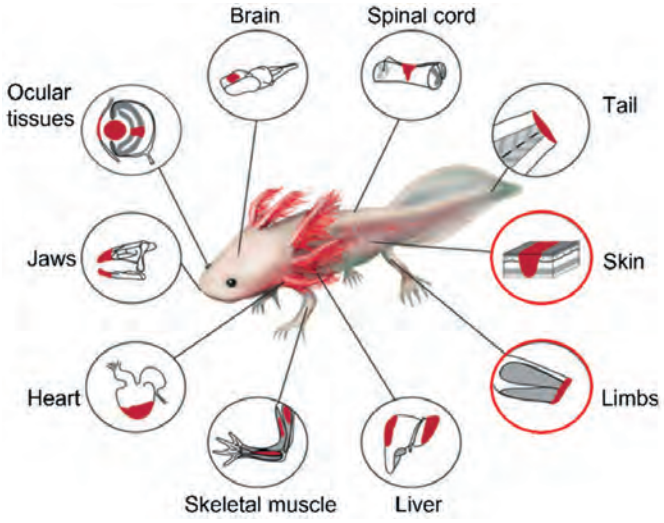

Figure 3. Summary of tissues/organs that can be regenerated by axolotls (*Ambystoma mexicanum*). The regeneration of skin and limbs, outlined in red, and the involvement of matrisome components is further explored in this review. Reproduced from ref. Debuque & Godwin [62] with permission from Springer International Publishing Switzerland, 2016, under the STM permissions guidelines.

Limb regeneration has been extensively investigated in axolotl. Following limb amputation, wound closure continues to blastema formation and limb development [26]. Wound closure takes several hours, and full regeneration of the limb typically occurs between 40 and 50 days [63]. The formation of a blastema is essential to the regeneration of a limb. Research using the Accessory Limb Model has uncovered three requirements for successful blastema-mediated limb regeneration: the presence of a wound epithelium, the occurrence of nerve signaling and the availability of positional cues provided by pattern forming cells [64]. Absence of any of these factors abrogates limb regeneration [65]. Formation of a closed wound epithelium involves migrating keratinocytes that cover the wound surface [26]. Under the influence of signals emanating from local nerve fibers, proliferation of this wound epithelium into a multilayered epithelium result in the apical epithelial cap [66]. This epithelial cap is characterized by specific molecular markers and by an immature basement membrane beneath the epidermis [67]. Nerve signaling causes basal epithelial cells to exit the cell cycle. This step is essential for the development of the blastema as cells of the apical epithelial cap will start secreting growth factors and enzymes that degrade ECM and facilitate migration[28]. Next, fibroblasts originating from the limb circumference gather underneath the apical epithelial cap. The interaction between these cells with different positional identities is crucial for maintaining the blastema and ensuring regeneration as the 'positional memory' dictates the pattern of the missing limb [26].

Transcriptomic analysis has revealed the importance of the immune system in axolotl wound healing and regeneration. There is a gradual increase of macrophages and fibroblast-like cells post amputation, whereas neutrophil populations decreased after wounding [68]. Neutrophils evoke anti-inflammatory macrophages, which leads to a reduction in pro-inflammatory cytokines [69]. Macrophages with anti-inflammatory and pro-resolving phenotypes were dominant in the first seven days of axolotl limb regeneration, thereby contributing to repressing the inflammatory response [70]. When macrophages were systemically depleted, limb regeneration failed. A fibrotic ECM was observed with increased type I collagen deposition and the presence of αSMA-positive cells [71] that could also inhibit apical epithelial cap formation and blastema-induction [72]. ECM remodeling is of key importance to rapidly reconstruct the matrix [70] and the ECM contains positional information required for limb pattern formation through location-specific differences in heparan sulfate sulfation. This was shown by grafting decellularized axolotl skin or decellularized mouse skin onto axolotl limb wounds [73]. Depending on the developmental stage, positional origin and heparan sulfate sulfation pattern of the graft, limb patterning was either supported or inhibited. These results

demonstrated that the ECM contains information, conveyed via heparan sulfate sulfation patterns, that can influence limb regeneration and this information is also present in the ECM of mice [73].

Axolotl skin, which regenerates without blastema formation, provides a platform to uncover drivers of regeneration in the absence of blastema. The skin of juvenile axolotls consists of a pseudostratified epithelium which contains epithelial and Leydig cells, and the dermis presents a loosely organized network of thin collagen fibrils in which fibroblasts and mucus glands are embedded [74]. A layer of compressed collagen fibers separates the hypodermis from the underlying muscle layer. Scarless skin wound healing has been reported in adult axolotls after making excisional wounds on the flanks. Wounds did not form scabs, instead epithelization was completed within 24 h and full skin healing including all skin appendages was completed within 80 days [67]. Overall, the regenerating tissue in axolotl was characterized by high levels of matrix remodeling enzymes, relatively low abundance of fibronectin and persistently high levels of tenascin C throughout the wound bed. Type III collagen deposition was followed by type I collagen deposition and maturation from day 14 onwards. Following a full-thickness wound, the collagen architecture in the dermis did not return to the normal lattice-like pattern, but was disorganized, even though the healed skin appeared identical to unwounded skin. However, after blastema-mediated skin regeneration following limb amputation, the dermis, including collagen architecture, does fully regenerate [75].

The healing capacity of the axolotl is unique and while directly translating regeneration in salamanders to mammals is difficult, some clues may be found in the regenerative response of axolotls. Axolotls display a minor inflammatory response with macrophages of a mostly anti-inflammatory phenotype. The fibrotic response is notably absent, ECM deposition is regulated, and matrix remodeling enzymes are prevalent (Figure 4A). These hallmarks are also observed in *Acomys* regeneration, suggesting regeneration shares similar mechanisms across both models. However, there are differences in intensity and duration of the different events in regenerative and non-regenerative mammals, indicating the importance of timing of the various phases (Figure 4B). The various wound healing responses described for the animals are summarized in Table 1 (full thickness skin wound healing) and Table 2 (blastema-mediated regeneration).

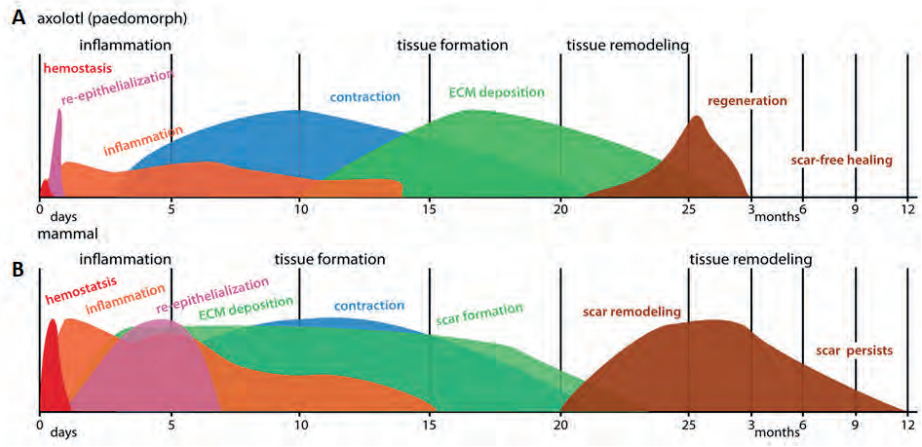

Figure 4. Schematic representation of the wound healing response in A) paedomorphic axolotls and B) mammals. Axolotl wound healing shows minimal hemostasis and very rapid re-epithelization followed by low levels of inflammation. ECM deposition occurs after wound contraction and tissue remodeling does not lead to a scar, but results in normal skin appearance. Contrary to that, in mammals, a strong inflammatory response is maintained even after re-epithelization is complete. Deposition of new ECM and wound contraction occur at the same time and scar tissue persists after completion of the months-long remodeling phase. Reproduced from Seifert *et al.* (2012) [67] with permission from © 2012 Seifert et al., under the Creative Commons Attribution License.

Table 1. Summary of processes observed during full-thickness skin wound healing.

Full-thickness skin wound healing	***Mus musculus* (mammal)**	***Acomys* sp. (mammal)**	**Axolotl (amphibian)**
Re-epithelialization	Slow (5-7 days) with a scab	Fast (3 days) with a scab	Fast (1 day) without a scab
Inflammation	High	Low	Low
	Fast neutrophil response	Delayed neutrophil response	Low neutrophil response
	High expression of M1 macrophages Pro-inflammatory cytokines ++	High expression of M2 macrophages Pro-inflammatory cytokines --	High expression of pro-resolving macrophages Pro-inflammatory cytokines --
Proliferation	Early matrix deposition	Delayed matrix deposition	Delayed matrix deposition
	Dense granulation matrix	Loose granulation matrix	Loose granulation tissue
	Collagen deposition +	Collagen depostion -	Matrix degradation +
Remodeling	Scar remodeling	Scar-free remodeling	Scar-free remodeling
	Type I collagen with parallel orientation No regeneration of skin appendages	Type I collagen with basket weave orientation Regeneration of hair follicles and sebaceous glands	Type I collagen did not return to normal lattice organization Regeneration of mucous glands

Table 2. Summary of processes observed during blastema-mediated regeneration.

Blastema-mediated regeneration	***Acomys* sp. (mammal)**	**Axolotl (amphibian)**
	Regeneration after ear punch via blastema-like process	Limb regeneration via blastema
Wound epithelium	Loss of basal-apical polarity in keratinocytes	Migrating keratinocytes close the wound
	Presence of keratin 17 (blastema marker)	Multi-layered epithelium forms (apical epithelial cap)
	Recruitment of mesenchymal stem cells	Immature basement membrane
Innervation	Upregulation of genes associated with axon guidance, neuron growth and neuroactivity	Apical epithelial cap (AEC) is innervated
	Cell proliferation is restricted to wound borders	Cells exit cell cycle
Blastema formation	Cell cycle re-entry, cell proliferation and cell division	Pro-migratory environment is formed (ECM degradation, growth factor secretion)
	Increase of matrix degradation enzymes	Fibroblasts with various positional identities migrate to the AEC
	Cartilage pattern re-established the ear	Limb pattern is established by ECM and cells
Differentiation	Regeneration of missing tissues	Cells redifferentiate to form missing limb

Identification of matrisome-related genes and proteins during regeneration using existing datasets

Comparing the matrisome and GAG-related components present during regeneration in *Acomys* and axolotl will aid in uncovering similarities between these two animals. Through this approach, we aim to identify shared pro-regenerative factors between species, which may be translated to other species (i.e. humans).

Selection of datasets

To select the databases that will be analyzed, papers that document regenerative wound healing in *Acomys* or axolotl were retrieved, with a focus on skin and blastema. Publications with either a proteomics or transcriptomics approach were extracted. For *Acomys* publications on both skin regeneration and ear hole closure were included in the search. A total of four papers were identified, of which three focused on the regeneration of full-thickness skin wounds [55, 57, 76] and one publication described ear hole closure [31]. The datasets of Brant *et al*. (2015) [55] and Brant *et al*. (2019) [76] were compared for overlap, as these publications investigate similar samples with different techniques. All genes identified by the 2015 publication were present in the 2019 publication. As the 2019 publication offered more data only this set was included for the comparison. Details of the selected papers are presented in Table 3.

Several papers focusing on axolotl were reviewed such as Monaghan *et al*. (2009) [77] and Wu *et al.* (2013) [78]. The limited availability of public transcriptomic datasets of *Acomys* led us to select publications on axolotl that best matched the timepoints and tissues analyzed in the selected *Acomys* publications. Proteomic and transcriptomic studies of the axolotl were selected based on their description of the regenerating limb blastema and/or non-blastema mediated skin regeneration, which resulted in the selection of three papers (Table 3). The paper by Monaghan *et al.* (2012) [79] describes both limb regeneration (via blastema) and regeneration of a full-thickness skin wound. Both Rao *et al.* (2009) [63] and Stewart *et al*. (2013) [80] exclusively describe hind-limb regeneration via blastema at the proteomic and transcriptomic level, respectively.

Table 3. Selected publications focusing on regeneration in *Acomys* and axolotl.

Publication	Title	Tissue	Timepoints	Technique	Dataset
Brant *et al* . 2019 (*Acomys)*	Comparative transcriptome analysis of dermal wound healing reveals *de novo* skeletal muscle regeneration in *Acomys cahirinus*	Dorsal skin, 8 mm skin punch	Day 0, 7, 14	*De novo* transcriptome assembly and comparative transcriptomics	Supplementary files: S7 data and S8 data
Gawriluk *et al* . 2016 (*Acomys*)	Comparative analysis of ear-hole closure identifies epimorphic regeneration as a discrete trait in mammals	Ear punch, 4 mm	Day 0, 5, 10, 15, 20	*De novo* transcriptome assembly and comparative transcriptomics	Supplementary file: dataset 1
Yoon *et al* . 2020 (*Acomys*)	Comparative proteomic analysis in scar-free skin regeneration in *Acomys cahirinus* and scarring *Mus musculus*	Dorsal skin, 8 mm skin punch	Day 0, 7, 14	Shotgun proteomics using LC-MS/MS	Table 1 of the publication
Monaghan *et al* . 2012 (axolotl)	Gene expression patterns specific to the regenerating limb of the Mexican axolotl	Flank skin outside of limb range, 4 mm skin punch	Day 0, 1, 3, 7	Microarray by Affymetrix GeneChips	Supplementary data in NCBI: GSE37198_RAW.tar
Stewart *et al* . 2013 (axolotl)	Comparative RNA-seq analysis in the unsequenced axolotl: The oncogene burst highlights early gene expression in the blastema	Right forelimbs at the mid-stylopod level	Hour 0, 3, 6, 12 and day 1, 3, 5, 7, 10, 14, 21, 28	*De novo* assembly of axolotl transcript, RNA-seq	Supplementary data in NCBI: GSE34394_RAW.tar
Rao *et al* . 2009 (axolotl)	Proteomic analysis of blastema formation in regenerating axolotl limbs	Bilateral hind limbs regenerating tissue and 1 mm of stump tissue	Day 0, 1, 4, 7	Proteomics by LC-MS/MS	Supplementary files: table 2

Identification of the matrisome and GAG-related components

We next addressed the differences in gene annotations of the selected datasets. The publications focusing on *Acomys* used mouse gene symbols to annotate data, whereas the axolotl datasets were annotated using human gene symbols. Detailed lists of matrisome related genes of various species are available through the Matrisome Project [15]. The mouse and human matrisome master lists contain 1110 and 1027 genes, respectively. As human-mouse orthologs are comparable the more extensive mouse matrisome was used for the selection of matrisome genes from all datasets.

The genes of the matrisome are divided into core matrisome genes and matrisome-associated genes [15]. The former is further subdivided into ECM glycoproteins,

collagens and proteoglycans while the latter is subdivided into ECM-affiliated proteins, ECM regulators and secreted factors (Figure 5, full gene list is available in Table S1). Closely associated with the matrisome, but not fully included in the matrisome lists, are glycosaminoglycans (GAGs). These polysaccharides are generally present in the ECM and mostly attached to a core protein, together known as proteoglycans [81]. Although the specialized role of GAGs in a multitude of biological processes is widely acknowledged, they are technically difficult to assess and are consequently often disregarded. After biosynthesis of the repeated disaccharide units, GAGs are extensively modified by enzymes that epimerize certain saccharides, remove acetyl groups and add sulfate groups at specific locations on the building blocks, resulting in highly heterogenous molecules. Methods such as a colorimetric staining or ELISA allow for the basic quantification of GAGs in various sample types [82]. Methods that assess GAGs on the disaccharide level, e.g. RP-HPLC, are suited for identifying the various disaccharides but lose positional information in the chain. Raman spectroscopy may struggle to separate the signals of complex samples [83]. Mass spectrometry has made significant progress with novel ionisation techniques, but is not yet a standard method for GAG analysis [84]. Given the importance of GAGs in many biological processes, we performed an additional investigation into the presence of GAG related enzymes during the regenerative processes in axolotl and *Acomys*. Currently there are no methods available to directly assess GAG biosynthesis and modification. Instead, the expression of genes involved in GAG biosynthesis provides information on the regulation of GAGs during biological processes. A paper published in 2018 by Uijtdewilligen *et al.* provides a curated list of genes involved in proteoglycan/glycosaminoglycan metabolism [85], dividing GAG-related genes into various categories based on their role in GAG homeostasis. The following four categories were selected for use in our comparison analysis: linkage region formation (8 genes), GAG chain polymerization (13 genes), GAG chain modification (32 genes), and GAG chain degradation (19 genes) (the complete gene list is available in Table S2). Several of these genes were also present in the greater matrisome list as part of the ECM regulators. These were GAG chain modificators *sulfatase 1* and *sulfatase 2*, *heparanase* and *hyaluronidase 1, 2* and *3*. The matrisome and GAG-related genes were extracted from each dataset. Any adaptions made to a dataset prior to gene extraction are covered in the results section for each publication. The next section focuses on the datasets that were compared.

Comparison of the matrisome and GAG components

The same biological processes (full-thickness skin wound regeneration or blastema-mediated regeneration) in *Acomys* and axolotl were compared at the transcriptome level. On the proteomic level this comparison could not be made due to absence

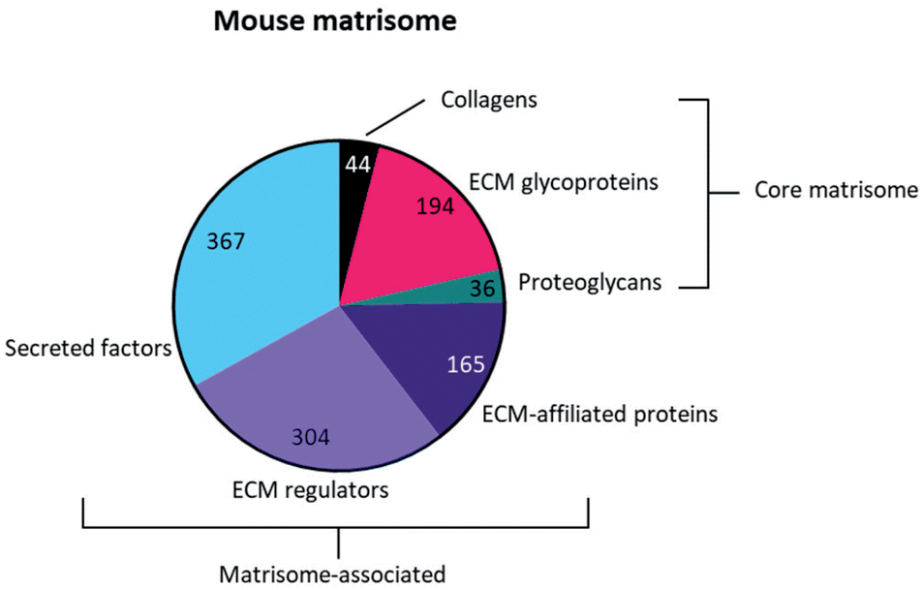

Figure 5. Schematic representation of the subdivision of genes in the mouse matrisome.

of proteomics studies on blastema-mediated regeneration in *Acomys* and skin regeneration in axolotl. Although the processes are different, we propose that comparing skin regeneration and blastema on the proteomic level could still yield beneficial information. Thus, the matrisome and GAG-related genes of the following datasets were compared:

- Transcriptomics of full-thickness skin wound regeneration in *Acomys* (Brant *et al*. 2019) versus in axolotl (Monaghan *et al*. 2012)
- Transcriptomics of the (mammalian) blastema in *Acomys* (Gawriluk *et al*. 2016) versus the (amphibian) blastema in axolotl (Stewart *et al*. 2013)
- Proteomics data of *Acomys* full-thickness skin wound healing (Yoon *et al*. 2020) versus proteomics data of axolotl blastema-mediated limb regeneration (Rao *et al*. 2009)

Results of the matrisome-GAG component analysis

In the following sections we describe the results of the matrisome and GAG gene comparisons. Each comparison is divided into three sections. Section 1 describes the preparation of the datasets in order to perform the comparison, section 2

highlights the matrisome components identified in the comparisons and section 3 focuses on the GAG-related components.

Comparison of the transcriptome profiles of regenerating full-thickness skin wounds on day 7 in Acomys (Brant et al. 2019) versus axolotl (Monaghan et al. 2012)

Preparation and matching of datasets

The work of Brant et al. (2019) [76] involved the transcriptomic profiling of full-thickness skin wounds with 8 mm diameter in *A. cahirinus*. Regenerating wounds at day 7 and 14 were compared to unwounded skin tissue (day 0). As the *Acomys* genome was unavailable at the time, these authors assembled a *de novo* transcriptome for *Acomys* which allowed the identification of differentially expressed genes expressed as fold changes compared to unwounded tissue with a p-value < 0.05. The data presented by the authors of Brant et al. (2019) [76] did not require any alterations and was ready for use. Monaghan et al. (2012) [79] studied the gene expression in full-thickness skin wounds of 4 mm diameter on axolotl flanks using *A. mexicanum* Affymetrix GeneChips (full microarray data can be found at the Gene Expression Omnibus (GSE37198)). Tissue was collected on day 0 (unwounded) and at days 1, 3 and 7 after wounding. The authors made a total of 16 comparisons. To identify differentially expressed genes on day 7, we ran our own expression analysis using the raw microarray data. Fold changes on day 7 (respective to unwounded tissue) were calculated using the software package Transcriptome Analysis Console (TAC 4). Significance was determined using Fisher's exact test for 2x2 contingency tables and genes with a p-value < 0.05 were identified (Table S3).

The only matching timepoint in both publications was day 7 after skin injury. Descriptive studies on skin wound healing in *Acomys* and axolotl reported complete re-epithelialization within the first 3-5 days in both species[46, 79]. Moreover, after wounding both animals exhibited a limited and low inflammatory response. After day 7 both animals start wound contraction, ECM deposition and new tissue formation [67, 86] . Therefore, *Acomys* and axolotl should be in a similar regeneration stage on day 7 after wounding and a comparison at this time point may highlight the matrisome and GAG genes involved during early regeneration. Thus, only the datasets of day 7 in *Acomys* and axolotl were compared. First, differentially expressed matrisome and GAG-related genes were identified in *Acomys* (Table S4) and axolotl (Table S5). Finally, the differentially expressed matrisome and GAG-related genes that were present in both *Acomys* and axolotl were identified (Table S6).

Expression of matrisome genes on day 7 of skin wound regeneration in Acomys vs. axolotl

The results of the matrisome matching process are visualized in Figure 5. In *Acomys* 3921 genes were differentially expressed 7 days after skin wounding, of which 535 genes (13.6%) belonged to the matrisome. In axolotl 861 genes were differentially expressed on day 7 and 133 of these genes (15.5%) belonged to the matrisome. A total of 99 differentially expressed matrisome genes were identified between *Acomys* and axolotl.

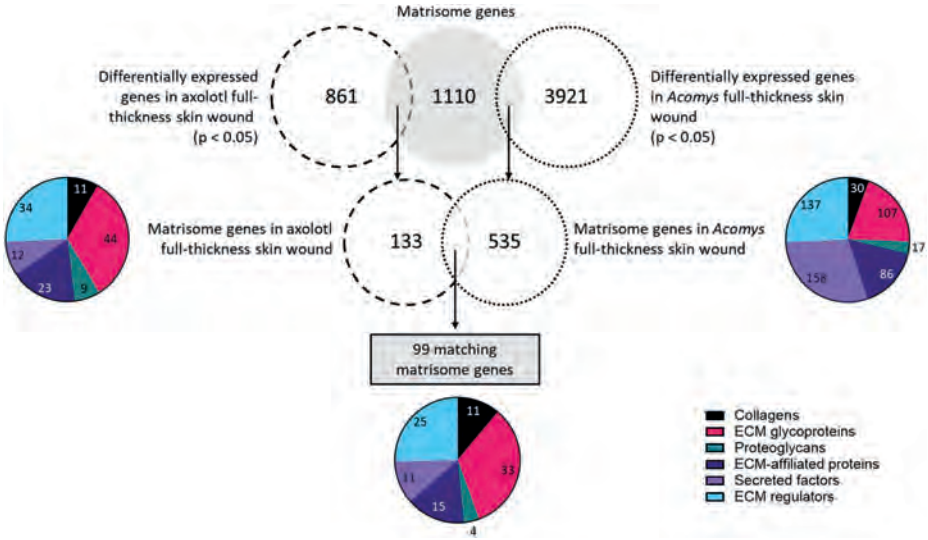

Figure 6. Schematic representation of the identification of matrisome genes in full-thickness skin wounds. In axolotl 861 genes were differentially expressed as demonstrated by significant fold change ($p < 0.05$) on day 7 compared to day 0 (determined by our own analysis). Within this dataset 133 matrisome genes were identified. In Acomys, 3921 genes were differentially expressed on day 7 compared to day 0 ($p < 0.05$) and a total of 535 matrisome genes could be identified in this list. After comparing the matrisome genes of axolotl and Acomys, 99 matching matrisome genes were identified, representing all six matrisome categories.

A comparison of the **collagens** expressed in the two species revealed 11 matching genes. Among the top upregulated genes in axolotl were *Col11a1, Col7a1, Col28a1, Col4a5 and Col12a1*. In *Acomys*, the highest fold changes belonged to *Col12a1, Col24a1*, *Col5a2*, *Col5a1* and *Col7a1*. All genes were upregulated in axolotl but in *Acomys* four genes were downregulated: *Col4a5, Col4a6, Col17a1,* and *Col28a1*. Amongst the **glycoproteins** a total of 33 matches were found. The most upregulated genes in both species were tenascin C (*Tnc*), fibronectin (*Fn1*), laminin alpha 1 (*Lama1*), thrombospondin 1 and 2 (*Thbs1, Thbs2*), peroxidasin homolog (*Pxdn*) and collagen triple helix repeat containing 1 (*Cthrc1*). The genes with the most negative

fold changes were adiponectin C1q collagen domain containing (*Adipoq*), spondin 2 (*Spon2*) and multimerin 1 (*Mmrn1*). Only four **proteoglycans** were present in both datasets, of which three were upregulated in both species: proteoglycan 4 (*Prg4*), serglycin (*Srgn*) and decorin (*Dcn*). Osteoglycin (*Ogn*) was downregulated in both axolotl and *Acomys*. Fifteen genes matched in the compartment of **ECM affiliated proteins**. Several of these genes were upregulated in both species, with the highest fold changes found in: C1q tumor necrosis factor related protein 1 (*C1qtnf1*), lectin galactose binding soluble 9 (*Lgals9*), syndecan 2 (*Sdc2*), complement component 1 q subcomponent B (*C1qb*), and C chain (*C1qc*). Only *C1qtnf2* was downregulated in both species. Notably, *Lgals8* and *Lgals2* were greatly downregulated in axolotl whereas their expression was barely affected in *Acomys*. Eleven **secreted factors** were identified in both datasets. Several genes were upregulated in both species, with the largest fold changes belonging to secreted frizzled-related protein 4 (*Sfrp4*), *Srfp2*, follistatin-like 1 (*Fstl1*) and angiopoietin-like 2 (*Angptl2*). Two genes were downregulated in both animals: chordin-like 1 (Chrdl1) and fibroblast growth factor 12 (*Fgf12*). A few notable differences in expression levels were present, the most notable being interleukin 1 beta (*Il6*) which was the most upregulated gene in *Acomys* but showed a downregulation in axolotl. Among the **ECM regulators** 25 matches were found. The top upregulated genes in both species were matrix metallopeptidase 2 (*Mmp2*), *Mmp3*, *Mmp13*, procollagen lysine 2-oxoglutarate 5-dioxygenase 2 (*Plod2*), proprotein convertase subtilisin/kexin type 5 (*Pcsk5*), tissue inhibitor of metalloproteinase 1 (*Timp1*), peptidase domain containing associated with muscle regeneration 1 (*Pamr1*) and lysyl oxidase-like 2 (*Loxl2*). Only one out of 25 genes was downregulated in axolotl: cathepsin S (*Ctss*). In *Acomys*, three out of 25 matching genes were downregulated: *Mmp28*, tolloid-like 1 (*Tll1*) and Kazal-type serine peptidase inhibitor domain 1 (*Kazald1*). Interestingly, *Kazald1* was the most upregulated gene in axolotl, but the most downregulated gene in *Acomys*.

In summary, of the 99 matrisome genes that were present in both species 77 genes (77%) had a similar expression pattern, where a gene was either upregulated (69 genes/70%) or downregulated (8 genes/8.1%) in both *Acomys* and axolotl. Twenty-two genes (22%) showed opposing expression patterns where a gene would be upregulated in one species but downregulated in the other species.

Description of GAG-related gene expression on day 7 of skin wound regeneration in axolotl vs. Acomys

Of all the differentially expressed genes in the axolotl dataset, only three GAG-related genes could be identified: these genes were all related to GAG chain modification. Conversely, all GAG gene categories were represented among

the differentially expressed genes in the *Acomys* data, of which 30 genes were upregulated and five were downregulated.

In *Acomys*, two genes involved with **linkage region preparation** were present: beta-1,4-galactosyltransferase 7 (*B4galt7)* and *B4galt2*, both were upregulated. Eleven genes related to **GAG chain polymerization** were found in *Acomys*, with the highest fold changes seen in hyaluronan synthase 1 (*Has1*), *Has2* and *Has3*. Only two genes were downregulated: exostoses (multiple)-like 1 (*Extl1*) and *Extl3*. In axolotl, three genes relating to **GAG chain modification** were found, these were all upregulated: carbohydrate sulfotransferase 2 (*Chst2*), *Chst11* and sulfatase 1 (*Sulf1*). In *Acomys* a total of 11 genes matched in this compartment, among which were the three genes identified in axolotl. Together with *Sulf2* these were amongst the most upregulated genes in *Acomys*. Only three genes were downregulated: sulfatase modifying factor 1 and 2 (*Sumf1*, *Sumf2)* and carbohydrate sulfotransferase 15 (*Chst15*). Finally, 11 genes involved with **GAG chain degradation** were present in *Acomys*. The most highly upregulated genes were glucuronidase beta (*Gusb*), hexosaminidase A (*Hexa*), arylsulfatase B and J (*Arsb, Arsj*). No genes were downregulated.

Comparison of the transcriptome profiles during blastemal regeneration in Acomys ear pinnae closure (Gawriluk et al. 2016) vs. axolotl stylopod amputation (Stewart et al. 2013)

Preparation and matching of the datasets

A transcriptomic study on blastema-mediated ear pinna regeneration in *Acomys* was performed by Gawriluk *et al*. (2016) [31]. Full-thickness ear wounds of 4 mm diameter at days 5, 10, 15 and 20 were compared to unwounded ear tissue and analyzed by RNAseq using a *de novo* transcriptome assembly. EBseq was used to determine differentially expressed genes (false discovery rate < 0.05). Differentially expressed genes that matched with the matrisome and GAG-related genes were extracted and are presented in supplementary Table S7. In the study of Stewart *et al.* (2013) [80] the researchers amputated forelimbs of axolotls; tissue from the amputation site was collected at 0 (healthy tissue control), 3, 6, and 12 hours and 1, 3, 5, 7, 10, 14, 21 and 28 days. Samples were subjected to RNAseq transcriptome analysis and data was generated as gene abundance using transcripts per million (TPM). Using the raw data containing TPM, we identified matches to the matrisome and GAG-related genes, then calculated a fold change for day 5, 10 and 14 ([TPM day X] / [TPM day 0]). Values of 0 < fold change > 1 were further converted to a negative number: -1/ fold change. As the original paper pooled three biological samples for analysis to

generate only one transcriptome per time point, it was not possible to test the acquired fold changes for statistical significance. Instead, we applied a threshold of at least 2-fold up or down regulation, thus excluding -2 < fold change > 2 from the dataset (full data available in Table S8). To be included in our selection, a gene was required to pass the threshold for at least one time point.

In this comparison we focused only on the blastema stage. In axolotl this stage lasts approximately from day 3-4 up to day 21 [71]. A similar timeframe is described by Gawriluk *et al*. (2016) [31] when investigating *Acomys* ear blastema. For this reason, we compare days 5, 10 and 14 in axolotl to days 5, 10 and 15 in *Acomys*. Later time points were excluded as they are not in the blastema stage in axolotl. The full dataset containing all matching matrisome and GAG-related genes of both species genes is available in the supplemental data (Table S9).

Description of matrisome related genes in ear pinna blastema in Acomys vs. forelimb blastema of axolotl

The results of the matching process are visualized in Figure 7. There were 14735 differentially expressed genes identified in *Acomys* ear pinna of which 638 genes (4.3%) were part of the matrisome. In axolotl, a total of 11928 genes were expressed in the regenerating limb. Following matching to the matrisome and application of the fold change threshold, 324 genes (2.7%) were extracted. Between *Acomys* and axolotl 278 matching matrisome genes were found.

Twenty-one genes that code for **collagen** proteins were present in both species during various points in the blastema formation. Of note, only three genes were upregulated in both models at all time points: *Col18a1*, *Col6a2* and *Col3a1*. One gene was downregulated on all time points: *Col22a1*. The remaining collagen genes showed opposite expression patterns in each species. For example, *Col4a6* was upregulated at all timepoints in axolotl but downregulated at all time points in *Acomys;* the reverse pattern was observed for *Col4a1*. In total 77 **glycoproteins** were identified in both species. Of the 17 genes that were upregulated in both species at all time points the top-upregulated genes were: collagen triple helix repeat containing 1 *(Cthrc1)*, laminin alpha 1 (*Lama1*), tenascin C (*Tnc*), transforming growth factor beta induced (*Tgfbi*), thrombospondin 2 (*Thbs2*), peroxidasin homolog (*Pxdn*), fibronectin 1 (*Fn1*), and elastin microfibril interfacer 1 (*Emilin1*). A total of 10 genes were downregulated in both axolotl and *Acomys*, with the lowest fold changes seen in: adiponectin, C1Q and collagen domain containing (*Adipoq*), tenascin XB (*Tnxb*), leucine-rich repeat LGI family member 1 (*Lgi1*) and gliomedin (*Gldn*). One gene, Tenascin N (*Tnn*), displayed a similar expression profile in axolotl

and *Acomys*. This gene was downregulated on day 5, but positive fold changes were observed on day 10 and day 14/15. The remaining genes showed differences in expression patterns such as matrilin 4 (*Matn4*), cartilage oligomeric matrix protein (*Comp*), fraser syndrome 1 homolog (*Fras1*) and nephronectin (*Npnt*), all of which were upregulated in axolotl but downregulated in *Acomys*. In contrast, matrilin 2 (*Matn2*) and connective tissue growth factor (*Ctgf*) were upregulated in *Acomys* but downregulated in axolotl. Among the **proteoglycan** genes, 13 matches were identified. Three of these genes were upregulated at all time points in both animals: proteoglycan 4 *(Prg4*), versican (*Vcan*) and serglycin (*Srgn*). Similar expression profiles were seen in osteoglycin (*Ogn*), which was downregulated on day 5 and 10 in both animals, a positive fold change was seen on day 14 in axolotl and on day 15 in *Acomys*. A contradicting profile was observed for neurocan (*Ncan*): this gene was highly upregulated on day 5 in axolotl after which fold changes < 2 were seen, whereas in *Acomys Ncan* was absent on day 5 but displayed high fold changes on day 10 and 15. Among the **ECM-affiliated** matrisome 41 genes matched between axolotl and *Acomys.* A total of 15 genes were upregulated in both animals: C-type lectin domain family 4 member e (*Clec4e*), lectin galactose binding soluble 1 (*Lgals1*), complement component q subcomponent alpha polypeptide (*C1qa*), plexin D1 and C1 (*Plxnd1*, *Plxnc1*) and syndecan 1 (*Sdc1*). Only four genes were downregulated in both animals and during all timepoints, of which the most downregulated genes were: C-type lectin domain family 3 member a (*Clec3a*) and family 2 member d (*Clec2d)*. The remaining genes in this compartment had opposing expression patterns. For example, Fras1 related extracellular matrix protein 2 (*Frem2*) was highly upregulated in axolotl but downregulated in *Acomys.* Surfactant associated protein C *(Sftpc*) was highly upregulated in *Acomys* but downregulated in axolotl. A total of 55 genes were found in the **secreted factors** subset. Seventeen genes were upregulated in both species at all timepoints, with the highest fold changes observed in chemokine C-X-C motif ligand 14 (*Cxcl14)*, multiple EGF-like-domains 11 (*Megf11*), platelet-derived growth factor C polypeptide (*Pdgfc*), wingless-related MMTV integration site 5A (*Wnt5a*), sonic hedgehog *(Shh*), transforming growth factor beta 3 (*Tgfb3*) and secreted frizzled-related protein 2 (*Sfrp2*). Three genes were downregulated in all datasets: chemokine C-X-C motif ligand 12 (*Cxcl12),* follistatin (*Fst*) and bone morphogenic protein 5 (*Bmp5)*. The remaining genes often showed opposing expression patterns. Heparin-binding EGF-like growth factor (*Hbegf*) and chemokine C-C motif ligand 5 (*Ccl5*), were downregulated in axolotl but upregulated in *Acomys*. The other way around: leptin (*Lep*) and macrophage stimulating 1 (*Mst1*) were upregulated in axolotl and downregulated in *Acomys*. Finally, 71 **regulator genes** matched between *Acomys* and axolotl of which 40 genes were upregulated at all timepoints in both datasets. The highest fold

changes belonged to several matrix metallopeptidases (*Mmp3*, *Mmp9, Mmp12, Mmp13, Mmp19)*, transglutaminase 3 E polypeptide (*Tgm3*), tolloid-like 2 (*Tll2*), tissue inhibitor of metalloproteinase 1 (*Timp1*), serine (or cysteine) peptidase inhibitor clade E member 1 (*Serpine1*), and cathepsin Z (*Ctsz*). Only one gene, tissue inhibitor of metalloproteinase 3 (*Timp3*), was downregulated in both animals across all days. Once again, the remaining genes displayed opposite expression patterns. This was the case for Kazal-type serine peptidase inhibitor domain 1 (*Kazald1*) and coagulation factor XIII A1 subunit (*F13a1*), which were among the most upregulated genes in axolotl but displayed downregulations in *Acomys*. The opposite was also seen: cathepsin H and S (*Ctsh, Ctss*) were downregulated in axolotl but upregulated in *Acomys*.

To summarize this comparison demonstrated that many matrisome genes are present in the blastema of both *Acomys* and axolotl. A total of 278 matching matrisome genes were identified and 115 of these genes (41%) showed similar expression patterns, being either upregulated (96 genes/35%) or downregulated (19 genes/7%) in both species.

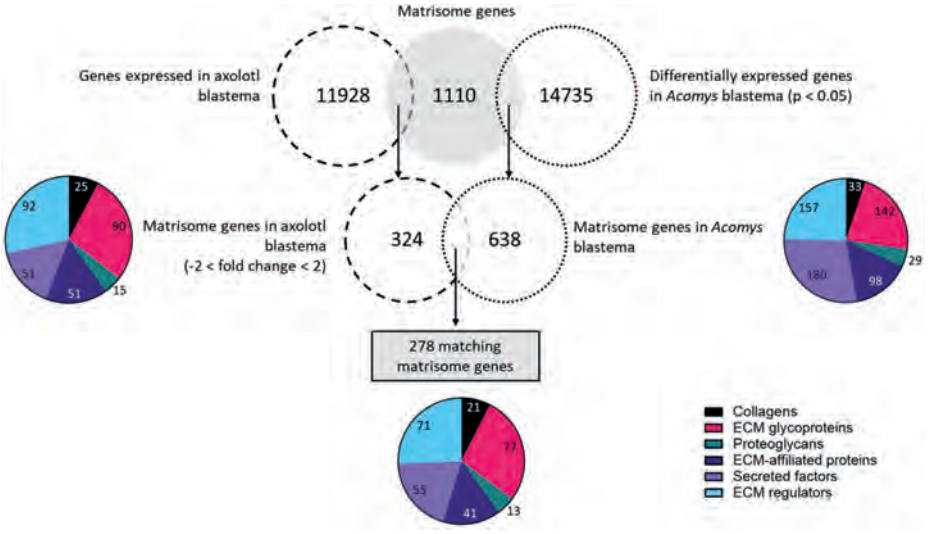

Figure 7. Schematic representation of the identification of matrisome genes in axolotl limb blastema and Acomys ear blastema. In axolotl a total of 11928 genes were expressed, of which 324 passed the threshold of -2 < fold change < 2 on day 5, 10 and 14 (differentially expressed genes could not be generated from this dataset). In Acomys, a total of 14735 genes were differentially expressed ($p < 0.05$) in ear blastema. Among these were 638 matrisome genes. Between axolotl and Acomys 278 matching matrisome genes were identified and all matrisome categories were represented.

Presence of GAG-related genes ear pinnae blastema in Acomys compared to forelimb blastema of axolotl

In the category of **linkage region preparation** three genes matched between the two models and all were upregulated across all timepoints. In axolotl the highest expression was observed for beta-1,4-galactosyltransferase (*B4galt7*), in *Acomys* the most upregulated gene was beta-1,4-galactosyltransferase 2 (*B4galt2*). The remaining beta-1,3-glucuronyltransferase 3 (*B3gat3*), was upregulated in axolotl on day 5 after which the fold changes did not exceed the threshold. In *Acomys* a slight upregulation was seen for all timepoints. In the compartment of genes related to glycosaminoglycan **chain polymerization** nine genes matched between species. The highest fold changes in all timepoints, for both species, were seen in chondroitin sulfate synthase 1 (*Chsy1*), hyaluronan synthase 2 (*Has2*) and exostatin-like glycosyltransferase 3 (*Extl3*). In axolotl only one gene was downregulated: hyaluronan synthase 1 (*Has1*) on day 14. In *Acomys* this gene was also downregulated on day 10 and 15. A total of eight genes related to glycosaminoglycan **chain modification** were identified. Three genes were always upregulated in both animals: carbohydrate sulfotransferase 2 (*Chst2*), sulfatase 1 (*Sulf1*) and carbohydrate sulfotransferase 11 (*Chst11*). No negative fold changes were observed in axolotl and in *Acomys* only sulfatase modifying factor (*Sumf2*) was consistently downregulated. Opposing expression patterns were observed in heparan sulfate glucosamine 3-O-sulfotransferase 3B1 (*Hs3st3b1*): this gene was upregulated in axolotl but downregulated in *Acomys*. Lastly, 10 genes in the compartment of glycosaminoglycan **chain degradation** were matched and these mostly displayed varying expression patterns. A single gene, glucuronidase beta (*Gusb*), was upregulated in axolotl and *Acomys* on all timepoints. No genes were consistently downregulated in both animals. Arylsulfatase family member K (*Arsk*) was downregulated across all days in *Acomys* but upregulated in Axolotl. In axolotl N-sulfoglucosamine sulfohydrolase (*Sgsh*) was downregulated on day 5.

Comparison of the proteomic profiles of skin regeneration in Acomys (Rao et al. 2009) vs. blastema-mediated limb regeneration in axolotl (Yoon et al. 2020)

In this section a comparison was performed of skin regeneration (absence of blastema) and limb regeneration (blastema mediated) on the proteomic level. The previous comparisons of transcriptome profiles each generated an extensive list of matrisome-related genes that were present in both species. However, up or downregulation on the transcriptional level does not necessarily translate to an increase or decrease in protein abundance, thus investigating regeneration at the proteomic level is important.

Comparing the matrisome-related proteins from the proteomics studies on *Acomys* skin regeneration (Yoon *et al.* 2020 [57]) and axolotl limb regeneration (Rao *et al.* 2009 [63]) revealed only four proteins that were present in both species. The data from Yoon does not provide a fold change for the variations in protein abundance. To be able to compare trends a simple fold change for the Yoon data was calculated: fold change = [protein QV on day X] / [protein QV on day 0]. Following this, values of 0 > fold change < 1 indicate a decrease in the protein and these values were converted to negative fold changes by calculating -1/fold change. Values of fold change >1 indicate an increase in protein abundance, but this difference could not be statistically tested for a differential increase or decrease. Data are represented in Table 4.

Table 4. Proteins identified in both axolotl and *Acomys*. Data represent a fold change compared to day 0.

Collagens		***Acomys* (fold change)**			**Axolotl (fold change)**		
Gene symbol	**Prot description**	**Day 3**	**Day 5**	**Day 7**	**Day 1**	**Day 4**	**Day 7**
Col12a1	Collagen alpha-1(XII) chain	-1.29	1.90	1.80	1.32	1.05	-1.12
Col1a1	Collagen alpha-1(I) chain	-1.32	1.87	1.62	1.43	1.44	1.92
ECM glycoproteins		***Acomys* (fold change)**			**Axolotl (fold change)**		
Gene symbol	**Prot description**	**Day 3**	**Day 5**	**Day 7**	**Day 1**	**Day 4**	**Day 7**
Fgb	Fibrinogen beta chain	1.83	1.97	2.10	3.39	1.63	1.14
Fgg	Fibrinogen gamma chain	1.13	1.21	1.36	4.64	2.17	1.24

Of the matrisome **collagens**, only collagen type XII alpha 1 (*Col12a1*) and *Col1a1* were found in both species. In *Acomys* the abundance of *Col12a1* was lower on day 3 compared to day 0, but abundance had risen on day 5 and 7 as demonstrated by a positive fold change. On the other hand, *Col12a1* abundance was increased in axolotl on day 1 and 4 but protein levels dropped with a negative fold change observed on day 7. The protein form of *Col1a1* was again less abundant in *Acomys* on day 3, but the protein abundance increased with positive fold changes observed on day 5 and 7. In axolotl the abundance of *Col1a1* was always increased. Among the **ECM glycoproteins**, only fibrinogen beta and gamma chain (*Fgb* and *Fgg)* matched between the datasets. No negative fold changes were observed in either animal. In *Acomys* the protein abundance of both *Fgb* and *Fgg* remained steady over all days, whereas in axolotl the fold change for both *Fgb* and *Fgg* was highest on day 1 with a decrease in protein abundance over the following days.

To conclude, only four matching matrisome proteins were identified and no matches were found among the GAG specific lists. This could be the result of comparing two distinct biological processes. While the axolotl hind limb regeneration is mediated by the blastema, the process of full-thickness skin regeneration in the spiny mouse has not been hallmarked as a blastema-mediated process [46]. The blastema

is a very specialized tissue, thus the proteins present during this process may not be present during skin regeneration in *Acomys*. An alternative explanation is that sample preparation methods resulted in biased protein sets in each species. A recent study that discusses methods to obtain ECM molecules from tissue samples states that the sample extraction method should be optimized to also obtain insoluble ECM [87], which was not done for the publications of Yoon et al. (2020) [57] and Rao et al. (2009) [63]. Proteins from *Acomys* tissue were extracted using a buffer made with Tris-Cl, NaCl, ethylenediaminetetraacetic acid (EDTA), phosphatase inhibitors and protease inhibitors. Soluble proteins were then separated from undissolved tissue using centrifugation. Tissue derived from axolotl was homogenized in a lysis buffer containing urea and dithiothreitol (DTT) followed by further peptide extraction from cell lysates using triethylphosphine, iodoethanol and finally trypsin digestion. To determine the engagement of the matrisome on the proteomics scale it will be necessary to conduct carefully designed experiments that are tailored to the analysis of ECM.

Discussion

Identifying key regulatory factors of regeneration is crucial to develop biomaterials that are capable of inducing regeneration in systems that respond to wounding with fibrosis. Research on *Acomys* demonstrates that regeneration in mammals is possible. Here, we focused on the extracellular matrix (ECM) by performing a direct comparison of the matrisome components present during two distinct regenerative processes in two regenerative species. These were blastema formation and skin wound healing in axolotl and *Acomys*. This approach identified the common ECM-related denominators in the regenerative wound healing processes that occur in both species. Neither axolotl nor *Acomys* can be directly compared to humans due to obvious differences in their (skin) biology. However, the identification of ECM-related factors that were present in both an amphibian and mammal support the existence of shared drivers of regeneration that exceed the differences in species. We propose that these matrisome factors play a vital role in regeneration and that specific matrisome factors should be incorporated into novel biomaterials to improve skin healing in non-regenerative species [27, 88].

Recent research provides evidence that regeneration can be induced using only a small selection of components. In axolotl the process of innervation is essential to achieve limb regeneration. In the absence of a nerve, the application of a combination of fibroblast growth factors (FGFs) and bone morphogenetic

proteins (BMPs) was enough to rescue limb regeneration [89]. Frogs (*Xenopus laevis*) lose the ability to replace amputated hind limbs through blastema after metamorphosis. Instead, adult individuals resolve amputated limbs through the formation of a cartilaginous spike. Murugan and colleagues reported on the ability of a functionalized device that induced hindlimb regeneration in adult *Xenopus leavis* [90]. A wearable dome-shaped bioreactor ('biodome') constructed of a silicone sleeve and containing a silk-based hydrogel loaded with five drugs was attached to the amputation site during the first 24 hours. Animals were followed for 18 months, during which functional hindlimbs regenerated that resembled wildtype hindlimbs. The five drugs in question had been selected for their individual pro-regenerative effects. 1,4-dihydrophenonthrolin-4-ene-3 carboxylic acid (1,4-DPCA), an inhibitor of prolyl 4-hydroxylase, is an enzyme involved in collagen formation [91]. Brain-derived neurotrophic factor (BDNF) is associated with neuron development and axon regeneration [92, 93]. Growth hormone (GH) has many functions and a recent study on the side effects of GH as an anti-aging therapeutic identified its role as an inhibitor of TGF-β1-mediated myofibroblast activation [94]. Resolvin D5, an oxidized lipid mediator, has anti-inflammatory properties by mediating immune cell behavior and recent work indicated this agent has a direct role during re-epithelialization [95, 96]. Finally, retinoic acid (a vitamin A metabolite) has been found in regenerating zebrafish tissues [97] and it was shown to enhance the production of ECM components during wound healing [98]. In another study, full-thickness skin wounds of 12 mm diameter were inflicted on the backs of fetal sheep [99]. At this wound size and gestational age (day 79 of 140-147 days) fetal sheep are not able to regenerate the skin and instead a fibrotic scar forms [33]. However, the regeneration of full-thickness skin wounds in fetal sheep was induced using type I collagen scaffolds functionalized with heparin, vascular endothelial growth factor (VEGF) and fibroblast growth factor 2 (FGF2) [99]. After postnatal analysis, there was an increase in the skin surface area, a reduction in myofibroblast numbers and evidence of hair follicle formation. In the regenerating ear tissue of *Acomys* sustained ERK activity was identified as a crucial pro-regenerative factor [100]. The application of ERK activators (FGF2 and neuregulin-1) to *Mus* ear punch wounds induced a pro-regenerative matrisome profile that was characterized by the presence of matrix metalloproteinase 9 and fibronectin 1 and in addition hair follicle neogenesis was stimulated. Together these studies emphasize the feasibility of driving a biological system towards regeneration using only a few selected components.

Before we elucidate on the matrisome components that were extracted in our study the limitations of our study should be addressed. A single study which compares differentially expressed genes in human partial-thickness skin wounds to axolotl

full-thickness skin wounds, using pre-existing datasets, is available. This study was seeking for genes that were upregulated in humans and downregulated in axolotl, and *vice versa* [101]. This work identified genes involved in collagen formation, biosynthesis and modification, as well as ECM organization, ECM-receptor interactions and connective tissue development. To date, no transcriptomic or proteomic studies have been published regarding healing of adult human skin following a full-thickness skin wound. Despite the widely acknowledged caveats of extrapolating animal data to humans, comparing datasets obtained from regenerating animal models may be useful to gain knowledge that can be applied to human wound healing. We found a compelling overlap between the matrisome transcriptomes of axolotl and *Acomys*. This suggests there is a possibility of shared ECM/matrisome based regenerative mechanisms between amphibians and mammals that could potentially also be present, albeit inactive, in humans [102, 103]. While there was a clear overlap found between the datasets, a direct comparison of numerical data was challenging due to differences in sample harvesting, experimental methodologies and data analyses. Each step from sample extraction to data normalization can affect the final dataset [104-106]. Therefore, the expression level of one gene cannot be directly compared between two datasets. For these reasons, our analysis will only show general trends of gene expression. Our approach also leaves out the effects of enzyme activity on protein synthesis, since an enzyme's gene expression does not need to be increased for the enzyme activity to be increased. An example of this may be found in the hyaluronan synthase genes, which were identified in only one comparison, even though hyaluronic acid is known to have positive effects on regeneration [107]. Second, different publications use different sets of temporal data points which did not always coincide. In particular, the early timepoints of blastema formation (day 0-4) have not been characterized in *Acomys*. Comparing only the later time points means early contributors to regeneration are left unexplored. Third, the age range of the animals used in the experiments should be briefly considered. The publications focusing on axolotl all used juvenile animals of 7-11 cm in length [63, 79, 80]. Axolotls reach sexual maturity after 9 to 12 months, when the animal is on average 15 cm long [89, 108]. The publications on *Acomys* used animals of varying ages; 6 weeks – 6 months[76], 6 months only [31], or 'sexually mature'[57]. Both male and female *Acomys* reach sexually maturity at 2-3 months of age [44], thus the majority of the individuals in the experiments would have been mature. Comparing the life phases of axolotl and *Acomys* is negligible as axolotls naturally retain their juvenile characteristics even after obtaining sexual maturity. Lastly, the proteomic analyses of the incorporated papers are limited to the soluble fractions of the ECM. For example, only four proteins were found in the proteomics datasets and two of these (**fibrinogen**

beta (*Fgb)* **and gamma chain** *(Fgg)*) are known soluble proteins.Fibrinogens have a well-known role in the healing response: after conversion to fibrin it assembles into a temporary support network. Fibrinogen-deficient mice have highlighted this role in wound stabilization and matrix organization [102]. Although many important ECM proteins are soluble, identification of insoluble components of the ECM remains elusive.

Our analysis found multiple matrisome related genes that had similar expression patterns in both models and these genes could therefore potentially be essential to regeneration. In this discussion we will focus solely on the genes that were upregulated in both skin regeneration and blastema, as these could be candidates to be included in pro-regenerative biomaterials.

Glycoproteins are essential molecules in the ECM and are known to be involved in wound healing [109]. The widespread functions of glycoproteins explain the presence of many highly upregulated glycoproteins during the regenerative processes. Glycoproteins that were highly upregulated in both axolotl and *Acomys* during skin regeneration and in the blastema were: **tenascin C, fibronectin, laminin alpha 1, thrombospondin 1 and 2, peroxidasin homolog and collagen triple helix repeat containing 1**. In general, tenascins are involved with cell adhesion modulation; thereby influencing cell proliferation and migration [110, 111]. **Tenascin C** is activated after injury in axolotl and is deposited in the wound margins [67]. Due to its anti-adhesive behavior and promotion of a softer matrix [112], Tenascin C is thought to lead to proliferation and migration of keratinocytes, fibroblasts, and endothelial cells [113]. Tenascin C has been indicated as a component of a "transitional matrix" in regeneration-competent species such as newts and zebrafish [114-116]. In humans, tenascin C is highly expressed during wound healing, inflammation and injury. A study using mice demonstrated that tenascin C polypeptides increased type I collagen expression, contributing to ECM strength in young skin [117]. **Fibronectin 1,** another component of the transitional matrix, was found in both *Acomys* and axolotl during skin regeneration and blastema-formation. Fibronectin is crosslinked to the fibrin matrix during hemostasis and enables fibroblast migration [118]. Mouse full-thickness skin wounds sealed with a combination of plasma fibrinogen and fibronectin demonstrated enhanced wound healing [119]. Similarly, pre-coating fibronectin on full-thickness skin wounds in mice before the application of autologous basal cells improved wound healing [120]. Furthermore, it has been shown that fibronectin regulates collagen assembly [121, 122]. An in depth review on the role of fibronectin and its potential in regeneration was recently published [123]. **Laminin alpha 1**, a protein that interacts with fibronectin, was present and upregulated

in all datasets. Laminin alpha 1 encodes the alpha I chain of the trimeric laminin protein and is a major component of the basement membrane, with an important role in re-epithelization and angiogenesis during wound healing [124]. Laminins are also important in growth factor regulation: the heparin-binding domains on laminin can bind growth factors and fibrin matrices functionalized with laminin improved wound healing in diabetic mice [125]. Another consistently upregulated gene during regeneration was the relatively unknown **peroxidasin homolog.** A study into the role of peroxidasin in the ECM demonstrated that human dermal fibroblasts treated with TGF-β1 to induce myofibroblasts secrete peroxidasin to the ECM where it may co-localize with fibronectin in thick bundles [126]. Peroxidasin may also contribute to ECM stabilization via tyrosine crosslinking of proteins [127] and it was identified as a catalyst in type IV collagen crosslinking through sulfilimine [128, 129]. Inhibition of peroxidasin reduced endothelial cell attachment and growth, and without peroxidasin the organization of type IV collagen, fibronectin and laminin into fibrillar networks was diminished [130]. The potential role of peroxidasin in ECM formation coupled with its consistent presence in the regenerating matrix indicates this peroxidasin may be an important player in wound healing. The consistent presence of both fibrin(ogen) and fibronectin, as well as their associated proteins, demonstrates their importance during regeneration in regenerative and non-regenerative systems alike. **Thrombospondin 1**, a large trimeric glycoprotein secreted by a plethora of cell types, has been implicated in many (patho)physiological processes [131]. Researchers demonstrated that the inhibition of thrombospondin 1 with antisense oligonucleotides in full-thickness skin wounds of mice markedly impaired the wound healing process [132]. Recently thrombospondin 1 has been implicated in fibrillar collagen organization through its inhibitory effect on lysyl oxidase, which is an enzyme responsible for collagen crosslinking in the ECM [133]. Thrombospondin 1 also indirectly inhibited myofibroblast differentiation through its effects on the organization of collagenous ECM [133]. **Thrombospondin 2**, like thrombospondin 1, is involved in ECM organization and it is secreted primarily by fibroblasts and smooth muscle cells [134]. In thrombospondin 2 knock-out mice the skin displayed disorganized collagen fibers, contrasting the parallel orientated fibers found in wild-type mice [135]. Additionally, the researchers demonstrated that dermal fibroblasts obtained from these mice produced more matrix metalloproteinase 2, indicating thrombospondin 2 may affect cell-matrix interactions. Taken together, the increased expression levels of thrombospondin 1 and 2 during regeneration underline the impact of ECM organization. **Collagen triple helix repeat containing 1 (***Cthrc1***)** is a secreted glycosylated protein that is usually present in embryonic and neonatal tissues. *Cthrc1* has shown the ability to inhibit type I and III collagen synthesis [136, 137]. In skin wounds, it has been localized at sites of collagen

deposition and in myofibroblast clusters [137]. Moreover, *Cthrc1* regulates and inhibits TGF-β1 production which may be a potential anti-fibrotic treatment in the skin [138, 139]. The consistent upregulation of Cthrc1 during regeneration is indicative of a need for controlled collagen synthesis.

Several genes involved in matrix degradation were upregulated in all transcriptomics datasets: **matrix metalloproteinase 3**, **matrix metalloproteinase 13** and **tissue inhibitor of metallopeptidase 1 (***Timp1)***.** Matrix remodeling is essential in wound healing, as demonstrated by the total of 14 differentially expressed MMPs that were found during healing of human split-thickness skin wounds, which do not scar [140]. It has been described that **matrix metalloproteinase 3** degrades both type I and III collagen [67]. Research in regenerating axolotl digits showed that the presence of matrix metalloproteinases was essential to effective digit regeneration [141]. **Matrix metalloproteinase 13** is capable of cleaving type I, II, and III collagen and various other fibrillar ECM components, thereby modulating fibroblast-matrix interactions and it is even upregulated in fetal wounds [142]. *Timp1* can inhibit all matrix metalloproteinase family members [143]. It has been shown that increased levels of this gene were implicated as a poor outcome marker for increased fibrosis in burn patients and persistence of foot ulcers in diabetic patients [144]. On the other hand, a study performed in newts indicated that increased levels of *Timp1* during regeneration is required to maintain optimal concentrations of matrix metalloproteinases [145].

Regarding proteoglycans associated with the matrisome, **proteoglycan 4** and **serglycin** were present and upregulated in all datasets. Proteoglycans consist of a core protein and one or more covalently attached glycosaminoglycan (GAG) side chains. They make up a major part of the ECM and have a range of purposes. **Proteoglycan 4**, also known as lubricin, contains the GAGs chondroitin sulfate and keratan sulfate. The biosynthesis of keratan sulfate was highly increased in the regenerating spinal cord of *Acomys* and, the expression of one related biosynthesis gene, beta-1,3-N-acetylglucosaminyltransferase 7 (*B3gnt7*), was identified as an axon growth enhancer [47]. Proteoglycan 4 is more formally associated with blastema formation because of its role in cartilage-bone protection [146]. In humans, proteoglycan 4 is associated with the regeneration of cartilage tissue between joint surfaces [147]. A recent study elaborated on the anti-fibrotic properties of proteoglycan 4 by demonstrating the ability of this proteoglycan to decrease synovial fibroblast activation *in vitro* and reduce fibrosis *in vivo* [148]. Its presence during skin regeneration in both *Acomys* and axolotl underscores the importance of proteoglycan 4 to regeneration in general. This finding is supported by the

results of Krawetz *et al*. (2022), who demonstrated proteoglycan 4 is essential in ear wound healing in mice [149]. They showed that proteoglycan 4 modulates macrophage polarization, increases vascularization and promotes cartilage regeneration. The proteoglycan **serglycin** was upregulated during both blastema and skin regeneration. Serglycin is a well-known intracellular proteoglycan and one of its main roles is the regulation of inflammatory mediators in the granules of mast cells [150]. After secrection serglycin may act as a vehicle for the extracellular delivery of the molecules inside granules, such as cytokines, or act as a scavenger in the ECM [151]. Thus, serglycin may have a role as an inflammation mediator. Moreover, serglycin is upregulated under the influence of TGF-β1 during epithelial-mesenchymal transition, this transition is an important process during wound healing [152]. Serglycin is densely packed with various GAGs, leading to a high density of GAG-binding proteins, and one of these associated GAGs is heparin [151]. Heparin is most commonly associated with anticoagulation and anti-inflammation and has widespread use in therapeutic applications [153]. For example, treatment of chronic ulcers with low molecular weight heparin resulted in increased numbers of healed patients and reduced wound recurrence rates [154, 155]. These findings illustrate the beneficial effects of heparin on the healing of chronic wounds.

Considering the upregulation of various proteoglycans, it is to be expected that several genes related to the linkage and modification of GAG chains were also upregulated during regeneration: **carbohydrate sulfotransferase 2, carbohydrate sulfotransferase 11** and **sulfatase 1.** Carbohydrate sulfotransferases are responsible for the transfer of sulfate groups onto carbohydrates. Our analysis returned two carbohydrate sulfotransferase genes that were always upregulated during regeneration. **Carbohydrate sulfotransferase 2**, also known as N-acetylglucosamine 6-O-sulfotransferase or GlcNAc6ST1, is associated with the biosynthesis of keratan sulfate [156]. This enzyme may play a direct role in the inflammatory response as it is a part of L-selectin ligand synthesis: these ligands are responsible for leukocyte rolling and capture in high endothelial venules [157, 158]. **Carbohydrate sulfotransferase 11,** or chondroitin-4-sulfotransferase 1, is an enzyme involved in the biosynthesis of chondroitin sulfate [159]. In Costello syndrome, where overexpression of the HRAS oncogene leads to a reduction in carbohydrate sulfotransferase 11, skin fibroblasts do not produce elastic fibers. Forced expression of carbohydrate sulfotransferase 11 rescued the elastic fiber production [160]. Chondroitin sulfate itself was shown to improve palatal wound healing by promoting fibroblast adhesion and proliferation [161]. **Sulfatase 1** is an extracellular enzyme that removes 6-O-sulfates from heparan sulfate and augments Wnt/β-catenin signaling. Following wounding of the corneal epithelium in mice sulfatase 1 was found in the wound edges and

knockdown of sulfatase 1 led to a decrease in cell migration and delayed wound healing [162]. Similarly, during hind limb regeneration in *Xenopus laevis* high levels of sulfatase 1 were present during the first three days in the blastema, which demonstrates its the importance in regeneration [163]. Moreover, it was found that sulfatase 1 is upregulated during mouse embryonic skin development and is likely involved in cellular signaling [85]. Taken together, the three enzymes found in the datasets regulate sulfation patterns of GAGs, which modulates the bioactivity. The GAG heparan sulfate (HS) binds many proteins, such as growth factors, that reside in the ECM and the interaction of HS-binding proteins and receptors is modulated by HS proteoglycans [164, 165]. Changes in sulfation patterns of GAGs may thus have far-reaching effects in modulating cell behavior.

Lastly, two collagens were identified in the proteomics datasets. These collagens, **type I collagen type alpha 1 chain** and **type XII collagen alpha 1 chain**, are important during regeneration albeit in different ways. As part of the core matrisome, collagens have a great influence on the overall structure of the ECM and cell behavior. **Type I collagen**, a member of the fibrillar collagens, contributes to over 90% of the collagen content in skin ECM [166]. Scar tissue consists of a dense collagenous matrix organized in thick parallel orientated bundles, in contrast to healthy dermis where the collagen is organized into a basket weave-like pattern [7]. In regenerating *Acomys* skin, type I collagen was loosely organized and less abundant as shown through trichrome staining, resembling undamaged skin [51]. To achieve skin regeneration, the architecture of type I collagen should match that of unwounded skin, which requires guiding the deposition and remodeling of type I collagen during wound healing. **Type XII collagen** is a member of the Fibril Associated Collagens with Interrupted Triple helices (FACIT). This collagen has binding sites for type I collagen, to assist in type I collagen packing, and GAGs (such as heparan sulfate) [167, 168]. Additionally, type XII collagen helps to maintain the structure of the ECM and responds to mechanical stretch by absorbing stress. Type XII collagen is expressed in the dermis during skin development in humans, however, after birth it is found only in the papillary dermis and surrounding hair follicles [169]. Following skin injury, the scarring *Mus musculus* displays significant increases in type XII collagen compared to *Acomys*, which indicates that an abundance of type XII collagen could also be detrimental to a regenerative matrix [51, 55]. Similarly, timing the deposition of type I and XII collagen has shown to play a key role in skin regeneration in the axolotl [103].

In summary, our analysis of matrisome factors revealed several genes that are upregulated during regeneration in both axolotl and *Acomys*. In some cases, they

encode proteins which are known to have a positive influence on wound healing in mammals or are in some way related to the structural organization of the ECM. The fact that fibrotic skin is characterized by the thick parallel organization of type I collagen while in undamaged skin a basket-weave pattern is seen suggests that a regenerative biomaterial should focus on re-establishing the normal ECM architecture and organization (Figure 8).

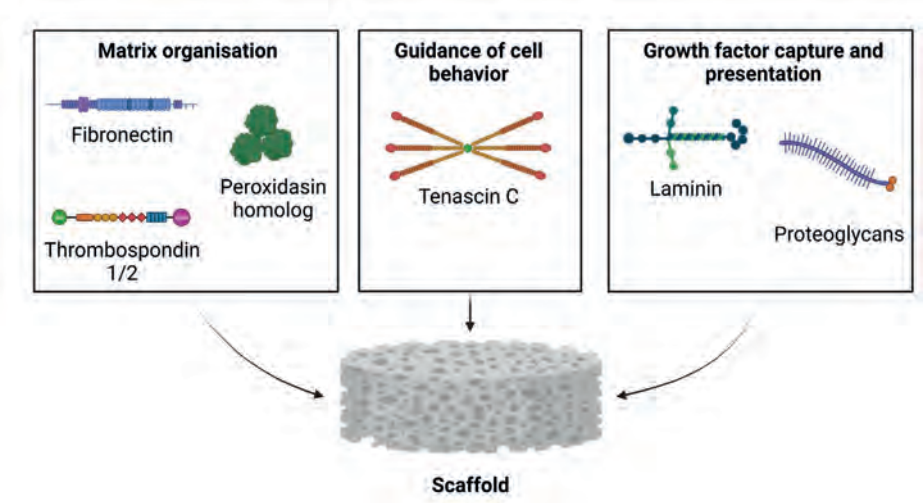

Figure 8. Components to be considered for incorporation in pro-regenerative biomaterials. Created with BioRender.com.

Several of the components identified in our analysis may be considered for use in a regenerative biomaterial. The incorporation of **fibronectin** in a biomaterial would aid in the regulation of collagen fiber assembly. Several other components can be considered to strengthen the matrix organizing properties, such as **thrombospondin 1 and/or 2**, as well as **peroxidasin homolog**. Growth factors are an integral part of regeneration, and their capture should be facilitated. This may be achieved through the incorporation of molecules that have growth factor binding abilities, such as **laminin alpha 1**, or various **proteoglycans** which may bind growth factors through their GAG chains. The glycoprotein **tenascin c** is known for its positive influence on wound healing by enhancing cell migration. Its constant presence in our datasets supports the inclusion of tenascin c in a pro-regenerative biomaterial. The proteoglycans **serglycin** and **proteoglycan 4** were an unexpected finding in our dataset, as their exact roles in skin wound healing are not well known. This warrants a more detailed investigation into the influence of the various proteoglycans on wound healing to determine which would be the most appropriate for incorporation in a pro-regenerative scaffold. Proteoglycan-

associated GAGs, such as heparin in serglycin and chondroitin sulfate or keratan sulfate in proteoglycan 4, have shown potential in promoting wound healing and should be considered for incorporation into the pro-regenerative biomaterial. Phan *et al.* (2021) showed that heparan sulfates, together with fibroblast growth factor signaling, are required to provide the correct positional information during axolotl limb regeneration [170].

There is a myriad of options available for the development and production of pro-regenerative biomaterials. Such materials may contain natural or synthetic components, or a combination of both. The application of natural-derived components is widespread. For example, decellularized tissues maintain the native tissue architecture and many of the signaling factors [171, 172]. A wide range of decellularized skin substitutes from human and animal sources are commercially available and have been used in clinical practice [173]. Decellularized human nail beds have been used to stimulate bone regeneration in rats [174, 175]. These examples establish the ability of the native ECM to promote regenerative processes. In addition to naturally derived components, chemically or enzymatically produced components may be considered. Standardized processes greatly decrease variations between batches and the low immunogenicity makes synthetic compounds an interesting alternative [176]. Besides the incorporation of proteinaceous compounds in biomaterials, carbohydrates - and GAGs in particular - encompass a class of molecules with diverse biological functions. Unlike proteins, they are more difficult to analyze due to the non-template driven biosynthesis and extensive structural heterogeneity of these long polysaccharides. In the context of biomaterial development their multitude of functions make them important to consider. GAGs are known for their role in organizing the extracellular matrix and for their ability to bind and present bioactive molecules, protecting these from proteolytic degradation, and regulating growth factor gradients [177]. Many examples of the exploitation of such functions can be found in the literature, from hyaluronan injectables [178] to collagen-based skin constructs containing dermatan sulfate and heparin [179]. However, one GAG may have various domains in the sulfation pattern and its structure can vary during development and (patho)physiology. To avoid the use of heterogenous natural GAGs with potential batch-to-batch variations, novel strategies have been developed to obtain more defined preparations. One approach includes the use of degradation-resistant carboxymethyl-dextran sulfates: these heparan sulfate mimetics are capable of binding and protecting growth factors already present in the wound matrix, thereby allowing the tissue to regenerate [180]. These ReGeneraTing Agents (RGTA®) have shown great potential during *in vivo* studies and were clinically used to treat ulcers [181, 182]. The basic research into defined

saccharides offers an original approach to their application in biomaterials [183]. In addition, chemo-enzymatic synthesis of well-characterized oligosaccharides with specific biological functions opens a whole new avenue in the field of regenerative medicine [184-186].

Future efforts should be directed towards functionality-based studies in order to elucidate the function of the matrisome components identified here in the regenerating matrix. This may be aided by improving the proteomic analysis of insoluble matrisome components. For example, the insoluble ECM pellet can be digested to allow proteomic analysis of insoluble matrisome components [87]. This can be achieved by digesting insoluble ECM pellets with hydroxylamine [187] or with a photocleavable linker such as 4-hexylphenylazosulfonate [188, 189]. Both approaches yield a solubilized ECM fraction compatible with proteomic analysis pipelines and are relatively easy to implement. Efforts are already being made to improve the proteomic coverage of the matrisome. A universal tool titled 'MatrisomeDB' is available to all researchers, and it facilitates the reuse of proteomic datasets with a focus on the matrisome [190]. To obtain robust insights in the trends in gene and protein expression patterns observed in both species, it would require a united effort to analyze all data via identical methods and with matching timepoints in the regenerative process. Furthermore, the investigation of early timepoints in *Acomys* is highly recommended to provide a detailed image of the processes that occur during the first phases of regeneration.

Conclusions

With the increasing knowledge on the complexity of regenerative environments, the next generation of biomaterials should focus on the rational incorporation of various pro-regenerative matrix molecules. By applying such knowledge to the development of biomaterials we open new avenues towards improving wound healing and obtaining regeneration in humans.

Conflicts of interest

There are no conflicts to declare.

Acknowledgements

The authors acknowledge Tahar van der Straaten, Field Applications Scientist, Microarray Support from Thermo Fisher Scientific for his support in the extraction

and analysis of the axolotl skin transcriptomics genes which were further used for the comparison with Acomys.

This work has received funding from the European Union's Horizon 2020 research and innovation programme under the Marie Skłodowska-Curie Grant Agreement No. 955722 (SkinTERM, NAM and HJ) and from a Radboudumc RIMLS Young Investigator Grant (RIMLS, MG).

Electronic supplementary information (ESI)

The following supporting information is available:
https://doi.org/10.1039/D3BM00835E
Description for supplement

Table S1. Murine matrisome masterlist

Table S2. List of GAG genes

Table S3. Monaghan 2012

Table S4. Brant 2019_matrisome and GAG matches_day 7 vs 14

Table S5. Monaghan 2012 analyzed for D7 vs D0

Table S6. Brant vs Monaghan

Table S7. Gawriluk 2016_matrisome and GAG matches

Table S8. Stewart 2013 with FC calculation and matching

Table S9. Stewart vs Gawriluk matching of blastema

References

1. P. K. Williams-Boyce and J. C. Daniel, Jr., *J Exp Zool*, 1980, **212**, 243-253.
2. P. G. ten Koppel, G. J. van Osch, C. D. Verwoerd and H. L. Verwoerd-Verhoef, *Biomaterials*, 2001, **22**, 1407-1414.
3. J. Price and S. Allen, *Philos Trans R Soc Lond B Biol Sci*, 2004, **359**, 809-822.
4. U. Kierdorf and H. Kierdorf, *Front Biosci (Elite Ed)*, 2012, **4**, 1606-1624.
5. L. Yu, M. J. Han, M. Q. Yan, J. Lee and K. Muneoka, *Developmental Biology*, 2012, **372**, 263-273.
6. J. Simkin, M. C. Sammarco, L. A. Dawson, P. P. Schanes, L. Yu and K. Muneoka, *Regeneration*, 2015, **2**, 93-105.
7. P. Martin, *Science*, 1997, **276**, 75-81.
8. J. H. W. Distler, A. H. Gyorfi, M. Ramanujam, M. L. Whitfield, M. Konigshoff and R. Lafyatis, *Nat Rev Rheumatol*, 2019, **15**, 705-730.
9. P. C. Esselman, *Arch Phys Med Rehabil*, 2007, **88**, S3-6.
10. J. M. Reinke and H. Sorg, *Eur Surg Res*, 2012, **49**, 35-43.
11. E. S. White and A. R. Mantovani, *J Pathol*, 2013, **229**, 141-144.
12. N. Di Caprio and E. Bellas, *Adv Biosyst*, 2020, **4**, e1900286.
13. M. F. Brizzi, G. Tarone and P. Defilippi, *Curr Opin Cell Biol*, 2012, **24**, 645-651.
14. F. Mercier, *Cell Mol Life Sci*, 2016, **73**, 4661-4674.
15. A. Naba, K. R. Clauser, H. Ding, C. A. Whittaker, S. A. Carr and R. O. Hynes, *Matrix Biol*, 2016, **49**, 10-24.
16. R. O. Hynes and A. Naba, *Cold Spring Harbor Perspectives in Biology*, 2012, **4**, a004903.
17. A. Heydemann, *Front Biol (Beijing)*, 2012, **7**, 522-538.
18. M. Suzuki, N. Yakushiji, Y. Nakada, A. Satoh, H. Ide and K. Tamura, *ScientificWorldJournal*, 2006, **6 Suppl 1**, 26-37.
19. J. F. Denis, M. Levesque, S. D. Tran, A. J. Camarda and S. Roy, *Adv Wound Care (New Rochelle)*, 2013, **2**, 250-260.
20. R. Richardson, K. Slanchev, C. Kraus, P. Knyphausen, S. Eming and M. Hammerschmidt, *J Invest Dermatol*, 2013, **133**, 1655-1665.
21. S. E. Mutsaers, J. E. Bishop, G. McGrouther and G. J. Laurent, *Int J Biochem Cell Biol*, 1997, **29**, 5-17.
22. G. Henry and W. L. Garner, *Surg Clin North Am*, 2003, **83**, 483-507.
23. T. Velnar, T. Bailey and V. Smrkolj, *J Int Med Res*, 2009, **37**, 1528-1542.
24. H. P. Ehrlich, A. Desmouliere, R. F. Diegelmann, I. K. Cohen, C. C. Compton, W. L. Garner, Y. Kapanci and G. Gabbiani, *Am J Pathol*, 1994, **145**, 105-113.
25. M. C. Vogg, Y. Wenger and B. Galliot, *Essays on Developmental Biology, Pt A*, 2016, **116**, 391-414.
26. C. McCusker, S. V. Bryant and D. M. Gardiner, *Regeneration*, 2015, **2**, 54-71.
27. A. W. Seifert and K. Muneoka, *Dev Biol*, 2018, **433**, 190-199.
28. A. Satoh, S. V. Bryant and D. M. Gardiner, *Developmental Biology*, 2012, **366**, 374-381.
29. G. G. Whitehead, S. Makino, C. L. Lien and M. T. Keating, *Science*, 2005, **310**, 1957-1960.
30. J. Girstmair, R. Schnegg, M. J. Telford and B. Egger, *EvoDevo*, 2014, **5**, 37.
31. T. R. Gawriluk, J. Simkin, K. L. Thompson, S. K. Biswas, Z. Clare-Salzler, J. M. Kimani, S. G. Kiama, J. J. Smith, V. O. Ezenwa and A. W. Seifert, *Nat Commun*, 2016, **7**, 11164.

32. B. J. Larson, M. T. Longaker and H. P. Lorenz, *Plastic and Reconstructive Surgery*, 2010, **126**, 1172-1180.
33. D. L. Cass, K. M. Bullard, K. G. Sylvester, E. Y. Yang, M. T. Longaker and N. S. Adzick, *J Pediatr Surg*, 1997, **32**, 411-415.
34. C. C. Yates, P. Hebda and A. Wells, *Birth Defects Res C Embryo Today*, 2012, **96**, 325-333.
35. P. Martin and J. Lewis, *Nature*, 1992, **360**, 179-183.
36. J. Brock, K. Midwinter, J. Lewis and P. Martin, *J Cell Biol*, 1996, **135**, 1097-1107.
37. I. V. Yannas and D. S. Tzeranis, *NPJ Regen Med*, 2021, **6**, 39.
38. M. M. W. Ulrich, in *Textbook on Scar Management: State of the Art Management and Emerging Technologies*, eds. L. Téot, T. A. Mustoe, E. Middelkoop and G. G. Gauglitz, Springer International Publishing, Cham, 2020, DOI: 10.1007/978-3-030-44766-3_1, pp. 3-9.
39. P. Vidal and M. G. Dickson, *J Hand Surg Br*, 1993, **18**, 230-233.
40. R. B. Borgens, *Science*, 1982, **217**, 747-750.
41. B. S. Douglas, *Aust Paediatr J*, 1972, **8**, 86-89.
42. S. K. Das and H. G. Brown, *Hand*, 1978, **10**, 16-27.
43. M. A. Storer, N. Mahmud, K. Karamboulas, M. J. Borrett, S. A. Yuzwa, A. Gont, A. Androschuk, M. V. Sefton, D. R. Kaplan and F. D. Miller, *Dev Cell*, 2020, **52**, 509-524 e509.
44. C. L. Haughton, T. R. Gawriluk and A. W. Seifert, *J Am Assoc Lab Anim Sci*, 2016, **55**, 9-17.
45. M. Maden and J. A. Varholick, *Development*, 2020, **147**, dev167718.
46. A. W. Seifert, S. G. Kiama, M. G. Seifert, J. R. Goheen, T. M. Palmer and M. Maden, *Nature*, 2012, **489**, 561-565.
47. J. Nogueira-Rodrigues, S. C. Leite, R. Pinto-Costa, S. C. Sousa, L. L. Luz, M. A. Sintra, R. Oliveira, A. C. Monteiro, G. G. Pinheiro, M. Vitorino, J. A. Silva, S. Simão, V. E. Fernandes, J. Provazník, V. Benes, C. D. Cruz, B. V. Safronov, A. Magalhães, C. A. Reis, J. Vieira, C. P. Vieira, G. Tiscórnia, I. M. Araújo and M. M. Sousa, *Developmental Cell*, 2022, **57**, 440-450.e447.
48. A. G. W. Sandoval and M. Maden, *Curr Opin Genet Dev*, 2020, **64**, 31-36.
49. M. Maden and J. O. Brant, *Exp Dermatol*, 2019, **28**, 436-441.
50. J. Simkin, T. R. Gawriluk, J. C. Gensel and A. W. Seifert, *Elife*, 2017, **6**, e24623.
51. J. O. Brant, J. H. Yoon, T. Polvadore, W. B. Barbazuk and M. Maden, *Wound Repair Regen*, 2016, **24**, 75-88.
52. J. L. Cyr, T. R. Gawriluk, J. M. Kimani, B. Rada, W. T. Watford, S. G. Kiama, A. W. Seifert and V. O. Ezenwa, *Integr Comp Biol*, 2019, **59**, 1138-1149.
53. Y. Kuninaka, Y. Ishida, A. Ishigami, M. Nosaka, J. Matsuki, H. Yasuda, A. Kofuna, A. Kimura, F. Furukawa and T. Kondo, *Scientific Reports*, 2022, **12**, 20327.
54. H. I. Harn, S. P. Wang, Y. C. Lai, B. Van Handel, Y. C. Liang, S. Tsai, I. M. Schiessl, A. Sarkar, H. Xi, M. Hughes, S. Kaemmer, M. J. Tang, J. Peti-Peterdi, A. D. Pyle, T. E. Woolley, D. Evseenko, T. X. Jiang and C. M. Chuong, *Nat Commun*, 2021, **12**, 2595.
55. J. O. Brant, M. C. Lopez, H. V. Baker, W. B. Barbazuk and M. Maden, *PLoS One*, 2015, **10**, e0142931.
56. J. H. Yoon, K. Cho, T. J. Garrett, P. Finch and M. Maden, *Sci Rep*, 2020, **10**, 8641.
57. J. H. Yoon, K. Cho, T. J. Garrett, P. Finch and M. Maden, *Sci Rep*, 2020, **10**, 166.
58. D. Matias Santos, A. M. Rita, I. Casanellas, A. Brito Ova, I. M. Araújo, D. Power and G. Tiscornia, *Regeneration (Oxf)*, 2016, **3**, 52-61.
59. J. Gresens, *Lab Animal*, 2004, **33**, 41-47.

60. A. Crowner, S. Khatri, D. Blichmann and S. R. Voss, *Frontiers in Endocrinology*, 2019, **10**.
61. S. R. Voss, H. H. Epperlein, E. M. Tanaka, S. Khattak, T. Richter, E. Nacu, D. Knapp, M. Kragl, R. B. Page and P. Cold Spring Harbor Laboratory, *Emerging Model Organisms: Laboratory Manual, Vol 2*, 2010, **2009**, 397-419.
62. R. J. Debuque and J. W. Godwin, *Stem Cells Biol Reg*, 2016, DOI: 10.1007/978-3-319-44996-8_1, 1-21.
63. N. Rao, D. Jhamb, D. J. Milner, B. B. Li, F. Y. Song, M. Wang, S. R. Voss, M. Palakal, M. W. King, B. Saranjami, H. L. D. Nye, J. A. Cameron and D. L. Stocum, *Bmc Biology*, 2009, **7**, 1-25.
64. T. Endo, S. V. Bryant and D. M. Gardiner, *Dev Biol*, 2004, **270**, 135-145.
65. C. S. Thornton, *J Exp Zool*, 1957, **134**, 357-381.
66. R. N. Christensen and R. A. Tassava, *Dev Dyn*, 2000, **217**, 216-224.
67. A. W. Seifert, J. R. Monaghan, S. R. Voss and M. Maden, *Plos One*, 2012, **7**, e32875.
68. A. K. Rodgers, J. J. Smith and S. R. Voss, *Experimental Cell Research*, 2020, **394**, 112149.
69. J. A. Marwick, R. Mills, O. Kay, K. Michail, J. Stephen, A. G. Rossi, I. Dransfield and N. Hirani, *Cell Death & Disease*, 2018, **9**.
70. H. B. Li, X. Y. Wei, L. Zhou, W. Q. Zhang, C. Wang, Y. Guo, D. H. Li, J. Y. Chen, T. B. Liu, Y. Y. Zhang, S. Ma, C. Y. Wang, F. J. Tan, J. S. Xu, Y. Liu, Y. Yuan, L. Chen, Q. R. Wang, J. Qu, Y. Shen, S. S. Liu, G. Y. Fan, L. Q. Liu, X. Liu, Y. Hou, G. H. Liu, Y. Gu and X. Xu, *Protein & Cell*, 2021, **12**, 57-66.
71. J. W. Godwin, A. R. Pinto and N. A. Rosenthal, *Proceedings of the National Academy of Sciences of the United States of America*, 2013, **110**, 9415-9420.
72. A. Satoh, A. Hirata and A. Makanae, *Zoological Science*, 2012, **29**, 191-197.
73. A. Q. Phan, J. Lee, M. Oei, C. Flath, C. Hwe, R. Mariano, T. Vu, C. Shu, A. Dinh, J. Simkin, K. Muneoka, S. V. Bryant and D. M. Gardiner, *Regeneration*, 2015, **2**, 182-201.
74. T. Demircan, A. E. Ilhan, N. Ayturk, B. Yildirim, G. Ozturk and I. Keskin, *Acta Histochem*, 2016, **118**, 746-759.
75. R. Kashimoto, S. Furukawa, S. Yamamoto, Y. Kamei, J. Sakamoto, S. Nonaka, T. M. Watanabe, T. Sakamoto, H. Sakamoto and A. Satoh, *iScience*, 2022, **25**, 104524.
76. J. O. Brant, J. L. Boatwright, R. Davenport, A. G. W. Sandoval, M. Maden and W. B. Barbazuk, *PLoS One*, 2019, **14**, e0216228.
77. J. R. Monaghan, L. G. Epp, S. Putta, R. B. Page, J. A. Walker, C. K. Beachy, W. Zhu, G. M. Pao, I. M. Verma, T. Hunter, S. V. Bryant, D. M. Gardiner, T. T. Harkins and S. R. Voss, *BMC Biol*, 2009, **7**, 1-19.
78. C. H. Wu, M. H. Tsai, C. C. Ho, C. Y. Chen and H. S. Lee, *BMC Genomics*, 2013, **14**.
79. J. R. Monaghan, A. Athippozhy, A. W. Seifert, S. Putta, A. J. Stromberg, M. Maden, D. M. Gardiner and S. R. Voss, *Biology Open*, 2012, **1**, 937-948.
80. R. Stewart, C. A. Rascon, S. L. Tian, J. Nie, C. Barry, L. F. Chu, H. Ardalani, R. J. Wagner, M. D. Probasco, J. M. Bolin, N. Leng, S. Sengupta, M. Volkmer, B. Habermann, E. M. Tanaka, J. A. Thomson and C. N. Dewey, *Plos Computational Biology*, 2013, **9**, e100293.
81. R. V. Iozzo and L. Schaefer, *Matrix Biol*, 2015, **42**, 11-55.
82. F. Kubaski, H. Osago, R. W. Mason, S. Yamaguchi, H. Kobayashi, M. Tsuchiya, T. Orii and S. Tomatsu, *Mol Genet Metab*, 2017, **120**, 67-77.
83. S. Heath, Y. Han, R. Hua, A. Roy, J. Jiang, J. S. Nyman and X. Wang, *Bone*, 2023, **171**, 116751.
84. M. Grabarics, M. Lettow, C. Kirschbaum, K. Greis, C. Manz and K. Pagel, *Chem Rev*, 2022, **122**, 7840-7908.
85. P. J. E. Uijtdewilligen, E. M. Versteeg, E. M. A. van de Westerlo, J. van der Vlag, W. F. Daamen and T. H. van Kuppevelt, *Biomed Res Int*, 2018, **2018**, 9873471.

86. T. R. Gawriluk, J. Simkin, C. K. Hacker, J. M. Kimani, S. G. Kiama, V. O. Ezenwa and A. W. Seifert, *Front Immunol*, 2020, **11**, 1695.
87. M. C. McCabe, L. R. Schmitt, R. C. Hill, M. Dzieciatkowska, M. Maslanka, W. F. Daamen, T. H. van Kuppevelt, D. J. Hof and K. C. Hansen, *Mol Cell Proteomics*, 2021, **20**, 100079.
88. S. Owlarn, F. Klenner, D. Schmidt, F. Rabert, A. Tomasso, H. Reuter, M. A. Mulaw, S. Moritz, L. Gentile, G. Weidinger and K. Bartscherer, *Nat Commun*, 2017, **8**, 2282.
89. W. A. Vieira, K. M. Wells and C. D. McCusker, *Gerontology*, 2020, **66**, 212-222.
90. N. J. Murugan, H. J. Vigran, K. A. Miller, A. Golding, Q. L. Pham, M. M. Sperry, C. Rasmussen-Ivey, A. W. Kane, D. L. Kaplan and M. Levin, *Sci Adv*, 2022, **8**, eabj2164.
91. T. Pihlajaniemi, R. Myllyla and K. I. Kivirikko, *J Hepatol*, 1991, **13 Suppl 3**, S2-7.
92. S. Bathina and U. N. Das, *Arch Med Sci*, 2015, **11**, 1164-1178.
93. C. E. McGregor and A. W. English, *Front Cell Neurosci*, 2018, **12**, 522.
94. I. S. Thorey, B. Hinz, A. Hoeflich, S. Kaesler, P. Bugnon, M. Elmlinger, R. Wanke, E. Wolf and S. Werner, *J Biol Chem*, 2004, **279**, 26674-26684.
95. H. W. Chun, J. Lee, T. H. Pham, J. Lee, J. H. Yoon, J. Lee, D. K. Oh, J. Oh and D. Y. Yoon, *J Microbiol Biotechnol*, 2020, **30**, 85-92.
96. J. Hellmann, B. E. Sansbury, B. Wong, X. Li, M. Singh, K. Nuutila, N. Chiang, E. Eriksson, C. N. Serhan and M. Spite, *J Invest Dermatol*, 2018, **138**, 2051-2060.
97. L. J. Gudas, *Biochim Biophys Acta*, 2012, **1821**, 213-221.
98. M. E. Polcz and A. Barbul, *Nutr Clin Pract*, 2019, **34**, 695-700.
99. C. Oostendorp, P. J. Geutjes, F. Smit, D. M. Tiemessen, S. Polman, A. Abbawi, K. M. Brouwer, A. J. Eggink, W. F. J. Feitz, W. F. Daamen and T. H. van Kuppevelt, *Tissue Eng Part A*, 2020, **27**, 10-25.
100. A. Tomasso, K. Bartscherer and A. W. Seifert, *bioRxiv*, 2022, DOI: 10.1101/2022.06.27.497314, 2022.2006.2027.497314.
101. E. K. Oktem, M. Yazar, G. Gulfidan and K. Y. Arga, *OMICS*, 2019, **23**, 389-405.
102. N. Suzuki and H. Ochi, *Dev Growth Differ*, 2020, **62**, 343-354.
103. J. R. Erickson, M. D. Gearhart, D. D. Honson, T. A. Reid, M. K. Gardner, B. S. Moriarity and K. Echeverri, *Npj Regenerative Medicine*, 2016, **1**, 16016.
104. A. Conesa, P. Madrigal, S. Tarazona, D. Gomez-Cabrero, A. Cervera, A. McPherson, M. W. Szczesniak, D. J. Gaffney, L. L. Elo, X. Zhang and A. Mortazavi, *Genome Biol*, 2016, **17**, 13.
105. A. Conesa, P. Madrigal, S. Tarazona, D. Gomez-Cabrero, A. Cervera, A. McPherson, M. W. Szczesniak, D. J. Gaffney, L. L. Elo, X. Zhang and A. Mortazavi, *Genome Biol*, 2016, **17**, 181.
106. A. Stupnikov, C. E. McInerney, K. I. Savage, S. A. McIntosh, F. Emmert-Streib, R. Kennedy, M. Salto-Tellez, K. M. Prise and D. G. McArt, *Comput Struct Biotechnol J*, 2021, **19**, 3470-3481.
107. M. Litwiniuk, A. Krejner, M. S. Speyrer, A. R. Gauto and T. Grzela, *Wounds*, 2016, **28**, 78-88.
108. L. Zambrano, E. Vega, L. G. Herrera, E. Prado and V. H. Reynoso, *Animal Conservation*, 2007, **10**, 297-303.
109. F. X. Maquart and J. C. Monboisse, *Pathol Biol (Paris)*, 2014, **62**, 91-95.
110. R. Chiquet-Ehrismann and R. P. Tucker, *Cold Spring Harb Perspect Biol*, 2011, **3**, a004960.
111. D. J. Donaldson, J. T. Mahan, H. Yang and K. L. Crossin, *Anat Rec*, 1991, **230**, 451-459.
112. T. Y. Huang, C. H. Wu, M. H. Wang, B. S. Chen, L. L. Chiou and H. S. Lee, *Biomed Research International*, 2015, **2015**, 1-10.
113. K. S. Midwood and G. Orend, *Journal of Cell Communication and Signaling*, 2009, **3**, 287-310.

114. S. Calve, S. J. Odelberg and H. G. Simon, *Developmental Biology*, 2010, **344**, 259-271.
115. S. E. Mercer, C. H. Cheng, D. L. Atkinson, J. Krcmery, C. E. Guzman, D. T. Kent, K. Zukor, K. A. Marx, S. J. Odelberg and H. G. Simon, *PLoS One*, 2012, **7**, e52375.
116. J. Govindan and M. K. Iovine, *Gene Expr Patterns*, 2015, **19**, 21-29.
117. Y. E. Choi, M. J. Song, M. Hara, K. Imanaka-Yoshida, D. H. Lee, J. H. Chung and S. T. Lee, *International Journal of Molecular Sciences*, 2020, **21**, 8693.
118. E. Makogonenko, G. Tsurupa, K. Ingham and L. Medved, *Biochemistry*, 2002, **41**, 7907-7913.
119. C. P. Jara, O. Wang, T. Paulino do Prado, A. Ismail, F. M. Fabian, H. Li, L. A. Velloso, M. A. Carlson, W. Burgess, Y. Lei, W. H. Velander and E. P. Araujo, *Bioact Mater*, 2020, **5**, 949-962.
120. P. Wang, Z. Hu, X. Cao, S. Huang, Y. Dong, P. Cheng, H. Xu, B. Shu, J. Xie, J. Wu, B. Tang and J. Zhu, *Stem Cell Res Ther*, 2019, **10**, 154.
121. J. A. Paten, C. L. Martin, J. T. Wanis, S. M. Siadat, A. M. Figueroa-Navedo, J. W. Ruberti and L. F. Deravi, *Chem-Us*, 2019, **5**, 2126-2145.
122. K. E. Kubow, R. Vukmirovic, L. Zhe, E. Klotzsch, M. L. Smith, D. Gourdon, S. Luna and V. Vogel, *Nat Commun*, 2015, **6**, 8026.
123. J. Patten and K. Wang, *Adv Drug Deliv Rev*, 2021, **170**, 353-368.
124. V. Iorio, L. D. Troughton and K. J. Hamill, *Adv Wound Care (New Rochelle)*, 2015, **4**, 250-263.
125. J. Ishihara, A. Ishihara, K. Fukunaga, K. Sasaki, M. J. V. White, P. S. Briquez and J. A. Hubbell, *Nat Commun*, 2018, **9**, 2163.
126. Z. Peterfi, A. Donko, A. Orient, A. Sum, A. Prokai, B. Molnar, Z. Vereb, E. Rajnavolgyi, K. J. Kovacs, V. Muller, A. J. Szabo and M. Geiszt, *Am J Pathol*, 2009, **175**, 725-735.
127. Z. Peterfi and M. Geiszt, *Trends Biochem Sci*, 2014, **39**, 305-307.
128. G. Bhave, C. F. Cummings, R. M. Vanacore, C. Kumagai-Cresse, I. A. Ero-Tolliver, M. Rafi, J. S. Kang, V. Pedchenko, L. I. Fessler, J. H. Fessler and B. G. Hudson, *Nat Chem Biol*, 2012, **8**, 784-790.
129. E. Lazar, Z. Peterfi, G. Sirokmany, H. A. Kovacs, E. Klement, K. F. Medzihradszky and M. Geiszt, *Free Radic Biol Med*, 2015, **83**, 273-282.
130. S. W. Lee, H. K. Kim, P. Naidansuren, K. A. Ham, H. S. Choi, H. Y. Ahn, M. Kim, D. H. Kang, S. W. Kang and Y. A. Joe, *FASEB J*, 2020, **34**, 10228-10241.
131. N. Esemuede, T. Lee, D. Pierre-Paul, B. E. Sumpio and V. Gahtan, *J Surg Res*, 2004, **122**, 135-142.
132. L. A. DiPietro, N. N. Nissen, R. L. Gamelli, A. E. Koch, J. M. Pyle and P. J. Polverini, *Am J Pathol*, 1996, **148**, 1851-1860.
133. S. Rosini, N. Pugh, A. M. Bonna, D. J. S. Hulmes, R. W. Farndale and J. C. Adams, *Sci Signal*, 2018, **11**, eaar2566.
134. N. E. Calabro, N. J. Kristofik and T. R. Kyriakides, *Biochim Biophys Acta*, 2014, **1840**, 2396-2402.
135. P. Bornstein, T. R. Kyriakides, Z. Yang, L. C. Armstrong and D. E. Birk, *J Investig Dermatol Symp Proc*, 2000, **5**, 61-66.
136. T. Durmus, R. J. LeClair, K. S. Park, A. Terzic, J. K. Yoon and V. Lindner, *Gene Expr Patterns*, 2006, **6**, 935-940.
137. M. T. Shekhani, T. S. Forde, A. Adilbayeva, M. Ramez, A. Myngbay, Y. Bexeitov, V. Lindner and V. A. Adarichev, *Arthritis Res Ther*, 2016, **18**, 171.
138. J. Li, J. Cao, M. Li, Y. Yu, Y. Yang, X. Xiao, Z. Wu, L. Wang, Y. Tu and H. Chen, *Br J Dermatol*, 2011, **164**, 1030-1036.
139. Z. Shen, T. Su, J. Chen, Z. Xie and J. Li, *Ann Transl Med*, 2021, **9**, 801.

140. K. Nuutila, A. Siltanen, M. Peura, J. Bizik, I. Kaartinen, H. Kuokkanen, T. Nieminen, A. Harjula, P. Aarnio, J. Vuola and E. Kankuri, *Wound Repair Regen*, 2012, **20**, 830-839.
141. T. Y. Huang, L. L. Zuo, S. K. Walczynska, M. Y. Zhu and Y. J. Liang, *Cell and Tissue Research*, 2021, **385**, 105-113.
142. M. J. Toriseva, R. Ala-aho, J. Karvinen, A. H. Baker, V. S. Marjomaki, J. Heino and V. M. Kahari, *J Invest Dermatol*, 2007, **127**, 49-59.
143. M. P. Vincenti, *Methods Mol Biol*, 2001, **151**, 121-148.
144. D. Ulrich, E. M. Noah, D. von Heimburg and N. Pallua, *Plast Reconstr Surg*, 2003, **111**, 1423-1431.
145. T. J. Stevenson, V. Vinarsky, D. L. Atkinson, M. T. Keating and S. J. Odelberg, *Dev Dyn*, 2006, **235**, 606-616.
146. H. Ogawa, E. Kozhemyakina, H. H. Hung, A. J. Grodzinsky and A. B. Lassar, *Genes & Development*, 2014, **28**, 127-139.
147. Y. Lee, J. Choi and N. S. Hwang, *Biomaterials Research*, 2018, **22**, 9.
148. M. Qadri, G. D. Jay, L. X. Zhang, H. Richendrfer, T. A. Schmidt and K. A. Elsaid, *Arthritis Res Ther*, 2020, **22**, 113.
149. R. J. Krawetz, S. Abubacker, C. Leonard, A. O. Masson, S. Shah, N. Narendran, P. Tailor, S. C. Regmi, E. Labit, N. Ninkovic, J. M. Corpuz, K. Ito, T. M. Underhill, P. T. Salo, T. A. Schmidt and J. A. Biernaskie, *NPJ Regen Med*, 2022, **7**, 32.
150. E. Ronnberg and G. Pejler, *Proteoglycans: Methods and Protocols*, 2012, **836**, 201-217.
151. S. O. Kolset and G. Pejler, *J Immunol*, 2011, **187**, 4927-4933.
152. M. Tellez-Gabriel, X. Tekpli, T. M. Reine, B. Hegge, S. R. Nielsen, M. Chen, L. Moi, L. S. Normann, L. R. Busund, G. A. Calin, G. M. Mælandsmo, M. Perander, A. D. Theocharis, S. O. Kolset and E. Knutsen, *Front Oncol*, 2022, **12**, 868868.
153. D. J. Tyrrell, A. P. Horne, K. R. Holme, J. M. Preuss and C. P. Page, *Adv Pharmacol*, 1999, **46**, 151-208.
154. R. Serra, G. Buffone, V. Molinari, R. Montemurro, P. Perri, D. M. Stillitano, B. Amato and S. de Franciscis, *Int Wound J*, 2015, **12**, 150-153.
155. C. Y. Huang and M. Y. Choong, *Int Wound J*, 2017, **14**, 589-590.
156. B. Caterson and J. Melrose, *Glycobiology*, 2018, **28**, 182-206.
157. B. N. Cook, S. Bhakta, T. Biegel, K. G. Bowman, J. I. Armstrong, S. Hemmerich and C. R. Bertozzi, *Journal of the American Chemical Society*, 2000, **122**, 8612-8622.
158. X. Li, L. Tu, P. G. Murphy, T. Kadono, D. A. Steeber and T. F. Tedder, *J Leukoc Biol*, 2001, **69**, 565-574.
159. M. Kluppel, *Prog Mol Biol Transl*, 2010, **93**, 113-132.
160. M. Kluppel, P. Samavarchi-Tehrani, K. Liu, J. L. Wrana and A. Hinek, *Eur J Hum Genet*, 2012, **20**, 870-877.
161. X. H. Zou, W. C. Foong, T. Cao, B. H. Bay, H. W. Ouyang and G. W. Yip, *J Dent Res*, 2004, **83**, 880-885.
162. I. Maltseva, M. Chan, I. Kalus, T. Dierks and S. D. Rosen, *PLoS One*, 2013, **8**, e69642.
163. Y. H. Wang and C. Beck, *Regeneration (Oxf)*, 2015, **2**, 19-25.
164. C. Lanzi and G. Cassinelli, *Biochem Pharmacol*, 2020, **178**, 114084.
165. D. Papy-Garcia and P. Albanese, *Glycoconj J*, 2017, **34**, 377-391.
166. G. Theocharidis and J. T. Connelly, *J Anat*, 2019, **235**, 418-429.
167. K. E. Keller, M. J. Kelley and T. S. Acott, *Investigative Ophthalmology & Visual Science*, 2007, **48**, 1164-1172.

168. S. Delbaere, T. Dhooge, D. Syx, F. Petit, N. Goemans, A. Destree, O. Vanakker, R. De Rycke, S. Symoens and F. Malfait, *Genet Med*, 2020, **22**, 112-123.

169. K. Schonborn, S. Willenborg, J. N. Schulz, T. Imhof, S. A. Eming, F. Quondamatteo, J. Brinckmann, A. Niehoff, M. Paulsson, M. Koch, B. Eckes and T. Krieg, *Matrix Biology*, 2020, **94**, 57-76.

170. D. N. Phan, M. Q. Khan, N. T. Nguyen, T. T. Phan, A. Ullah, M. Khatri, N. N. Kien and I. S. Kim, *Carbohydr Polym*, 2021, **252**, 117175.

171. S. Ullah and X. Chen, *Applied Materials Today*, 2020, **20**, 100656.

172. M. Brovold, J. I. Almeida, I. Pla-Palacin, P. Sainz-Arnal, N. Sanchez-Romero, J. J. Rivas, H. Almeida, P. R. Dachary, T. Serrano-Aullo, S. Soker and P. M. Baptista, *Adv Exp Med Biol*, 2018, **1077**, 421-449.

173. J. Y. Park, T. G. Lee, J. Y. Kim, M. C. Lee, Y. K. Chung and W. J. Lee, *Arch Craniofac Surg*, 2014, **15**, 14-21.

174. Y. Yu, H. Cui, C. Zhang, D. Zhang, J. Yin, G. Wen and Y. Chai, *J Mater Chem B*, 2020, **8**, 4067-4079.

175. Y. Yu, H. Cui, D. Zhang, B. Liang, Y. Chai and G. Wen, *J Tissue Eng Regen Med*, 2019, **13**, 1770-1778.

176. G. BaoLin and P. X. Ma, *Sci China Chem*, 2014, **57**, 490-500.

177. A. Varki, *Glycobiology*, 2017, **27**, 3-49.

178. E. V. Maytin, *Glycobiology*, 2016, **26**, 553-559.

179. S. T. Nillesen, G. Lammers, R. G. Wismans, M. M. Ulrich, E. Middelkoop, P. H. Spauwen, K. A. Faraj, J. Schalkwijk, W. F. Daamen and T. H. van Kuppevelt, *Acta Biomater*, 2011, **7**, 1063-1071.

180. V. Rouet, A. Meddahi-Pelle, H. Q. Miao, I. Vlodavsky, J. P. Caruelle and D. Barritault, *J Biomed Mater Res A*, 2006, **78**, 792-797.

181. M. Tong, M. M. Zbinden, I. J. Hekking, M. Vermeij, D. Barritault and J. W. van Neck, *Wound Repair Regen*, 2008, **16**, 294-299.

182. M. Tong, B. Tuk, I. M. Hekking, M. Vermeij, D. Barritault and J. W. van Neck, *Wound Repair Regen*, 2009, **17**, 840-852.

183. P. Chopra, M. T. Logun, E. M. White, W. Lu, J. Locklin, L. Karumbaiah and G. J. Boons, *ACS Chem Biol*, 2019, **14**, 1921-1929.

184. W. Lu, C. Zong, P. Chopra, L. E. Pepi, Y. Xu, I. J. Amster, J. Liu and G. J. Boons, *Angew Chem Int Ed Engl*, 2018, **57**, 5340-5344.

185. T. J. Boltje, T. Buskas and G. J. Boons, *Nat Chem*, 2009, **1**, 611-622.

186. D. Xu, K. Arnold and J. Liu, *Curr Opin Struct Biol*, 2018, **50**, 155-161.

187. A. S. Barrett, M. J. Wither, R. C. Hill, M. Dzieciatkowska, A. D'Alessandro, J. A. Reisz and K. C. Hansen, *J Proteome Res*, 2017, **16**, 4177-4184.

188. K. A. Brown, T. Tucholski, C. Eken, S. Knott, Y. Zhu, S. Jin and Y. Ge, *Angew Chem Int Ed Engl*, 2020, **59**, 8406-8410.

189. S. J. Knott, K. A. Brown, H. Josyer, A. Carr, D. Inman, S. Jin, A. Friedl, S. M. Ponik and Y. Ge, *Anal Chem*, 2020, **92**, 15693-15698.

190. X. H. Shao, C. D. Gomez, N. Kapoor, J. M. Considine, C. Grams, Y. Gao and A. Naba, *Nucleic Acids Research*, DOI: 10.1093/nar/gkac1009.

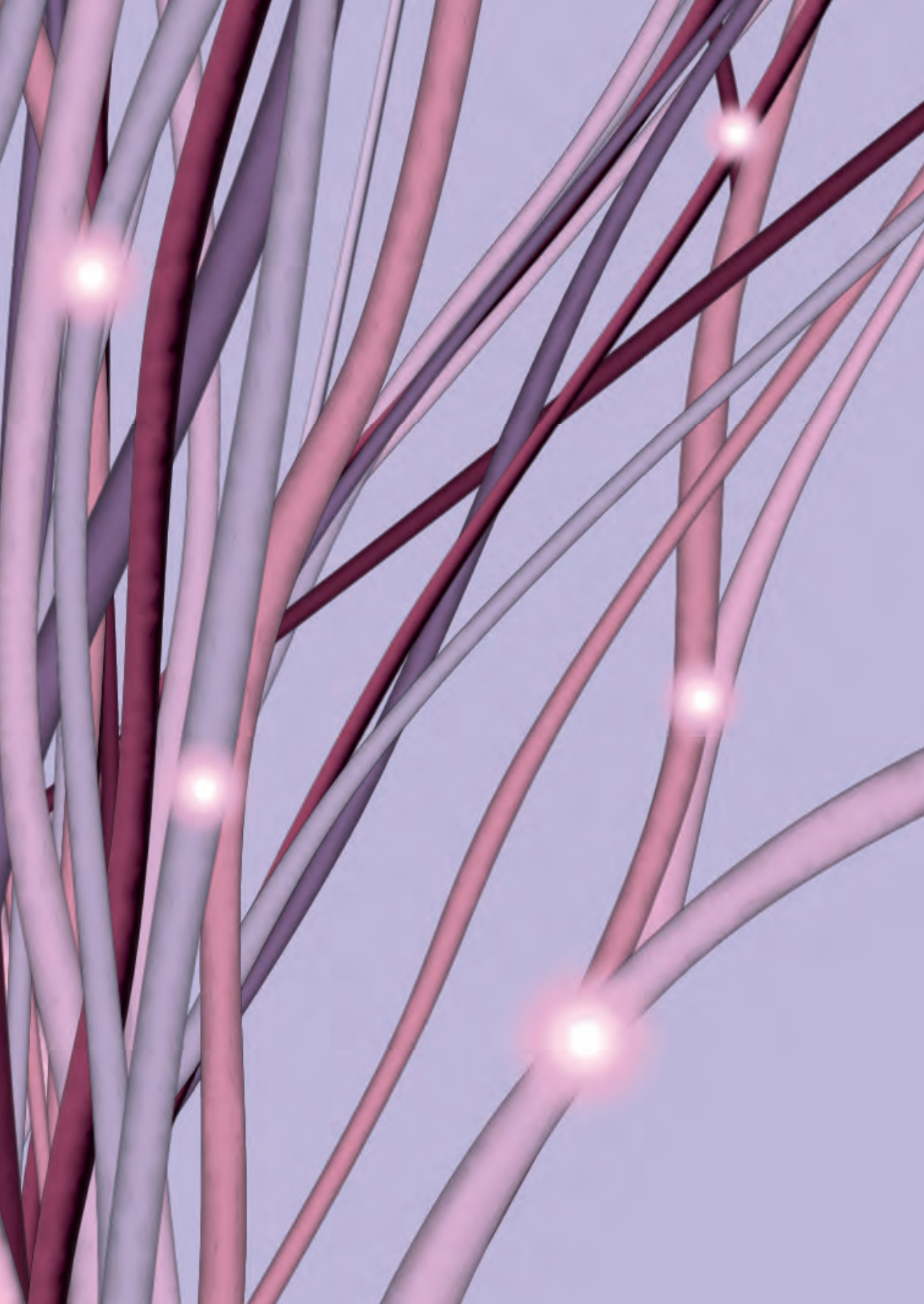

Chapter 3

Effect of Hyaluronan in Collagen Biomaterials on Human Macrophages and Fibroblasts *In Vitro*

Nancy Avila-Martinez [1], Maren Pfirrmann [1], Madalena L. N. P. Gomes [2,3,4,5], Roman Krymchenko [1], Elly M. M. Versteeg [1], Marcel Vlig [5], Martijn Verdoes [1,6], Toin H. van Kuppevelt [1], Bouke K. H. L. Boekema [3,4,5] and Willeke F. Daamen [1]

[1] Department of Medical BioSciences, Research Institute for Medical Innovation, Radboud university medical center, 6525 GA Nijmegen, The Netherlands

[2] Department of Pathology, Amsterdam University Medical Center (AUMC), Location AMC, 1081 HV Amsterdam, The Netherlands

[3] Tissue Function and Regeneration, Amsterdam Movement Sciences Research Institute, 1081 HV Amsterdam, The Netherlands

[4] Department of Plastic, Reconstructive and Hand Surgery, Amsterdam University Medical Center (AUMC), Location AMC, 1081 HV Amsterdam, The Netherlands

[5] Alliance of Dutch Burn Care, Burn Research Lab, 1941 AJ Beverwijk, The Netherlands

[6] Department of Immunology, Leiden University Medical Center (LUMC), 2333 ZA Leiden, The Netherlands

J Funct Biomat. 2025;16(5)-167. Doi: 10.3390/jfb16050167

Abstract

In adults, scars are formed after deep skin wound injuries like burns. However, the fetal microenvironment allows for scarless skin regeneration. One component that is abundantly present in the fetal extracellular matrix is hyaluronan (HA). To study whether biomaterials with HA improve wound healing, type I collagen scaffolds with and without HA were prepared and characterized. Their immune effect was tested using macrophages and their phenotypes were analyzed through cell surface markers and cytokine expression after 48 h. Since fibroblasts are the main cellular component in the dermis, adult, fetal and eschar-derived cells were cultured on scaffolds for 14 days and evaluated using histology, gene and protein expression analyses. Biochemical assays demonstrated that HA was successfully incorporated and evenly distributed throughout the scaffolds. Macrophages (M0) cultured on Col I+HA scaffolds exhibited a profile resembling the M2c-like phenotype (CD206^{high}, CD163^{high} and IL10^{high}). HA did not significantly affect gene expression in adult and fetal fibroblasts, but significantly reduced scarring-related genes, such as transforming growth factor beta 1 (TGFB1) and type X collagen alpha 1 chain (COL10A1), in myofibroblast-like eschar cells. These findings highlight the potential of incorporating HA into collagen-based skin substitutes to improve the wound healing response.

Keywords: hyaluronic acid; scaffolds; skin regeneration; dermal; fetal; eschar

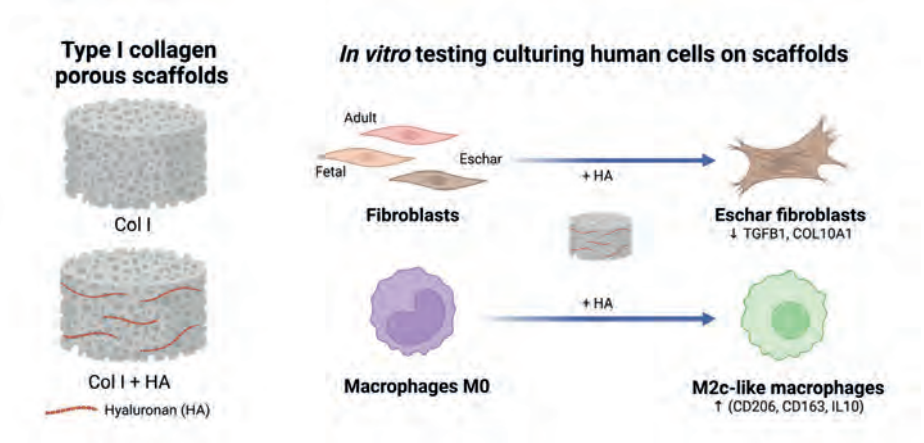

1. Introduction

Effective skin wound healing is vital for quality of life but remains a significant global medical challenge [1]. Standard care for full-thickness burns includes autologous split-thickness skin grafting, which replaces the epidermis and part of the dermis [2]. Biocompatible skin substitutes, particularly natural biomaterials like collagen, emerged in the wound care market as they support dermal restoration. From the premise that fetal wounds can heal without scars, researchers have widely explored hyaluronan, an abundant component of the fetal extracellular matrix [3–5].

Hyaluronan (HA), also known in its protonated form as hyaluronic acid, is a non-sulfated glycosaminoglycan that carries a significant overall negative charge and contains carboxylate and acetamido functional groups [6]. HA has a remarkable capacity to bind and retain water, which results in the moisturization of the dermal extracellular matrix. During the wound healing process, HA binds primarily to the CD44 receptor on the cell surface, facilitating cell adhesion and migration [7].

During hemostasis and inflammation, circulatory monocyte-derived macrophages (M0) migrate to the wound site, gradually replacing short-lived neutrophils [8]. Macrophages serve as important regulators as they can polarize into M1-type macrophages, which secrete pro-inflammatory cytokines during proliferation. A persistent response from this phenotype might lead to more scarring. M1s are later replaced by M2-type macrophages, which release anti-inflammatory/pro-healing cytokines in the remodeling stage, making them key targets for improving wound healing outcomes [9]. Macrophages have a high CD44 expression and play a major role in HA uptake and degradation, where the M1-like subtype favors HA binding and the M2-like subtype shows improved HA internalization [10].

Fibroblasts are important cells in the proliferation and remodeling phases of wound healing, but their behavior depends on the life stage of the patient and their cellular origin. For instance, adult fibroblasts showed a four times lower CD44 expression compared to their fetal equivalent [11]. Additionally, adult wounds showed increased transforming growth factor beta 1 (TGFβ1) expression, with low levels of TGFβ3, whereas an opposite pattern was observed in fetal wounds [12]. The role of cellular origin is exemplified by adult eschar fibroblasts obtained from burnt tissue after debridement. These eschar fibroblasts have been associated with a myofibroblast-like phenotype due their expression of alpha smooth muscle actin (α-SMA) and ability to contract collagen scaffolds in vitro [13].

Several studies have indicated the benefits of using HA in wound dressings and its effect on skin cells, such as dermal fibroblasts and macrophages [14,15]. While commercial HA-based products are mainly available in cream or gel form, porous sponges offer distinct advantages, especially for full-thickness wounds, such as a larger surface area for cell attachment [16,17]. In this study, HA was chemically crosslinked to porous collagen scaffolds and compared to bare collagen scaffolds to evaluate the effect of HA addition on primary cells, such as on macrophage polarization, as well as on particular fibrotic gene expression levels in fetal, healthy adult and adult eschar fibroblasts.

2. Materials and Methods

2.1. Preparation and Characterization of Type I Collagen Scaffolds with Hyaluronan

Porous collagen scaffolds (Col I) were prepared by adding 0.8% (*w/v*) collagen fibrils from bovine tendon, obtained from a slaughterhouse, to 0.25 M acetic acid and swelling overnight at 4 °C under constant agitation. For collagen scaffolds with hyaluronan (Col I+HA), 0.05% (*w/v*) hyaluronic acid sodium salt from *Streptococcus equi* (Sigma-Aldrich, St. Louis, MO, USA) was dissolved in 0.25 M acetic acid, and 0.8% (*w/v*) type I collagen fibrils were added. The suspension was mixed, swollen overnight at 4 °C, homogenized, poured into molds (4 mL suspension/960 mm^2, 6-well plate) and lyophilized using a Lyoph-pride 03 freeze dryer (ilShin Biobase Europe, Ede, The Netherlands). Scaffolds were chemically crosslinked for 3 h using 33 mM 1-ethyl-3-dimethyl aminopropyl carbodiimide (EDC) and 6 mM N-hydroxysuccinimide (NHS) in 50 mM 2-morpholinoethane sulphonic acid buffer (Sigma-Aldrich) containing 40% ethanol (Merck, Darmstadt, Germany) at pH 5.0 (MES buffer) (8 mg scaffold/mL crosslinking solution). Non-crosslinked control scaffolds were treated similarly, but without EDC/NHS. Scaffolds were washed in 0.1 M Na_2HPO_4 (2 × 1 h), 1 M NaCl (2 × 30 min), 2 M NaCl (2 × 30 min) and demineralized water until their conductivity was less than 200 µS, and lyophilized. Scaffolds were cut to ∅12 mm for in vitro studies.

The morphology of the scaffolds was analyzed using scanning electron microscopy (SEM). Dry scaffolds were fixed on a stub with double-sided carbon tape, sputtered with gold twice for 60 s using an Edwards Scancoat Six Sputter Coater (Crawley, UK) and examined with a Zeiss Sigma 300 Field Emission Scanning Electron Microscope (Jena, Germany) at an accelerating voltage of 3 kV.

For HA localization, frozen scaffolds in TissueTek O.C.T. compound (Sakura Finetek, Alphen aan den Rijn, The Netherlands) were cut to 7 µm sections and mounted on Superfrost™ plus adhesion microscope slides (Epredia, Kalamazoo, MI, USA). After 10 min fixation in 4% paraformaldehyde in phosphate-buffered saline (PBS), sections were blocked with PBS containing 0.5% bovine serum albumin (BSA, fraction V, Roche, Basel, CH) and stained with biotinylated HA binding protein (400763-1A, Seikagaku, Japan), 1:200 diluted in 0.5% BSA in PBS. The signal was amplified by incubating the sample with the Vectastain avidin/biotin ABC complex HRP kit (PK-4000, Vector Laboratories, Newark, CA, USA) for 1 h. Finally, ImmPACT AEC (3-amino-9-ethylcarbazole) was added to produce a red reaction product over 15 min, followed by rinsing with water for 5 min. The sections were mounted with a cover glass using VectorMount® AQ Aquos Mounting Medium (H-5501, Vector Laboratories).

The degree of crosslinking was determined by the loss of primary amine groups after crosslinking using 2,4,6-trinitrobenzene sulfonic acid (TNBS) [18]. Briefly, scaffolds before and after crosslinking were incubated in 4% $NaHCO_3$, left to react with 0.08% (*w*/*v*) TNBS for 2 h at 40 °C and hydrolyzed in 6 M HCl for 1.5 h at 60 °C. Glycine was used for the calibration curve. The absorbances were measured at 420 nm using a SpectraMax iD3 spectrophotometer (Molecular Devices, San Jose, CA, USA).

The HA content in the scaffolds was measured using the Stains-All colorimetric assay using a carbocyanine dye suitable for staining HA (Sigma-Aldrich). Scaffolds were digested overnight at 65 °C using 2.5 U/mL papain (P3125, Merck), 2 mM EDTA and 2 mM cysteine in 50 mM sodium phosphate (pH 6.5). A staining solution, containing 0.0056% (*w*/*v*) Stains-All dissolved in 5% (*v*/*v*) isopropanol (Merck), 5% (*v*/*v*) 0.01 M ascorbic acid (Sigma-Aldrich) and 0.2% (*v*/*v*) 1 M acetic acid (Merck) in demineralized water, was added to the digested samples alongside a calibration curve of HA, and the absorbances were measured at 650 nm.

The molecular weight of the incorporated HA in the scaffolds was estimated using agarose gel electrophoresis. Briefly, 1% LE agarose (SeaKem, Lonza, Rockland, ME, USA) was dissolved in TAE buffer (40 mM Tris, 20 mM acetic acid, 1 mM EDTA, pH 8.0), heated and poured into a tray. Papain-digested collagen scaffolds with and without HA (as described in HA quantification), along with undigested HA and papain-digested HA, were loaded on the gel, and Smart Ladder (MW-1700-10, Eurogentec, Seraing, Belgium) and Lambda DNA/Hind III marker (G171A, Promega, Madison, WI, USA) were used as the molecular weight standards. Their base pair size was converted to molecular weight (MW) size using bioline.com to assess HA

size in the gel. The gel was run for ~2 h at 50 V and was fixed for 2 × 1 h in 25% (*v*/*v*) isopropanol and 10% (*v*/*v*) acetic acid in demineralized water. The gel was stained overnight in the dark under constant agitation with 0.01% (*w*/*v*) Stains-All, 7.5% (*v*/*v*) formamide and 25% (*v*/*v*) isopropanol in 4 mM Tris pH 8.8 and destained with 25% isopropanol for two days, changing the solution four times. The gel was scanned using the Gel Doc XR+ Imaging System (Bio-Rad, Hercules, CA, USA).

For the differential scanning calorimetry assay (DSC), approximately 1 mg of sample was placed in T_{zero} pans (TA Instruments, New Castle, DE, USA), which were tightly sealed with T_{zero} hermetic lids, and heated from 1 to 220 °C at a scanning rate of 5 °C/min using a TA Q1000 DSC (TA Instruments, New Castle, DE, USA) equipped with a RCS40 cooler with Universal Analysis software version 5.5.24. T_{onset} was selected to detect the denaturation temperature of the collagen peaks [19].

2.2. Macrophage Culture and Analysis

Peripheral blood mononuclear cells (PBMCs) were isolated from buffy coats from three healthy donors (Sanquin, Nijmegen, NL). Informed consent was given in accordance with the Declaration of Helsinki and the Dutch national and Sanquin internal ethics boards. Monocytes were isolated using $CD14^+$ MACS MicroBeads (130-050-201, Miltenyi Biotech, Teterow, Germany) following the manufacturer's protocol. Monocytes were plated in T75 flasks (10^6 cells in 10 mL for M0 differentiation and 0.5×10^6 cells for M1/M2 differentiation) in RPMI 1640 (including HEPES, Gibco by Thermo Fisher Scientific, Grand Island, NY, USA), 10% fetal bovine serum (FBS, Gibco), 1% stable glutamine (STA-B, Capricorn, Ebsdorfergrund, Germany) and 1% antibiotic–antimycotic (Gibco), and differentiated with 50 ng/mL macrophage colony-stimulating factor (M-CSF, 300-25, PeproTech by Thermo Scientific, Waltham, MA, USA) for 6 days to obtain monocyte-derived macrophages. The macrophages were either left unstimulated (M0 macrophages) or were stimulated for 24 h with 100 ng/mL lipopolysaccharides (LPS, vac-3pelps, InvivoGen, San Diego, CA, USA) + 20 ng/mL interferon gamma (IFNγ, 300-02, PeproTech) to polarize them to M1-like macrophages, or treated with 20 ng/mL interleukin 4 (IL4, 170-076-135, Miltenyi Biotec) + 20 ng/mL interleukin 13 (IL13, 130-112-412, Miltenyi Biotech) to polarize them to M2-like macrophages. On day 7, the cells were collected after 30 min of incubation with PBS and 2 mM EDTA. A total of 200,000 cells were seeded on each scaffold and cultured for 48 h (Figure 1). M0 macrophages were seeded on Col I and Col I+HA scaffolds to observe their polarization, while M1-like and M2-like macrophages were seeded separately in Col I scaffolds as controls.

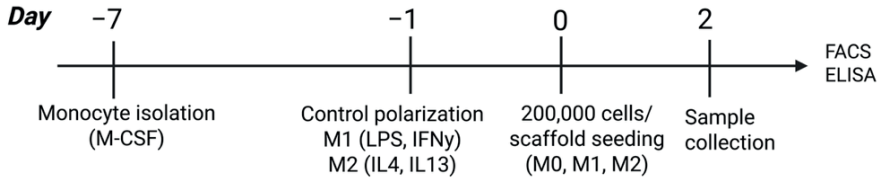

Figure 1. Timeline for macrophage culture on scaffolds. Analyses performed after two days and included fluorescence-activated cell sorting (FACS) and enzyme-linked immunoassay (ELISA). Created in BioRender. Avila, N. (2025) https://BioRender.com/i2p6ff7.

For flow cytometric analysis, cells were isolated from scaffolds by incubation with 0.25 U/mL collagenase A (10103578001, Roche, Mannheim, Germany) at 37 °C in a shaking water bath for 30 min. All the following incubations were performed at 4°C. PBS with 2 mM EDTA was added to cell-seeded scaffolds and incubated for 30 min under constant agitation, filtered using a 70 µm cell strainer (Falcon, Durham, NC, USA), centrifuged at 257 g for 10 min and transferred to a 96-well V-bottom plate for staining. Isolated cells were incubated with eFluor 780-APC+Cy7, dilution 1:2000 (65-0865-14, ThermoFisher, Carlsbad, CA, USA), for 20 min in the dark and washed with PBA (PBS +1% BSA + 0.05% NaN_3) for 25 min. CD163, CD206, CD80, MerTK, HLA-DR and PDL1 antibodies were used for labeling (Supplementary Table S1). Marker expression was measured with the BD FACSVerse Cell Analyzer flow cytometer (BD BioSciences, NJ, USA). Data analysis was performed using FlowJo X (vX 0.7, Tree STAR, Ashland, OR, USA). Cells were gated on live cells and $CD45^+$ cells, and mean fluorescence intensity (MFI) for each marker was assessed (Supplementary Figure S1).

ELISA kits for IL12 (88-7126), IL6 (88-7066) and IL10 (88-7106) (Invitrogen, ThermoFisher, Vienna, Austria) were used to measure the concentrations of cytokines in the supernatants according to the manufacturer's instructions. Supernatants from M1 control were diluted 10×. The absorptions were measured at 450 nm using the iMark™ Microplate Absorbance Reader (Bio-Rad, Basel, Switzerland).

2.3. Fibroblast Culture and Analysis

Fibroblasts were obtained from three different sources, either healthy adult skin (adult), burn wound tissue (eschar) or fetal skin (fetal), as described [20,21]. Cells were isolated from three different donors per tissue type. In total, nine donors were tested. Adult fibroblasts were isolated from healthy skin samples obtained from adult patients who underwent elective surgery at the Department of Plastic and

Reconstructive Surgery of the Red Cross Hospital (Beverwijk, NL). Eschar material was obtained from patients undergoing debridement between day 13 and 19 post-burn as part of their treatment in the Burn Center of the Red Cross Hospital. Fetal fibroblasts were isolated from fetal skin after pregnancy termination between gestational weeks 16 and 22. Fetal skin was obtained with the informed and written consent of the pregnant women from the Center for Contraception, Abortion and Sexuality (CASA, Leiden and The Hague, NL). Consent for the use of anonymized residual tissue was received through the informed opt-out protocol in accordance with national guidelines (https://www.coreon.org/, accessed on 23 November 2020) and was approved by the institutional privacy officer. Cells were cultured in fibroblast medium (FBM) including DMEM with 10% fetal bovine serum (FBS), 1% penicillin/streptomycin and 1% GlutaMAX (all from Gibco, Paisley, UK). Cells were incubated at 37 °C with 5% CO_2.

A total of 100,000 cells between passage 3 and 4 were seeded per scaffold (Col I and Col I+HA), having been pre-wetted in PBS. Seeding was performed in triplicate per donor in 24-well suspension culture plates (Cellstar, Frickenhausen, DE). Media were changed at days 3, 7 and 11. Control scaffolds without cells were treated like seeded scaffolds. On day 14, samples were collected (Figure 2). Samples were stored for different analyses in one of three ways: (1) placed in TRIzol™ reagent (Invitrogen, Waltham, MA, USA) and frozen at −80°C; (2) placed in a cryotube and frozen at −80°C; (3) placed in Kryofix solution (50% ethanol, 3% PEG300). The samples in Kryofix were embedded in paraffin, sectioned at 5 µm thickness and stained with hematoxylin and eosin (H&E). Images were visualized using Case Viewer 2.4 software.

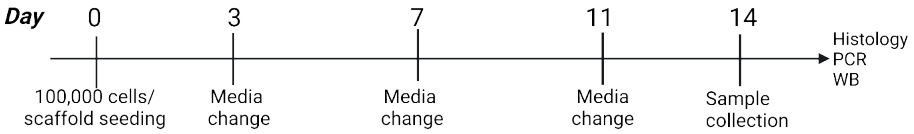

Figure 2. Timeline for fibroblast culture on scaffolds. Analyses performed on day 14 and included histology using H&E staining, real-time quantitative polymer chain reaction (PCR) and Western blotting (WB). Created in BioRender. Avila, N. (2025) https://BioRender.com/3udm9r4.

Protein expression was analyzed through Western blotting using a 10% SDS-PAGE gel from all the samples. The primary antibody anti-alpha smooth muscle actin (α-SMA) was used in dilution 1:2000 (clone 1A4, A-2547, Merck) in combination with anti-GAPDH diluted 1:1000 (clone 14C10, ID218, Cell Signaling Technology, Danvers, MA, USA). As secondary antibodies, 1:10,000-diluted goat polyclonal anti-mouse

IgG—IRDye 800CW-conjugated (LI-COR Biotechnology Inc., 926-32210, Lincoln, NE, USA)—and 1:15,000-diluted goat anti-rabbit polyclonal IgG antibodies—IRDye 680CW-conjugated (LI-COR Biotechnology, 926-32221)—were used. Blots were analyzed using Odyssey CLx (LI-COR).

The samples stored in TRIzol reagent were processed for RNA isolation. In short, scaffolds were crushed with a pipet tip and incubated for 20 min at room temperature, followed by brief centrifugation at 12,000× *g* at 4°C. The supernatant was transferred to a new tube and RNA was isolated using the RNeasy mini kit (74106, QIAGEN, Hilden, Germany) and RNase-free DNase set (79254, Qiagen). RNA yield and purity were quantified using the NanoDrop spectrophotometer (Thermos Scientific, Rockford, IL, USA). Gene expression levels were measured using reverse transcription–quantitative polymerase chain reaction (RT-qPCR), as described in Oostendorp et al. [22]. Primer sets included ACTA2, EN1, TGFB1 TGFB3, COL10A1 and COL14A1, using GAPDH and YWHAZ as reference genes (Supplementary Table S2). A normalized expression (ΔΔCq) calculation was performed according to the CFX Maestro™ software User Guide Version 1.0 (Bio-Rad), using the relative quantity of the target gene normalized to the quantities of the reference genes.

2.4. Statistical Analysis

Data were analyzed and visualized using GraphPad prism 10.4.0 (La Jolla, CA, USA). Regarding biochemical analyses, descriptive statistics and a one-way ANOVA with Tukey's multiple comparison test were used. For in vitro studies, comparisons between scaffolds and cell type groups were conducted under two-way ANOVA using Tukey's multiple comparison test, e.g., average adult vs. fetal vs. eschar in Col I and Col I+HA. For comparisons between the same donors, a paired two-tailed t test with a confidence level of 95% was used, e.g., Col I vs. Col I+HA with fetal cells (3 donors).

3. Results

3.1. Incorporation of HA in Collagen Scaffolds

Porous collagen scaffolds with and without HA were prepared and characterized. Scanning electron microscopy images revealed that the covalent binding of HA slightly impacted on the morphology of the collagen scaffolds, making the pores more compact while giving them a wavy, velvety appearance (Figure 3B). Immunohistochemical staining for HA showed an even distribution in the scaffold, thereby confirming its incorporation (Figure 3C).

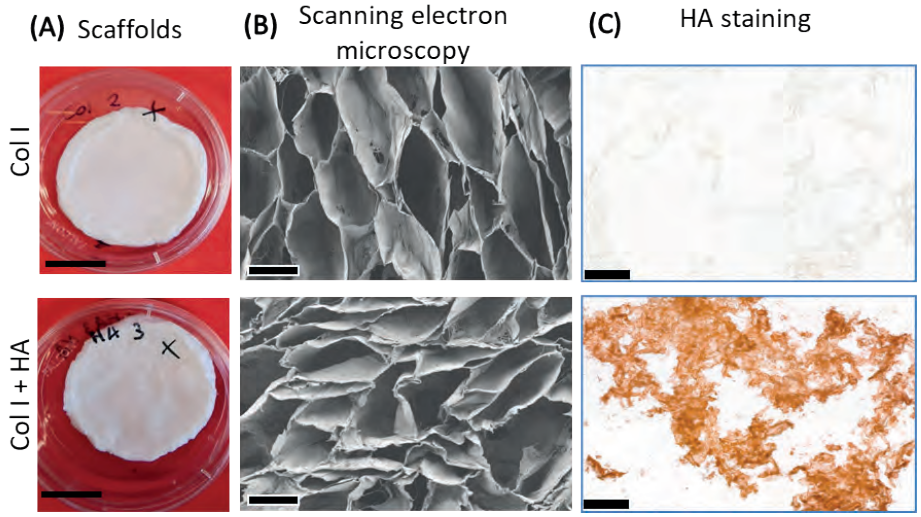

Figure 3. Scaffold structure and distribution of hyaluronan. Top images show Col I and bottom images show Col I+HA. (**A**) Macroscopic images of crosslinked scaffolds. (**B**) Scanning electron microscopy (SEM) shows pore morphology of collagen-only and collagen–hyaluronan scaffold cross-sections. (**C**) Immunostaining of collagen-only scaffold shows absence of hyaluronan in comparison with overall presence of hyaluronan in scaffold with HA, as stained with biotinylated HA binding protein. HA: hyaluronan. Scale bars for macroscopic images: 10 mm; SEM: 120 µm; immunostaining: 100 µm.

Table 1 gives an overview of the biochemical analysis of the scaffolds with and without HA before and after chemical crosslinking. Although the collagen scaffolds had slightly more primary amine groups per mg, the crosslinking degree was 42% for both scaffolds. Chemical crosslinking made the scaffolds more stable, seen as the denaturation temperature (Td) increased by 18±7 and 17±9 °C for Col I and Col I+HA, respectively.

Table 1. Characteristics of type I collagen scaffolds with and without hyaluronan. N = 3 ± SD.

Scaffold Type	**Amine group Content (nmol/mg Scaffold)**		**Denaturation Temperature Td (°C)**		**Hyaluronan Content (µg/mg Scaffold)**	
Crosslinked	No	Yes	No	Yes	No	Yes
Col I	361 ± 49	206 ± 19	59 ± 1	78 ± 0	1 ± 1	1 ± 1
Col I+HA	341 ± 36	197 ± 23	58 ± 1	76 ± 0	19 ± 4	43 ± 2

Papain digestion was used to degrade the collagen scaffolds and quantify the amount of HA present. HA quantification showed that chemical crosslinking was necessary to capture HA, as the HA content in the crosslinked scaffolds was considerably higher than in the non-crosslinked scaffolds. As the non-crosslinked scaffolds received the same incubation steps as their crosslinked counterparts, this illustrates that the HA was partially washed out. The Col I+HA scaffolds were also evaluated in an agarose gel to estimate their molecular weight (MW, Supplementary Figure S2). The HA dissolved in water demonstrated a MW of ~800 kDa, which matches the manufacturer's information. When HA was digested by papain, its MW decreased to ~100 kDa, similar to its size in the crosslinked Col I+HA scaffolds. It seems that the papain preparation used also affected the molecular weight of the HA, making it challenging to accurately assess HA size in the scaffolds. The non-crosslinked and untreated scaffolds with HA showed higher MWs in a range from 93 to 370 kDa. HA was not observed in the Col I scaffolds by agarose gel electrophoresis.

3.2. Effect of Hyaluronan-Containing Scaffolds on Macrophage Polarization

Since the immune response has an important role in wound healing, especially in the phases of inflammation and remodeling, the effect of scaffold composition on macrophages was evaluated. Chemically crosslinked scaffolds were used for the biological analysis. M0 macrophages were seeded in Col I scaffolds ± HA, while M1 or M2 macrophages were seeded in Col I scaffolds as controls. After 2 days, the cells were analyzed by flow cytometry using the MFI of the cell surface markers (Figure 4). The expression of CD80 in the M0 macrophages was not significantly affected by the presence of HA. The control M1-like cells in the scaffolds showed significantly higher CD80 expression than the M0 macrophages in both scaffold types (Figure 4A). PDL-1 and HLA-DR were also not induced on the M0 macrophages by HA, while slightly higher, non-significant expression was seen for the M1-like phenotype. The marker profile of the M0 macrophages in scaffolds resembled the M2-like control more than the M1-like control, especially for CD206 and MerTK (Figure 4B). The expression of CD163 was low in the control with M2-like-induced macrophages, with values similar to the M1-like-induced macrophages.

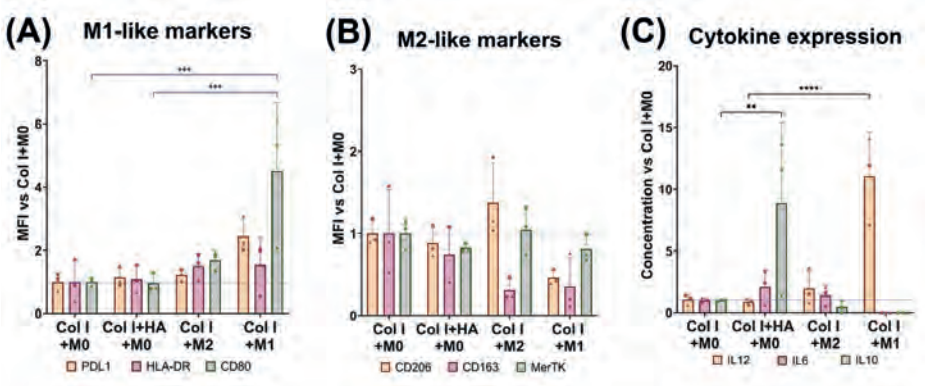

Figure 4. Macrophage CD markers and cytokine expression levels after 48 h of culture on collagen scaffolds. Flow cytometry for (**A**) M1-like markers for PDL1, HLA-DR and CD80 and (**B**) M2-like markers for CD206, CD163 and MerTK. (**C**) Analysis of cytokine expression of IL12, IL6 and IL10 in culture supernatant. Donors represented as follows: ● donor 1; ■ donor 2; ▲ donor 3. Comparison between groups analyzed using two-way ANOVA. ** = $p < 0.01$, *** = $p < 0.001$, **** = $p < 0.0001$.

Regarding cytokine expression, IL12 was statistically higher in the control with the M1 macrophages, thereby confirming their M1 subtype. IL10 levels were notably elevated in the M0 macrophages cultured on the Col I+HA scaffolds (Figure 4C). IL-6 levels were similar for the scaffolds seeded with M0 or M2 macrophages in Col I+HA and Col I, respectively.

3.3. Effect of Hyaluronan on Different Fibroblast Types

Fibroblasts from different sources—adult, fetal and eschar—exhibit different markers during wound healing. To investigate whether the use of HA influenced the regenerative or fibrotic responses of these cells, fibroblasts were seeded on chemically crosslinked scaffolds and characterized through histology and gene and protein expression studies.

In H&E staining, slightly more fetal fibroblasts seem to be present on the scaffolds after two weeks of culture, followed by the adult and eschar cells, which correlates with the amount of isolated RNA (Supplementary Table S3) and growth rate in 2D culture (Supplementary Figure 3). The adult and fetal cells showed slightly higher migration in both scaffold types than the eschar cells, which mostly remained on the surface (Figure 5). The fetal cells formed cellular aggregates, which may have been due to their higher proliferation rate. Cellular morphology varied somewhat between donors, regardless of the presence of HA. Overall, the fetal and adult fibroblasts had a more roundish shape, while the eschar cells were more elongated (Supplementary Figure S4). As histology only shows sections of the scaffolds, we

used mRNA and protein expression to obtain more representative results from larger specimens.

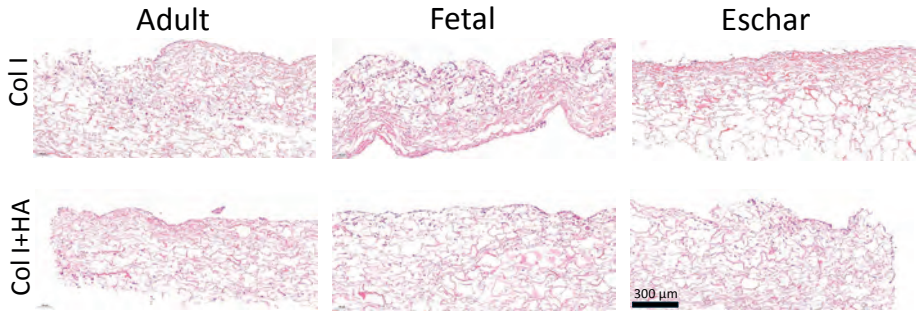

Figure 5. Cellular distribution in scaffolds after 14 days of culture with either adult, fetal or eschar fibroblasts using H&E staining. Collagen stained in pink; cells stained in purple. Scale bar: 300 µm.

The protein expression of α-SMA was evaluated as a marker for myofibroblast presence. α-SMA expression was not affected by the addition of HA to the Col I scaffolds (Figure 6 and Supplementary Figure S5), but it differed between fibroblast types, although not significantly. High expression of α-SMA was observed for the fetal and eschar cells, while the expression of α-SMA was very low or hardly detectable for the adult dermal cells, except for donor 3 in the HA scaffolds (Figure 6A).

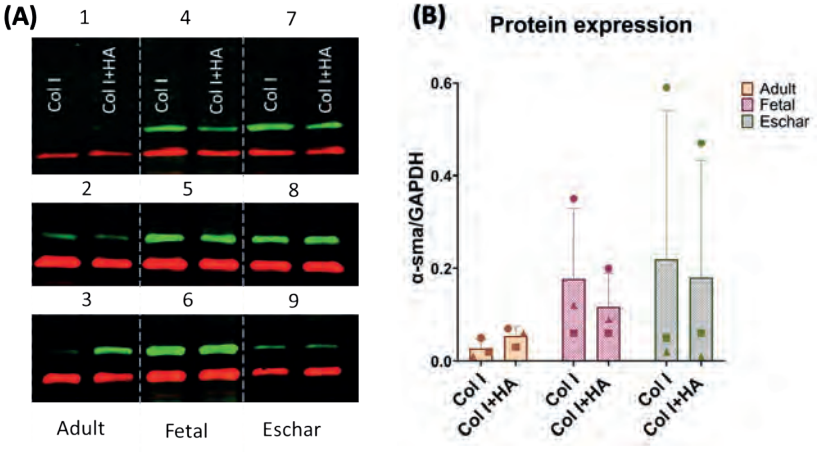

Figure 6. α-SMA protein expression after culturing different types of fibroblasts in scaffolds for 14 days. (**A**) Western blot results for α-SMA of human fibroblast donors 1-9. Molecular weight of α-SMA (green): 42 kDa; GAPDH (red): 36 kDa. (**B**) α-SMA/GAPDH quantification of Western blot results. Individual donors represented by different symbols as follows: ● donor 1/4/7; ■ donor 2/5/8; and ▲ donor 3/6/9.

To corroborate the Western blot results at the mRNA level, RT-qPCR was performed (Figure 7). The expression of ACTA2, which encodes the protein α-SMA, was more affected by cell origin than by the presence of HA (Figure 7A), similarly to the observed protein levels in Figure 6. The expression of α-SMA in the adult cells was increased in Col I+HA, whereas its expression in the fetal and eschar cells was not significantly affected by the presence of HA. ACTA2 expression in the Col I scaffolds was increased in the eschar cells compared to the adult and fetal cells.

TGFβ1 can induce the conversion of fibroblasts into myofibroblasts, leading to fibrosis [23]. The expression of TGFB1 was slightly but significantly reduced in the eschar cells when using HA in the scaffolds, as assessed by paired testing (Figure 7B).

Another gene related to myofibroblasts is COL10A1, which is regulated by TGFβ1 [24,25]. Among all the genes analyzed in this study, this gene showed the highest expression in the eschar cells compared to the other cell types (Figure 7C). In the presence of HA, COL10A1 expression was significantly reduced in the eschar cells.

Engrailed-1 (EN1) plays an important role in the reorganization of the cytoskeleton [26,27]. Its expression is low during early pregnancy and during wound regeneration but high when scarring occurs [28]. The expression of the EN1 gene was not affected by HA being added to the scaffolds (Figure 7D).

TGFβ3 is highly expressed in fetal wounds and has been associated with skin regeneration [29]. Surprisingly, its highest expression level was observed in the eschar cells (Figure 7E), with no significant difference between the adult and fetal cells. The expression of COL14A1, associated with embryogenesis and the regulation of collagen fibrillogenesis, was similar between the adult, fetal and eschar cells in both scaffold types (Figure 7F).

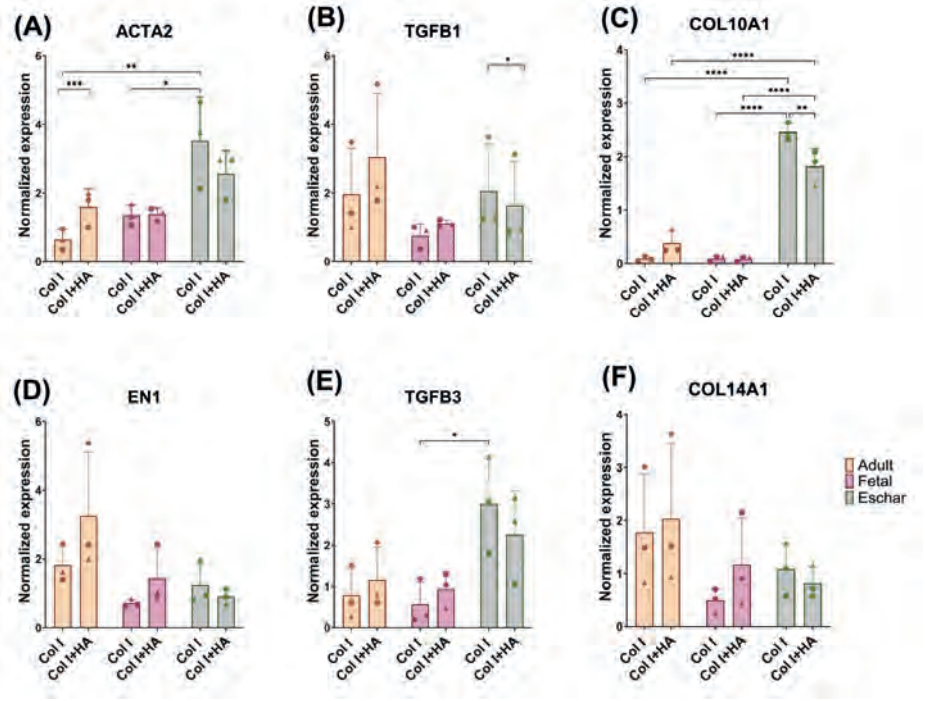

Figure 7. Effect of hyaluronan in collagen scaffolds on mRNA expression by adult, fetal and eschar fibroblasts after 14 days of culture. Normalized expression (ΔΔCq) of (**A**) alpha smooth muscle actin 2 (ACTA2), (**B**) transforming growth factor beta 1 (TGFB1), (**C**) type X collagen alpha 1 chain (COL10A1), (**D**) engrailed-1 (EN1), (**E**) transforming growth factor beta 3 (TGFB3) and (**F**) type XIV collagen alpha 1 chain (COL14A1). Individual donors represented by different symbols: ● donor 1/4/7; ■ donor 2/5/; ▲ donor 3/6/9. ΔΔCq calculated using relative quantity of target gene normalized to quantities of reference genes. Note: Comparison between groups analyzed using two-way ANOVA; paired t tests applied for comparison between same donors. *= $p < 0.05$, ** = $p < 0.01$, *** = $p < 0.001$, **** = $p < 0.0001$.

4. Discussion

Hyaluronan (HA) is a component widely used in skin care products and in promising dermal templates to treat burn injuries, such as Hyalomatrix®. Many studies have focused on the effect of HA on a specific cell type, predominantly in the form of hydrogels. In this study, we created porous collagen sponges biofunctionalized with HA and showed their promising regenerative effect on macrophages and fibroblasts of different origins.

The concentration of 0.05% HA for our collagen scaffolds was selected based on the study by Uijtdewilligen et al. [3], where the highest incorporation of this

glycosaminoglycan was obtained at this concentration. SEM images showed the fluffy edges of the cross-section of the scaffolds, which might be some HA coating the scaffold walls. Similar observations were made for chitosan [30] and silk [31] scaffolds supplemented with HA. Immunostaining proved that HA was distributed evenly in the scaffolds when mixed during its production. We achieved ~43 µg HA/mg scaffolds, which was twice of what has been reported [3]. Overall, the incorporation of HA into the scaffold did not modify its crosslinking degree nor its denaturation temperature, indicating a minimal indirect impact on mechanical properties [32]. The largest effect came from the chemical crosslinking, which resulted in a higher temperature being required to denature the collagen, as observed in previous studies [19].

It is well known that fetal wounds are able to regenerate free of scars and that the amount of HA in the extracellular matrix of the skin in mammals is higher during the early embryonic life stage [33,34]. Here, we mimicked this aspect of the fetal microenvironment by creating Col I+HA scaffolds and studied the subsequent response of macrophages and fibroblasts, after confirming the incorporation of HA in the collagen scaffolds.

The activation of specific macrophage phenotypes during different stages of wound healing could make the difference between proper skin remodeling and scarring [35]. We noticed that, upon seeding M0 macrophages on our scaffolds containing either Col I or Col I+HA, the macrophages started to resemble a phenotype closer to M2-like macrophages ($CD80^{low}$, $CD206^{high}$, $CD163^{high}$ and $MerTK^{high}$). This phenotype, however, differed from the control macrophages that were stimulated using IL4 and IL13 (M2-like cells) and seeded on Col I scaffolds. The M2 control was more similar to an M2a subset of macrophages ($CD80^{low}$, $CD206^{high}$, $CD163^{low}$ [36]), whereas macrophages collected from the scaffolds were more similar to M2c-like macrophages ($CD163^{high}$, $CD206^{high}$) [37]. This was confirmed by the increased IL10 production under conditions with HA, as M2c macrophages secrete large amounts of IL10 [38]. Additionally, it is known that IL10 is essential in regenerative wound healing in fetal tissue [39] and that it can elevate HA deposition in the ECM of fetal fibroblasts [40].

Several studies have explored the effects of HA on macrophage activation, with low-MW HA promoting pro-inflammatory and angiogenic responses, while high-MW HA reduces inflammation and angiogenesis [41]. In our study, the HA within crosslinked scaffolds (~100 kDa) exhibited a reduced MW after papain digestion, but this was also seen after HA digestion alone. Interestingly, macrophage polarization

in chemically crosslinked HA–collagen hydrogels is reportedly not significantly affected by the MW of the HA [42]. We observed an M2c-like macrophage profile in our Col I+HA scaffolds, and it is known that M2-like subtypes show significant CD44 upregulation, enhancing responsiveness to HA [43,44]. In this context, M2c-like macrophages contribute to wound healing by secreting IL10, which could downregulate TGFβ signaling, thereby inhibiting fibroblast-to-myofibroblast differentiation and showing promise in reducing excessive scarring [45].

Histological images showed that the number of fibroblasts in the scaffolds was somewhat higher for the fetal fibroblasts, followed by the adult and eschar cells, regardless of whether they were seeded in Col I or Col I+HA scaffolds. This may be related to a higher proliferation rate [42], as was seen during their expansion in 2D culture, and by the larger amounts of isolated RNA for fetal samples. Although small fragments of HA (6–20 monosaccharides in length) could attract fibroblasts to the wound site through CD44 signaling during the proliferation phase [46], we did not see an increased migration when using Col I+HA scaffolds, which may be due to the static culture in combination with the crosslinking of HA to collagen, which could restrict the available binding sites.

Scarring is caused by a fibrotic response during wound healing and is characterized by high α-SMA expression in fibroblasts [47]. Our findings revealed that fetal fibroblasts produced more α-SMA than adult fibroblasts at the protein level when cultured in collagen scaffolds, consistent with studies using these two cell types on dermal templates (Novomaix) [48]. However, α-SMA expression was not affected by the presence of HA. The eschar fibroblasts, which exhibited a myofibroblast-like profile [13], showed an approximately two-fold increase in COL10A1 mRNA levels compared to the adult and fetal fibroblasts. This response was decreased in the presence of HA. While ACTA2, EN1 and TGFB1 are regarded as fibrotic genes [26], they play crucial roles in embryogenesis and skin wound healing [49–51]. COL10A1 may serve as a potential marker to identify scar-associated cells like eschar fibroblasts [52,53], as its expression was notably higher in these cells. This could aid in distinguishing fibroblasts involved in excessive scarring in order to develop new strategies to reduce these cells, ultimately contributing to improved wound healing and reduced scarring in patients.

Skin regeneration has been observed during fetal wound healing [54]. Therefore, we investigated COL14A1 and TGFB3, as these genes have been related to regeneration and embryogenesis [55]. However, we did not observe a high expression of these genes in fetal cells, irrespective of the use of HA in scaffolds. Fibroblasts are

mechanosensitive, which was shown by the reduced α-SMA expression when the cells were exposed to a softer 3D environment compared to a 2D one in plastic [56]. It is possible that our fetal fibroblasts did not upregulate TGFB3 or COL14A1 expression because they were present in a 3D scaffold and not surrounded by a fibrotic environment [57], which would otherwise activate fibrillogenesis [55]. Overall, the largest differences were related to fibroblast origin rather than the incorporation of HA.

While our study provides valuable insights about the potential of HA to improve wound healing, certain considerations might enhance the applicability of these findings. We observed some variability in expression levels across cell donors in our in vitro studies, although a consistent trend was noted in their expression profiles. To address this, we recommend increasing the cell density to 200,000/cm^2 for fibroblasts and macrophages, and expanding the number of donors to increase the heterogeneity [58]. Since normal adult fibroblasts may not accurately reflect the responses observed in a fibrotic environment, fibrotic cells like eschar fibroblasts or wound models are better suited for such studies. For future experiments, it would be interesting to seed M2-like and M1-like stimulated macrophages on Col I+HA to observe if their phenotypes maintain or switch.

5. Conclusions

In conclusion, by chemical crosslinking we successfully incorporated HA into collagen scaffolds, which may be used as a prototype for dermal substitutes in the future. Our results demonstrated that Col I+HA scaffolds increased IL10 cytokine expression, a marker of M2c-like macrophages. Additionally, the scaffolds containing HA reduced the expression of scarring-associated genes (TGFB1, COL10A1) in primary eschar fibroblasts, further supporting their potential to promote a reparative rather than fibrotic response.

Supplementary Materials: The following supporting information can be downloaded at: https://www.mdpi.com/article/doi/s1, Figure S1: Representative gating strategy to select CD45+ macrophages; Figure S2: Molecular weight of hyaluronan decreased after digestion with papain and crosslinking with collagen scaffolds using an agarose gel stained with Stains-All; Figure S3: Microscopic images displaying higher proliferation of fetal fibroblasts in a tissue culture flask, prior to seeding on the scaffolds; Figure S4: H&E staining of scaffolds after 14 days of culture with fibroblasts of different origins; Figure S5: α-SMA protein expression

after culturing different types of fibroblasts in scaffolds for 14 days; Table S1: Antibody panels used to characterize macrophages by flow cytometry; Table S2: Primer sequences for quantitative polymerase chain reaction; Table S3: RNA quantification in fibroblasts seeded on scaffolds after 14 days of culturing.

Author Contributions: Conceptualization: N.A.-M., M.P., B.K.H.L.B., T.H.v.K. and W.F.D.; methodology: N.A.-M., R.K., M.L.N.P.G., M.P., M.V. (Marcel Vlig) and E.M.M.V.; validation: N.A.-M., M.P., M.V. (Marcel Vlig) and E.M.M.V.; formal analysis: N.A.-M. and M.P.; investigation: N.A.-M. and M.P.; resources: M.V. (Martijn Verdoes), B.K.H.L.B. and W.F.D.; writing—original draft: N.A.-M.; writing—review and editing: all authors; visualization: N.A.-M.; supervision: B.K.H.L.B., T.H.v.K. and W.F.D.; funding acquisition: T.H.v.K. and W.F.D. All authors have read and agreed to the published version of the manuscript.

Funding: This work received funding from the European Union's Horizon 2020 research and innovation program under the Marie Skłodowska-Curie Grant, Agreement No. 955722 (SkinTERM, NAM, RK, MLNPG), and from Radboud university medical center PhD round 2020 (awarded to MP).

Institutional Review Board Statement: The study was conducted in accordance with the Declaration of Helsinki. For human fibroblasts derived from dermal tissue, The Medical Ethics Review Committee assessed that the research is not subject to the Medical Research Involving Human Subjects Act. Consent for the use of anonymized, post-operative residual tissue samples was received through the informed opt-out protocol of the Red Cross Hospital, which was in accordance with the national guidelines (https://www.coreon.org/, accessed on 23 November 2020) and approved by the institutional privacy officers. Informed consent for the use of fetal material was obtained. For human cells derived from blood specimens, the experiments using these cells were approved by the local ethical committee. Privacy and data protection are covered by the Standard Operating Procedures of the Sanquin Bloodbank, following National and International legislation, principles and guidelines.

Informed Consent Statement: Informed consent from the humans whose cells were used in this study were obtained from all subjects, as specified in the Materials and Methods section per cell type.

Data Availability Statement: The original contributions presented in this study are included in the article/Supplementary Materials. Further inquiries can be directed to the corresponding author.

Acknowledgments: The authors would like to thank Radboud Technology Center—Microscopy for the use of their microscopy facilities to take the Scanning Electron Microscope images, and Theo Hafmans (Dept. of Medical BioSciences) for aid with scaffold sectioning and immunostaining. Finally, we appreciate the help from Patricia Suurs (Marel Townsend Further Processing, Boxmeer) in performing differential scanning calorimetry.

Conflicts of Interest: The authors confirm that there are no conflicts of interest associated with this publication.

References

1. Mamun, A.; Shao, C.; Geng, P.; Wang, S.; Xiao, J. Recent advances in molecular mechanisms of skin wound healing and its treatments. *Front. Immunol.* **2024**, *15*, 1395479. https://doi.org/10.3389/fimmu.2024.1395479.
2. Chacon, M.A.; Haas, J.; Hansen, T.C.; Mushin, O.P.; Bell, D.E. Thin and Ultra-Thin Split-Thickness Skin Grafts Are Safe and Efficacious in the Burn Population. *J. Burn Care Res.* **2019**, *41*, 849–852. https://doi.org/10.1093/jbcr/irz208.
3. Uijtdewilligen, P.J.E.; Versteeg, E.M.M.; Gilissen, C.; van Reijmersdal, S.V.; Schoppmeyer, R.; Wismans, R.G.; Daamen, W.F.; van Kuppevelt, T.H. Towards embryonic-like scaffolds for skin tissue engineering: Identification of effector molecules and construction of scaffolds. *J. Tissue Eng. Regen. Med.* **2016**, *10*, E34–E44. https://doi.org/10.1002/term.1725.
4. Estes, J.; Adzick, N.; Harrison, M.; Longaker, M.; Stern, R. Hyaluronate metabolism undergoes an ontogenic transition during fetal development—Implications for scar-free wound-healing. *J. Pediatr. Surg.* **1993**, *28*, 1227–1231. https://doi.org/10.1016/s0022-3468(05)80303-3.
5. Gomes, M.; Krijnen, P.A.J.; Middelkoop, E.; Niessen, H.W.M.; Boekema, B. Fetal Skin Wound Healing: Key Extracellular Matrix Components and Regulators in Scarless Healing. *J. Investig. Dermatol.* **2025**, *145*, 280–302. https://doi.org/10.1016/j.jid.2024.05.027.
6. Dovedytis, M.; Liu, Z.J.; Bartlett, S. Hyaluronic acid and its biomedical applications: A review. *Eng. Regen.* **2020**, *1*, 102–113. https://doi.org/10.1016/j.engreg.2020.10.001.
7. Acharya, P.S.; Majumdar, S.; Jacob, M.; Hayden, J.; Mrass, P.; Weninger, W.; Assoian, R.K.; Puré, E. Fibroblast migration is mediated by CD44-dependent TGFβ activation. *J. Cell Sci.* **2008**, *121*, 1393–1402. https://doi.org/10.1242/jcs.021683.
8. Potter, D.A.; Veitch, D.; Johnston, G.A. Scarring and wound healing. *Br. J. Hosp. Med.* **2019**, *80*, C166–C171. https://doi.org/10.12968/hmed.2019.80.11.C166.
9. Zheng, H.; Cheng, X.; Jin, L.; Shan, S.; Yang, J.; Zhou, J. Recent advances in strategies to target the behavior of macrophages in wound healing. *Biomed. Pharmacother.* **2023**, *165*, 115199. https://doi.org/10.1016/j.biopha.2023.115199.
10. Rios de la Rosa, J.M.; Tirella, A.; Gennari, A.; Stratford, I.J.; Tirelli, N. The CD44-Mediated Uptake of Hyaluronic Acid-Based Carriers in Macrophages. *Adv. Healthc. Mater.* **2017**, *6*, 1601012. https://doi.org/10.1002/adhm.201601012.
11. Alaish, S.M.; Yager, D.; Diegelmann, R.F.; Cohen, I.K. Biology of fetal wound healing: Hyaluronate receptor expression in fetal fibroblasts. *J. Pediatr. Surg.* **1994**, *29*, 1040–1043. https://doi.org/10.1016/0022-3468(94)90275-5.
12. Soo, C.; Hu, F.-Y.; Zhang, X.; Wang, Y.; Beanes, S.R.; Lorenz, H.P.; Hedrick, M.H.; Mackool, R.J.; Plaas, A.; Kim, S.-J.; et al. Differential Expression of Fibromodulin, a Transforming Growth Factor-β Modulator, in Fetal Skin Development and Scarless Repair. *Am. J. Pathol.* **2000**, *157*, 423–433. https://doi.org/10.1016/S0002-9440(10)64555-5.
13. Van Der Veen, V.C.; Vlig, M.; Van Milligen, F.J.; De Vries, S.I.; Middelkoop, E.; Ulrich, M.M.W. Stem Cells in Burn Eschar. *Cell Transplant.* **2012**, *21*, 933–942. https://doi.org/10.3727/096368911x600993.
14. David-Raoudi, M.; Tranchepain, F.; Deschrevel, B.; Vincent, J.; Bogdanowicz, P.; Boumediene, K.; Pujol, J. Differential effects of hyaluronan and its fragments on fibroblasts: Relation to wound healing. *Wound Repair Regen.* **2008**, *16*, 274–287. https://doi.org/10.1111/j.1524-475X.2007.00342.x.

15. Yang, H.; Song, L.; Sun, B.; Chu, D.; Yang, L.; Li, M.; Li, H.; Dai, Y.; Yu, Z.; Guo, J. Modulation of macrophages by a paeoniflorin-loaded hyaluronic acid-based hydrogel promotes diabetic wound healing. *Mater. Today Bio* **2021**, *12*, 100139. https://doi.org/10.1016/j.mtbio.2021.100139.
16. O'Brien, F.; Harley, B.; Yannas, I.; Gibson, L. The effect of pore size on cell adhesion in collagen-GAG scaffolds. *Biomaterials* **2005**, *26*, 433–441. https://doi.org/10.1016/j.biomaterials.2004.02.052.
17. Liu, J.-Y.; Li, Y.; Hu, Y.; Cheng, G.; Ye, E.; Shen, C.; Xu, F.-J. Hemostatic porous sponges of cross-linked hyaluronic acid/cationized dextran by one self-foaming process. *Mater. Sci. Eng. C* **2018**, *83*, 160–168. https://doi.org/10.1016/j.msec.2017.10.007.
18. Buttafoco, L.; Engbers-Buijtenhuijs, P.; Poot, A.A.; Dijkstra, P.J.; Daamen, W.F.; van Kuppevelt, T.H.; Vermes, I.; Feijen, J. First steps towards tissue engineering of small-diameter blood vessels: Preparation of flat scaffolds of collagen and elastin by means of freeze drying. *J. Biomed. Mater. Res. B Appl. Biomater.* **2006**, *77B*, 357–368. https://doi.org/10.1002/jbm.b.30444.
19. Schroepfer, M.; Meyer, M. DSC investigation of bovine hide collagen at varying degrees of crosslinking and humidities. *Int. J. Biol. Macromol.* **2017**, *103*, 120–128. https://doi.org/10.1016/j.ijbiomac.2017.04.124.
20. van den Bogaerdt, A.J.; van Zuijlen, P.P.; van Galen, M.; Lamme, E.N.; Middelkoop, E. The suitability of cells from different tissues for use in tissue-engineered skin substitutes. *Arch. Dermatol. Res.* **2002**, *294*, 135–142. https://doi.org/10.1007/s00403-002-0305-3.
21. Akershoek, J.J.; Vlig, M.; Talhout, W.; Boekema, B.K.H.L.; Richters, C.D.; Beelen, R.H.J.; Brouwer, K.M.; Middelkoop, E.; Ulrich, M.M.W. Cell therapy for full-thickness wounds: Are fetal dermal cells a potential source? *Cell Tissue Res.* **2016**, *364*, 83–94. https://doi.org/10.1007/s00441-015-2293-6.
22. Oostendorp, C.; Geutjes, P.J.; Smit, F.; Tiemessen, D.M.; Polman, S.; Abbawi, A.; Brouwer, K.M.; Eggink, A.J.; Feitz, W.F.J.; Daamen, W.F.; et al. Sustained Postnatal Skin Regeneration Upon Prenatal Application of Functionalized Collagen Scaffolds. *Tissue Eng. Part A* **2021**, *27*, 10–25. https://doi.org/10.1089/ten.tea.2019.0234.
23. Kim, K.K.; Sheppard, D.; Chapman, H.A. TGF-β1 Signaling and Tissue Fibrosis. *Cold Spring Harb. Perspect. Biol.* **2018**, *10*, a022293. https://doi.org/10.1101/cshperspect.a022293.
24. Li, T.; Huang, H.; Shi, G.; Zhao, L.; Li, T.; Zhang, Z.; Liu, R.; Hu, Y.; Liu, H.; Yu, J.; et al. TGF-β1-SOX9 axis-inducible COL10A1 promotes invasion and metastasis in gastric cancer via epithelial-to-mesenchymal transition. *Cell Death Dis.* **2018**, *9*, 849. https://doi.org/10.1038/s41419-018-0877-2.
25. Kutluoğlu, G.C.; Vlig, M.; Elgersma, A.; Boekema, B.; Daamen, W.F.; Doberenz, C.; Manikowski, D. Comparison of dermal and eschar fibroblasts in full skin equivalents. *Wound Repair Regen.* **2025**, *33*, e70001. https://doi.org/10.1111/wrr.70001.
26. Györfi, A.; Matei, A.; Fuchs, M.; Liang, C.; Rigau, A.; Hong, X.; Zhu, H.; Luber, M.; Bergmann, C.; Dees, C.; et al. Engrailed 1 coordinates cytoskeletal reorganization to induce myofibroblast differentiation. *J. Exp. Med.* **2021**, *218*, e20201916. https://doi.org/10.1084/jem.20201916.
27. Rinkevich, Y.; Walmsley, G.G.; Hu, M.S.; Maan, Z.N.; Newman, A.M.; Drukker, M.; Januszyk, M.; Krampitz, G.W.; Gurtner, G.C.; Lorenz, H.P.; et al. Skin fibrosis. Identification and isolation of a dermal lineage with intrinsic fibrogenic potential. *Science* **2015**, *348*, aaa2151. https://doi.org/10.1126/science.aaa2151.
28. Mascharak, S.; DesJardins-Park, H.E.; Davitt, M.F.; Griffin, M.; Borrelli, M.R.; Moore, A.L.; Chen, K.; Duoto, B.; Chinta, M.; Foster, D.S.; et al. Preventing *Engrailed*-1 activation in fibroblasts yields wound regeneration without scarring. *Science* **2021**, *372*, eaba2374. https://doi.org/10.1126/science.aba2374.
29. Lichtman, M.K.; Otero-Vinas, M.; Falanga, V. Transforming growth factor beta (TGF-β) isoforms in wound healing and fibrosis. *Wound Repair Regen.* **2016**, *24*, 215–222. https://doi.org/10.1111/wrr.12398.

30. Correia, C.R.; Moreira-Teixeira, L.S.; Moroni, L.; Reis, R.L.; van Blitterswijk, C.A.; Karperien, M.; Mano, J.F. Chitosan Scaffolds Containing Hyaluronic Acid for Cartilage Tissue Engineering. *Tissue Eng. Part C Methods* **2011**, *17*, 717–730. https://doi.org/10.1089/ten.tec.2010.0467.

31. Yu, L.; Liu, T.; Ma, Y.; Zhang, F.; Huang, Y.; Fan, Z. Fabrication of Silk-Hyaluronan Composite as a Potential Scaffold for Tissue Repair. *Front. Bioeng. Biotech.* **2020**, *8*, 578988. https://doi.org/10.3389/fbioe.2020.578988.

32. Zhu, K.; Slusarewicz, P.; Hedman, T. Thermal analysis reveals differential effects of various crosslinkers on bovine annulus fibrosis. *J. Orthop. Res.* **2011**, *29*, 8–13. https://doi.org/10.1002/jor.21189.

33. Mast, B.; Flood, L.; Haynes, J.; Depalma, R.; Cohen, I.; Diegelmann, R.; Krummel, T. Hyaluronic-acid is a major component of the matrix of fetal rabbit skin and wounds—Implications for healing by regeneration. *Matrix* **1991**, *11*, 63–68. https://doi.org/10.1016/s0934-8832(11)80228-3.

34. Ulrich, M.M.W. Fetal Wound Healing. In *Textbook on Scar Management: State of the Art Management and Emerging Technologies*, Téot, L., Mustoe, T.A., Middelkoop, E., Gauglitz, G.G., Eds.; Springer International Publishing: Cham, Switzerland, 2020; pp. 3–9.

35. Hesketh, M.; Sahin, K.B.; West, Z.E.; Murray, R.Z. Macrophage Phenotypes Regulate Scar Formation and Chronic Wound Healing. *Int. J. Mol. Sci.* **2017**, *18*, 1545. https://doi.org/10.3390/ijms18071545.

36. Mondadori, C.; Chandrakar, A.; Lopa, S.; Wieringa, P.; Talò, G.; Perego, S.; Lombardi, G.; Colombini, A.; Moretti, M.; Moroni, L. Assessing the response of human primary macrophages to defined fibrous architectures fabricated by melt electrowriting. *Bioact. Mater.* **2023**, *21*, 209–222. https://doi.org/10.1016/j.bioactmat.2022.07.014.

37. Spiller, K.L.; Anfang, R.R.; Spiller, K.J.; Ng, J.; Nakazawa, K.R.; Daulton, J.W.; Vunjak-Novakovic, G. The role of macrophage phenotype in vascularization of tissue engineering scaffolds. *Biomaterials* **2014**, *35*, 4477–4488. https://doi.org/10.1016/j.biomaterials.2014.02.012.

38. Lu, J.; Cao, Q.; Zheng, D.; Sun, Y.; Wang, C.; Yu, X.; Wang, Y.; Lee, V.W.S.; Zheng, G.; Tan, T.K.; et al. Discrete functions of M2a and M2c macrophage subsets determine their relative efficacy in treating chronic kidney disease. *Kidney Int.* **2013**, *84*, 745–755. https://doi.org/10.1038/ki.2013.135.

39. Liechty, K.W.; Kim, H.B.; Adzick, N.S.; Crombleholme, T.M. Fetal wound repair results in scar formation in interleukin-10–deficient mice in a syngeneic murine model of scarless fetal wound repair. *J. Pediatr. Surg.* **2000**, *35*, 866–873. https://doi.org/10.1053/jpsu.2000.6868.

40. King, A.; Balaji, S.; Le, L.D.; Marsh, E.; Crombleholme, T.M.; Keswani, S.G. Interleukin-10 regulates fetal extracellular matrix hyaluronan production. *J. Pediatr. Surg.* **2013**, *48*, 1211–1217. https://doi.org/10.1016/j.jpedsurg.2013.03.014.

41. Yang, P.; Lu, Y.; Gou, W.; Qin, Y.; Tan, J.; Luo, G.; Zhang, Q. Glycosaminoglycans' Ability to Promote Wound Healing: From Native Living Macromolecules to Artificial Biomaterials. *Adv. Sci.* **2024**, *11*, 2305918. https://doi.org/10.1002/advs.202305918.

42. Oates, T.C.; Boyd, J.; Dolan, L.; Kergariou, C.d.; Toye, A.; Perriman, A.W.; Boussahel, A. The Immobilization of Hyaluronic Acid in 3D Hydrogel Scaffolds Modulates Macrophage Polarization. *bioRxiv* **2024**. https://doi.org/10.1101/2024.04.10.588451.

43. Sapudom, J.; Ullm, F.; Martin, S.; Kalbitzer, L.; Naab, J.; Möller, S.; Schnabelrauch, M.; Anderegg, U.; Schmidt, S.; Pompe, T. Molecular weight specific impact of soluble and immobilized hyaluronan on CD44 expressing melanoma cells in 3D collagen matrices. *Acta Biomater.* **2017**, *50*, 259–270. https://doi.org/10.1016/j.actbio.2016.12.026.

44. Zhang, Q.; Wang, X.; Liu, Y.; Xu, H.; Ye, C. Pan-cancer and single-cell analyses identify CD44 as an immunotherapy response predictor and regulating macrophage polarization and tumor progression in colorectal cancer. *Front. Oncol.* **2024**, *14*, 1380821. https://doi.org/10.3389/fonc.2024.1380821.

45. Sapudom, J.; Karaman, S.; Mohamed, W.K.E.; Garcia-Sabaté, A.; Quartey, B.C.; Teo, J.C.M. 3D in vitro M2 macrophage model to mimic modulation of tissue repair. *npj Regen. Med.* **2021**, *6*, 83. https://doi.org/10.1038/s41536-021-00193-5.

46. Rooney, P.; Wang, M.; Kumar, P.; Kumar, S. Angiogenic oligosaccharides of hyaluronan enhance the production of collagens by endothelial cells. *J. Cell Sci.* **1993**, *105*, 213–218. https://doi.org/10.1242/jcs.105.1.213.

47. Schulz, J.; Plomann, M.; Sengle, G.; Gullberg, D.; Krieg, T.; Eckes, B. New developments on skin fibrosis—Essential signals emanating from the extracellular matrix for the control of myofibroblasts. *Matrix Biol.* **2018**, *68–69*, 522–532. https://doi.org/10.1016/j.matbio.2018.01.025.

48. Walraven, M.; Akershoek, J.; Beelen, R.; Ulrich, M. In vitro cultured fetal fibroblasts have myofibroblast-associated characteristics and produce a fibrotic-like environment upon stimulation with TGF-β1: Is there a thin line between fetal scarless healing and fibrosis? *Arch. Dermatol. Res.* **2017**, *309*, 111–121. https://doi.org/10.1007/s00403-016-1710-3.

49. Nakamura, M.; Yoshida, H.; Moriyama, Y.; Kawakita, I.; Wlizla, M.; Takebayashi-Suzuki, K.; Horb, M.E.; Suzuki, A. TGF-β1 signaling is essential for tissue regeneration in the Xenopus tadpole tail. *Biochem. Biophys. Res. Commun.* **2021**, *565*, 91–96. https://doi.org/10.1016/j.bbrc.2021.05.082.

50. McAndrews, K.; Miyake, T.; Ehsanipour, E.; Kelly, P.; Becker, L.; McGrail, D.; Sugimoto, H.; LeBleu, V.; Ge, Y.; Kalluri, R. Dermal αSMA+ myofibroblasts orchestrate skin wound repair via β1 integrin and independent of type I collagen production. *EMBO J.* **2022**, *41*, e109470. https://doi.org/10.15252/embj.2021109470.

51. Huettl, R.E.; Luxenhofer, G.; Bianchi, E.; Haupt, C.; Joshi, R.; Prochiantz, A.; Huber, A.B. Engrailed 1 mediates correct formation of limb innervation through two distinct mechanisms. *PLoS ONE* **2015**, *10*, e0118505. https://doi.org/10.1371/journal.pone.0118505.

52. Tabib, T.; Huang, M.; Morse, N.; Papazoglou, A.; Behera, R.; Jia, M.; Bulik, M.; Monier, D.; Benos, P.; Chen, W.; et al. Myofibroblast transcriptome indicates *SFRP2*^{hi} fibroblast progenitors in systemic sclerosis skin. *Nat. Commun.* **2021**, *12*, 4384. https://doi.org/10.1038/s41467-021-24607-6.

53. Gao, Y.; Li, J.; Cheng, W.; Diao, T.; Liu, H.; Bo, Y.; Liu, C.; Zhou, W.; Chen, M.; Zhang, Y.; et al. Cross-tissue human fibroblast atlas reveals myofibroblast subtypes with distinct roles in immune modulation. *Cancer Cell* **2024**, *42*, 1764–1783.e10. https://doi.org/10.1016/j.ccell.2024.08.020.

54. Lorenz, H.P.; Lin, R.Y.; Longaker, M.T.; Whitby, D.J.; Adzick, N.S. The fetal fibroblast—The effector cell of scarless fetal skin repair. *Plast. Reconstr. Surg.* **1995**, *96*, 1251–1259. https://doi.org/10.1097/00006534-199511000-00001.

55. Ansorge, H.L.; Meng, X.; Zhang, G.; Veit, G.; Sun, M.; Klement, J.F.; Beason, D.P.; Soslowsky, L.J.; Koch, M.; Birk, D.E. Type XIV Collagen Regulates Fibrillogenesis*. *J. Biol. Chem.* **2009**, *284*, 8427–8438. https://doi.org/10.1074/jbc.M805582200.

56. Smithmyer, M.E.; Cassel, S.E.; Kloxin, A.M. Bridging 2D and 3D culture: Probing impact of extracellular environment on fibroblast activation in layered hydrogels. *AIChE J.* **2019**, *65*, e16837. https://doi.org/10.1002/aic.16837.

57. Xue, K.; Zhang, J.; Li, C.; Li, J.; Wang, C.; Zhang, Q.; Chen, X.; Yu, X.; Sun, L.; Yu, X. The role and mechanism of transforming growth factor beta 3 in human myocardial infarction-induced myocardial fibrosis. *J. Cell. Mol. Med.* **2019**, *23*, 4229–4243. https://doi.org/10.1111/jcmm.14313.

58. Pipiya, V.V.; Gilazieva, Z.E.; Issa, S.S.; Rizvanov, A.A.; Solovyeva, V.V. Comparison of primary and passaged tumor cell cultures and their application in personalized medicine. *Explor. Target. Antitumor Ther.* **2024**, *5*, 581–599. https://doi.org/10.37349/etat.2024.00237.

Supplementary material

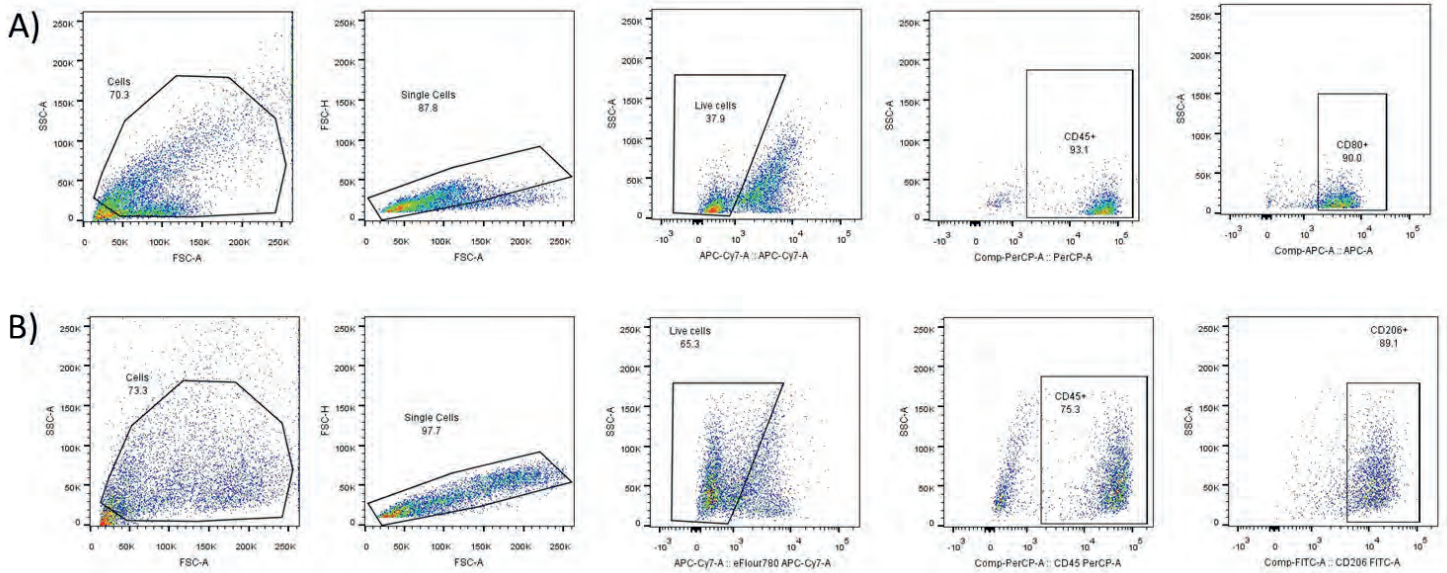

Figure S1. Representative gating strategy to select CD45$^+$ macrophages. A) CD80$^+$ in sample Col I+M1-like macrophages and B) CD206$^+$ in sample Col I+M2-like macrophages.

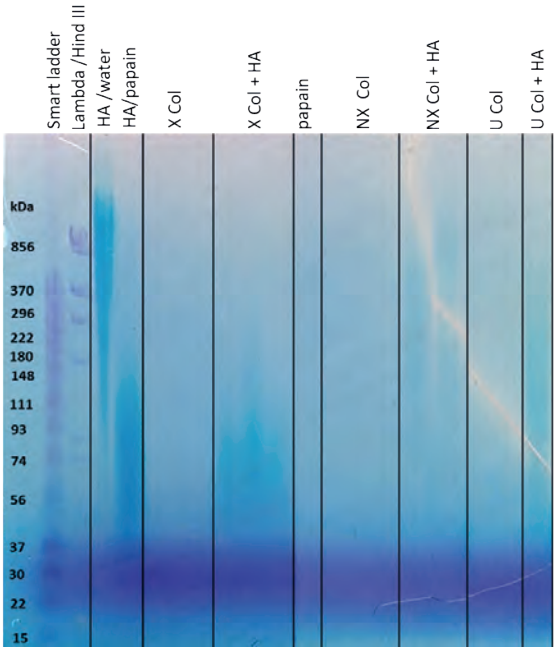

Figure S2. Molecular weight of hyaluronan decreased after digestion with papain and crosslinking with collagen scaffolds using an agarose gel stained with Stains-All. Papain-digested scaffolds from different batches were applied to the gel for the following conditions: crosslinked (X), non-crosslinked (NX) and untreated (U) made by type I collagen (Col I) or type I collagen + hyaluronan (Col I +HA). HA dissolved in demineralized water (HA/water) and digested in papain (HA/papain) were included as controls. DNA ladders were used for the estimation of the molecular weight and converted from pair base to polysaccharide kDa.

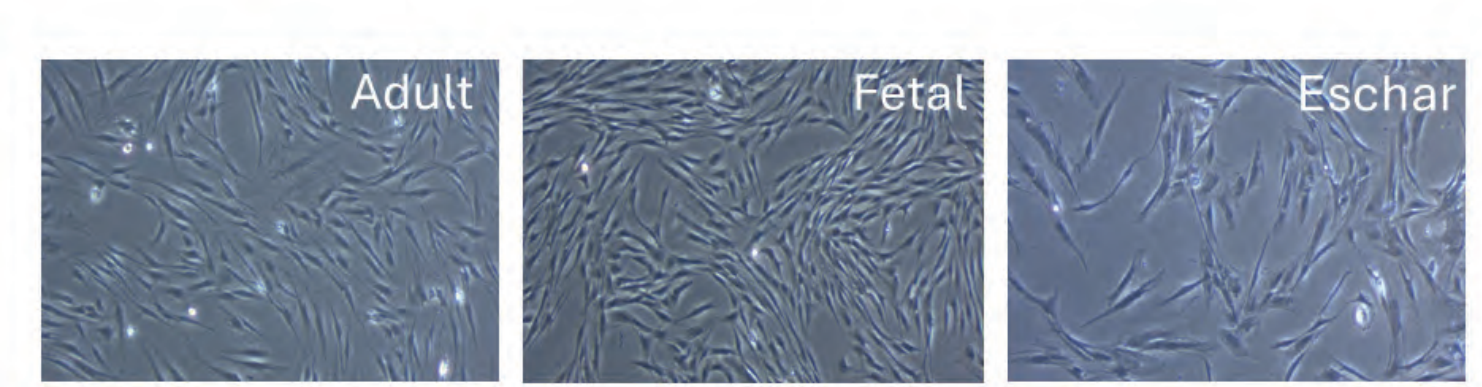

Figure S3. Microscopic images displaying higher proliferation of fetal fibroblasts in a tissue culture flask, prior to seeding on the scaffolds. 0.9 x 10^6 cells/T175 flask were seeded in each condition and photos were captured after 7 days of culture. Original magnification 10x.

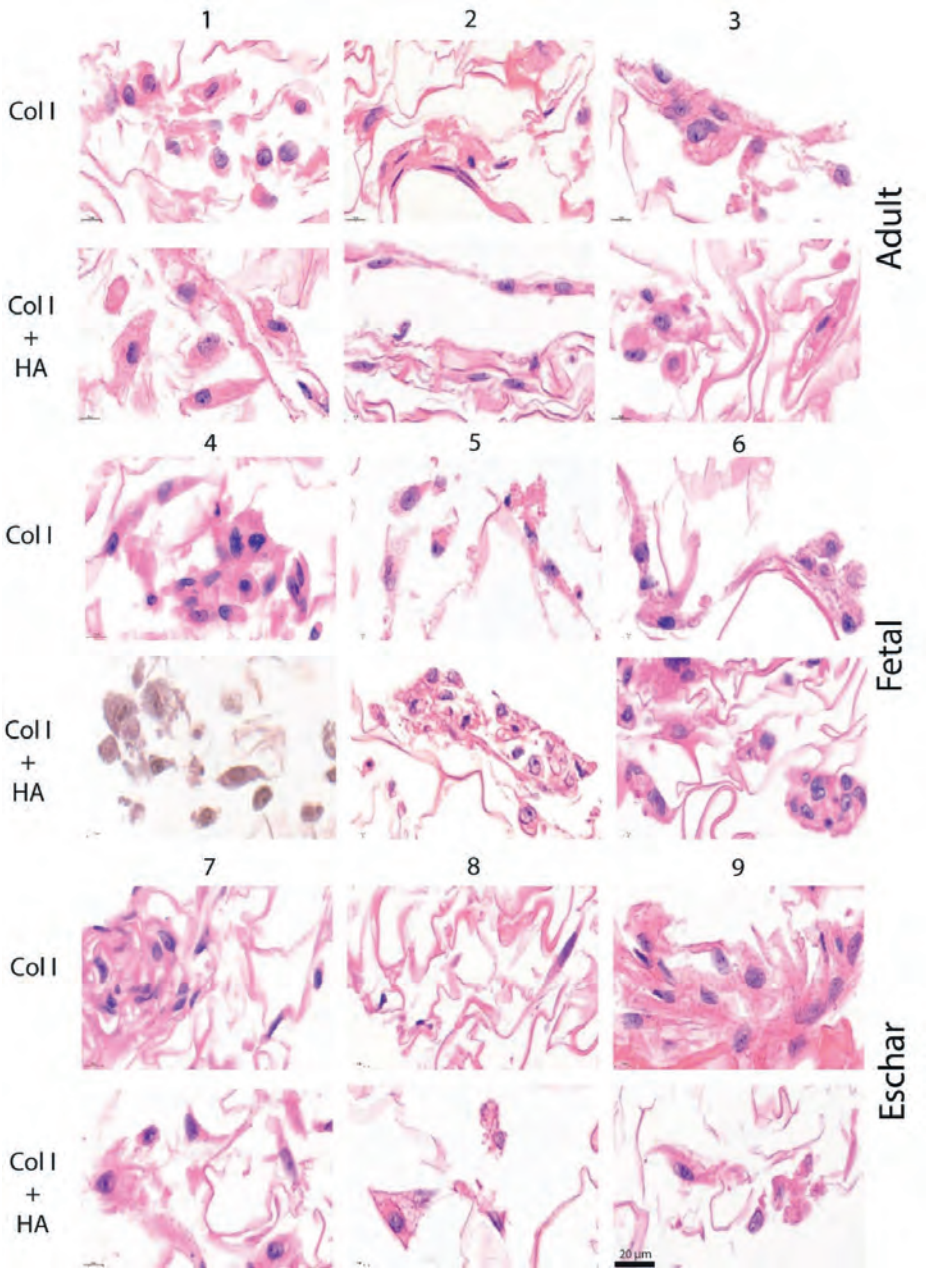

Figure S4. H&E staining of scaffolds after 14 days of culture with fibroblasts of different origins. Adult (donor 1, 2, 3), fetal (donor 4, 5, 6) and eschar (donor 7, 8, 9) fibroblasts were used. Scale bar is 20 µm.

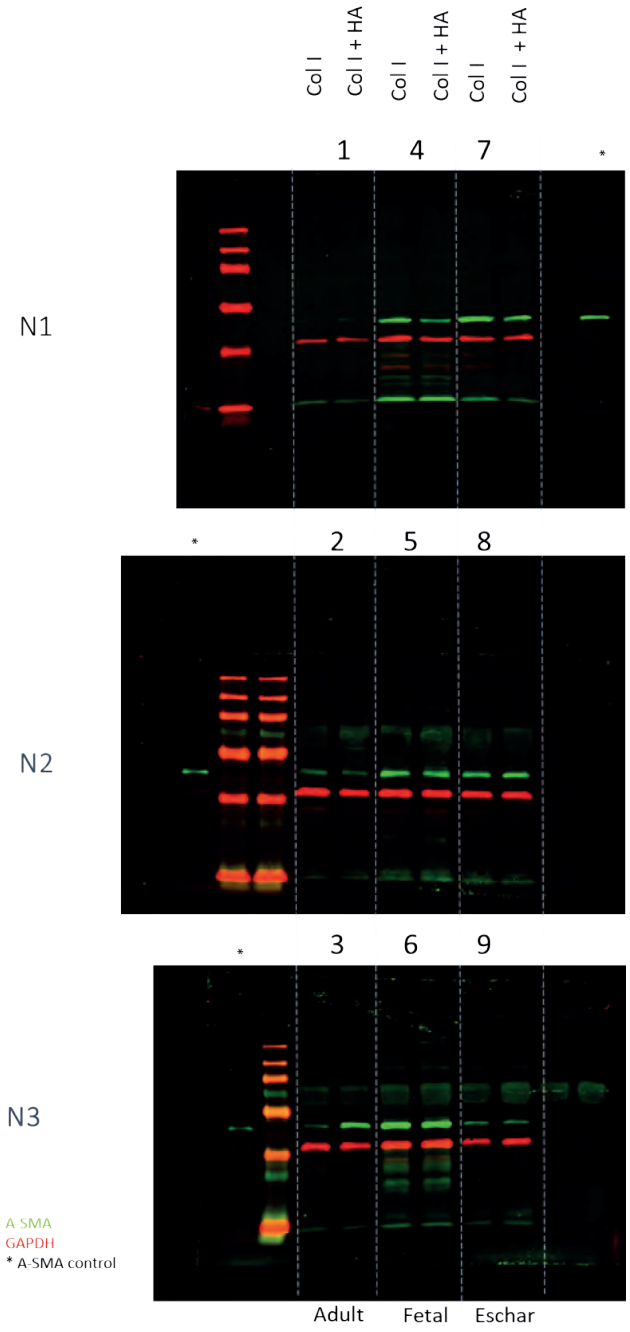

Figure S5. α-SMA protein expression after culturing different types of fibroblasts in scaffolds for 14 days. A) Western blot results for α-SMA of human fibroblast donors 1-9. Molecular weight of α- SMA (in green) is 42 kDa and GAPDH (in red) is 36 kDa.

Table S1. Antibody panels used to characterize macrophages by flow cytometry.

Panel 1			
Label/fluorophore	**Surface marker**	**Dilution**	**Cat. No., Company**
BV421	CD163	1:40	562643, BD Biosciences
FITC	CD206	1:40	551135, BD Biosciences
APC	CD80	1:20	305220, BioLegend
PeCy7	MerTK	1:50	367610, BioLegend
PerCP	CD45	1:20	304026, BioLegend
Panel 2			
Antibody	**Surface marker**	**Dilution**	**Description**
PE	PDL1	1:30	557924, BD Biosciences
BV510	HLA-DR	1:20	307646, BioLegend
PerCP	CD45	1:20	304026, BioLegend

Note: Companies location BD Biosciences, Franklin Lakes, NJ, USA and BioLegend, San Diego, CA, USA.

Table S2. Primer sequences for quantitative polymerase chain reaction.

Gene	**Name**	**Sequence**
GAPDH	Glyceraldehyde-3-phosphate dehydrogenase	5′ TGG GTG TGA ACC ATG AGA AG 3′ 3′ AGT TGT CAT GGA TGA ACC TTG G 5′
YWHAZ	Tyrosine 3-monooxygenase / Tryptophan 5-monooxygenase activation protein zeta	5′ CAT CTT GGA GGG TCG TCT CA 3′ 3′ ACT TTG CTC TCT GCT TGT GAA 5′
ACTA2	Alpha smooth muscle actin 2	5′ CCG ACC GAA TGC AGA AGG A 3′ 3′ ACA GAG TAT TTG CGC TCC GAA 5′
EN1	Engrailed-1	5′ TGA CTC GCA GCA GCC TCT CGT 3′ 3′ AAC GTG TGC AGT ACA CCC AGG C 5′
TGFB1	Transforming growth factor beta 1	5′ CGC GTG CTA ATG GTG GAA A 3′ 3′ TGT GTG TAC TCT GCT TGA ACT TGT CA 5′
TGFB3	Transforming growth factor beta 3	5′ CAA TTA CTG CTT CCG CAA CTT G 3′ 3′ GAT CCT GTC GGA AGT CAA TGT AGA 5′
COL10A1	Type X collagen alpha 1 chain	5′ GGG AGT GCC ATC ATC GAT CT 3′ 3′ CCA TTT GAC TCG GCA TTG GG 5′
COL14A1	Type XIV collagen alpha 1 chain	5′ TGT GGA TGA CTT TGA CGC CT 3′ 3′ GTT GCT GAT GCT GTT TCG CA 5′

Table S3. RNA quantification in fibroblasts seeded on scaffolds after 14 days of culturing.

Nucleic acid concentration (ng/µl)	**Adult**	**Fetal**	**Eschar**
Col I	121 ± 18	223 ± 64	100 ± 37
Col I + HA	125 ± 53	206 ± 40	126 ± 70

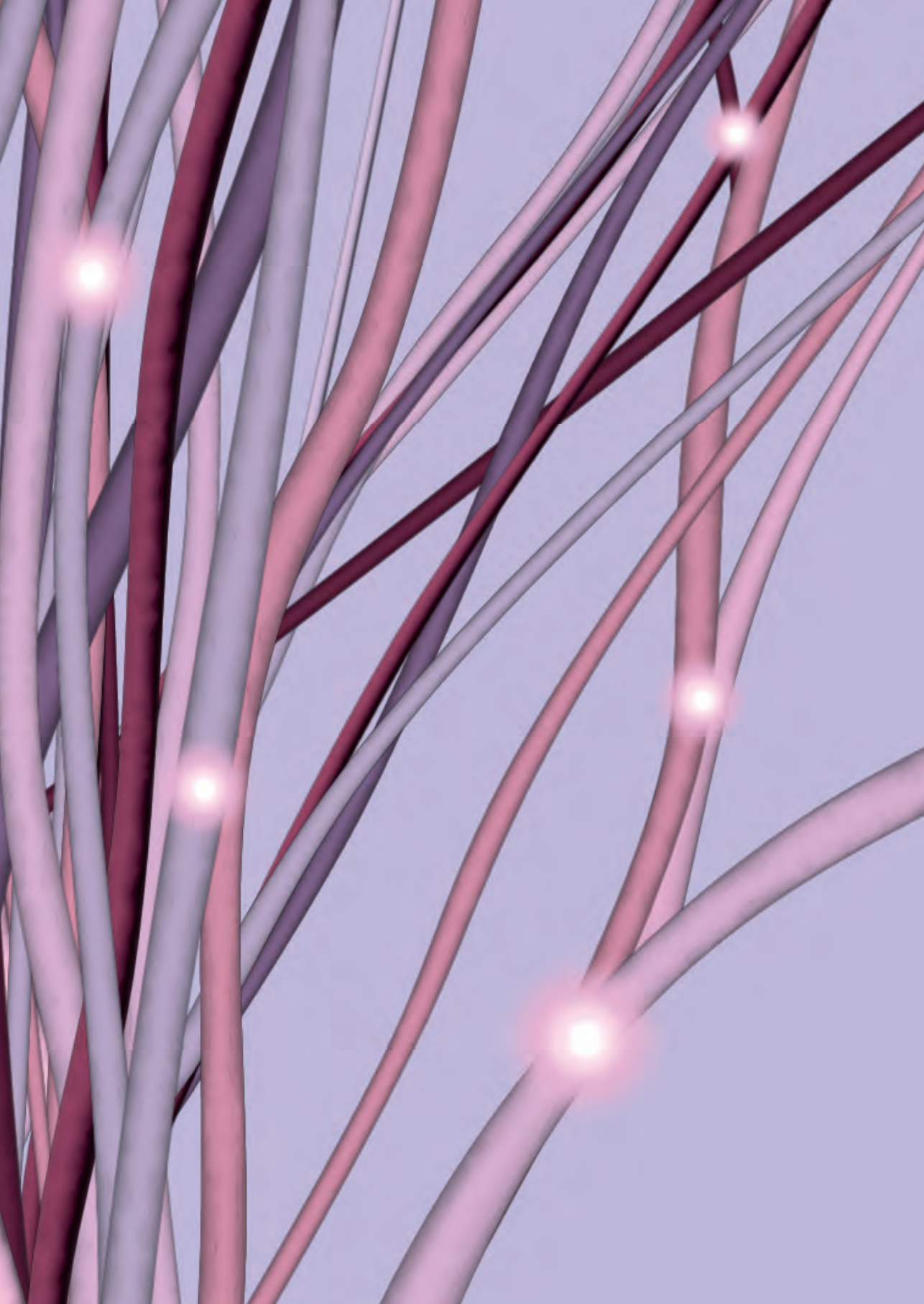

Chapter 4

Type III collagen-containing scaffolds modulate skin wound healing

Nancy Avila-Martinez[1], Roman Krymchenko[1], Martin Konovalov[1], Merel Gansevoort[1], Maren Pfirrmann[1], Marcel Vlig[2], Martijn Verdoes[1,3], Bouke K. H. L. Boekema[2,4,5], Toin H. van Kuppevelt[1], Willeke F. Daamen[1*]

[1] Radboud university medical center, Research Institute for Medical Innovation, Department of Medical BioSciences, Nijmegen, The Netherlands

[2] Alliance of Dutch Burn Care, Burn Research Lab, Beverwijk, The Netherlands

[3] LUMC, Department of Immunology, Leiden, The Netherlands

[4] Department of Plastic, Reconstructive and Hand Surgery, AUMC, location AMC, Amsterdam, The Netherlands

[5] Tissue Function and Regeneration, Amsterdam Movement Sciences Research Institute, Amsterdam, The Netherlands

Manuscript in preparation

Abstract

As a major dermal component of adult skin, type I collagen (Col I) has been widely used for skin substitutes, yet minimizing scarring remains a clinical challenge. In contrast, fetal skin heals without scarring and contains high levels of type III collagen (Col III), which decline with aging. To investigate the role of Col III in wound healing, porous crosslinked sponges with different Col I/III ratios mimicking three developmental stages were created. Atelocollagen enriched in Col III was successfully obtained from human placenta. Upon combining Col III atelocollagen with Col I collagen fibrils in Col I + III scaffolds, a high Col III concentration altered pore morphology and reduced scaffold stiffness. *In vitro*, Col III-containing scaffolds downregulated fibrotic associated markers (ACTA2 and TGFB1) in human dermal fibroblasts. M0 macrophages cultured on these scaffolds exhibited surface marker profiles consistent with an M2-like phenotype. In a rat full-thickness wound model, Col III led to lower deformation in the wound morphology, an epidermal thickness resembling native skin, and faster scaffold degradation than untreated wounds after 28 days. These findings highlight the potential of Col III to regulate wound healing, offering promising implications for improving skin treatments, such as for burn injuries.

Keywords: Collagen III, fetal skin, macrophages, fibroblasts, scar, rat model

1. Introduction

Collagen-based sponges are widely used in clinical settings for treating severe burns, including third-degree injuries [1]. These skin substitutes primarily consist of type I collagen (Col I), the dominant protein in the dermis (~80%) [2]. Despite their effectiveness, they do not prevent scarring, which is the typical outcome of the wound healing process of deep wounds in adults [3]. In contrast, in the fetal stage skin regeneration occurs before 24 weeks of gestation [4], with key differences in among others the extracellular matrix (ECM), such as a higher occurrence of type III collagen (Col III) compared to adult skin [5].

In adults, Col III is the second most abundant collagen in the skin after Col I [6]. While exact values vary in the literature and among individuals, studies have reported a Col I/III ratio in humans of 0.6:1 in a 15-week fetus, shifting to 1:1 at 24 weeks gestation and at birth, and increasing to 2-3:1 for adults [7-9]. Col III plays an important role in early wound healing by forming a fine provisional matrix during inflammatory-proliferative phases, which supports cell migration to the wound site and the formation of granulation tissue [10, 11]. Subsequently, it is gradually replaced by mature Col I, which provides increased tensile strength to the skin. However, an excessive accumulation of dense, parallel fibers and an imbalanced Col I/III ratio can negatively affect scar quality with reports of even 4:1 for hypertrophic scars [8, 12].

The interaction between cells and the ECM is essential for effective wound healing. Matrix stiffness, in particular, plays a key regulatory role: fibroblasts sense mechanical cues through focal adhesions like integrin α11β1, which promotes myofibroblast activation, a cell type associated with scar formation [13]. These myofibroblasts are characterized by α-smooth muscle actin (α-SMA) stress fibers and the release of transforming growth factor beta 1 (TGFβ1), contributing to fibrosis when they persist in the wound environment [14, 15]. Macrophages are also influenced by matrix mechanics; softer matrices tend to support a pro-healing M2-like phenotype, whereas a stiffer matrix promotes the pro-inflammatory M1 subtype [16, 17]. Col III contributes to lower ECM stiffness [18], probably because these fibrils are thinner and more flexible than the thicker, more rigid fibrils of Col I [19].

Obtaining sufficient Col III for dermal template creation is challenging due to its lower natural abundance compared to other ECM components. Placenta contains a wide range of collagens such as type I, III, IV, V and VI collagen [20], making it a valuable source for Col III. Effective isolation requires precise methods to separate

Col III while minimizing contaminants. A critical step in this process is pepsin digestion, which cleaves all collagen telopeptides to produce atelocollagen, whose enhanced solubility facilitates downstream purification procedures [21]. Understanding the structural differences between Col I and Col III and their properties further aids in selective extraction. Col I is a heterotrimer consisting of two α1(I) chains (139 kDa) and one α2(I) chain (129 kDa) (UniProtKB, P02452, P08123), whereas Col III is a homotrimer of α1(III) chains, each weighing 138 kDa (UniProtKB, P02461). Their amino acid composition influences solubility, with both collagens precipitating in acidic conditions at 0.7 M NaCl. However, Col III favorably precipitates in neutral buffer at 1.8 M NaCl, enabling its selective separation during purification [22].

Col III has been incorporated into hydrogels for repairing wounds [23], but sponges provide a more stable healing template for deep and extensive wounds. In this study, Col III was isolated from human placenta and used to develop chemically crosslinked porous scaffolds. Various Col I/III ratios were tested to mimic different life stages: 1:2 (early fetal), 1:1 (newborn), and 3:1 (adult). The impact of Col III atelocollagen and insoluble Col I fibrils in scaffolds was evaluated *in vitro* using fibroblasts and macrophages and further analyzed *in vivo* using a Wistar rat model with full-thickness excisional wounds.

2. Materials and methods

2.1 Col III isolation and characterization

Placentas from uncomplicated pregnancies were obtained with informed consent from women undergoing elective caesarean sections. Tissue was either processed on the same day or stored at 4 °C for up to 24 h before processing. To obtain blood-free basal placenta, the chorion and amniotic sac were removed using a scalpel. The basal placenta was subsequently washed 6 times with 2 L of demineralized water and rinsed with 25 mL of ACK buffer (0.1 mM EDTA, 10 mM $KHCO_3$, 150 mM NH_4Cl, pH 7.2) into each artery. Peripheral blood vessels were injected with 150 mL of ACK buffer, plus an additional injection of 300 mL into the basal tissue to remove remaining erythrocytes. The basal tissue was homogenized using a blender (MultiQuick 3 Vario, Braun, Neu-Isenburg, DE) and centrifuged at 7270 × g for 10 min in 500 mL of ACK buffer. The pellet was washed 10 times with fresh buffer. Finally, the pellet was snap-frozen in liquid nitrogen, and stored at -80 °C.

All incubations were performed at 4 °C under constant agitation (Supplementary Fig. 1). Blood-free basal placenta (200 g) was resuspended in 1 L of 0.25 M acetic acid for 2 h, followed by the slow addition of 1 L of 4 M NaOH and incubation for 1 h. The solution was neutralized with 6 M HCl, filtered using 850 µm sieves on top of 90 µm sieves, and resuspended in NaCl buffer (1 M NaCl, 50 mM Tris, 20 mM EDTA, pH 7.2) for sequential incubations of 2 h, overnight, and 4 h. After sieving, the sample was washed five times with demineralized water until conductivity reached <50 µS and left overnight. The isolate was resuspended in 1 L of 0.5 M acetic acid with 1 g of pre-diluted porcine pepsin (P6887, Merck, Darmstadt, DE) for 6 h, followed by an additional 1 g of pepsin and overnight incubation. After centrifugation (12,500 × g, 1 h), the supernatant was adjusted to 0.7 M NaCl using 3.6 M NaCl/0.5 M acetic acid and stirred at 200 rpm for 6 h. The precipitate was collected by centrifugation (12,500 × g, 1.5 h) and resuspended in 1 M NaCl/50 mM Tris (pH 8), homogenized, and adjusted to 1.8 M NaCl. The solution was centrifuged (12,500 × g, 1 h), and the pellet was dissolved in 750 mL of 0.5 M acetic acid overnight while stirring. Filtration was performed using a 100 kDa MWCO membrane (Vivaflow 50 Crossflow Cassette, Sartorius, Göttingen, DE) against three volumes of 0.5 M acetic acid using a peristaltic pump at 20 ml/min. The solution was then adjusted to 0.7 M NaCl, stirred overnight, and centrifuged (12,500 × g, 1 h). The final pellet was dissolved in 0.05 M acetic acid, dialyzed with a 100 kDa (131417, Biotech CE, Waltham, MA, USA) membrane and the solution was changed 3 times. The final isolate was lyophilized using a Lyoph-pride 03 freeze dryer (ilShin Biobase Europe, Ede, NL) and stored at -20 °C.

Collagen purity was assessed using 8% SDS-PAGE run at 100 V for 3 h. Samples were diluted in sample reduction buffer [24] and boiled for 10 min. Bovine insoluble type I collagen (isolated at Radboudumc) and bovine soluble type III collagen (001-001-105, Rockland, Limerick, PA, USA) were used as controls. Gels were stained with Coomassie blue and imaged with Bio-Rad Molecular Imager Gel Doc XR (Bio-Rad, Hercules) system on a White Light Conversion Screen in grayscale. The intensities of the bands were used to calculate the α1/α2 ratio in the sample to assess Col III content for the construction of the scaffolds. The other gels were transferred to nitrocellulose membranes (162-0112, Bio-Rad, Hercules, CA, USA) for Western blotting and blocked with 2% bovine serum albumin (BSA) in PBST (0.1% Tween-20 in PBS) overnight. Immunostaining was performed with anti-type I collagen rabbit polyclonal antibodies (1:5000, ab34710, Abcam, Cambridge, UK) and anti-type III collagen mouse monoclonal antibodies (1:2500, ab6310, Abcam) for 1 h. Secondary antibodies included IRDye 680CW goat anti-rabbit IgG (1:15000, 926-32221, LI-COR, Lincoln, NE, USA) and IRDye 800CW goat anti-mouse IgG

(1:10000, 926-32210, LI-COR). Blots were scanned using the Odyssey CLx imager (LI-COR), and signal quantification was performed with Image Studio™ Version 5.0 (LI-COR).

For DNA and glycosaminoglycans (GAGs) quantification, lyophilized placenta and Col III isolate were enzymatically digested overnight at 65 °C using 2.5 U/ml papain (P3125, Merck), 2 mM EDTA, 2 mM cysteine in 50 mM sodium phosphate (pH 6.5). DNA content was measured using Hoechst 33258 fluorescence dye assay [25]. In short, papain digested samples were diluted in TEN buffer (10 mM Tris, 1 mM EDTA, 100 mM NaCl in demineralized water, pH 7.4) and calf thymus DNA (D1501, Merck) was used for calibration curve. Fluorescence was measured at 360/40 and 460/40 in the BioTek ELISA plate reader (ClarioSTAR, BMG Labtech, Offenburg, DE). GAG content was determined using a dot blot colorimetric assay with Alcian blue staining. A polyvinylidene fluoride (PVDF) membrane (0.45 µm, Thermo Scientific, Waltham, MA, USA) was activated by sequentially submerging in methanol, 30% isopropanol, and 0.25% (w/v) cetylpyridinium chloride (CPC) in 30% isopropanol, followed by two washes in PBS. The membrane was placed in a dot blot apparatus with two wet filter papers at the base, and samples were spotted alongside a chondroitin sulfate A (C8529, Sigma-Aldrich) as a GAG standard. The membrane was incubated in 10× diluted Alcian blue solution for 30 min, as described by Clausen *et al.* [26], then destained in demineralized water for 5 min. Imaging was performed using a Molecular Imager Gel Doc XR system with a White Light Conversion Screen in grayscale.

Protein content was quantified using the A205 method (Thermo Fisher) following the manufacturer's instructions. Isolates were dissolved in 0.05 M acetic acid, while placenta samples were prepared in 8 M urea with 10 mM Tris-HCl (pH 8). Measurements were taken using a NanoDrop™ 2000 spectrophotometer (Thermos Scientific, Rockford, IL, USA) at 205 nm, with appropriate negative controls.

Calculations of the Col III and Col I content were made based on the α1/α2 chains intensities on the SDS-PAGE gel. Ratios of collagens in the isolate were also assessed by mass spectrometry (MS). Pulverized placenta tissue (containing insoluble collagens) and Col III isolate (containing soluble atelocollagens) were analyzed at Radboud Technology Center for Mass Spectrometry (n=1). Data were analyzed using the Peaks Studio X software (Ontario, CA).

2.2 Preparation and characterization of type I/III collagen scaffolds

Four types of scaffolds were prepared using insoluble bovine type I collagen fibrils and soluble atelocollagen type III isolated from human placenta (Table 1). The

incorporated Col III content was calculated assuming the preparation enriched in Col III contained only protein and that the intensity of the Col I α2 band on the gel was 15%, which would mean that the Col I α1 band needs to comprise 30% (Col I consists of two α1 and one α2 polypeptide), thus indicating 55% Col III in the final product.. A 0.8% (w/v) collagen suspension in 0.25 M acetic acid was prepared and allowed to dissolved overnight, homogenized, frozen at -20 °C for 4 h, and lyophilized. For *in vitro* and *in vivo* testing, scaffolds were chemically crosslinked (X) using 33 mM 1-ethyl-3-(3-dimethylaminopropyl)-carbodiimide (EDC) and 6 mM N-hydroxysuccinimide (NHS) in 50 mM 2 morpholinoethane sulphonic acid (MES) for 3 h. They were then washed in 0.1 M Na_2HPO_4, 1 M NaCl, 2 M NaCl, and demineralized water, followed by freezing at -20 °C and lyophilization. Scaffolds were cut into Ø 12 mm disks and gamma sterilized (25 kGy, Steris, Ede, NL). Untreated scaffolds (U) without crosslinking served as controls.

Table 1. Composition of collagen scaffolds.

#	Condition	Components	Description
1	Col I	Type I collagen	Control
2	Col I/III 3:1	75% type I collagen + 25% type III collagen	Mimics adult skin
3	Col I/III 1:1	50% type I collagen + 50% type III collagen	Mimics newborn skin
4	Col I/III 1:2	33% type I collagen + 67% type III collagen	Mimics fetal skin

The degree of crosslinking was determined by the loss of primary amine groups after crosslinking using 2,4,6-trinitrobenzene sulfonic acid (TNBS). Glycine was used for the calibration curve. Absorbances were measured at 420 nm using a spectrophotometer (SpectraMax iD3, Austria). The morphology of the scaffolds was analyzed using Scanning electron microscopy (SEM). Dry scaffolds were fixed on a stub with double-sided carbon tape, sputtered with gold twice for 60 s (Scancoat Six Sputter Coater, Edwards, Crawley, United Kingdom) and examined with a Zeiss Sigma 300 Field Emission Scanning Electron microscope (Zeiss, Jena, DE) at an accelerating voltage of 3 kV.

The distribution of Col III in the scaffolds was assessed using indirect fluorescence microscopy (IFA). Cryosections (7 µm) of frozen scaffolds in TissueTek O.C.T. compound (Sakura Finetek, Alphen aan den Rijn, NL) were mounted on glass slides and air-dried for 30 min. For IFA, sections were blocked with 2% BSA-PBST and incubated for 1 h with anti-rabbit type I collagen polyclonal antibody (1:500, ab34710) and anti-mouse type III collagen monoclonal antibody (1:100, ab6310). After three 5-min PBST washes, secondary antibodies from Molecular Probes Inc. (Eugene, OR, USA), goat anti-rabbit IgG Alexa Fluor 488 (1:500, A-11008) and goat

anti-mouse IgG Alexa Fluor 594 (1:500, A-11032), were applied for 1 h. Sections were dehydrated in 100% ethanol and mounted in Mowiol (Merck, Darmstadt, DE). Imaging was performed with the Zoe™ Fluorescent Cell Imager (Bio-Rad).

To measure the stiffness of the scaffolds, the compressive strength was measured in a materials testing device (Bose Corp. ElectroForce Systems Group, MN, USA) with a 22 N load cell. Specimens were compressed at a displacement rate of 10 mm/min, up to a maximum load of 15 N (or 132 kPa). 10 specimens were used per condition. The compressive tests typically resulted in a non-linear stress-strain curve, with an initial toe region with low stiffness, followed by increased stiffening due to compaction of the porous scaffolds. A simplified compressive modulus of the scaffolds representing the stiffness was calculated as the ratio of stress and strain at a strain level of 95% strain, using the stress-strain graphs.

In vitro analysis of scaffolds using fibroblasts

Primary human dermal fibroblasts (3 donors) were cultured in Dulbecco's modified eagle medium (DMEM) supplemented with 1x GlutaMax, pen-strep, (all from Gibco, Paisley, UK), 10 % fetal bovine serum (FBS, 205 HyClone™, Cytiva Life Sciences, Marlborough, MA, USA) and maintained in a culture incubator at 37 °C with 5% CO_2. All donor cells were confirmed mycoplasma free as assessed by the Lonza MycoAlert mycoplasma detection kit. Cells were harvested at passage 2 and seeded onto scaffolds at passage 3. A total of 200,000 cells were seeded per pre-wetted scaffold in a 24-well plate. Medium was refreshed on days 3 and 6. Samples were collected at days 1 and 7 for PCR and WB analysis.

Cell viability was evaluated using alamarBlue assay (Invitrogen, Carlsbad, CA, USA). The reagent was added in 1:10 diluted in culture medium to the scaffolds at days 1 and 7. After 4 h incubation, the supernatant was transferred to a 96 well-plate and fluorescence was measured using a SpectraMax iD3 (Molecular Devices, San Jose, CA, USA) with excitation/emission wavelengths of 530/590 nm.

For mRNA quantification, samples were collected in Trizol, frozen at -80 °C, or processed for RNA isolation. Scaffolds were crushed with a pipette tip at room temperature for 20 min, followed by centrifugation at 12,000 g for 10 min at 4 °C. The supernatant was transferred to a new tube, and RNA was isolated using the RNeasy Mini Kit (74106, Qiagen, Hilden, DE) with the RNase-Free DNase Set (79254, Qiagen). RNA yield and purity were assessed at 260 nm using the NanoDrop 2000 spectrophotometer. cDNA synthesis was performed using the iScript™ cDNA Synthesis Kit (Bio-Rad) following the manufacturer's protocol. Quantitative PCR was

conducted with iQ™ SYBR® Green Supermix (Bio-Rad), for the primer sets: GAPDH (5' TGG GTG TGA ACC ATG AGA AG 3'-3' AGT TGT CAT GGA TGA ACC TTG G 5'), ACTA2 (5' CCG ACC GAA TGC AGA AGG A 3'- 3' ACA GAG TAT TTG CGC TCC GAA 5'), TGFB1 (5' CGC GTG CTA ATG GTG GAA A 3' - 3' TGT GTG TAC TCT GCT TGA ACT TGT CA 5') and TGFB3 (5' CAA TTA CTG CTT CCG CAA CTT G 3' - 3' GAT CCT GTC GGA AGT CAA TGT AGA 5') (Biolegio, Nijmegen, NL). Amplifications were performed in duplicate on a CFX96 Touch Deep Well or CFX Connect Real-Time PCR Detection System (Bio-Rad) under the following conditions: 3 min at 95 °C, followed by 40 cycles of 15 s at 95 °C and 30 s at 60 °C with plate reading, and a final melt curve analysis (10 s, 65-95 °C). Gene expression fold changes were calculated using the $2^{-\Delta\Delta Ct}$ method relative to Col I at day 1. Data were processed using CFX Maestro™ Software (Bio-Rad) and visualized as heatmap using GraphPad Prism.

Protein expression was analyzed through Western blotting in a 10% SDS-PAGE gel. Primary antibody anti-α-SMA was used (1:2000, clone 1A4, A-2547, Merck) in combination with anti-GAPDH (1:1000, clone 14C10, ID218, Cell Signaling Technology). As secondary antibodies goat polyclonal anti-mouse IgG, IRDye 800CW conjugated (1:10,000, 926-32210, LI-COR) and goat anti-rabbit polyclonal IgG antibodies, IRDye 680CW conjugated (1:15,000, 926-32221, LI-COR) were used and read in the Odyssey CLx imager (LI-COR).

In vitro analysis of scaffolds using macrophages

Primary human monocytes (3 donors), isolated from buffy coats of healthy donors, were differentiated to M0 macrophages for six days with 50 ng/ml macrophage colony-stimulating factor (M-CSF, 300-25, PeproTech in RPMI 1640 media with 10% FBS, 1% ultraglutamine and 1% antibiotic/antimycotic at 37 °C in 5% CO_2. As secondary controls for the cell surface markers, M0 macrophages were further polarized for 24 h into M1-like macrophages using 100 ng/ml lipopolysaccharides (LPS, vac-3pelps, InvivoGen) and 20 ng/ml interferon-gamma (IFNγ, 300-02, PeproTech), or into M2-like macrophages using 20 ng/ml interleukin-4 (IL4, 170-076-135) and 20 ng/ml interleukin-13 (IL13, 130-112-412) (both from Miltenyi Biotech). On day 7, cells were harvested and 200,000 M0 macrophages were seeded on scaffolds and incubated for 48 h. The secondary controls M1-like and M2-like differentiated macrophages were seeded on Col I scaffolds only.

Macrophages were enzymatically retrieved using 0.25 U/ml collagenase A (Roche, Mannheim, DE) in a shaking water bath for 30 min at 37 °C. PBS containing EDTA was added to the scaffolds and incubated for 30 min at 4 °C. Viable cells were detected with eFluor 780-APC+Cy7 (1:2000, 65-0865-14, ThermoFisher). Cell surface markers

from BD Biosciences (Franklin Lakes, NJ, USA) or BioLegend (San Diego, CA, USA) included CD45 (1:20, 304026), CD80 (1:20, 305220), HLA-DR (1:20, 307646), CD206 (1:40, 551135), and CD163 (1:40, 562643). Mean fluorescence intensity (MFI) was measured using a BD FACSVerse Cell Analyzer (BD Biosciences) and analyzed with FlowJo X (vX 0.7, Tree STAR, Ashland, OR, USA). Gating involved singlets, live CD45+ cells, and specific CD markers as presented in Avila-Martinez *et al.* (2025) [27].

Rat full-thickness skin wound model for *in vivo* evaluation of scaffolds

Fifteen male Wistar rats (3 months old, 300–400 g, WI:WU Charles River) were used to establish a full-thickness skin wound model. All procedures were approved by the local Animal Experiments Committee. Rats were housed with *ad libitum* access to booster food (Ssniff Spezialdiäten, Soest, DE), and water with controlled amounts of sunflower seeds, one day before surgery and 2 weeks post-surgery. Upon arrival, they were labeled with an ear punch and handled for 1–2 weeks before surgery.

Rats were anesthetized with 1.5–2.5% isoflurane, and eye cream (Ophtosan®, AST Farma, Oudewater, NL) was applied. Their backs were trimmed with a hair clipper, and hair was further removed using Veet cream (Reckitt Benckiser, Slough, UK). Four full-thickness wounds (Ø 12 mm) were created on each rat's back using a biopsy punch (220701, SMI AG, St. Vith, BE) and curved scissors. Sterile scaffolds were placed to fit the wound edges and secured with 6–8 resorbable sutures (100L6P, Monocryl™ 4-0, Ethicon, Raritan, NJ, USA). Wounds were covered with a silicone dressing (Mepilex Border Flex Lite, Mölnlycke, Gothenburg, SE), an elastic bandage (PetFlex, Andover Healthcare, Portsmouth, NH, USA), and fixed with adhesive plaster (Leukoplast®, Hamburg, DE). Post-operative analgesia (carprofen, 0.1 ml/100 g) was administered for three days.

Experimental design: Pilot experiments were conducted for 14 days (6 rats) to refine surgical techniques and select conditions for the final experiment (Supplementary Fig. 2). Treatments included untreated and Col I controls. The first pilot tested Col I/III 1:2, while the second tested Col I/III 1:1 and 3:1. For the final experiment (9 rats, endpoint at day 28), Col I/III 1:1 was selected. An additional condition, not related to this study, was included. Treatment locations were randomized (randomizator.org) to avoid repetition, with four wound sites (A–D) assigned per rat.

Wound healing was monitored for the final experiment through digital photography at days 0, 7, 14, 21, and 28 during dressing changes. At day 28, rats were euthanized

by CO_2 inhalation, and scaffolds with surrounding tissue were collected. Half of the tissue was fixed in 4% paraformaldehyde (PFA) in phosphate buffer pH 7.4 overnight, then stored in 1% PFA prior to paraffin embedding. The other half was embedded in TissueTek and frozen at -80 °C.

Macroscopic analysis: Wound contraction (%) was calculated using Equation 1**,** while wound morphology was determined using Equation 2. A morphology value closer to 1 indicates a more circular wound, suggesting less contraction. Two axes were measured: the length was defined as the vertical distance along the head-to-tail axis of the animal, and the width as the horizontal distance perpendicular to this axis. Measurements were taken directly across the wound area, with the rat positioned dorsally (back facing up).

$$Wound\ contraction\ (\%) = \frac{Ao - An}{Ao} \cdot 100 \qquad \textit{Equation 1}$$

$$Morphology\ (1) = \frac{length\ (cm)}{width\ (cm)} \qquad \textit{Equation 2}$$

Where A_0 is the original wound area, and A_n is the wound area at days 7, 14, 21, or 28.

Microscopic analysis: Paraffin-embedded sections (5 µm) were stained with hematoxylin and eosin (H&E) or Masson's trichrome blue to assess skin layers, appendages, and scaffold remnants. For immunostaining, tissues were stained for α-SMA (1:2000, clone 1A4, A-2547) to identify mature blood vessels and myofibroblasts, and CD68 (1:200, MCA341R) to detect macrophages. Immunoreactivity was visualized using AEC staining as follows. Paraffin-embedded sections were first deparaffinized and incubated in 0.5% hydrogen peroxide (K44653709, Merck) for 1 h to block endogenous peroxidase activity. After a 5-min rinse in demineralized water, antigen retrieval was performed by boiling the sections for 10 min in citrate buffer (10 mM tri-sodium citrate, pH 6.0), followed by cooling for 40 min. Sections were then rinsed twice in demineralized water (2 × 2 min) and incubated for 30 min in blocking solution (0.5% BSA in PBS containing 0.05% Triton X-100). Primary antibodies were applied for 45 min. Next, sections were incubated with biotinylated goat anti-mouse IgG (H+L) secondary antibody (1:200, BA-9200, Vector Laboratories) for 45 min. The Elite® ABC peroxidase kit (PK-6100) was applied for 1 h, followed by AEC substrate (SK-4205) development for 5–8 min. Finally, sections were counterstained with hematoxylin and mounted using VectorMount® (H-5501). Sections were scanned (3DHISTECH, Budapest, HU) and visualized using CaseViewer 2.4.

Epidermal thickness was measured three times at different locations using H&E staining. Wound width was assessed at both the middle and upper parts of the wound. Hair follicles and sebaceous glands were counted within and around the wound area. Healed tissue was semi-quantitatively scored by two independent evaluators (NA, RK) for myofibroblast presence, macrophage infiltration, angiogenesis, and residual collagen using AEC and trichrome blue staining. Scores ranged from 0 (absent) to 3 (abundant). Discrepancies between evaluators were resolved through re-evaluation until a consensus was reached.

2.6 Statistical analysis

Data were analyzed statistically and visualized using GraphPad prism 10.4.1 (GraphPad Software, San Diego, CA, USA). Comparison between conditions were calculated with one-way ANOVA, repeated measurements, with Tukey's multiple comparison test. When more than two groups per condition were evaluated (e.g. days or sterilization), a two-way ANOVA with Tukey's multiple comparison test was used. A p-value of <0.05 (95% confidence interval) was considered statistically significant. To assess inter-rater reliability in the histological scoring, the intraclass correlation coefficient was calculated using IBM SPSS Statistics 29 (Armonk, NY, USA). Values ≥ 0.75 indicate substantial agreement.

3. Results

3.1 Col III isolation and characterization

We developed and optimized a method to enrich Col III in a preparation from human basal blood-free placenta tissue, employing pepsin digestion and selective salt precipitation, based on available protocols [22, 28, 29]. Hereafter, the term "placenta" refers specifically to the blood-free basal placental tissue. The purity of the isolated collagen was assessed using SDS-PAGE, followed by Coomassie blue staining. Col III isolates from different batches consistently exhibited a prominent band around 130 kDa (Fig. 1A), corresponding to the α1 chains (α1) in both type I and III collagen. Western blot analysis (Fig. 1A) confirmed that this band primarily represented Col III, as indicated by green immunostaining, while Col I was detected in red. Additionally, β (two α chains) and γ chains (three α chains) were observed on the blot (Fig. 1A, Supplementary Fig. 3). The placenta-derived bands appeared faint, likely because the insoluble collagen did not migrate into the gel. Band quantification showed 85% α1 and 15% α2 chains. Given the 2:1 α1:α2 ratio of Col I, we estimate 30% of α1 chains belong to Col I and 55% to Col III. From 100 g of wet placental tissue, 1.02 ± 0.17 g of lyophilized isolated material

was obtained. After isolation, DNA and GAG content were reduced 10-fold and 100-fold, respectively compared to placenta (Fig. 1B). Due to insolubility of proteins in placenta, protein quantification was only possible in the soluble isolates, which had a mean protein concentration of 91%. MS analysis revealed that Col III α1 made up 40% of the detected collagenous proteins in the isolate, followed by Col I α1 (29%), Col VI (21%), Col I α2 (6%) and Col IV α1 (4%) (Supplementary table 1). In contrast, nine collagen types were identified in placenta, but Col III α1 and Col I α2 were undetectable, while Col I α1 was present at only 2% likely due to the insolubility of native collagen compared to the soluble atelocollagens in the isolate. Comparing Col I and Col III levels, Col III α1 comprised 53% vs. 47% Col I (α1+α2). These results support SDS-PAGE estimates, where Col III represents ~55% of the isolate, the value used for scaffold calculations.

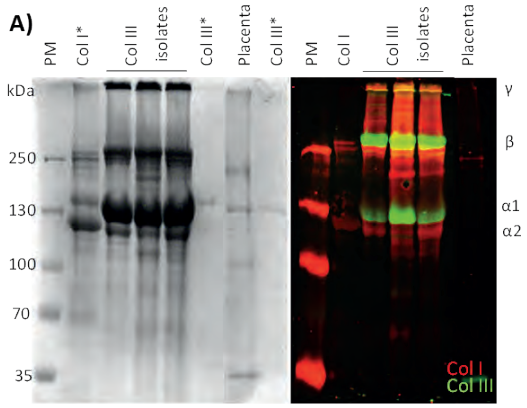

B)

Parameter	Isolate	Placenta
Yield (isolate /placenta)	~ 1%	-
DNA content (µg/mg sample)	4.9 ± 0.3	60.5 ± 0.3
GAG content (µg/mg sample)	0.3 ± 0.1	4.9 ± 0.4
Protein concentration (%)	91%	-

Figure 1. Type III collagen purification analysis. A) Left image is a Coomassie-blue stained 8% SDS-PAGE gel including protein marker (PM), three different Col III isolates, placenta and controls (*) for Col I and Col III (bovine source). Right image corresponds to an immunoblot staining with Col III in green and Col I in red. The molecular weight of collagen chains is around 110, 130, 250 and >300 kDa for α2, α1, β and γ respectively. Pre-stained protein marker is also visualized with these settings. Individual channels for Western blotting show the specific stainings for each antibody (Supplementary Fig. 3). B) Summarizing table of different quantification parameters from the isolate as mean ± standard deviation (SD).

3.2 Characterization of type I/III collagen scaffolds

Scaffolds with different ratios of Col I/III were constructed using insoluble Col I (fibrils) and soluble Col III (atelocollagen) and chemically crosslinked, with Col I-only scaffolds serving as controls. Scanning electron microscopy revealed pore compression with increasing Col III content. Double immunostainings confirmed successful Col III integration, with overlapping Col I/III observed in the 3:1

condition, while scaffolds with higher Col III content displayed collagen distribution in distinct regions.

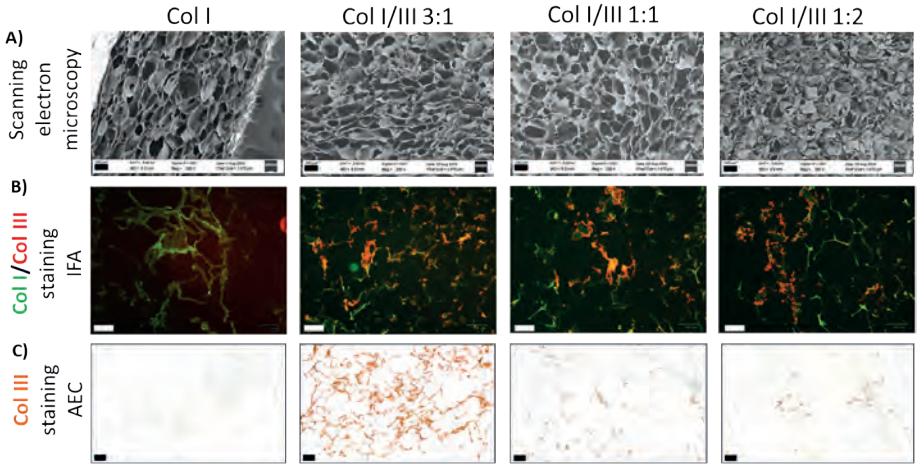

Figure 2. Scanning EM images and Col III incorporation of scaffolds. A) Morphology of the pores was visualized using scanning electron microscopy, B) Detection of Col I (green) and Col III (red) using fluorescence immunostaining assay. Individual channels showed the specific staining for each antibody (Supplementary Fig. 4). All images show cross-sections of scaffolds. Scale bar is 100 µm in all images.

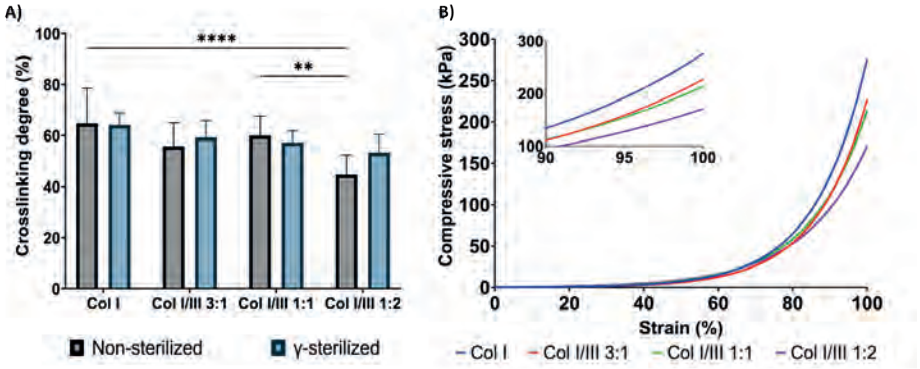

C)

Conditions	Col I	Col I/III 3:1	Col I/III 1:1	Col I/III 1:2
Compressive stress (kPa)	193	159	155	128

Figure 3. Mechanical behavior and crosslinking degree of different scaffolds. A) Percentage of amine groups bound after crosslinking before and after sterilization (n=3). Shown is mean ± standard deviation (SD). Two-way ANOVA was used for comparison between groups of sterilization, ** = $p < 0.01$, **** = $p < 0.0001$. B) Stress-strain curves obtained after fitting the compression test data (n=10 scaffolds from three independent batches) into one curve. Insert in the graph zooms in at the compressive stress at 90-100% strain. C) Table depicting compression stress values (kPa) at 95% strain in compressive testing.

Gamma irradiation was used to sterilize the scaffolds for *in vitro* and *in vivo* testing. Since this method can introduce new crosslinks and cause chain scission [30], the crosslinking degree was assessed before and after sterilization. The values remained around 55-60% for all conditions except for Col I/III 1:2 condition before sterilization (~45%), indicating that amine group content did not change due to sterilization (Fig. 3A).

Given that scaffolds were made using Col I fibrils combined with atelocollagen, weaker mechanical properties were expected with increasing Col III content. To evaluate this, compression assays were performed on sterilized, crosslinked scaffolds. Compression resistance was highest in Col I-only scaffolds and decreased with increasing Col III content (Fig. 3B). At 95% strain, stress values were similar between Col I/III 3:1 and 1:1, showing a 20% reduction in strength compared to Col I. However, in Col I/III 1:2 scaffolds, strength was nearly halved (~44% reduction).

In vitro analysis of scaffolds using human fibroblasts

Fibroblasts, the predominant dermal cell type, are essential for wound healing [31]. To evaluate how scaffold composition affects cell viability, we performed alamarBlue assay on primary human dermal fibroblasts seeded on scaffolds. After 7 days of culture, metabolic activity remained stable across all conditions, indicating that Col III incorporation did not affect the metabolic activity (Fig. 4A).

To evaluate myofibroblast presence, α-SMA protein expression was analyzed via Western blot, which remained below detection levels at both day 1 and day 7 across all scaffold conditions (Supplementary Fig. 5). Gene expression analysis was conducted using RT-qPCR on days 1 and 7 (Fig. 4B-C). Although not significant due to large donor variation, differences were found in ACTA2 and TGFB1 with trends per donor. By day 7 after cell culture on scaffolds, the Col I-only scaffold exhibited the highest ACTA2 (α-SMA) expression (2.3-fold change), with a progressive decrease as Col III content increased, to 1.6, 1.4 and 1.3-fold, respectively (Fig. 4B). In the case of TGFB1, a lower expression was observed by day 7 when Col III was incorporated into scaffolds (Fig. C). Significant differences were found for TGFB3 levels that showed reduced expression for Col I/III 3:1 and 1:1 compared to Col I-only. Additionally, Col I and Col I/III 3:1 showed significantly increased TGFB3 expression between day 1 and 7 (Fig. 5D).

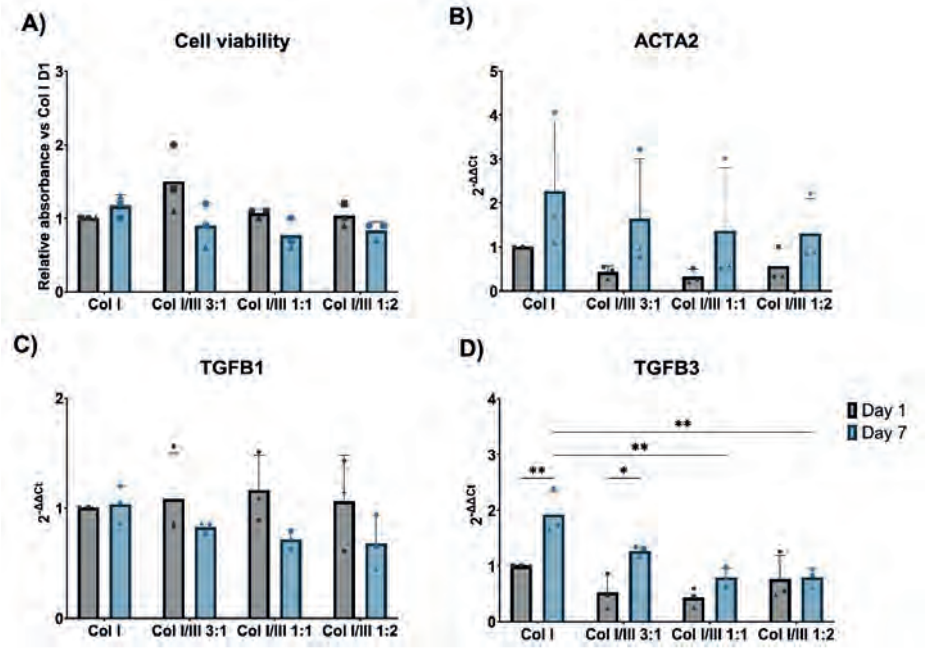

Figure 4. Effect of Col I and Col I/III scaffolds on primary human dermal fibroblasts. A) Cell viability analyzed by alamarBlue assay, normalized to Col I Day 1. mRNA expression assessed by RT-qPCR and compared to Col I D1. B) α-smooth muscle actin gene expression levels (ACTA2). C–D) Transforming growth factor β1 (TGFB1) and β3 (TGFB3). Individual donors are represented by different symbols as ● donor 1, ■ donor 2 and, ▲ donor 3. Two-way ANOVA was applied for comparison between groups. All values are presented as (mean ± SD). *= $p < 0.05$, ** = $p < 0.01$.

In vitro analysis of scaffolds using human macrophages

Type III collagen is abundant in early granulation tissue, a stage where macrophages typically transition from a pro-inflammatory (M1-like) to a pro-healing (M2-like) phenotype [32, 33].

Macrophages were seeded in different scaffolds and analyzed by flowcytometry after 48 h. Although limited by donor variability (n=3), we observed a reduction in the MFI of CD80 in scaffolds incorporating Col I and Col III seeded with M0 macrophages (Fig. 5A), with the Col I/III 1:1 scaffold showing significantly less expression of CD80 than M0 in Col I. A non-significant decrease for HLA-DR was observed in Col III-containing scaffolds (MFI 0.5) compared to M1-like control (MFI 1.5). The decrease of these two markers, associated with M1-like macrophages, suggests a shift away from the pro-inflammatory state. Notably, M0 macrophages seeded on the Col I/III 1:2 condition exhibited elevated CD206 expression in two out of three donors, reaching mean values (MFI 1.3) comparable to M2-like

macrophages in Col I scaffolds (MFI 1.4). (Fig. 5C). In addition, Col I increased (non-significantly) CD163 expression on M0 compared to other conditions, while M0 in Col III-containing scaffolds exhibited CD163 levels similar to secondary M1 and M2-like controls, based on MFI (Fig. 5D). While these findings indicate that Col III may influence macrophage polarization, potentially favoring a transition toward a regenerative phenotype, further studies with a large donor pool are needed to confirm these observations.

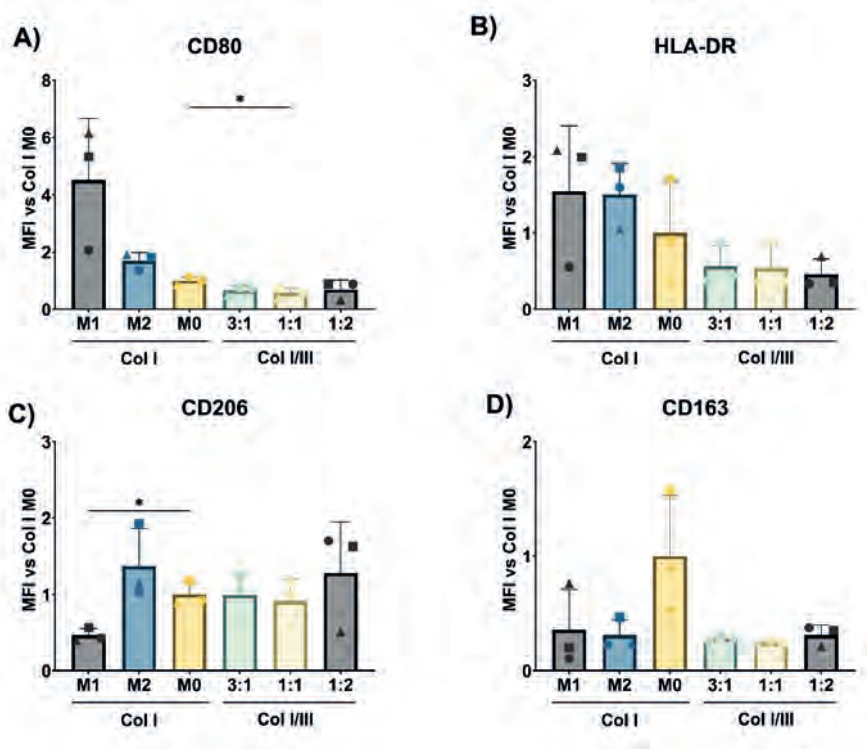

Figure 5. Effect of Col III on cell-surface expression in primary human macrophages (3 donors) after 48 h of culture on collagen scaffolds. A-B) M1-like macrophage markers (CD80 and HLA-DR**).** C-D) M2-like macrophage markers (CD206 and CD163). Macrophages seeded on Col I/III scaffolds were M0. Values represent relative mean fluorescence intensity (MFI) normalized to the Col I + M0 control (mean ± SD). Individual donors are represented by different symbols as ● donor 1, ■ donor 2 and, ▲ donor 3. Scaffold comparisons were analyzed using repeated measurements One way ANOVA with Tukey's multiple comparison test., *= $p<0.05$.

Rat full-thickness skin wound model for *in vivo* evaluation of scaffolds

To compare the wound healing efficiency, Col I and Col I/III scaffolds were implanted in full-thickness wound in rats. Two pilot animal studies were conducted until 14 days post-surgery to determine the optimal Col I/III scaffold composition for the final experiment. In the first pilot, four rats were assigned to different treatments: no scaffold, Col I and Col I/III 1:2. Col I/III 1:2 scaffolds, however, were too fragile for proper handling, requiring replacement of the scaffold during surgery as they tore easily during suturing. In the second pilot, two rats were used to test Col I/III 1:1 and 3:1 scaffolds. Both performed similarly during suturing, consistent with the results of mechanical testing (Fig. 3). The Col I/III 1:1 condition was selected for the final study, as it contained more Col III. Results from the pilot studies indicated that untreated wounds contracted more rapidly and exhibited a less circular morphology (Supplementary Table 2).

For the final experiment, nine rats were scheduled for a 28-day full-thickness skin implantation study. Two animals did not complete the study: one was found dead in its cage on day 21, likely due to bandage-related distress, and another was euthanized upon reaching a humane endpoint after significant weight loss and signs of discomfort. The remaining seven animals completed the study as planned. Macroscopic wound analysis was feasible only up to day 14 (n=9), as the scab dried and remained attached, resulting in inaccurate measurements of wound size and morphology beyond this time point (Fig. 6A). At day 14, wound contraction was similar for 1:1 and Col I-only scaffolds, but significantly lower than untreated wounds (Fig. 6B). Wounds treated with Col III-containing scaffolds significantly exhibited a more circular morphology than Col I or untreated wounds (Fig. 6C).

Histological images from the pilot study (day 14) and the final experiment (days 21 and 28) provided insights into wound healing progression (Fig. 7). At day 14, re-epithelialization was still ongoing in scaffold-treated wounds but already complete in untreated wounds. Wounds showed significant cellular infiltration, likely corresponding to the inflammatory-proliferative phase. The wound edges in untreated conditions appeared more contracted, which explains complete re-epithelialization. By day 21, re-epithelialization was nearly complete in scaffold-treated wounds. In untreated wounds, some areas showed the formation of new collagen fibers, indicating a transition toward the remodeling phase. In scaffold-treated conditions, particularly Col I, healing remained within the proliferative phase. By day 28, wound areas had reduced in size in both untreated and Col I/III-treated conditions.

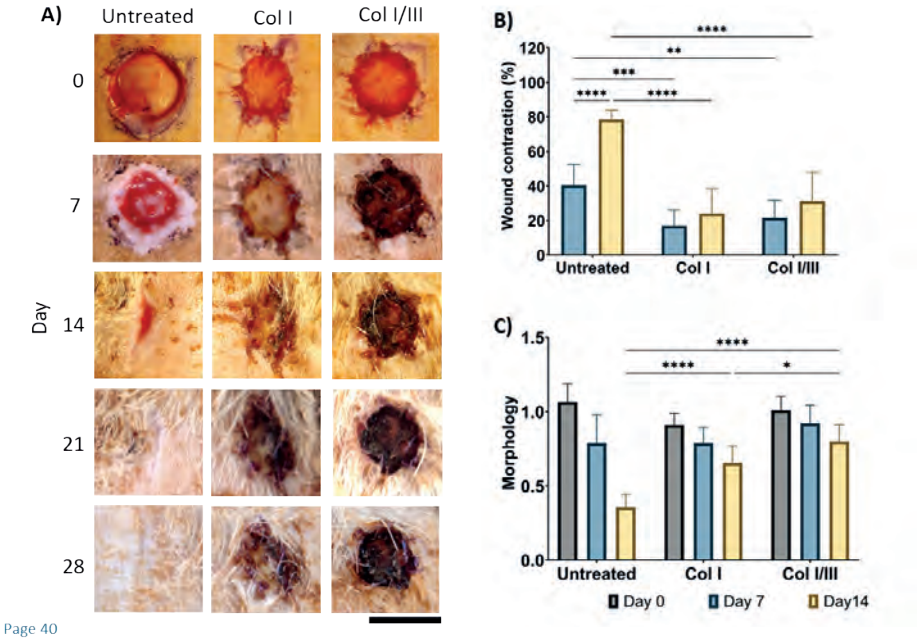

Page 40

Figure 6. Macroscopic evaluation of the skin healing time in untreated, Col I scaffold, and Col I/III scaffold treated wounds. A) Representative photos of the wound. B) Wound contraction compared to day 0. C) Morphology of the wound assessed by width-to-length ratio, where 1 indicates a symmetric circular shape. Data shown as mean ± SD (n = 9). Group comparisons were performed using two-way ANOVA with Tukey's multiple comparison test. * = p<0.05 ** = p < 0.01, *** = p < 0.001, **** = p < 0.0001. Scale bar is 1 cm.

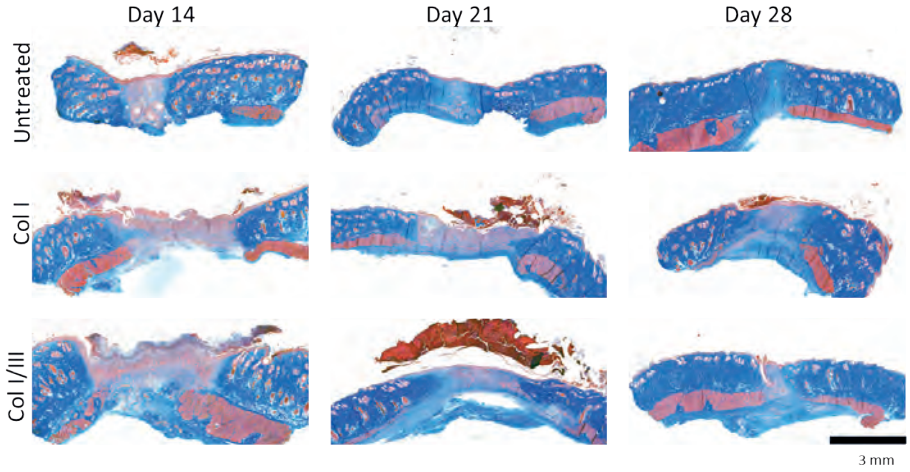

Figure 7. Histological evaluation during the wound healing process of different rats at day 14, 21 and 28. Masson's trichrome blue staining shows mature connective tissue, such as collagen bundles, in dark blue, whereas transitional connective tissue stains light blue and the red/pink/brown colors indicate among others cytoplasm, red blood cells, and blood vessels. Scale bar is 3 mm.

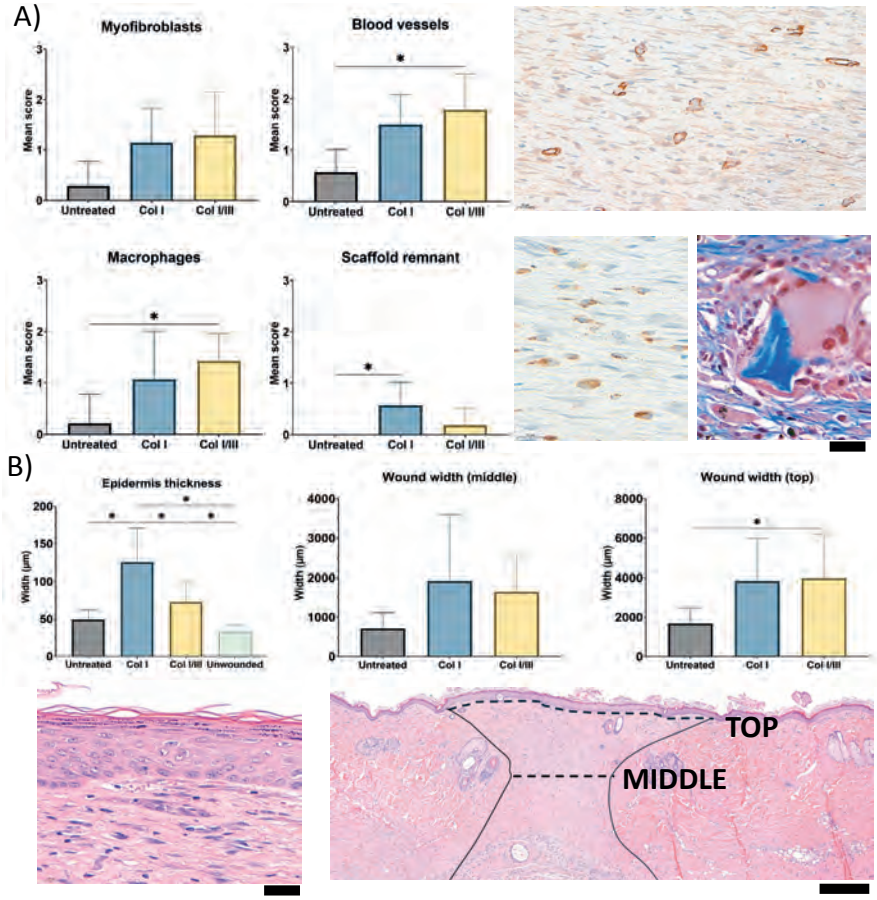

Figure 8. Histological analysis of wounds at day 28 (n=7 rats) for the different treatments. A) Samples were scored from 0 (not present) to 3 (abundant) for myofibroblasts and mature blood vessels identified by α-SMA staining in red/brown, macrophages infiltration assessed using CD68 staining in red and collagen remnants in blue, visualized with Masson's trichrome staining. Scale bar is 40 µm. B) H&E staining was used to assess epidermal thickness, wound width beneath the basal epidermis, as well as the mid wound width. Scale bar for epidermal image (left) is 40 µm and for overview of the wound (right) 500 µm. Repeated measurements One-way ANOVA was used for comparison between treatments with Tukey's multiple comparison test, *= $p<0.05$ ** = $p < 0.01$.

Immunostainings of the wounds revealed that scaffolds showed a significantly higher presence of mature blood vessels and macrophages in Col I/III scaffolds, while Col I also showed similar non-significant trends compared to untreated wounds (Fig. 8A). Moderate presence of myofibroblasts was observed across all conditions with no significant difference. These results indicate an ongoing transition between the proliferative and remodeling phase in the Col I/III condition. More scaffold remnants were observed in Col I scaffolds, indicating that scaffold degradation occurred more rapidly in the Col III condition. Wounds and surrounding tissue were histologically stained with H&E to measure the thickness of the epidermis and the wound width (Fig. 8B). At day 28, the epidermis was thicker in Col I treated wounds followed by Col III containing scaffolds and untreated wounds. The width of wounds at the top and middle location in the dermis was larger for wounds with scaffolds than untreated wounds, especially, the top width for Col I/III was significantly larger compared to untreated wounds (4.0 against 1.7 mm).

4. Discussion

The ratio of type I and III collagen (Col I/III) is a key factor in wound healing and scar formation in adult mammals [12]. Scar-free healing models, including the human fetus [34], axolotl, and *Acomys* [35], naturally exhibit higher Col III levels, suggesting a potential association between elevated Col III and enhanced regenerative capacity. These observations emphasize the relevance of Col III in modulating ECM properties and influencing tissue remodeling outcomes. A major challenge for scaffold construction, is obtaining sufficient Col III while minimizing immunological risks.

Our isolate was highly enriched in Col III, with reduced DNA and GAG content compared to raw placenta, minimizing the potential for immune responses. While previous studies reported collagen yields of 0.20–0.55% from placenta [28, 36], our modified protocol—featuring NaCl-based cleaning prior to pepsin digestion—achieved a 1% yield of atelocollagen. The sample was prepared at 1 mg/mL, and protein concentration measured by NanoDrop A205 was 0.91 mg/mL, suggesting ~91% of the sample consisted of protein. This may be an underestimate, as A205 primarily detects aromatic residues [37], which are present in collagen but at relatively low levels. Gel and MS analyses confirmed Col III as the dominant collagen in the isolate, along with smaller amounts of Col I, IV and VI. Notably, MS performed on rat placenta identified only 5% of all protein as Col III [38]. Given that

our scaffolds were designed to include both Col I and Col III, the presence of Col I in the isolate was acceptable and was accounted for in scaffold formulation.

To enhance structural stability, soluble atelocollagen was chemically crosslinked with fibrillar Col I. Immunostaining confirmed its successful incorporation. In high Col III content, both collagens appeared interspersed, but at lower ratios, Col III mainly overlapped Col I. Higher Col III content also altered pore morphology from rounded to flattened edges, consistent with pore collapse seen in similar compositions in gels [39]. Gamma sterilization increased crosslinking, especially in Col I/III 1:2 scaffolds, likely due to degradation exposing reactive sites [40]. As expected, mechanical strength decreased with higher atelocollagen Col III, reflecting its lower stiffness and lack of fibrillar reinforcement [19].

Col III supports wound healing by attracting fibroblasts, likely due to its role in creating a more flexible and permissive ECM that facilitates cell migration and tissue remodeling [32]. To evaluate the impact of Col III, fibroblasts were seeded onto scaffolds with varying composition. Fibroblasts seeded on scaffolds did not show αSMA expression at protein level, possibly due to insufficient mechanical stimulation. Fibroblast-to-myofibroblast transition requires a Young's modulus of at least 5 kPa [41], while collagen scaffold prepared in our laboratory had reported values of ~0.4 kPa [42]. At the mRNA level, scaffolds with Col III content were associated with lower ACTA2 and TGFB1 expression in a dose-dependent manner, indicating a potential antifibrotic effect. A more suitable model for assessing fibrosis reduction would involve pre-differentiated myofibroblasts with TGFβ stimulation or the use of eschar fibroblasts [43].

Modulating macrophage polarization may help reduce scarring, as M1 macrophages stimulate myofibroblast proliferation and transdifferentiation [44]. M0 macrophages seeded on Col I scaffolds exhibited a profile similar to M2-like control and Col III-containing scaffolds, except for a high expression of CD163, suggesting a shift towards the M2c-like subtype [45]. In contrast, Col I/III scaffolds induced a macrophage profile characterized by $CD206^{hi}$, $CD163^{lo}$, $CD80^{lo}$ and $HLA\text{-}DR^{lo}$ resembling the M2a-like subtype (IL-4, IL-13 stimulated). M2a macrophages exhibit anti-inflammatory properties such as enhanced endocytic activity, promotion of matrix synthesis and remodeling during healing [46, 47]. Consistently, a chronic endometriosis model showed that Col III solution skewed M1-like macrophages towards to M2 macrophages [48], supporting our findings.

Col III is primarily produced during the proliferative phase of wound healing, which typically begins around day 3 post-injury and overlaps with the inflammatory phase [49]. Macroscopic and histological analysis showed that untreated wounds contracted more rapidly, explaining the fast re-epithelization. H&E images showed wound width reduction from 12 mm to 1–2 mm in untreated and 2–4 mm in scaffold-treated groups, confirming the macroscopic contraction analysis trends. Meanwhile wounds treated with Col III-containing scaffolds retained a rounder shape compared to Col I or untreated conditions. Despite being mechanically weaker, Col III scaffolds reduced contraction, likely by decreasing ECM tension and preventing the mechanical cues that trigger pro-contractile signaling in cells [50]. While faster wound contraction shortens healing time, it often leads to increased scar formation [51]. A notable observation in this study was the slower ECM deposition in wounds treated with scaffolds. A delay in ECM deposition has been linked to improved skin regeneration in species like axolotls [52]. In mammals such as *Acomys*, Col III plays a role in regulating matrix architecture after injury [53].

The presence of scaffolds influenced cellular responses and neovascularization. Col III has been shown to enhance endothelial cell proliferation and capillary formation [54], aligning with the increased mature blood vessels observed in Col III-treated wounds. While myofibroblasts are essential for collagen remodeling, their prolonged presence post-closure can lead to scarring [55]. Notably, Col III has been reported to reduce myofibroblast activation and persistence at 35 days post-injury [53], suggesting a longer study could provide further insights. By day 28 post-injury, macrophage presence is typically minimal, yet our results showed a moderate presence in Col I/III scaffolds. Similarly, species with regenerative capacities exhibit immune cell persistence during healing but lower initial inflammatory responses [56]. To better understand macrophage subtypes during the inflammatory phase and their role in Col III-based healing, earlier time points, such as day 3, could be analyzed using specific markers like iNOS and CD206 for M1 and M2 macrophages.

While the modified isolation protocol improved collagen yield, complete separation of Col I and Col III was not achieved, likely due to overlapping solubility profiles after pepsin digestion. Further purification via additional precipitation or chromatography [57] could enhance specificity but would reduce yield and require more time and material. During MS sample preparation, insoluble proteins remained in the pellet limiting protein quantification to soluble fractions. Applying improved extraction protocols for ECM proteins [58] could enable more accurate protein analysis. *In vitro*, some variability in expression was observed across cell donors, however, similar response patterns were observed across conditions.

Expanding the number of donors could further strengthen reproducibility and capture donor heterogeneity. *In vivo*, chemically crosslinked scaffolds were used, which may have temporarily delayed contraction and subtly affected the host response as they degraded and integrated into the tissue**.** While rats are widely used for wound healing studies, their faster healing kinetics compared to humans can affect long-term remodeling processes, such as matrix turnover or late-stage scarring. Later time points (e.g., day 40) should be examined to better understand Col III's role in wound healing and remodeling.

5. Conclusion

In this study, we established an improved method to obtain a preparation enriched in type III atelocollagen from human placenta. *In vitro*, Col III atelocollagen in scaffolds downregulated scarring-related genes and promoted macrophage polarization toward the M2a-like phenotype. *In vivo*, Col I/III 1:1 scaffolds promoted a more balanced wound healing with moderate contraction, which may reduce scarring. These findings highlight the potential of incorporating Col III into skin substitutes for (burn) wound treatment.

Acknowledgements

The authors thank the Radboud Technology Center Microscopy for use of the Scanning Electron Microscope and Hans Wessels for the guidance and performance of Mass Spectrometry analysis of the isolates. Additionally, we thank Joris M. van Drongelen and Hedwig van Hove for providing placentas from Caesarian sections for the isolation process. We also acknowledge Dennis Janssen and Richard van Swam for their contributions to the design and performance of the compression tests. We appreciate the help from Steven Teerenstra with the power analysis for rat experiments as well as Hans Smola (Hartmann AG) for clinical advice about wound dressings for the rat experiments. We thank Maikel School, Tim Peters and the animal research facility staff for their support with the rat experiments.

Informed consent statement

The study was conducted in accordance with the Declaration of Helsinki. Use of human placenta was approved by the institutional medical ethical committee (CMO Arnhem/Nijmegen File 2022-13523). The study can be found at clinicaltrials.gov: NCT02438631 under the name PIANO2 version 6. For human fibroblasts derived from dermal tissue, The Medical Ethics Review Committee assessed that the research is not subject to the Medical Research Involving Human Subjects Act.

Consent for the use of anonymized, post-operative residual tissue samples was received through the informed opt-out protocol of the Red Cross Hospital, which was in accordance with the national guidelines (https://www.coreon.org/, accessed on 23 November 2020) and approved by the institutional privacy officers. For human cells derived from blood specimens, the experiments using these cells were approved by the local ethical committee. Privacy and data protection are covered by the Standard Operating Procedures of the Sanquin Blood bank, following National and International legislation, principles and guidelines. For animal experiments, all procedures were performed according to the Institute of Laboratory Animal Research guide for Laboratory Animals. The protocol study was approved by the Ethics Committee of the Radboud University Nijmegen DEC 2023-0016 under the project license AVD10300202317189.

Funding

This work received funding from the European Union's Horizon 2020 research and innovation programme under the Marie Skłodowska-Curie Grant Agreement No. 955722 (SkinTERM, NAM, RK) and from Radboud university medical center PhD round 2020 PI and MSc competition, respectively (MG and MP).

Conflict of interest

The authors confirm that there are no conflicts of interest associated with this publication.

References

1. Chattopadhyay, S. and R.T. Raines, *Review collagen-based biomaterials for wound healing.* Biopolymers, 2014. **101**(8): p. 821-33.
2. Briquez, P.S., J.A. Hubbell, and M.M. Martino, *Extracellular Matrix-Inspired Growth Factor Delivery Systems for Skin Wound Healing.* Advances in Wound Care, 2015. **4**(8): p. 479-489.
3. Marshall, C.D., et al., *Cutaneous Scarring: Basic Science, Current Treatments, and Future Directions.* Advances in Wound Care, 2018. **7**(2): p. 29-45.
4. Lorenz, H.P., et al., *The fetal fibroblast - the effector cell of scarless fetal skin repair.* Plastic and Reconstructive Surgery, 1995. **96**(6): p. 1251-1259.
5. Larson, B.J., M.T. Longaker, and H.P. Lorenz, *Scarless Fetal Wound Healing: A Basic Science Review.* Plastic and Reconstructive Surgery, 2010. **126**(4): p. 1172-1180.
6. Bode, M.K. *Characterization of type I and type III collagens in human tissues*. 2000.
7. Epstein, E.H., *[a1(III)]3 Human Skin Collagen: RELEASE BY PEPSIN DIGESTION AND PREPONDERANCE IN FETAL LIFE.* Journal of Biological Chemistry, 1974. **249**(10): p. 3225-3231.
8. Cheng, W., et al., *The content and ratio of type I and III collagen in skin differ with age and injury.* African Journal of Biotechnology, 2011. **10**(13): p. 2524-2529.
9. Sykes, B., et al., *The estimation of two collagens from human dermis by interrupted gel electrophoresis.* Biochemical and Biophysical Research Communications, 1976. **72**(4): p. 1472-1480.
10. Singh, D., V. Rai, and D.K. Agrawal, *Regulation of Collagen I and Collagen III in Tissue Injury and Regeneration.* Cardiol Cardiovasc Med, 2023. **7**(1): p. 5-16.
11. Fu, R., et al., *Type III Collagen Promotes Pseudopodium-Driven Cell Migration.* Chem & Bio Engineering, 2025. **2**(2): p. 97-109.
12. Kim, H.Y., et al., *Correlation between Collagen Type I/III Ratio and Scar Formation in Patients Undergoing Immediate Reconstruction with the Round Block Technique after Breast-Conserving Surgery.* Biomedicines, 2023. **11**(4).
13. Carracedo, S., et al., *The Fibroblast Integrin α11β1 Is Induced in a Mechanosensitive Manner Involving Activin A and Regulates Myofibroblast Differentiation*.* Journal of Biological Chemistry, 2010. **285**(14): p. 10434-10445.
14. Pakshir, P., et al., *The myofibroblast at a glance.* Journal of Cell Science, 2020. **133**(13).
15. Gibb, A.A., M.P. Lazaropoulos, and J.W. Elrod, *Myofibroblasts and Fibrosis.* Circulation Research, 2020. **127**(3): p. 427-447.
16. Lee, M., et al., *Mechanosensing in macrophages and dendritic cells in steady-state and disease.* Frontiers in Cell and Developmental Biology, 2022. **10**.
17. Luo, T., et al., *A Review on the Design of Hydrogels With Different Stiffness and Their Effects on Tissue Repair.* Frontiers in Bioengineering and Biotechnology, 2022. **10**.
18. Hance, A.J. and R.G. Crystal, *Rigid control of synthesis of collagen Types I and III by cells in culture.* Nature, 1977. **268**(5616): p. 152-154.
19. Asgari, M., et al., *In vitro fibrillogenesis of tropocollagen type III in collagen type I affects its relative fibrillar topology and mechanics.* Scientific Reports, 2017. **7**.
20. Franczyk, M., et al., *Extracellular matrix proteins in healthy and retained placentas, comparing hemochorial and synepitheliochorial placentas.* Placenta, 2017. **50**: p. 19-24.
21. Zhang, X., et al., *Factors affecting thermal stability of collagen from the aspects of extraction, processing and modification.* Journal of Leather Science and Engineering, 2020. **2**(1): p. 19.

22. Miller, E.J. and R.K. Rhodes, *PREPARATION AND CHARACTERIZATION OF THE DIFFERENT TYPES OF COLLAGEN.* Methods in Enzymology, 1982. **82**: p. 33-64.
23. Yang, Y., et al., *Recombinant Human Collagen-Based Bioinks for the 3D Bioprinting of Full-thickness Human Skin Equivalent.* Int J Bioprint, 2022. **8**(4): p. 611.
24. Gansevoort, M., et al., *Next-Generation Biomaterials for Wound Healing: Development and Evaluation of Collagen Scaffolds Functionalized with a Heparan Sulfate Mimic and Fibroblast Growth Factor 2.* Journal of Functional Biomaterials, 2025. **16**(2): p. 51.
25. Kim, Y.-J., et al., *Fluorometric assay of DNA in cartilage explants using Hoechst 33258.* Analytical Biochemistry, 1988. **174**(1): p. 168-176.
26. Clausen, T.M., et al., *A simple method for detecting oncofetal chondroitin sulfate glycosaminoglycans in bladder cancer urine.* Cell Death Discovery, 2020. **6**(1).
27. Avila-Martinez, N., et al., *Effect of Hyaluronan in Collagen Biomaterials on Human Macrophages and Fibroblasts In Vitro.* Journal of Functional Biomaterials, 2025. **16**(5): p. 167.
28. Hackethal, J., et al., *An Effective Method of Atelocollagen Type 1/3 Isolation from Human Placenta and Its In Vitro Characterization in Two-Dimesional and Three-Dimensional Cell Culture Applications.* Tissue Engineering Part C-Methods, 2017. **23**(5): p. 274-285.
29. Macarak, E.J., P.S. Howard, and E.T. Lally, *PRODUCTION AND CHARACTERIZATION OF A MONOCLONAL-ANTIBODY TO HUMAN TYPE-III COLLAGEN.* Journal of Histochemistry & Cytochemistry, 1986. **34**(8): p. 1003-1011.
30. Hemmerich, K., et al., *Gamma Irradiation of Animal Serum: Theoretical Basis of Impacts of Gamma Irradiation on Biological and Synthetic Polymers.* BioProcessing Journal, 2019. **18**.
31. Knoedler, S., et al., *Fibroblasts - the cellular choreographers of wound healing.* Front Immunol, 2023. **14**: p. 1233800.
32. Volk, S.W., et al., *Diminished Type III Collagen Promotes Myofibroblast Differentiation and Increases Scar Deposition in Cutaneous Wound Healing.* Cells Tissues Organs, 2011. **194**(1): p. 25-37.
33. Krzyszczyk, P., et al., *The Role of Macrophages in Acute and Chronic Wound Healing and Interventions to Promote Pro-wound Healing Phenotypes.* Frontiers in Physiology, 2018. **9**.
34. Cuttle, L., et al., *Collagen in the scarless fetal skin wound: Detection with Picrosirius-polarization.* Wound Repair and Regeneration, 2005. **13**(2): p. 198-204.
35. Avila-Martinez, N., et al., *Matrisomal components involved in regenerative wound healing in axolotl and Acomys: implications for biomaterial development.* Biomater Sci, 2023. **11**(18): p. 6060-6081.
36. Klasson, S.C., et al., *THE EFFECTS OF TISSUE PRETREATMENT AND PEPSIN LEVELS ON THE ISOLATION OF COLLAGENS FROM HUMAN-PLACENTA.* Collagen and Related Research, 1986. **6**(5): p. 397-408.
37. Anthis, N.J. and G.M. Clore, *Sequence-specific determination of protein and peptide concentrations by absorbance at 205 nm.* Protein Sci, 2013. **22**(6): p. 851-8.
38. Pataridis, S., et al., *Determination and Quantification of Collagen Types in Tissues Using HPLC-MS/MS.* Current Analytical Chemistry, 2009. **5**(4): p. 316-323.
39. Roman, B., et al., *A Model for Studying the Biomechanical Effects of Varying Ratios of Collagen Types I and III on Cardiomyocytes.* Cardiovascular Engineering and Technology, 2021. **12**(3): p. 311-324.
40. Jeong, J.-O., et al., *One step gamma-ray induced crosslinking and sterilization of electrospun poly(ε-caprolactone)/collagen composite scaffolds.* Materials Advances, 2025.
41. Balestrini, J.L., et al., *The mechanical memory of lung myofibroblasts.* Integrative Biology, 2012. **4**(4): p. 410-421.

42. Versteegden, L.R., et al., *A salt-based method to adapt stiffness and biodegradability of porous collagen scaffolds.* Rsc Advances, 2019. **9**(63): p. 36742-36750.
43. Kutluoğlu, G.C., et al., *Comparison of dermal and eschar fibroblasts in full skin equivalents.* Wound Repair Regen, 2025. **33**(1): p. e70001.
44. Lodyga, M., et al., *Cadherin-11–mediated adhesion of macrophages to myofibroblasts establishes a profibrotic niche of active TGF-β.* Science Signaling, 2019. **12**(564): p. eaao3469.
45. Spiller, K.L., et al., *The role of macrophage phenotype in vascularization of tissue engineering scaffolds.* Biomaterials, 2014. **35**(15): p. 4477-4488.
46. Sapudom, J., et al., *3D in vitro M2 macrophage model to mimic modulation of tissue repair.* npj Regenerative Medicine, 2021. **6**(1): p. 83.
47. Montaner, L.J., et al., *Type 1 and Type 2 Cytokine Regulation of Macrophage Endocytosis: Differential Activation by IL-4/IL-13 as Opposed to IFN-γ or IL-101.* The Journal of Immunology, 1999. **162**(8): p. 4606-4613.
48. You, S., et al., *Recombinant humanized collagen remodels endometrial immune microenvironment of chronic endometritis through macrophage immunomodulation.* Regen Biomater, 2023. **10**: p. rbad033.
49. Clore, J.N., I.K. Cohen, and R.F. Diegelmann, *Quantitation of collagen types I and III during wound healing in rat skin.* Proc Soc Exp Biol Med, 1979. **161**(3): p. 337-40.
50. Ibrahim, M.M., et al., *Myofibroblasts contribute to but are not necessary for wound contraction.* Laboratory Investigation, 2015. **95**(12): p. 1429-1438.
51. Yannas, I.V. and D.S. Tzeranis, *Mammals fail to regenerate organs when wound contraction drives scar formation.* Npj Regenerative Medicine, 2021. **6**(1).
52. Seifert, A.W., et al., *Skin Regeneration in Adult Axolotls: A Blueprint for Scar-Free Healing in Vertebrates.* Plos One, 2012. **7**(4).
53. Stewart, D.C., et al., *Type III Collagen Regulates Matrix Architecture and Mechanosensing during Wound Healing.* Journal of Investigative Dermatology, 2024.
54. Wang, H., et al., *Study on the Effect of Type III Recombinant Humanized Collagen on Human Vascular Endothelial Cells.* Tissue Engineering Part C: Methods, 2024. **30**(2): p. 53-62.
55. D'Urso, M. and N.A. Kurniawan, *Mechanical and Physical Regulation of Fibroblast-Myofibroblast Transition: From Cellular Mechanoresponse to Tissue Pathology.* Frontiers in Bioengineering and Biotechnology, 2020. **8**.
56. Li, H.B., et al., *Dynamic cell transition and immune response landscapes of axolotl limb regeneration revealed by single-cell analysis.* Protein & Cell, 2021. **12**(1): p. 57-66.
57. Deyl, Z. and I. Mikší k, *Advanced separation methods for collagen parent α-chains, their polymers and fragments.* Journal of Chromatography B: Biomedical Sciences and Applications, 2000. **739**(1): p. 3-31.
58. McCabe, M.C., et al., *Evaluation and Refinement of Sample Preparation Methods for Extracellular Matrix Proteome Coverage.* Mol Cell Proteomics, 2021. **20**: p. 100079.

Supplementary material

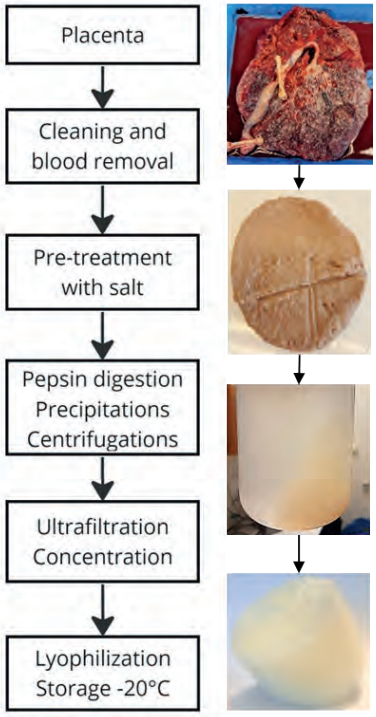

Supplementary Figure 1. Concise diagram of the main steps for enriching Col III from human placenta.

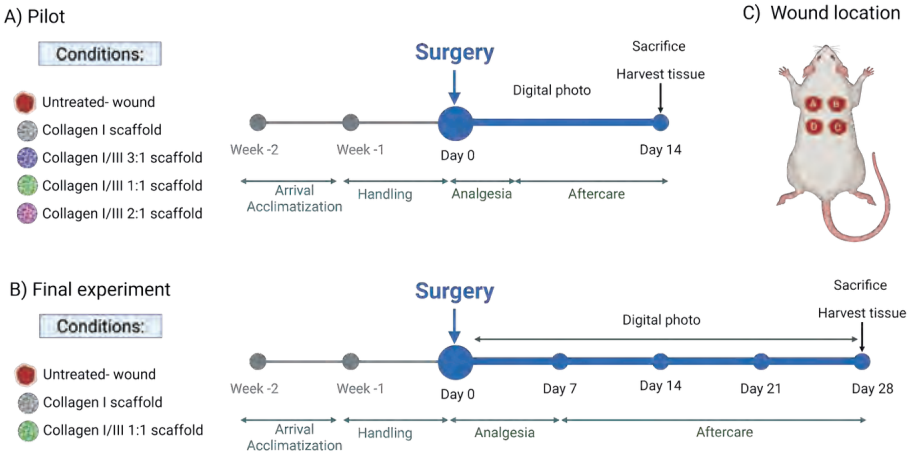

Supplementary Figure 2. Timeline for rat experiments. A) Pilot study (6 rats) until day 14 and B) Final experiment (9 rats) until day 28, including two deceased rats by day 21. C) Wound location on the back of the rat used for randomization.

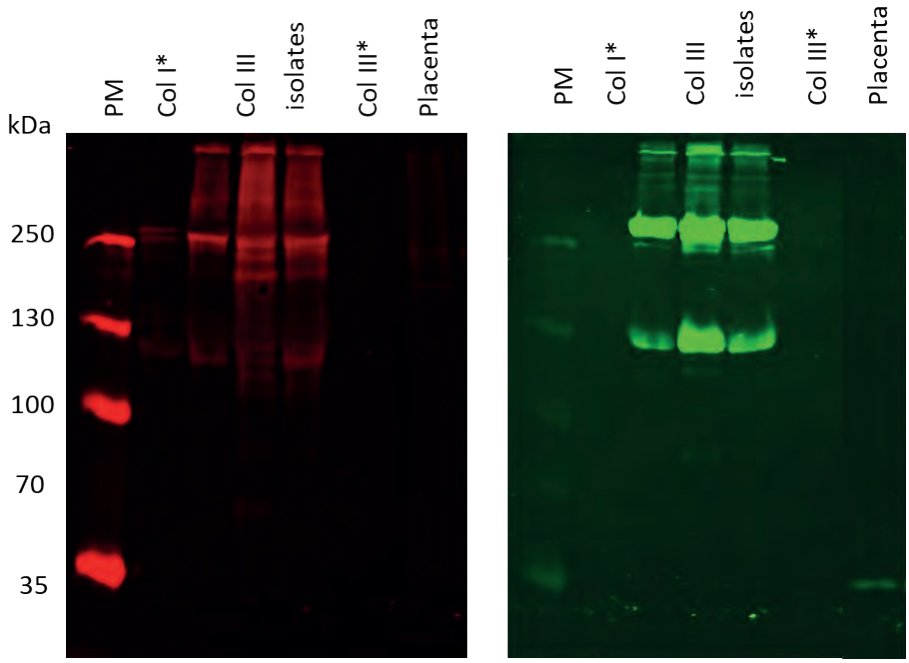

Supplementary Figure 3. Immunostaining for collagen in blots via Western blotting in the two analyzed channels. Left image was stained using anti-Col I in red (700 CW) and right image with anti-Col III in green (800 CW). PM is protein marker and Col I* and Col III* are standards from bovine origin.

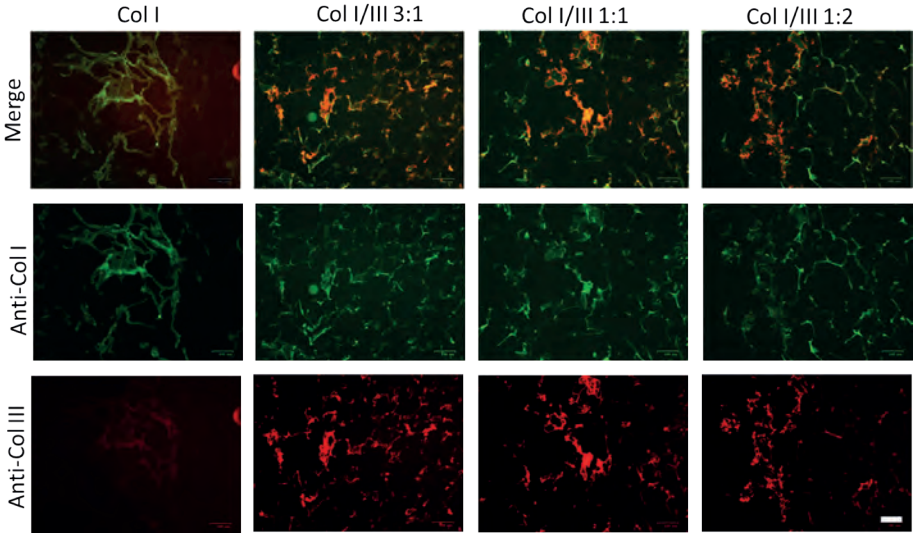

Supplementary Figure 4. Images of prepared scaffolds stained with fluorescence immunostaining assay for Col I in green and Col III in red. Scale bar is 100 µm.

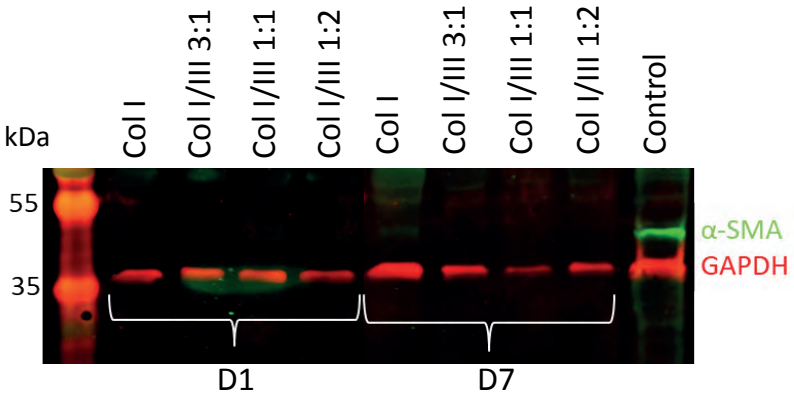

Supplementary Figure 5. α-SMA protein expression in human dermal fibroblasts after 7 days of culture by western blotting. Fibroblasts cultured in 2D with TGFβ1 served as a control. Molecular weight of α-SMA (in green) is 42 kDa and GAPDH (in red) is 36 kDa.

Supplementary Table 1. Mass spectrometry results from placenta and isolate showing identified collagens.

				Intensities		Percentages (%)	
Accession	**PTM**	**Avg. Mass**	**Collagens**	**Placenta**	**Isolate**	**Placenta**	**Isolate**
P02452|CO1A1_HUMAN	Oxidation (M)	138942	Collagen alpha-1(I)	8889.8	14335	2	29
P08123|CO1A2_HUMAN	Oxidation (M)	129314	Collagen alpha-2(I)		2957	0	6
P02461|CO3A1_HUMAN	Oxidation (M)	138564	Collagen alpha-1(III)		19797	0	40
P02462|CO4A1_HUMAN	Carbamidomethylation; Oxidation (M)	160611	Collagen alpha-1(IV)	10777		3	0
P08572|CO4A2_HUMAN	Carbamidomethylation; Oxidation (M)	167553	Collagen alpha-2(IV)	18155	1894	5	4
P12109|CO6A1_HUMAN	Carbamidomethylation; Oxidation (M)	108529	Collagen alpha-1(VI)	44550		12	0
P12110|CO6A2_HUMAN	Carbamidomethylation	108579	Collagen alpha-2(VI)	26507		7	0
P12111|CO6A3_HUMAN	Carbamidomethylation; Oxidation (M)	343668	Collagen alpha-3(VI)	203910	10438	54	21
Q05707|COEA1_HUMAN	Carbamidomethylation; Oxidation (M)	193513	Collagen alpha-1(XIV)	48281		13	0
P39059|COFA1_HUMAN	Oxidation (M)	141720	Collagen alpha-1(XV)	9891.9		3	0
P39060|COIA1_HUMAN		178187	Collagen alpha-1(XVIII)	3794.7		1	0

Percentages based on total collagen intensity per sample.

Supplementary Table 2. Results of the wound contraction and morphology of the wounds at day 14 post-surgery.

	Untreated (n=6)	**Col I (n=6)**	**Col I/III 3:1 (n=2)**	**Col I/III 1:1 (n=2)**	**Col I/III 1:2 (n=4)**
Wound contraction (%)	81 ± 11	29 ± 21	36 ± 8	23 ± 21	20 ± 5
Morphology (ratio width/length)	0.25 ± 0.08	0.50 ± 0.22	0.65 ± 0.21	0.60 ± 0.14	0.85 ± 0.10
Image	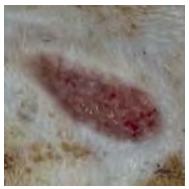	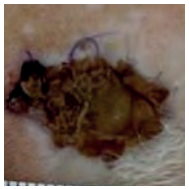	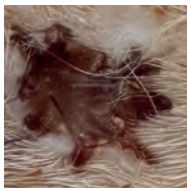	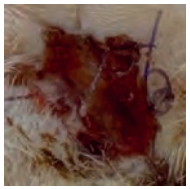	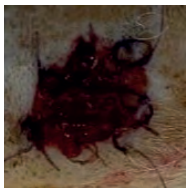

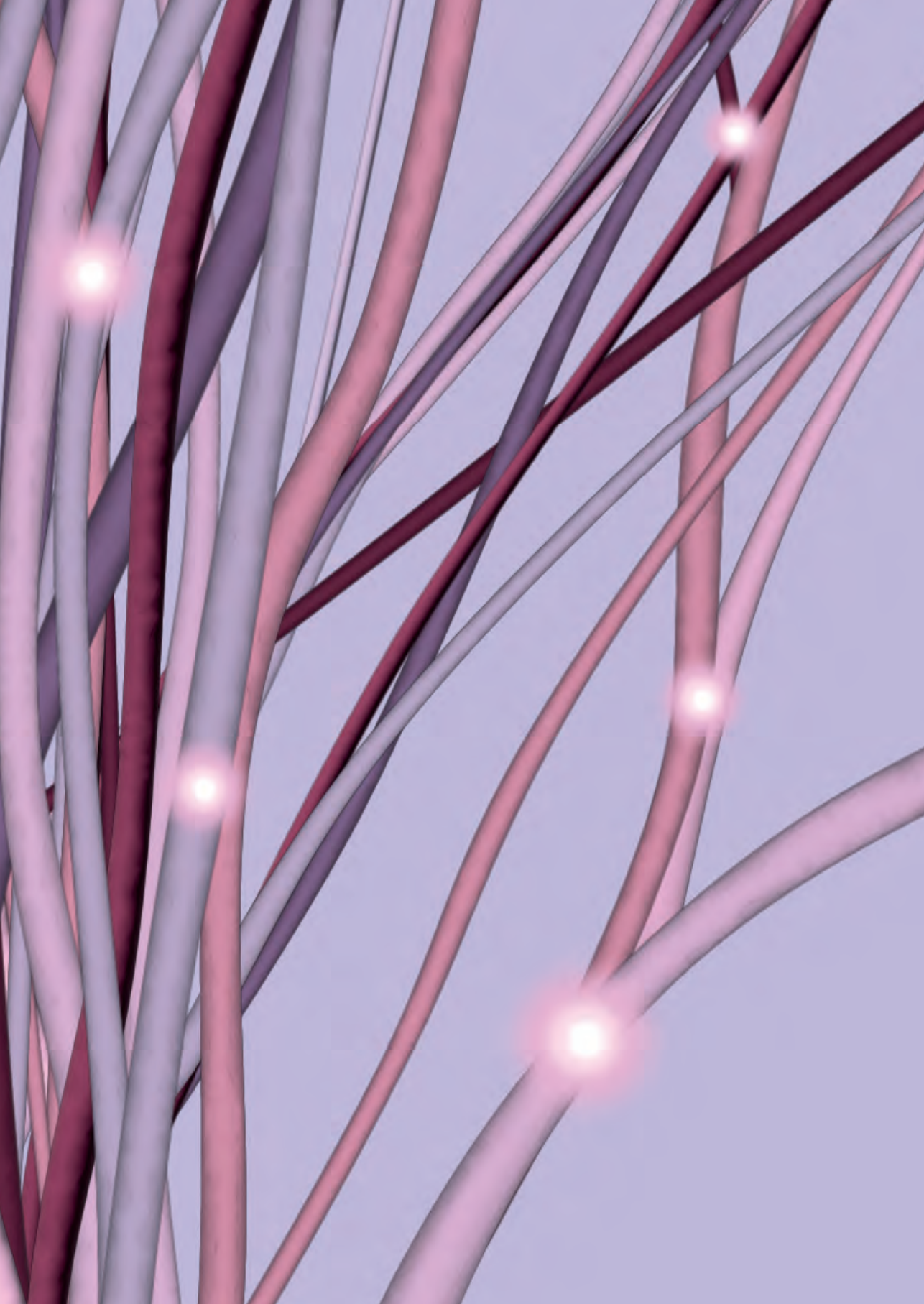

Chapter 5

Potential of heparan sulfate mimetics integrated into collagen scaffolds for enhanced skin wound healing

Nancy Avila-Martinez MSc[1], Roman Krymchenko MSc [1], Merel Gansevoort MSc [1], Maren Pfirrmann MSc [1], Sofia Aparicio BSc [1], Agnes Choppin PhD[2], Franck Chiappini DVM PhD [2], Denis Barritault PhD [2], Martijn Verdoes PhD [1,3], Toin H. van Kuppevelt PhD [1], Bouke K.H.L. Boekema PhD [4,5], Willeke F. Daamen PhD [1]

[1] Radboud university medical center, Research Institute for Medical Innovation, Department of Medical BioSciences, Nijmegen, The Netherlands

[2] OTR3, Paris, France

[3] Current address: LUMC, Department of Immunology, Leiden, The Netherlands

[4] Alliance of Dutch Burn Care, Burn Research Lab, Beverwijk, The Netherlands

[5] Department of Plastic, Reconstructive and Hand Surgery, AUMC, location VUmc, Amsterdam, The Netherlands

Submitted for publication

Abstract

Optimal healing of full-thickness skin wounds remains a clinical challenge. While current skin substitutes aid-burn wound management, there is still a need to effectively minimize scarring. Therefore, we developed type I collagen scaffolds with covalently bound ReGeneraTing Agent (RGTA®) OTR4120 (OTR), a synthetic heparan sulfate analog resistant to glycanase degradation (Col I+OTR). To further stimulate skin regeneration, collagen scaffolds with and without OTR4120 were subsequently loaded with sonic hedgehog (SHH), a key effector molecule in embryogenesis. The presence of OTR4120 and SHH in scaffolds was biochemically and histologically confirmed after crosslinking and sterilization. SHH was found deeper into collagen scaffolds in the presence of OTR4120. Addition of SHH to scaffolds showed lower expression of M1-like cell surface markers, while Col I+OTR significantly enhanced IL-10 production. The potential of OTR4120 in wound healing was further evaluated *in vivo* using a rat full-thickness wound model over 28 days. By day 14, macroscopic images revealed that OTR-treated wounds better maintained the original wound shape. Histological analysis showed increased blood vessel formation, fewer scaffold remnants, and more contiguous sebaceous glands in the granulation tissue with Col I+OTR scaffolds. This study demonstrates that OTR4120 could be a promising addition to acellular skin substitutes for improving acute wound healing.

1. Introduction

Deep and extensive injuries, such as burns, often lead to significant scarring, which can cause contraction and mobility limitation to patients [1]. Full-thickness skin wounds compromise the integrity of the epidermis and dermis, including appendages, creating a need for skin replacement to avoid complications [2]. Gold standard treatment for this type of wound involves split thickness skin transplants [3]. However, this method not only creates an additional superficial wound in the patient but can also lead to incomplete skin repair, often resulting in fibrotic tissue [4]. Dermal templates, such as collagen scaffolds, can provide structural support for dermal restoration during the wound healing process [5, 6].

Wound healing stages consist of overlapping phases: hemostasis, inflammation, proliferation, and remodeling [7]. Hemostasis initiates wound healing by rapidly constricting blood vessels, forming a fibrin clot to stop bleeding, and releasing signaling molecules that recruit immune cells [8]. During inflammation, monocyte-derived macrophages (M0) arrive at the wound site and polarize towards M1 (pro-inflammatory) macrophages to remove debris and pathogens, which are replaced by M2 (pro-healing) macrophages that help resolve inflammation and signal the start of proliferation [9-11]. During this phase, fibroblasts transform into myofibroblasts and secrete extracellular matrix (ECM) components to form granulation tissue and contract the wound, while endothelial cells promote angiogenesis to support tissue growth [12]. Fast wound contraction during the skin healing process usually leads to scarring [13]. Keratinocytes cover the wound and the provisional ECM is degraded to allow tissue reconstruction [14], while (myo)fibroblasts deposit type I collagen [15].

One way to improve the function of dermal templates is through biofunctionalization with molecules present in the ECM. Several studies described incorporating heparin in collagen scaffolds for its potential to bind growth factors, which can enhance skin wound healing [16, 17]. However, after an injury the environment is characterized by a catabolic activity leading to a rapid degradation of heparan sulfate and other molecules [18]. To tackle this, dextran-derived analogues, such as ReGeneraTing Agents (RGTA®) have been developed to mimic the structural and functional properties of heparan sulfate but are resistant to degradation by heparanases, chondroitinases, hyaluronidase and dextranase [19, 20], due to the presence of β1-6 bonds between the monosaccharides instead of the natural α1-4 glycosidic bonds in heparan sulfates [21]. We therefore decided to construct collagen scaffolds with RGTA® OTR4120 (OTR) to evaluate its potential as a dermal template in acute wounds.

Effector molecules are essential for ECM signaling during wound healing [22]. Sonic hedgehog (SHH) is a key regulator in the hedgehog pathway that influences tissue formation, hair follicle development, cell fate, and epidermal patterning during embryogenesis [23]. Higher SHH expression has been observed in embryonic mice with regenerated wounds compared to older mice that developed scars [24, 25]. Sulfation of heparan sulfate is crucial for SHH binding, as a study demonstrated SHH dimers assemble on heparin chains with three sulfate groups per disaccharide [26]. The formed complex enhances SHH bioavailability, a principle that can be applied in scaffolds. Moreover, SHH has shown to act as a chemoattractant for macrophages *in vivo* [27]. The incorporation of SHH and OTR4120 in collagen scaffolds may thus impact macrophage polarization. Recently, our research group described an anti-fibrotic effect of type I collagen scaffolds functionalized with OTR4120 in combination with FGF2 in an *in vitro* model using fibroblasts [28]. In this study, we evaluate the binding capacity of OTR4120 for SHH in collagen scaffolds, as well as its effect on macrophages *in vitro*. The wound healing potential of OTR4120 bound to collagen scaffolds is further evaluated *in vivo* using a rat full-thickness wound model.

2. Materials and methods

2.1 Scaffold construction and characterization

Porous collagen scaffolds (Col I) were prepared using 0.8 % (w/v) collagen fibrils in 0.25 M acetic acid, swollen overnight at 4 °C under constant agitation. The collagen was isolated from bovine Achilles tendon obtained from a local slaughterhouse [29]. For collagen scaffolds with RGTA® OTR4120 (Col I+OTR), 0.025 (w/v) % of heparan sulfate mimetic (OTR3, Paris, FR) [30] was added to the 0.8 % (w/v) collagen suspension. The suspensions were homogenized and poured into standard suspension culture plates (6-well format, Cellstar®, Greiner Bio-One, cat. no. 657185) at 4 mL per well (corresponding to 960 mm^2 surface area per well). The plates were then frozen at −20 °C before lyophilization using a Lyoph-pride 03 freeze dryer (ilShin BioBase Europe, Ede, NL) creating untreated non-crosslinked scaffolds (U). Scaffolds for characterization, *in vitro* and *in vivo* testing were chemically crosslinked (X) for 3 h applying 33 mM 1-ethyl-3-(3-dimethylaminopropyl)-carbodiimide (EDC) and 6 mM N-hydroxysuccinimide (NHS) in 50 mM 2-morpholinoethane sulphonic acid (MES, pH 5.0) (Sigma-Aldrich, St. Louis, MO, USA) containing 40 % ethanol. Scaffolds were washed with 0.1 M Na_2HPO_4, 1 M NaCl, 2 M NaCl and demineralized water, and lyophilized. Finally, Ø 12 mm scaffolds were gamma sterilized (Steris company, Ede, NL) with a minimum dose of 25 kGy.

Col I+OTR/SHH scaffolds were prepared by incubating dry Col I+OTR scaffolds in 3.5 µg/mL human sonic hedgehog C24II (Lot. 5221207908, SHH, Miltenyi Biotec, Teterow, DE) in phosphate buffered saline (PBS, pH 7.2) overnight. Scaffolds without OTR4120 (Col I+SHH) were used as a control for characterization. Scaffolds were washed 3 x 15 min in PBS to remove unbound SHH and processed for further analysis. Samples for *in vitro* studies were used immediately. Samples for characterization, including the supernatants from the washing steps, were stored either in sample buffer (1.0 % w/v sodium dodecyl sulfate (SDS), 1.25 % v/v 2-mercaptoethanol, 2.5 % v/v glycerol, and 0.04 % w/v bromophenol blue in 31.25 mM Tris-HCl in Milli-Q water) at -20 °C or in Tissue-Tek O.C.T. compound (Sakura Finetek, Alphen aan den Rijn, NL) at -80 °C.

The extent of crosslinking was evaluated by measuring the residual primary amine groups through 2,4,6-trinitrobenzene sulfonic acid (TNBS) assay [31]. Glycine solutions (0–80 µg/mL) prepared in 4 % $NaHCO_3$ were used for calibration, and absorbance was measured at 420 nm using a SpectraMax iD3 plate reader (Molecular Devices, CA, USA). Pore structure of the scaffolds was visualized using scanning electron microscopy (SEM). In short, the cross-sectional side of scaffolds was attached to carbon tape, coated with gold in an Edwards Scancoat Six Sputter Coater (Crawley, UK) and imaged with a Zeiss Sigma 300 SEM (Jena, DE) at 3 kV.

The amount of OTR4120 bound to the scaffolds was determined by performing a dot blot colorimetric assay with Alcian blue staining. Scaffolds were digested at 65 °C overnight using 2.5 U/ml papain (P3125, Merck, Darmstadt, DE) in 50 mM sodium phosphate, 2 mM EDTA and cysteine (pH 6.5). The samples were spotted on a polyvinylidene fluoride membrane (0.45 µm, Thermo Scientific, Waltham, MA, USA) activated with 0.25 (w/v) % cetylpyridinium chloride (CPC) in methanol with 30 % isopropanol alongside a serial dilution of OTR4120 starting from 500 ng. Alcian blue staining solution contained 2.5 (w/v) % Alcian blue (Sigma) in de-staining solution (40 mM guanidinium chloride, 1.8 mM H_2SO_4 and 0.025 v/v % Triton-X-100 in 50 % aqueous ethanol). Membranes were stained for 30 min in Alcian blue solution, following 5 min incubation in de-staining solution and 5 min in demineralized water [32]. Membranes were imaged with Molecular Imager Gel Doc XR system (Bio-Rad) on a White Light Conversion Screen (Bio-Rad, Hercules, CA, USA) in grayscale. The OTR4120 content of the samples was measured as µg OTR4120/mg collagen.

2.2 SHH quantification and localization

The amount of SHH bound to the scaffolds was measured using Western blotting. Samples and SHH for calibration curve in sample buffer were boiled for 10 min.

Samples including a Protein Ladder (PageRuler™ Plus, Thermo Scientific) were run on a 12 % SDS-PAGE gel for 1.5 h at 100 V. Proteins on the gel were blotted onto a nitrocellulose membrane (0.2 µm, Bio-Rad) at 100 V for 1 h in blotting buffer (25 mM Tris, 40 mM glycine, in 20 % aqueous methanol with 0.4 % SDS). Membranes were blocked with 2 % bovine serum albumin (BSA) in PBST (0.1 % Tween-20 in PBS) overnight at 4 °C under constant agitation. Immunostaining was performed by incubating the membrane with rabbit anti-human SHH (1:5000, sc-9024 Santa Cruz Biotechnology, Dallas, TX, USA) for 1 h, followed by goat-anti rabbit IRDye 680 CW conjugated (1:5000, 929-32221, Li-COR Biotechnology, Lincoln, NE, USA) for 1 h. Blots were washed with PBST for 3 x 5 min between antibody incubations. Blots were scanned using the Odyssey CLx imager (Li-COR) and the signal was quantified using Image Studio™ Version 6.0 (LI-COR).

The distribution of OTR4120 and SHH was visualized using indirect fluorescence microscopy. 7 µm cryosections of scaffold cross sections were blocked with 2 % BSA in PBST for 30 min. All antibodies were diluted in blocking solution (BSA-PBST) and left for incubation 1 h followed by washes of PBST 3 x 5 min between labelling steps. Three antibodies were used to stain OTR4120; primary single chain antibody HS4C3V with a VSV tag (1:10 periplasmic fraction, produced in house), secondary mouse anti-VSV P5D4 hybridoma supernatant (1:10, produced in house) [33], tertiary goat anti-mouse IgG (H+L) Alexa 488 conjugated (1:500, A-11001, Molecular Probes Inc). To visualize SHH, anti-rabbit SHH (1:100, Santa Cruz) was used, followed by secondary goat anti-rabbit IgG (H+L) Alexa 594 conjugated (1:500, A-11012, Molecular probes Inc). Slides were fixated in absolute ethanol and mounted with Mowiol 4-88 (Merck). Images were taken using ZOE Fluorescence Cell Imager (Bio-Rad).

2.3 *In vitro* analysis with human macrophages

Primary human monocytes were isolated from peripheral blood mononuclear cells of healthy donors (3 donors), using magnetic activated beads, $CD14^+$ (130-050-201, Miltenyi Biotech, Teterow, DE). Each donor was tested in an independent experiment performed at separate times. Informed consent was given in accordance with the Declaration of Helsinki and Dutch national and Sanquin internal ethic boards. Monocytes were stimulated with 50 ng/ml macrophage colony-stimulating factor (M-CSF, PeproTech by Thermo Scientific, Waltham, MA, USA) for 6 days to obtain M0 macrophages. As controls, M0 macrophages were stimulated for 24 h with 100 ng/ml lipopolysaccharides (LPS, vac-3pelps, InvivoGen, San Diego, CA, USA) with 20 ng/ml interferon gamma (IFNγ, PeproTech) to polarize them to M1-like macrophages or with 20 ng/ml interleukin 4 (IL4, 170-076-135) + 20 ng/ml interleukin 13 (IL13, 130-

112-412) to polarize them to M2-like macrophages (both from Miltenyi Biotech). On day 7, cells were harvested with a cell scraper using 2 mM EDTA in PBS. 200,000 M0 macrophages were seeded onto crosslinked collagen-based scaffolds, which included the following experimental conditions: Col I (control), Col I+OTR, and Col I+OTR/SHH. As additional controls, Col I scaffolds were also seeded with either M1- or M2-like macrophages that were pre-differentiated. Macrophages were cultured on scaffolds for 48 h in RPMI 1640 medium containing 10 % foetal bovine serum (FBS, Gibco), 1 % ultraglutamine and 1 % antibiotic/antimycotic with their respective stimulators (M0: /; M1: LPS+ IFNγ; M2: IL4 + IL13) during the differentiation process and without these factors during scaffold culture.

Cell phenotype was evaluated using flow cytometry. Macrophages were enzymatically retrieved from the scaffolds using 0.25 U/ml collagenase A (Roche, Mannheim, DE) in a shaking water bath for 30 min at at 37 °C. PBS containing EDTA was added to the scaffolds and incubated for 30 min at 4 °C. Isolated cells were labelled with eFluor 780-APC-Cy7 (1:2000, 65-0865-14, ThermoFisher, Carlsbad, CA, USA) to detect viable cells. For cell surface labelling, antibodies were used from either BD Biosciences (Franklin Lakes, NJ, USA) or BioLegend (San Diego, CA, USA) and corresponded to CD45 (1:20, 304026), CD80 (1:20, 305220), PD-L1 (1:30, 557924), HLA-DR (1:20, 307646), CD206 (1:40, 551135), CD163 (1:40, 562643) and MerTK (1:50, 367610). Mean fluorescence intensity (MFI) was measured with BD FACSVerse Cell Analyzer flow cytometer (BD BioSciences) and calculated using FlowJo X (vX 0.7, Tree STAR, Ashland, OR, USA). Gating strategy consisted of spotting singlet live cells, $CD45^{+}$cells, and a specific CD marker.

Cytokine concentrations in supernatants were quantified using ELISA kits for IL-12 (88-7126), IL-6 (88-7066), and IL-10 (88-7106) (Invitrogen, ThermoFisher, Vienna, AT), following manufacturer's instructions. Absorbances were recorded at 450 nm using the iMark™ Microplate Absorbance Reader (Bio-Rad, Basel, CH).

2.4 *In vivo* analysis with rats

All procedures were performed according to the Institute of Laboratory Animal Research guide for Laboratory Animals. The study was approved by the Ethics Committee of the Radboud University Nijmegen DEC 2023-0016 under the project license AVD10300202317189. A powered analysis based on a similar approach by Nillesen *et al.* 2011 [16] was performed, taking into account the wound contraction percentage between untreated and collagen-based substitute, calculating a relevant detectable contrast of 20 %. This resulted in a sample size of 9 rats for a power of 80 % and alpha= 0.05 (two sided). Nine Wistar rats (male, 3 months old,

weight 300-400 g, WI (WU), Charles River) were purchased and housed with two rats per cage. They were fed with pellets, sunflower seeds, booster food (Ssniff Spezialdiäten, Soest, DE) and water *ad libitum*. The rats were labelled by ear punch upon arrival and were handled and trained for a period of 1-2 weeks before surgery.

The experimental design consisted of the following treatment groups: untreated wound, Col I scaffold, and Col I+OTR scaffold. Note that the experiment contained another collagen-based condition not related to this study. The treatment location was randomized using randomizator.org to avoid repetitions of sets. Spots were assigned A-D on the back of the rats and treatments 1-4 were allocated in a different order. Rats were sacrificed at day 28 after implantation (Supplementary Fig. 1).

Rats were anesthetized with isoflurane 1.5-2.5 %. Eye cream (Ophtosan®, AST Farma, Oudewater, NL) was applied on their eyes. Their backs were trimmed using a hair clipper and hair removed by applying Veet cream (Reckitt Benckiser, Slough, UK). Four full-thickness wounds of Ø 12 mm were made on the back of each rat, between the shoulders and hind legs using a biopsy punch (220701, SMI AG, St. Vith, BE) and curved scissors. Sterile scaffolds were placed on the wounds in such a way they fitted exactly and touched the wound edge. The scaffolds were kept in place using 6-8 resorbable sutures (100L6P, Monocryl™ 4-0, Ethicon, Raritan, NJ, USA). Wounds were covered with a silicone dressing (Mepilex Border Flex Lite, 581277, Mölnlycke, Gothenburg, SE), elastic bandage (PetFlex 10009403914, Andover healthcare, Portsmouth, NH, USA), and adhesive plaster (250, Leukoplast®, Hamburg, DE). Post-operative analgesia was given after surgery and for the next three days with 0.1 ml/100 g body weight injections of carprofen (5 mg/ml, Rimadyl, Capelle a/d IJssel, NL). Wound dressing and bandaging were replaced when needed, generally 1-3 times per week.

Digital photos of the wounds were taken at days 0, 7, 14, 21 and 28 post surgery, plus when dressings and bandages were changed. Rats were sacrificed on day 28 by CO_2 inhalation and scaffolds with surrounding tissue were harvested. Half of the tissue was stored in 4 % paraformaldehyde (PFA) in PBS overnight and replaced with 1 % PFA in PBS thereafter. The other half was snap-frozen in liquid N_2, stored in TissueTek and frozen at -80 °C.

2.4.1 Morphology and wound contraction analysis

Macroscopic images were processed in FIJI 1.53t (ImageJ software, Bethesda, MD, USA) and calibrated using the photographed ruler in each photo to obtain the width, length and wound area by manually tracing the wound edge ($n \leq 9$). The

morphology was evaluated according to the ratio observed between the width and length of the wound (Supplementary Fig. 2). A morphology closer to 1 represents a rounder wound, which is an indication for less contraction. The formula used was:

$$Morphology\ (1) = \frac{width\ (cm)}{length\ (cm)}$$

Wound contraction was evaluated by determination of the remaining wound area using the photographs at the different timepoints (7, 14, 21, and 28 days) compared to day 0 (*i.e.* 100 % of the wound area) per condition. The formula used to calculate the wound contraction was:

$$Wound\ contraction\ (\%) = \frac{Ai - Ax}{Ai} \cdot 100\ \%$$

where: Ai = Initial wound area at day 0; Ax= Wound area at the timepoint (i.e. day 7, 14, 21, or 28).

2.4.2 Microscopical analysis

Histological analysis: PFA fixed samples were embedded in paraffin and sections of 5 µm thickness were cut. Sections were stained with hematoxylin and eosin (H&E) or Masson's trichome blue and scanned with a whole-slide scanner (3DHISTECH, Budapest, HU). CaseViewer 2.4 software was used to analyze the histological sections and immunostainings. The stainings were used to visualize skin layers, appendages and scaffold remnants.

Immunohistochemistry: Samples were stained for alpha smooth muscle actin (α-SMA, 1:2000, clone 1A4, A-2547, Merck) to visualize myofibroblasts and mature blood vessels and for cluster of differentiation 68 (CD68, 1:200, MCA341R, AbD Serotec) to study macrophages. Sections were deparaffinized and incubated with 0.5 % hydrogen peroxide (K44653709, Merck) for 1 h. After washing with demineralized water for 5 min, the samples were incubated for 10 min in boiling citrate buffer (10 mM tri-sodium citrate, pH 6.0). After cooling for 40 min, sections were rinsed in demineralized water for 2 x 2 min and incubated with blocking solution (0.5 % BSA in PBS + 0.05% Triton X-100) for 30 min. All antibodies used in this methodology and ABC kit were diluted in blocking solution and washed with PBS 2 x 5 min. Primary antibodies were incubated for 45 min. From this point, reagents were from Vector Laboratories (Newark, CA, USA). Secondary antibody goat anti-mouse IgG (H+L) biotinylated (1:200, BA-9200) was incubated for 45 min.

Elite® ABC kit, peroxidase (PK-6100) was applied for 1 h. AEC substrate kit, peroxidase (SK-4205) was incubated for 5-8 min. Sections were counterstained with haematoxylin and mounted using VectorMount® (H-5501).

Quantitative measurements: Using H&E, the epidermal thickness at both the wound and unwounded healthy skin was measured at three different areas. The wound area was marked by the presence of granulation tissue. The number of hair follicles and sebaceous glands were counted within the wound and in the adjacent area. The histological wound deformation was calculated by dividing the width of the middle of the wound by the width of the wound just below the epidermis.

$$Deformation\ (1) = \frac{Width\ from\ the\ middle\ dermis\ (\mu m)}{Width\ from\ the\ top\ dermis\ (\mu m)}$$

Semi-quantitative scoring: The healed tissue was semi-quantitatively scored by two independent individuals (NA, RK) for presence of myofibroblasts, macrophages, angiogenesis and residual collagen based on AEC and trichrome blue staining. Scores were assigned from 0 (not present) to 1, 2 or 3 (low, medium, high abundance, respectively). If differences occurred between observers (when intraclass correlation coefficient, ICC < 0.75), slides were re-evaluated to obtain consensus.

2.5 Statistical analysis

Data were analyzed and visualized using GraphPad prism 10.4.1. Scaffolds characterization and histological analysis from rat tissues were evaluated using one-way ANOVA with Tukey's multiple comparisons test. For *in vitro* studies and macroscopical analyses of *in vivo* studies, two-way ANOVA with Tukey's multiple comparison test was performed. Type I error was set at 5 % (*i.e.* α= 0.05). IBM SPSS statistics 29 (Armonk, NY, USA) was used to determine the ICC to evaluate if the reliability was good (> 0.75) or excellent (> 0.9) between scorers in the histology section (Supplementary Table 1).

3. Results

3.1 Effect of sterilization and crosslinking on OTR4120 bound to collagen scaffolds

Porous scaffolds were prepared containing type I collagen (Col I) or type I collagen with 0.025 % OTR4120 (Col I+OTR). Scanning electron microscopy images revealed that crosslinked Col I+OTR scaffolds showed more compressed pores than Col I, but

pore morphology was similar in both untreated (non-crosslinked) scaffolds (Fig. 1A and Supplementary Fig. 3). For *in vitro* and *in vivo* studies, scaffolds were sterilized by gamma radiation. Then, the amount of free amine groups was used to calculate the crosslinking degree (i.e. ~62 %), which did not change after sterilization (Fig. 1B). The amount of bound OTR4120 to collagen scaffolds remained constant with 24 ± 5 µg OTR4120/mg collagen scaffold in crosslinked scaffolds before and after sterilization, showing that gamma sterilization did not affect the amount of OTR4120 bound to scaffolds after crosslinking. However, the OTR4120 amount slightly increased in untreated Col I+OTR after sterilization (Fig. 1B).

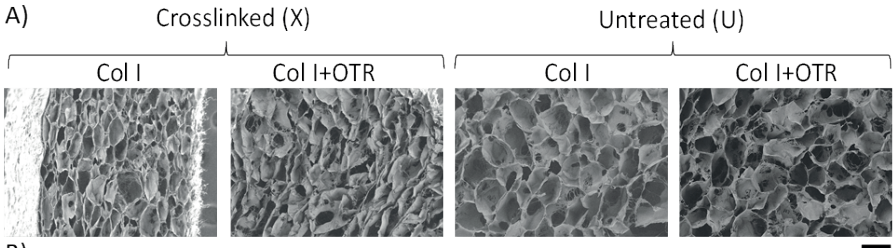

B)

Scaffold type	Free amine groups (nmol/mg scaffold)		OTR4120 quantification (µg OTR4120/mg scaffold)	
Sterilized	No	Yes	No	Yes
X Col I	65 ± 9	75 ± 10	-	-
U Col I	198 ± 43*	211 ± 15*	-	-
X Col I+OTR	65 ± 13	74 ± 11	24 ± 5	24 ± 7
U Col I+OTR	187 ± 24*	208 ± 22*	26 ± 4	36 ± 5

Figure 1. Effect of crosslinking and gamma sterilization of scaffolds. A) Representative images of the pore morphology in cross-section of crosslinked (X) and untreated (U) collagen scaffolds using scanning electron microscopy. Scale bar is 200 µm. B) Table displaying the characteristics of Col I scaffolds with and without OTR4120, before and after sterilization. "-" represents below detection limits. N= 3 (mean ± SD). Two-way ANOVA followed by Tukey's multiple comparison test was performed for primary amine groups. *Significant reduction in primary amine group content was observed in crosslinked scaffolds compared to their non-crosslinked counterparts ($p < 0.001$).

3.2 Presence of OTR4120 and SHH in collagen-based scaffolds

OTR4120 is a heparan sulfate mimetic capable of binding heparin binding sites of proteins such as effector molecules and, to a lesser extent, collagen. SHH has positively charged amino acid residues that interact with OTR4120. Col I and Col I+OTR scaffolds captured similar amounts of SHH, as quantified by Western blotting (Fig. 2A-B). Col I contained 0.15 ± 0.10 µg SHH/mg scaffold and Col I+OTR captured 0.13 ± 0.20 µg/mg. After consecutive washes, the SHH was not detected in the

wash solutions (Supplementary Fig. 4). The distribution of OTR4120 and SHH in the scaffolds was visualized using immunofluorescence assays. The antibody for heparan sulfate cross-reacts with OTR4120. Staining for heparan sulfate showed an even localization of OTR4120 in the whole scaffold of Col I+OTR, while there was no staining in the Col I scaffold. SHH bound to both types of scaffolds but was concentrated at the edge of Col I scaffolds. SHH penetrated deeper inside the Col I+OTR scaffold showing some overlap in the merged image of OTR4120 and SHH (Fig. 2C).

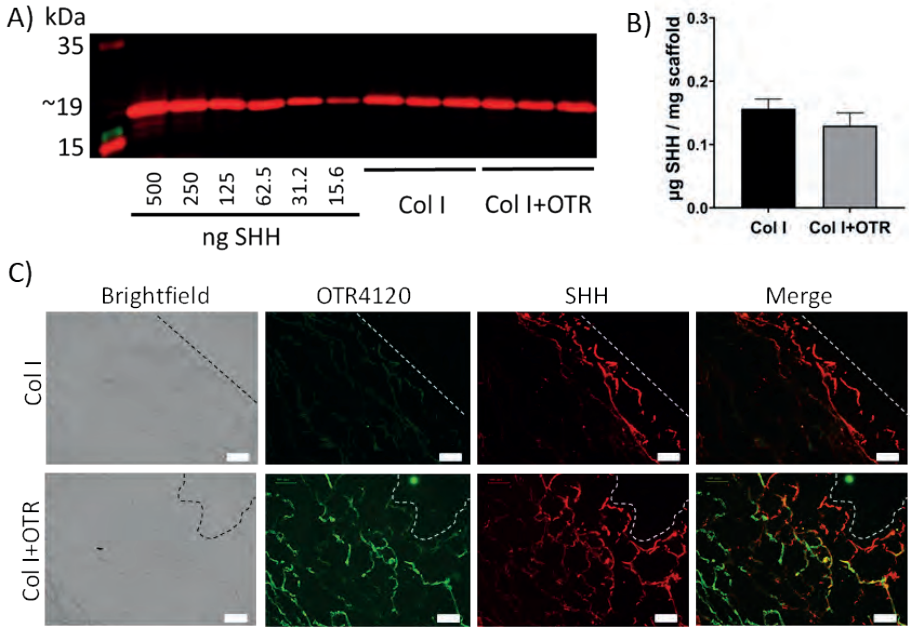

Figure 2. SHH bound to Col I and Col I+OTR scaffolds after incubation with 3.5 µg SHH/ml overnight. A) SHH detection using western blotting. Positive bands are stained in red around 19 kDa. The image shows the calibration curve, Col I and Col I+OTR scaffolds from three different batches. B) Quantification of SHH bound to scaffolds from bands on Western blots (n= 3) gave no significant differences. C) Detection of OTR4120 (green) and SHH (red) using immunostaining. OTR4120 was identified with single chain antibody HS4C3 against heparan sulfate. SHH was concentrated at the edge of the Col I scaffold while it showed a deeper penetration in OTR-containing scaffolds. Dashed line indicates the outer edge of the scaffold. Scale bar is 100 µm.

3.3 *In vitro* analysis with human macrophages

Since incorporation of OTR4120 and SHH in collagen scaffolds may affect the macrophage phenotype, we seeded M0 macrophages to evaluate whether scaffold components would convert the cells towards an M1 (pro-inflammatory) or M2 (pro-healing) subtype, Flow cytometry was used to measure the cell surface markers.

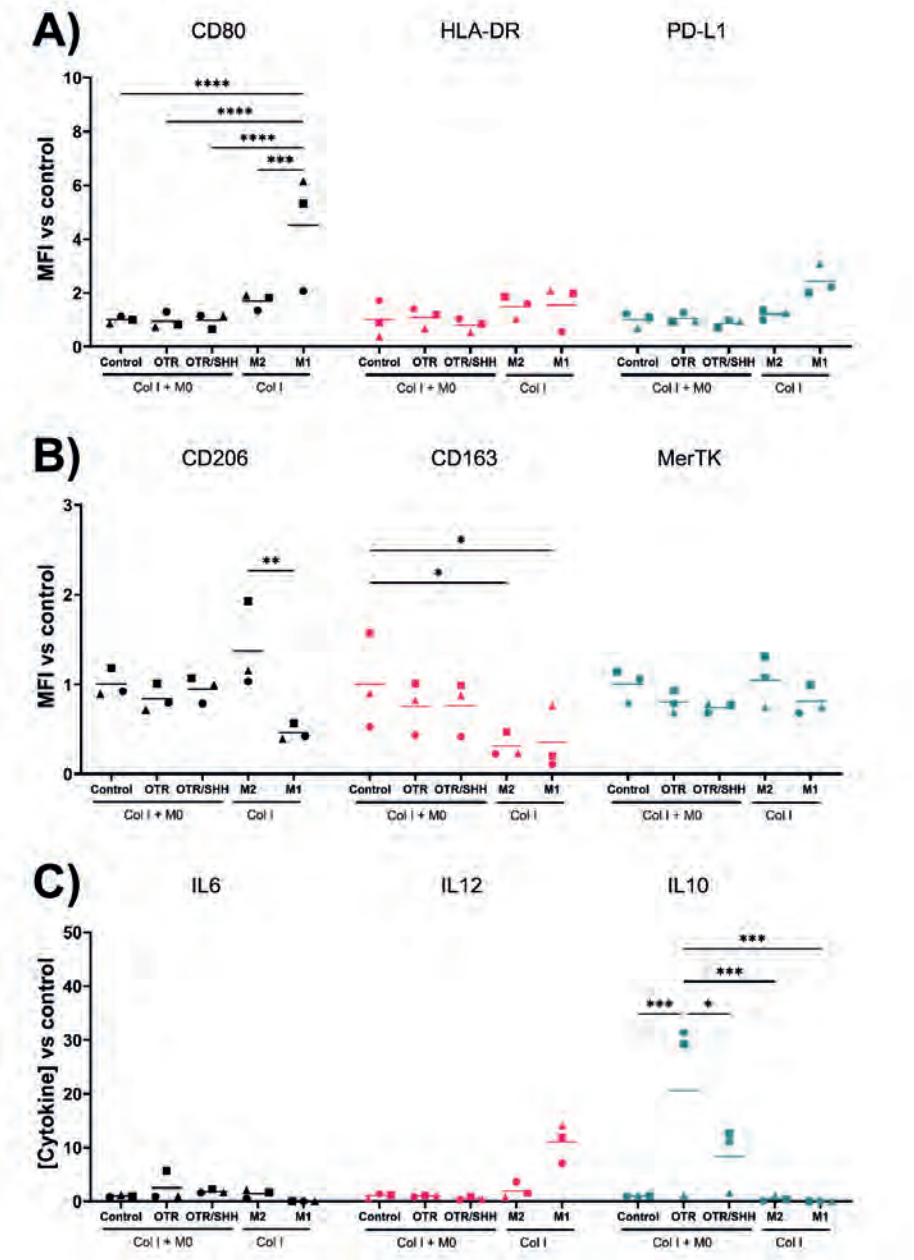

Figure 3. Effect of OTR4120 and/or SHH in collagen scaffolds on primary human macrophages. Type I collagen scaffolds with M0 macrophages were used as control. As secondary controls, Col I with either M1 or M2 macrophages were included. Mean fluorescence intensity (MFI) was measured by flow cytometry for A) M1 associated markers and B) M2 associated markers. C) Cytokine concentrations in the supernatants. Every donor is represented with a different symbol. Data are represented as mean ± SD (n= 3). $p < 0.05$, ** $p < 0.01$, ***$p<0.001$, and ****$p<0.0001$

Additional controls included M1-like and M2-like macrophages, which were seeded on Col I scaffolds to analyze the cell surface markers on non-functionalized scaffolds.

OTR4120 and SHH appeared to modulate macrophage polarization by slightly reducing certain pro-inflammatory markers and modestly enhancing anti-inflammatory cytokine production. The three conditions, Col I, Col I+OTR and Col I+OTR/SHH, tended to show lower expression of CD markers associated with pro-inflammatory phenotypes, such as CD80, HLA-DR, and PD-L1 (Fig. 3A), than the M1-like macrophages control. In contrast, M2-associated markers showed no significant differences across scaffold conditions seeded with M0 macrophages (Fig. 3B), although CD163 expression was significantly higher in control and slightly elevated in OTR ($p= 0.26$) and SHH ($p= 0.25$) compared to the M2-like control. Cytokine analysis of culture supernatants (Fig. 3G-I) revealed reduced IL12 levels in all M0-seeded scaffold conditions—Col I ($p= 0.11$), OTR ($p= 0.10$), and SHH ($p= 0.08$)—relative to M1-like macrophages. IL10 was significantly higher (~30-fold) in the Col I+OTR condition compared to all conditions, while the 10-fold increase in OTR/SHH was not statistically significant ($p= 0.22$). These findings suggest a trend toward an anti-inflammatory profile, particularly with OTR treatment, though variability between donors limits definitive conclusions.

3.4 OTR4120 in Col I scaffolds enhance wound healing

Col I and Col I+OTR scaffolds were implanted in full thickness wounds in rats. To compare the wound healing efficiency, untreated wounds were used as controls for scaffold treatment, while Col I was used as a control to assess the effect of incorporation of OTR4120. After surgery, rats experienced weight loss and discomfort from bandaging. To improve well-being, adjustments were made, including substituting the elastic band (Petflex) to a softer cotton material (2310057, Kruidvat, NL). Despite these efforts, two rats died during the third postoperative week, one was found dead in its cage, likely due to bandage-related distress, and another was euthanized at a humane endpoint following marked weight loss and signs of discomfort. The remaining seven animals completed the 28-day study period.

Macroscopic photos of the wound area were taken at day 0, 7, 14, 21, and 28, but accurate wound measurements could not be performed after day 14 due to scab formation (Fig. 4A). To avoid disrupting the underlying neo-epidermis and granulation tissue, scabs were left intact, as they typically detached only after 5 weeks in this full-thickness wound model, consistent with previous observations in a similar study with porous collagen biomaterials that followed healing up to 56 days[34]. On day 14,

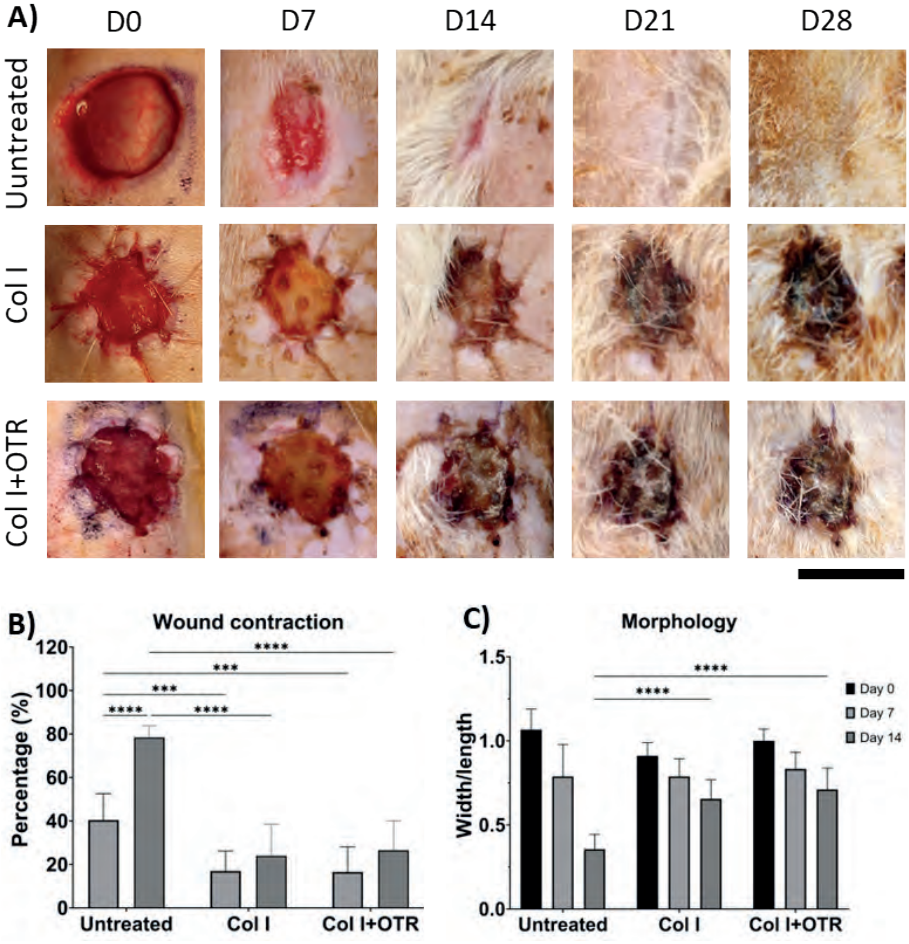

Figure 4. Wound contraction and morphology assessment in rats. 12 mm wounds were created on the back of the rats and left untreated or treated with Col I or Col I+OTR scaffolds. A) Representative macroscopical images of the wounds, from day 0 to day 28. Scale bar is 1 cm. B) Wound contraction at day 7 and day 14 compared to day 0. C) Wound morphology assessment using the width to length ratio of the wound., where 1 represents a symmetric circular shape. Note that circular patterns visible in Col I and Col I+OTR groups result from the texture of the wound dressing. These superficial imprints persist in the scabs due to drying but did not interfere with the underlying healing process. Values are represented as the mean ± SD (n= 9). Comparison between groups was analyzed using 2-way ANOVA. ** $p < 0.01$, *** $p < 0.001$, **** $p < 0.0001$.

wounds treated with scaffolds presented less wound contraction at day 7 with 17 % in Col I and Col I+OTR compared to 40 % in the untreated group. This difference increased by day 14 where the untreated wounds had contracted more than 78 % in contrast to the treated scaffolds with 24 % and 26 % for Col I and Col I+OTR, respectively (Fig. 4B). These trends suggest that scaffold-treated wounds exhibit more gradual contraction. The morphology of wounds during closing may impact the development of scars. The full-thickness wounds created on the back of the rats were a round circle of 12 mm diameter at day 0 with a width/length of ~1. On day 14, the untreated wounds tended to become oval shaped with a width/length ratio close to 0.36 in comparison to 0.65 in Col I and 0.71 in Col I+OTR (Fig. 4C).

The full wound areas with surrounding healthy skin were taken at day 28 and analyzed using (immuno) histochemistry. H&E staining of cross-sections of day 28 reflected our macroscopic observations of a significant contraction from untreated condition followed by collagen scaffolds with and without OTR4120. Granulation tissue formed an hourglass shape, which was most pronounced in untreated wounds as observed with the dotted line, indicating a higher wound deformation compared to scaffold conditions (Fig. 5A-B). The epidermis was significantly thicker in Col I followed by Col I+OTR with untreated condition featuring a similar thickness to unwounded skin (Fig. 5C). The wound area was larger in Col I condition compared to untreated wounds, probably due to the reduced skin contraction (Fig. 5D).

To evaluate the degradation of scaffolds, residual collagen material was scored. Collagen scaffold remnants can be easily differentiated from native collagen due to their thicker collagen bundles and intense blue staining using Masson's trichrome blue (Fig. 6A). By day 28, there were still some remnants in Col I condition, followed by OTR4120-containing scaffolds but with a mean score of less than 1. We semi quantitatively scored myofibroblasts, macrophages and blood vessels within the granulation tissue to evaluate whether the different conditions influenced cell recruitment and/or proliferation. No significant differences were found in the number of myofibroblasts (Fig. 6B). An overview with α-SMA staining showed that myofibroblasts had migrated to the wound area from the bottom and the wound edges (Supplementary Fig. 5). Treatment with OTR-containing scaffolds was associated with an increased number of macrophages (Fig. 6C). Scaffold treatments also appeared to increase angiogenesis compared to the untreated wounds (Fig. 6D).

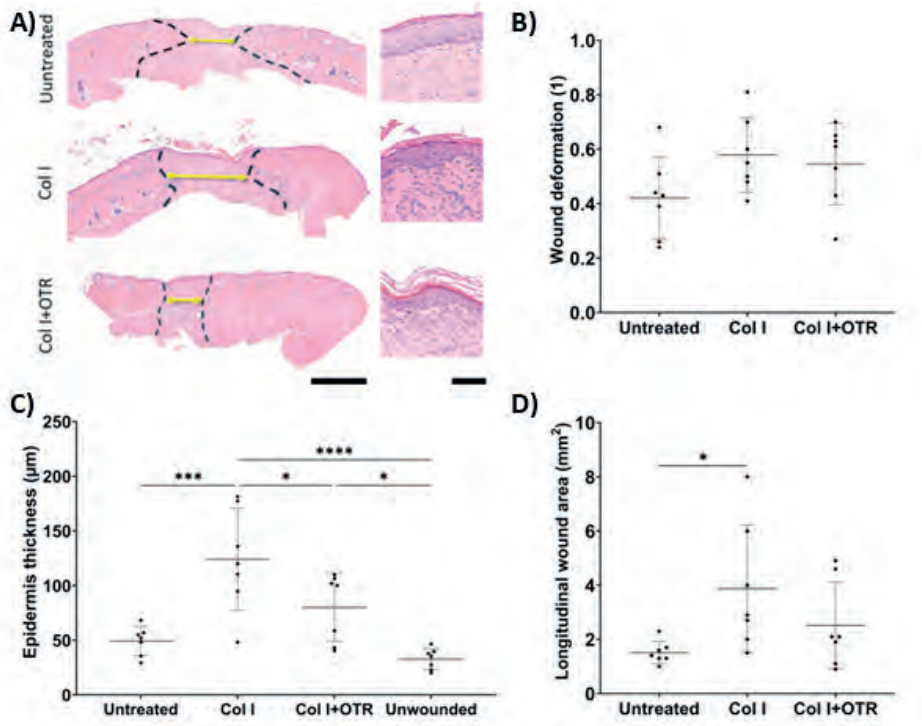

Figure 5. Histological analysis of wound areas on day 28. A) H&E staining of representative tissue sections. The dotted line is the interface between granulation tissue and unwounded skin, whereas the yellow arrow indicates the middle width of the dermis in the wound. Left images depict the complete tissue sample, while images on the right are an enlargement of the epidermal layer on the wound. Scale bar for skin overview is 2 mm and for epidermis 60 µm. B) Microscopical wound deformation calculated as a comparison between the length of the wound between the middle and top of the dermis. Values closer to 0 represent a higher deformation. C) Epidermal thickness above the granulation tissue. D) Wound area in the longitudinal plane visible by granulation tissue and delimited by dotted lines on histology. Data represent mean ± SD (n= 7). One-way ANOVA with Tukey's multiple comparison test was used for statistical analysis. * $p < 0.05$, *** $p < 0.001$, **** $p < 0.0001$.

Appendages such as hair follicles and sebaceous glands appeared next to the wound margins (approximately 300 µm away from the margin) (Fig. 7A). The density of hair follicles per area remained similar in all conditions (Fig. 7B). In contrast, Col I+OTR slightly increased the content of sebaceous glands at the wound edge compared to untreated wounds (Fig. 7C).

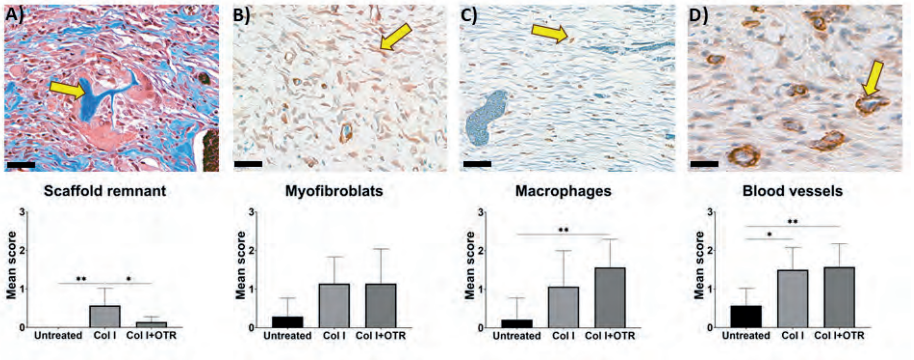

Figure 6. Histological analysis of day 28 tissue samples of various treatments. The top row shows histological examples, and the bottom row presents the semi-quantitative scoring. A) Remaining collagen scaffold visualized using trichrome blue. OTR-containing scaffold showed more degradation, B) Myofibroblasts stained for alpha-smooth muscle actin (α-SMA) visualized as elongated cells with blue nuclei. C) Macrophages stained with CD68 marker, Col I+OTR showed higher numbers. D) Blood vessels were identified using α-SMA staining for mature blood vessels. More angiogenesis was seen for scaffold-treated wounds. Arrows depict examples of the corresponding parameter. Sections were scored for these aspects from 0 (not present) to 3 (abundant). Data are represented as mean ± SD (n= 7). Scale bars are 40 µm. * $p < 0.05$, ** $p < 0.01$.

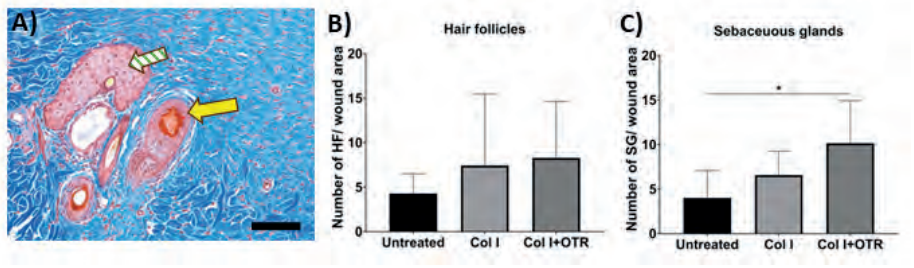

Figure 7. Quantitative histological analysis of appendages in healed skin. A) Representative histological image showing hair follicles (HF, yellow arrow) and sebaceous glands (SG, gray arrow) in the transitional wound area visualized with Masson's trichrome blue staining. B-C) Quantification of hair follicles (B) and sebaceous glands (C) in the adjacent wound area (<300 µm). Scale bar is 100 µm. * $p < 0.05$, ** $p < 0.01$.

4. Discussion

Scarring remains a significant clinical challenge, often leading to morbidity and impaired skin regeneration. Therefore, there is a pressing need for advanced biomaterials capable of promoting effective skin healing. In this study, we created innovative collagen scaffolds containing RGTA® OTR4120, a heparan sulfate mimetic molecule proven to improve wound healing in liquid format, such as CACIPLIQ20® [35].

In order to use skin substitutes *in vivo*, scaffolds were chemically crosslinked and sterilized by gamma irradiation. This sterilization step did not affect the crosslinking degree nor the amount of OTR4120 retained on crosslinked scaffolds, as OTR4120 was already covalently bound prior to sterilization. Interestingly, untreated (non-crosslinked) Col I+OTR scaffolds showed a slightly higher signal for OTR4120 after sterilization compared to their non-sterilized counterparts. Gamma rays can induce free radical formation and chemical modifications even in freezedried scaffolds, including chain scission or formation of new covalent bonds through oxidative pathways [36-38]. These alterations may facilitate more efficient papain digestion by breaking collagen chains and increasing the release of embedded OTR4120. In contrast, chemically crosslinked scaffolds are more resistant to such changes, and the amount of retained OTR4120 remained consistent before and after sterilization.

We also tested the capability of OTR4120 to bind the effector molecule SHH, which is a promising effector molecule for skin regeneration. It is upregulated during embryonic development promoting nerve growth [39], epidermal development [23] and hair follicle morphogenesis [40]. OTR4120 has been reported to bind heparin binding growth factors such as FGF, VEGF, TGFβ [21]. In our study, collagen scaffolds with and without OTR4120 bound similar amounts of the heparin-binding growth factor SHH (0.13-0.15 µg SHH/mg scaffold). Similarly, another study on Col I+OTR showed similar amount of FGF-2 binding compared to Col I but revealed a more gradual release of FGF2 in OTR-containing scaffolds [28]. A slower release of SHH may benefit later stages of wound healing, such as re-epithelization and stimulation of hair follicle neogenesis. Immunostainings showed that SHH penetrated deeper in Col I+OTR scaffolds, while concentrating at the edges in Col I. A previous study using collagen-heparin scaffolds incubated with 10 µg/ml SHH (nearly three times our 3.5 µg/ml) also found SHH primarily at the edges [25].

To assess the effect of OTR4120 and SHH on immune cells, *in vitro* testing was performed by culturing M0 macrophages on collagen scaffolds. Overall, it seems that collagen scaffolds seeded with M0 macrophages promote a macrophage

phenotype more akin to M2-like than M1-like phenotypes. Although not statistically significant, Col I+OTR/SHH treatment consistently showed lower mean expression of M1-associated markers, indicating a trend toward reduced pro-inflammatory macrophage activation. This aligns with previous reports where SHH reduced M1-related markers in macrophage cultures [41]. The largest effect of OTR4120 was observed in the expression of IL10 being nearly 30 times higher in two donors compared to Col I. IL10 is mainly produced by the M2c-like phenotype [42], and can reduce inflammation, inhibits the transformation of fibroblasts into myofibroblasts and increases collagen reorganization [43-45], resulting in skin repair with less scarring.

To study the effect of OTR4120 in acute deep wounds, collagen scaffolds with incorporated OTR4120 were applied on full-thickness wounds in a rat model over 28 days. By day 14, scaffold-treated wounds showed less macroscopic contraction compared to untreated wounds. A rapid contraction often leads to fibrosis and scar formation, a hallmark of mammalian healing but less pronounced in rodents [46]. In contrast, species capable of scarless regeneration, such as axolotls, exhibit delayed contraction and ECM deposition [47]. While we did not assess biomechanical properties of the scaffolds in this study, similar crosslinked type I collagen scaffolds had a Young's modulus of approximately 0.4 kPa [48], which is considerably lower than the ~5 kPa threshold reported to induce fibroblast-to-myofibroblast transition [49], suggesting that our scaffolds are relatively soft and unlikely to mechanically restrain the wound or hold it open. In addition, Col I+OTR scaffolds helped preserve a more rounded wound shape, which may suggest a more uniform healing that could lead to less scar formation [50]. Although round wounds were initially created to evenly distribute mechanical forces, untreated wounds contracted faster and formed an oval shape. Histological analysis revealed that untreated wounds, despite faster macroscopic contraction, exhibited greater deformation, indicating less coordinated healing and a higher risk of contractures. In contrast, scaffold-treated wounds showed slower, more organized closure with reduced deformation, supporting a more controlled healing process and potentially minimizing scarring [51, 52]. Re-epithelialization was complete across all conditions, but OTR-treated wounds showed a trend toward an epidermal thickness closer to native skin and with a slightly smaller wound area in the longitudinal section than Col I alone, which may be the result of a less rigid skin [53] and improved wound healing.

Immunostaining revealed that scaffolds delayed ECM deposition, with more presence of granular tissue and slightly elevated levels of myofibroblasts and macrophages than in untreated wounds. Porous scaffolds facilitated cell infiltration from wound edges and deeper layers. Particularly, OTR-treated wounds displayed

a higher macrophage presence as evidenced by CD68 staining, which might be related to the faster scaffold degradation (Fig. 6A & B). In contrast, a previous study in a fetal sheep model using collagen-heparin scaffolds with growth factors found more residual scaffold and lower macrophage presence (scoring <1, scale 0-3) [17]. This suggests that OTR4120 influences macrophage recruitment in adult rats, leading to accelerated scaffold degradation. A higher number of blood vessels was seen in scaffold-treated wounds, aligning with the proliferative phase [54]. While OTR4120 did not affect hair follicle abundance, it increased the number of sebaceous glands in the adjacent wound area. Given OTR4120 ability to bind heparin-binding effector molecules [55], it may interact with local growth factors, such as WNT, SHH, BMP and FGF [56], which are involved in sebaceous gland development [57].

A limitation of this study is that the Col I+OTR/SHH scaffold and OTR4120 alone were not evaluated *in vivo*. *In vitro* studies with SHH were limited to macrophages, thereby missing potential interactions with other relevant cells such as dermal papilla cells, neurons, and epidermal cells. Future research should explore these interactions to better understand SHH broader potential in skin regeneration. Additionally, the animal model presents limitations, as rats possess a panniculus carnosus layer which produces rapid wound contraction which is absent in human skin [58]. Unlike general practice in humans and larger animal studies, we did not apply split-thickness skin graft in these rodents, as this is highly challenging, limiting the ability to fully replicate skin treatments in humans. Pigs, with ECM skin more similar to human skin and comparable healing times, could be considered as an alternative animal model for future preclinical studies [46].

In conclusion, we successfully constructed chemically crosslinked porous collagen scaffolds with bound RGTA® OTR4120, which remained stable after gamma sterilization. These scaffolds retained the ability to bind the effector molecule SHH and showed a trend toward a pro-healing M2-like macrophage phenotype in culture. In a rat full-thickness wound model, collagen-OTR scaffolds modestly influenced wound healing dynamics by supporting ECM remodeling, maintaining improved wound morphology, and moderating epidermal thickness, which may contribute to reduce fibrosis and improve skin regeneration outcomes. This study provides preliminary evidence that OTR4120 could be a promising addition to acellular skin substitutes for improving acute wound healing.

Funding

This work received funding from the European Union's Horizon 2020 research and innovation program under the Marie Skłodowska-Curie Grant Agreement No.

955722 (SkinTERM, NAM, RK) and from Radboud university medical center PhD round 2020 PI and MSc competition, respectively (MG and MP).

Acknowledgements

The authors thank the Radboud Technology Center Microscopy for use of the Scanning Electron Microscope and Elly Versteeg for the development and optimization of the used dot blot method. We appreciate the help from Steven Teerenstra with the power analysis for rat experiments as well as Hans Smola (Hartmann AG) for clinical advice about wound dressings for the rat experiments. We thank Maikel School, Tim Peters and the animal research facility staff for their support with the rat experiments.

Conflicts of Interest

AC and FC are current employees of OTR3, DB is CEO of OTR3. However, the views presented in this research article remain independent and were not influenced by the company.

References

1. Schaefer TJ, Nunez Lopez O. Burn Resuscitation and Management. StatPearls. Treasure Island (FL): StatPearls Publishing Copyright © 2025, StatPearls Publishing LLC.; 2023.
2. Takeo M, Lee W, Ito M. Wound healing and skin regeneration. Cold Spring Harb Perspect Med. 2015;5(1):a023267. Epub 20150105. doi: 10.1101/cshperspect.a023267. PubMed PMID: 25561722; PMCID: PMC4292081.
3. Cancio LC, Barillo DJ, Kearns RD, Holmes JHt, Conlon KM, Matherly AF, et al. Guidelines for Burn Care Under Austere Conditions: Surgical and Nonsurgical Wound Management. J Burn Care Res. 2017;38(4):203-14. doi: 10.1097/bcr.0000000000000368. PubMed PMID: 27355660.
4. García-Salinas AS, Mecott GA, García-Pérez M, Castro-Govea Y, Pérez-Porras S, Chacón-Moreno H, et al. Decreased pain in split-thickness skin graft donor sites with the use of a non-adherent polyurethane dressing. Medicina Universitaria. 2015;17(69):196-202. doi: 10.1016/j.rmu.2015.07.001.
5. Bloemen MCT, van Leeuwen MCE, van Vucht NE, van Zuijlen PPM, Middelkoop E. Dermal Substitution in Acute Burns and Reconstructive Surgery: A 12-Year Follow-Up. Plast Reconstr Surg. 2010;125(5):1450-9. doi: 10.1097/PRS.0b013e3181d62b08. PubMed PMID: 00006534-201005000-00017.
6. van den Bosch AS, Verwilligen RAF, Pijpe A, Bosma E, van der Vlies CH, Lucas Y, et al. Outcomes of dermal substitutes in burns and burn scar reconstruction: A systematic review and meta-analysis. Wound Repair Regen. 2024;32(6):960-78. Epub 20241022. doi: 10.1111/wrr.13226. PubMed PMID: 39435560; PMCID: PMC11584356.
7. Karppinen SM, Heljasvaara R, Gullberg D, Tasanen K, Pihlajaniemi T. Toward understanding scarless skin wound healing and pathological scarring. F1000Res. 2019;8. Epub 2019/06/25. doi: 10.12688/f1000research.18293.1. PubMed PMID: 31231509; PMCID: PMC6556993.
8. Zaidi A, Green L. Physiology of haemostasis. Anaesthesia & Intensive Care Medicine. 2022;23(2):111-7. doi: https://doi.org/10.1016/j.mpaic.2021.10.023.
9. Su Y, Gao J, Kaur P, Wang Z. Neutrophils and Macrophages as Targets for Development of Nanotherapeutics in Inflammatory Diseases. Pharmaceutics. 2020;12(12). Epub 20201217. doi: 10.3390/pharmaceutics12121222. PubMed PMID: 33348630; PMCID: PMC7766591.
10. Silva MT. Macrophage phagocytosis of neutrophils at inflammatory/infectious foci: a cooperative mechanism in the control of infection and infectious inflammation. J Leukoc Biol. 2011;89(5):675-83. Epub 20101217. doi: 10.1189/jlb.0910536. PubMed PMID: 21169518.
11. Zheng H, Cheng X, Jin L, Shan S, Yang J, Zhou J. Recent advances in strategies to target the behavior of macrophages in wound healing. Biomed Pharmacother. 2023;165. doi: 10.1016/j.biopha.2023.115199. PubMed PMID: WOS:001057130700001.
12. Alhajj M, Goyal A. Physiology, Granulation Tissue. StatPearls. Treasure Island (FL): StatPearls Publishing. Copyright © 2025, StatPearls Publishing LLC.; 2025.
13. Yannas IV, Tzeranis DS. Mammals fail to regenerate organs when wound contraction drives scar formation. NPJ Regen Med. 2021;6(1):39. Epub 2021/07/24. doi: 10.1038/s41536-021-00149-9. PubMed PMID: 34294726; PMCID: PMC8298605.
14. Piipponen M, Li D, Landén NX. The Immune Functions of Keratinocytes in Skin Wound Healing. Int J Mol Sci. 2020;21(22). Epub 20201120. doi: 10.3390/ijms21228790. PubMed PMID: 33233704; PMCID: PMC7699912.

15. Li B, Wang JH. Fibroblasts and myofibroblasts in wound healing: force generation and measurement. J Tissue Viability. 2011;20(4):108-20. Epub 20091207. doi: 10.1016/j.jtv.2009.11.004. PubMed PMID: 19995679; PMCID: PMC2891362.

16. Nillesen STM, Lammers G, Wismans RG, Ulrich MM, Middelkoop E, Spauwen PH, et al. Design and in vivo evaluation of a molecularly defined acellular skin construct: Reduction of early contraction and increase in early blood vessel formation. Acta Biomater. 2011;7(3):1063-71. doi: 10.1016/j.actbio.2010.10.011. PubMed PMID: WOS:000287643900016.

17. Oostendorp C, Geutjes PJ, Smit F, Tiemessen DM, Polman S, Abbawi A, et al. Sustained Postnatal Skin Regeneration Upon Prenatal Application of Functionalized Collagen Scaffolds. Tissue Eng Part A. 2021;27(1-2):10-25. doi: 10.1089/ten.tea.2019.0234. PubMed PMID: WOS:000508888400001.

18. Bame KJ. Heparanases: endoglycosidases that degrade heparan sulfate proteoglycans. Glycobiology. 2001;11(6):91R-8R. doi: 10.1093/glycob/11.6.91R.

19. Neck J, Tuk B, Barritault D, Tong M. Heparan Sulfate Proteoglycan Mimetics Promote Tissue Regeneration: An Overview. Tissue Regeneration - From Basic Biology to Clinical Application2012.

20. Ikeda Y, Charef S, Ouidja M-O, Barbier-Chassefière V, Sineriz F, Duchesnay A, et al. Synthesis and biological activities of a library of glycosaminoglycans mimetic oligosaccharides. Biomaterials. 2011;32(3):769-76. doi: https://doi.org/10.1016/j.biomaterials.2010.09.043.

21. Barritault D, Gilbert-Sirieix M, Rice KL, Siñeriz F, Papy-Garcia D, Baudouin C, et al. RGTA® or ReGeneraTing Agents mimic heparan sulfate in regenerative medicine: from concept to curing patients. Glycoconj J. 2017;34(3):325-38. doi: 10.1007/s10719-016-9744-5.

22. Potekaev NN, Borzykh OB, Medvedev GV, Pushkin DV, Petrova MM, Petrov AV, et al. The Role of Extracellular Matrix in Skin Wound Healing. Journal of Clinical Medicine. 2021;10(24):5947. PubMed PMID: doi:10.3390/jcm10245947.

23. Abe Y, Tanaka N. Roles of the Hedgehog Signaling Pathway in Epidermal and Hair Follicle Development, Homeostasis, and Cancer. Journal of Developmental Biology. 2017;5(4). doi: 10.3390/jdb5040012. PubMed PMID: WOS:000419225800003.

24. Takaya K, Aramaki-Hattori N, Sakai S, Okabe K, Kishi K. Effect of Sonic Hedgehog on the Regeneration of Epidermal Texture Patterns. Biomedicines. 2022;10(12). doi: 10.3390/biomedicines10123099. PubMed PMID: WOS:000900465100001.

25. Uijtdewilligen PJE, Versteeg EMM, Gilissen C, van Reijmersdal SV, Schoppmeyer R, Wismans RG, et al. Towards embryonic-like scaffolds for skin tissue engineering: identification of effector molecules and construction of scaffolds. J Tissue Eng Regen Med. 2016;10(1):E34-E44. doi: 10.1002/term.1725. PubMed PMID: WOS:000368577300007.

26. Whalen DM, Malinauskas T, Gilbert RJ, Siebold C. Structural insights into proteoglycan-shaped Hedgehog signaling. Proc Natl Acad Sci U S A. 2013;110(41):16420-5. Epub 20130923. doi: 10.1073/pnas.1310097110. PubMed PMID: 24062467; PMCID: PMC3799379.

27. Chakrabarti J, Dua-Awereh M, Schumacher M, Engevik A, Hawkins J, Helmrath MA, et al. Sonic Hedgehog acts as a macrophage chemoattractant during regeneration of the gastric epithelium. npj Regenerative Medicine. 2022;7(1):3. doi: 10.1038/s41536-021-00196-2.

28. Gansevoort M, Wentholt S, Li Vecchi G, de Vries M, Versteeg EMM, Boekema BKHL, et al. Next-Generation Biomaterials for Wound Healing: Development and Evaluation of Collagen Scaffolds Functionalized with a Heparan Sulfate Mimic and Fibroblast Growth Factor 2. J Funct Biomater. 2025;16(2):51. PubMed PMID: doi:10.3390/jfb16020051.

29. Pieper JS, Oosterhof A, Dijkstra PJ, Veerkamp JH, van Kuppevelt TH. Preparation and characterization of porous crosslinked collagenous matrices containing bioavailable chondroitin sulphate. Biomaterials. 1999;20(9):847-58. doi: 10.1016/s0142-9612(98)00240-3. PubMed PMID: WOS:000079761800006.

30. Papy-Garcia D, Barbier-Chassefière V, Rouet V, Kerros M-E, Klochendler C, Tournaire M-C, et al. Nondegradative Sulfation of Polysaccharides. Synthesis and Structure Characterization of Biologically Active Heparan Sulfate Mimetics. Macromolecules. 2005;38(11):4647-54. doi: 10.1021/ma048485p.

31. Elias J, Matheson BA, Gower L. Influence of Crosslinking Methods on Biomimetically Mineralized Collagen Matrices for Bone-like Biomaterials. Polymers (Basel). 2023;15(9). Epub 20230422. doi: 10.3390/polym15091981. PubMed PMID: 37177129; PMCID: PMC10180878.

32. Clausen TM, Kumar G, Ibsen EK, Orum-Madsen MS, Hurtado-Coll A, Gustavsson T, et al. A simple method for detecting oncofetal chondroitin sulfate glycosaminoglycans in bladder cancer urine. Cell Death Discovery. 2020;6(1). doi: 10.1038/s41420-020-00304-z. PubMed PMID: WOS:000556318500001.

33. Damen LAA, van de Westerlo EMA, Versteeg EMM, van Wessel T, Daamen WF, van Kuppevelt TH. Construction and evaluation of an antibody phage display library targeting heparan sulfate. Glycoconj J. 2020;37(4):445-55. Epub 20200528. doi: 10.1007/s10719-020-09925-z. PubMed PMID: 32468289; PMCID: PMC7329785.

34. Krymchenko R, Avila-Martinez N, Gansevoort M, Bakker G-J, Gomes MLNP, Vlig M, et al. Collagen-elastin dermal scaffolds enhance tissue regeneration and reduce scarring in preclinical models. Mater Today Bio. 2025:102239. doi: https://doi.org/10.1016/j.mtbio.2025.102239.

35. Barritault D. Overview of 10 years of practice with CACIPLIQ20® matrix therapy as a healing agent for hard to heal wounds: Efficacy, cost-effectiveness and future perspectives. Wound Medicine. 2020;28:100180. doi: https://doi.org/10.1016/j.wndm.2020.100180.

36. Patel JM, Jackson RC, Schneider GL, Ghodbane SA, Dunn MG. Carbodiimide cross-linking counteracts the detrimental effects of gamma irradiation on the physical properties of collagen-hyaluronan sponges. Journal of Materials Science: Materials in Medicine. 2018;29(6):75. doi: 10.1007/s10856-018-6056-2.

37. Crocker DB, Hering TM, Akkus O, Oest ME, Rimnac CM. Dose-dependent effects of gamma radiation sterilization on the collagen matrix of human cortical bone allograft and its influence on fatigue crack propagation resistance. Cell Tissue Bank. 2024;25(3):735-45. doi: 10.1007/s10561-024-10135-2.

38. Jeong SM, Kim HH, Ryu SH, Kang WS, Lee JE, Kim SR, et al. Effects of Gamma Irradiation on Inhibition of Urease Activity and Fishy Smell in Mackerel (Scomber japonicus) during Refrigerated Storage. J Microbiol Biotechnol. 2022;32(6):808-15. Epub 20220513. doi: 10.4014/jmb.2112.12037. PubMed PMID: 35637171; PMCID: PMC9628912.

39. Belgacem YH, Hamilton AM, Shim S, Spencer KA, Borodinsky LN. The Many Hats of Sonic Hedgehog Signaling in Nervous System Development and Disease. Journal of Developmental Biology [Internet]. 2016; 4 4.

40. Sun X, Are A, Annusver K, Sivan U, Jacob T, Dalessandri T, et al. Coordinated hedgehog signaling induces new hair follicles in adult skin. eLife. 2020;9:e46756. doi: 10.7554/eLife.46756.

41. Zhang J, He Z, Xiong C, Yao Y, Zhang C, Yao W, et al. SHH induces macrophage oxidative phosphorylation and efferocytosis to promote scar formation. Cell Communication and Signaling. 2024;22(1):336. doi: 10.1186/s12964-024-01692-w.

42. Chen C, Liu T, Tang Y, Luo G, Liang G, He W. Epigenetic regulation of macrophage polarization in wound healing. Burns Trauma. 2023;11:tkac057. Epub 20230117. doi: 10.1093/burnst/tkac057. PubMed PMID: 36687556; PMCID: PMC9844119.

43. Singampalli KL, Balaji S, Wang X, Parikh UM, Kaul A, Gilley J, et al. The Role of an IL-10/Hyaluronan Axis in Dermal Wound Healing. Front Cell Dev Biol. 2020;8:636. Epub 20200717. doi: 10.3389/fcell.2020.00636. PubMed PMID: 32850791; PMCID: PMC7396613.

44. Shi J, Li J, Guan H, Cai W, Bai X, Fang X, et al. Anti-fibrotic actions of interleukin-10 against hypertrophic scarring by activation of PI3K/AKT and STAT3 signaling pathways in scar-forming fibroblasts. PLoS One. 2014;9(5):e98228. Epub 20140530. doi: 10.1371/journal.pone.0098228. PubMed PMID: 24878845; PMCID: PMC4039501.

45. Henderson J, Ferguson MWJ, Terenghi G. The reinnervation and revascularization of wounds is temporarily altered after treatment with interleukin 10. Wound Repair Regen. 2011;19(2):268-73. doi: https://doi.org/10.1111/j.1524-475X.2011.00667.x.

46. Supp DM. Animal Models for Studies of Keloid Scarring. Adv Wound Care (New Rochelle). 2019;8(2):77-89. Epub 20190213. doi: 10.1089/wound.2018.0828. PubMed PMID: 31832272; PMCID: PMC6906757.

47. Avila-Martinez N, Gansevoort M, Verbakel J, Jayaprakash H, Araujo IM, Vitorino M, et al. Matrisomal components involved in regenerative wound healing in axolotl and Acomys: implications for biomaterial development. Biomater Sci. 2023;11(18):6060-81. Epub 20230912. doi: 10.1039/d3bm00835e. PubMed PMID: 37525590.

48. Versteegden LR, Sloff M, Hoogenkamp HR, Pot MW, Pang J, Hafmans TG, et al. A salt-based method to adapt stiffness and biodegradability of porous collagen scaffolds. Rsc Advances. 2019;9(63):36742-50. doi: 10.1039/c9ra06651a. PubMed PMID: WOS:000498519000028.

49. Balestrini JL, Chaudhry S, Sarrazy V, Koehler A, Hinz B. The mechanical memory of lung myofibroblasts. Integrative Biology. 2012;4(4):410-21. doi: 10.1039/c2ib00149g.

50. Yin J, Zhang S, Yang C, Wang Y, Shi B, Zheng Q, et al. Mechanotransduction in skin wound healing and scar formation: Potential therapeutic targets for controlling hypertrophic scarring. Front Immunol. 2022;13:1028410. Epub 20221017. doi: 10.3389/fimmu.2022.1028410. PubMed PMID: 36325354; PMCID: PMC9618819.

51. Goel A, Shrivastava P. Post-burn scars and scar contractures. Indian J Plast Surg. 2010;43(Suppl):S63-71. doi: 10.4103/0970-0358.70724. PubMed PMID: 21321660; PMCID: PMC3038392.

52. Soller EC, Tzeranis DS, Miu K, So PTC, Yannas IV. Common features of optimal collagen scaffolds that disrupt wound contraction and enhance regeneration both in peripheral nerves and in skin. Biomaterials. 2012;33(19):4783-91. doi: https://doi.org/10.1016/j.biomaterials.2012.03.068.

53. Wei JCJ, Edwards GA, Martin DJ, Huang H, Crichton ML, Kendall MAF. Allometric scaling of skin thickness, elasticity, viscoelasticity to mass for micro-medical device translation: from mice, rats, rabbits, pigs to humans. Sci Rep. 2017;7(1):15885. doi: 10.1038/s41598-017-15830-7.

54. Sorg H, Tilkorn DJ, Hager S, Hauser J, Mirastschijski U. Skin Wound Healing: An Update on the Current Knowledge and Concepts. European Surgical Research. 2017;58(1-2):81-94. doi: 10.1159/000454919. PubMed PMID: WOS:000395772500007.

55. Rouet V, Hamma-Kourbali Y, Petit E, Panagopoulou P, Katsoris P, Barritault D, et al. A synthetic glycosaminoglycan mimetic binds vascular endothelial growth factor and modulates angiogenesis. J Biol Chem. 2005;280(38):32792-800. Epub 20050713. doi: 10.1074/jbc.M504492200. PubMed PMID: 16014624.

56. Papy-Garcia D, Albanese P. Heparan sulfate proteoglycans as key regulators of the mesenchymal niche of hematopoietic stem cells. Glycoconj J. 2017;34(3):377-91. Epub 20170602. doi: 10.1007/s10719-017-9773-8. PubMed PMID: 28577070.

57. Coulson-Thomas VJ, Gesteira TF, Esko J, Kao W. Heparan Sulfate Regulates Hair Follicle and Sebaceous Gland Morphogenesis and Homeostasis*. J Biol Chem. 2014;289(36):25211-26. doi: https://doi.org/10.1074/jbc.M114.572511.

58. Masson-Meyers DS, Andrade TAM, Caetano GF, Guimaraes FR, Leite MN, Leite SN, et al. Experimental models and methods for cutaneous wound healing assessment. Int J Exp Pathol. 2020;101(1-2):21-37. doi: 10.1111/iep.12346. PubMed PMID: WOS:000522321900001.

Supplementary Material

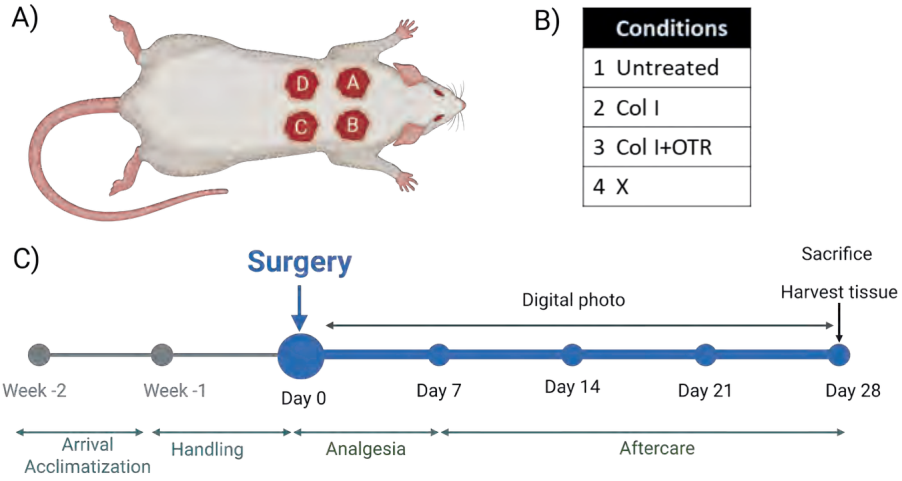

Supplementary Figure 1. Experimental design for the full-thickness wound model in rats. A) Location of wounds on the back of the rat. B) Treatment conditions for the wounds including untreated, type I collagen (Col I), type I collagen with RGTA® OTR4120 (Col I+OTR) and a treatment using collagen-base scaffolds not related with this study (X). The treatment location was randomized using randomizator.org to avoid repetitions of sets. C) Timeline of the experiment from arrival of the animals until sample collection. Digital photos of the wounds were taken on day 0, 7, 14, 21 and 28. Created in BioRender. Avila, N. (2025) https://BioRender.com/g85v9nc.

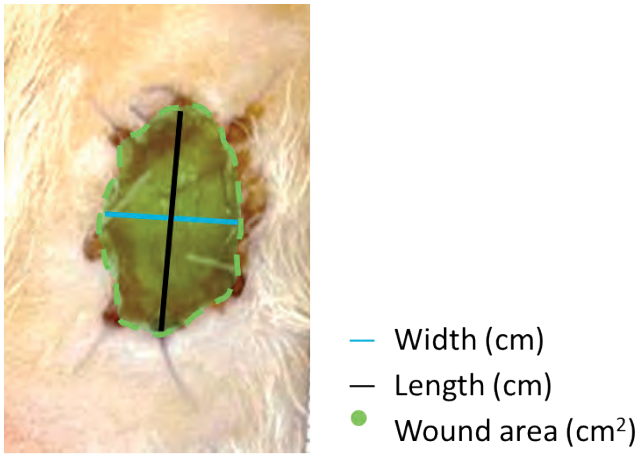

Supplementary Figure 2. Representative lines for the wound measurement process. In blue is the width, in black is the length and in green line is the outline of the wound area performed by manually tracing the wound edge.

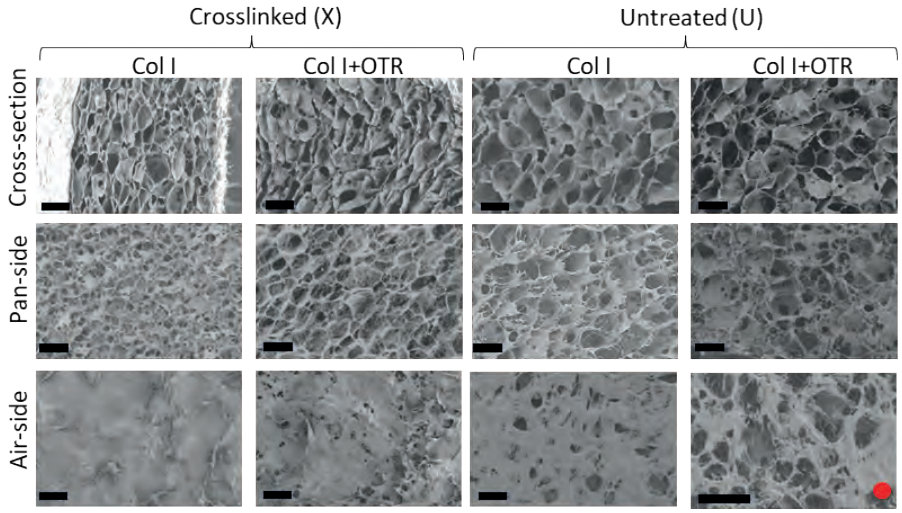

Supplementary Figure 3. Morphology of collagen scaffolds via scanning electron microscopy. Crosslinked and untreated collagen scaffold with and without OTR4120. Images include the cross-section, pan-side and air-side of the scaffolds. Note: U Col I+OTR air-side (red dot) was taken at a higher magnification (see scale bar). Scale bars are 200 µm.

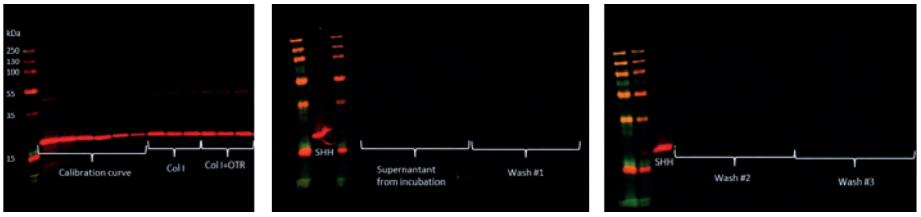

Supplementary Figure 4. Sonic hedgehog (SHH) detection using western blotting. Left image shows a dilution range for the calibration curve using SHH from 500.0 to 15.6 ng, and Col I and Col I+OTR scaffolds incubated with (3.5 µg/ml) SHH. A faint band around 45 kDa corresponds to the SHH precursor, while, at 19 kDa, the mature form of N-SHH is visualized. The center image shows the results of supernatants from the scaffold incubation and the first wash with PBS. The right image shows the supernatants from the second and third washing steps. Note that the same order of Col I and Col I+OTR scaffolds was used for the center and right image as in the left one. A positive control of 62.5 ng SHH is included in the middle and right images. SHH staining is in red.

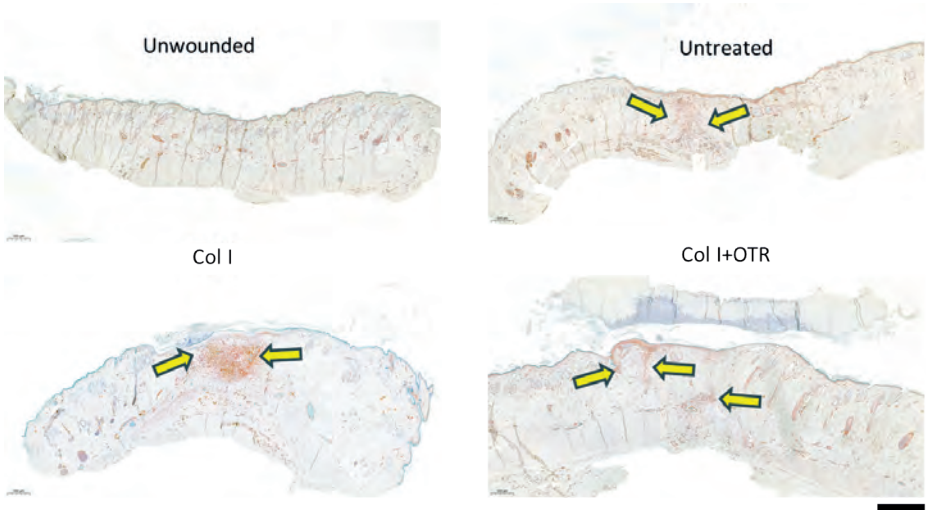

Supplementary Figure 5. Myofibroblast localization into the wound. Yellows arrows point at cells stained for alpha-smooth muscle actin (α-SMA). Scale bar is 1 mm.

Supplementary Table 1. Interclass Correlation Coefficient (ICC) for histological scoring

Parameter	Myofibroblasts	Macrophages	Blood vessels	Scaffold remnant
Interclass correlation (average measures)	1.000	0.927	0.832	0.804

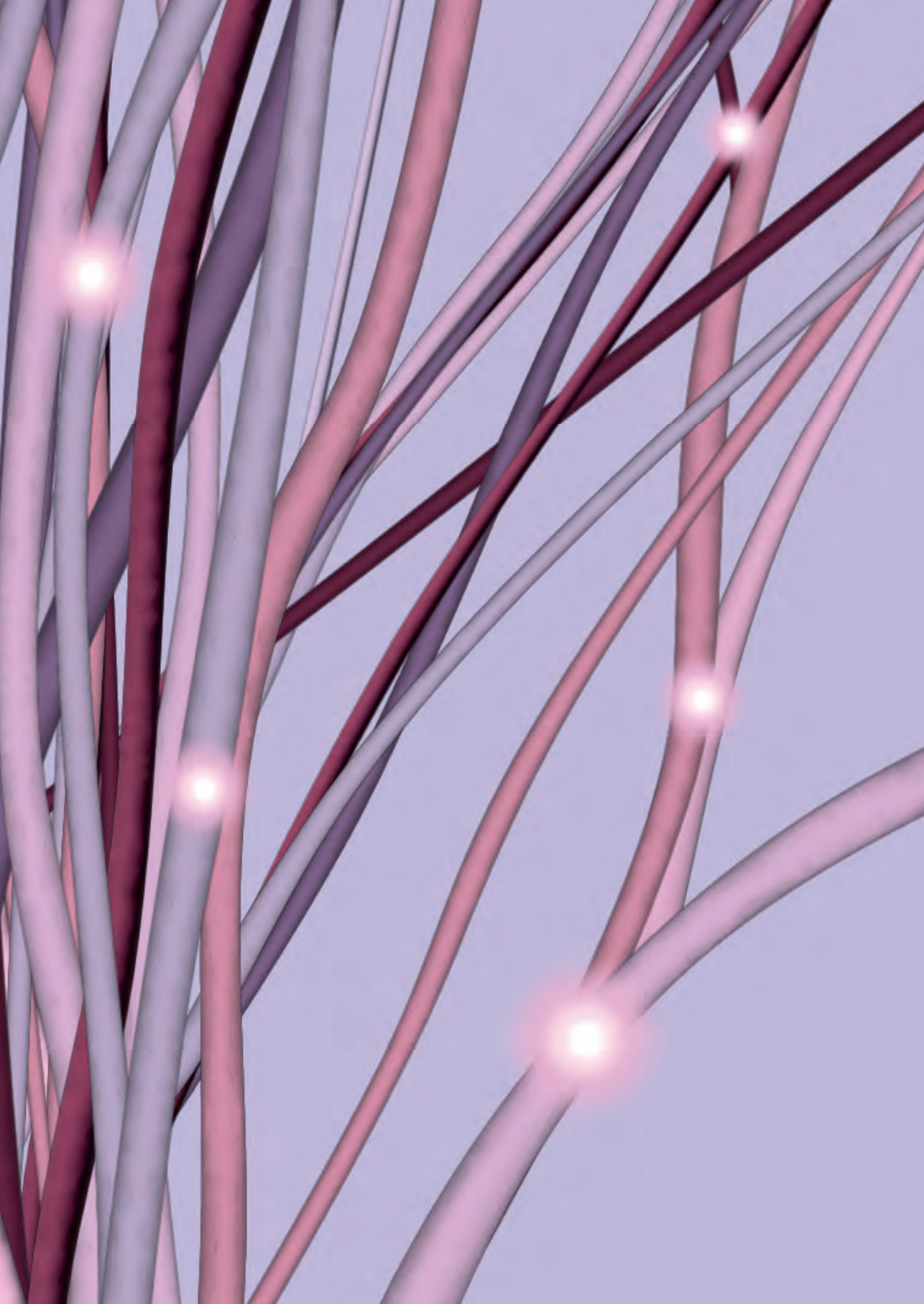

Chapter 6

General discussion and future perspectives

Despite significant advances in biomaterials and cell culture technologies, skin tissue engineering continues to face major challenges. Effective dermal substitutes must go beyond mimicking the mechanical strength and barrier function of native skin, they must also support critical processes such as vascularization, immune modulation, and the regeneration of skin appendages [1]. Clinical limitations remain substantial, including the scarcity of autologous donor sites, and risks of immune rejection in allogeneic or xenogeneic grafts [2]. As a result, many current skin substitutes yield suboptimal outcomes, often resulting in (hypertrophic) scarring, contractures, and the absence of skin appendages [3, 4]. In particular, contractures in joint regions can severely limit patient mobility [5]. Clinical evidence has shown that prompt and effective burn wound treatment can significantly improve healing outcomes [6]. Acellular biomaterials offer a distinct advantage in this context due to their immediate availability and off-the-shelf application [7].

This thesis draws inspiration from regenerative species such as Acomys, axolotls, and fetal mammalian models, which exhibit scarless healing and rapid tissue regeneration. These models have highlighted unique extracellular matrix (ECM) signatures that contrast sharply with those observed in typical adult wound healing [8]. By leveraging these regenerative cues, we aimed to identify and integrate key ECM components into engineered skin constructs to promote improved healing in patients with full-thickness injuries, such as burns. A critical aspect of this approach lies in selecting appropriate wound models for evaluation, as this directly influences the accurate assessment of the efficacy and functional performance of skin substitutes. In the following discussion, we reflect on the challenges encountered in this study and propose future strategies that may further advance the field of skin regeneration.

A new era of ECM skin substitute design

The field of regenerative medicine has steadily evolved over the past century, with continuous innovations in materials and biologics [9]. A significant paradigm shift has been the transition from using inert scaffolds to designing bioactive materials that actively shape the wound environment. Natural biomaterials, particularly type I collagen (Col I), have long been favored for skin scaffolds due to their biocompatibility [10]. However, skin is a complex organ regulated by a diverse array of ECM components, collectively known as the matrisome [11]. The composition and ratio of these components are now recognized as key regulators of wound healing and its ultimate outcome.

Although the mechanisms underlying scarless healing in regenerative species remain incompletely understood, advanced molecular tools such as transcriptomics, proteomics, and single-cell sequencing have helped identify unique matrisome components [12, 13] that could inform the design of next-generation biomaterials as discussed in the **Chapter 2**. Within the collagen family, types III, XII, and XIV are notably upregulated during wound healing in species such as Acomys and fetal mammals [14, 15]. Despite their potential, collagens like types XII and XIV are difficult to source in large quantities [16], making recombinant engineering an attractive, though costly, alternative. Apart from being abundantly present in the skin of regenerative species, type III collagen (Col III) also plays an important role in adult human wound healing and its ratio between Col I/III changes with aging [17]. In **Chapter 4** we observed the potential of Col III combined with Col I scaffolds in wound healing modulation, correlating with previous studies where it was demonstrated that Col III regulates matrix architecture and mechanosensing compared to Col III deficient knockdown mice [18].

Other extracellular matrix components, such as fibronectin, laminin, tenascin, hyaluronan, and heparan sulfate, are also enriched during regenerative wound healing. For instance, early fibronectin deposition in fetal rabbit wounds is thought to promote fibroblast attachment and accelerate closure [19], while tenascin has been shown to enhance collagen fibrillogenesis and fibroblast migration [20, 21]. In this thesis (**Chapters 3 and 5**), the regenerative potential of the glycosaminoglycan hyaluronan and of a heparan sulfate mimetic in wound healing applications were explored. Effector molecules, which influence cellular signaling and behavior, are an emerging focus in regenerative strategies. Members of the TGF-β family, particularly TGF-β1 (pro-fibrotic) and TGF-β3 (anti-fibrotic), play opposing roles in scarring [22, 23]. However, TGF-β3 is overexpressed in systemic sclerosis, a rare disease involving fibrosis in the skin, and treatment with an anti-TGF-β3 antibody has been shown to inhibit fibrosis in affected skin biopsies [24]. Similarly, VEGF, which increases during fetal development, enhances angiogenesis and re-epithelialization [25]. Fibroblast growth factors (FGFs), especially FGF2 (anti-fibrotic) and FGF7 (crucial for hair follicle development), are also more highly expressed in fetal fibroblasts [26, 27]. Recently, sonic hedgehog (SHH), upregulated in embryonic mice skin [28], has gained attention for its association with epidermal development, innervation, and hair follicle morphogenesis [29, 30].

This raises an important question for adult skin replacement: should we attempt to recreate fetal skin? The short answer is no. Adult human skin has evolved superior barrier function by structural, compositional and functional differences

[31]. However, temporarily mimicking key features of fetal or regenerative ECM composition could improve healing without compromising adult skin integrity. In this thesis, we identified and incorporated selected components related to a regenerative matrix, including Col III, HA, as well as SHH delivered in combination with the heparan sulfate mimetic OTR4120, into engineered dermal substitutes. Their individual performances were evaluated across **Chapters 3, 4, and 5**. Future studies should explore combinations of these constituents to determine whether synergistic effects could further promote wound healing and reduce scarring.

An effective enhancement to the scaffolds developed in **Chapters 3 and 5** could be the incorporation of gradients of glycosaminoglycans (GAGs) and bioactive molecules. In native skin, GAGs like HA and heparan sulfate are distributed non-uniformly [32, 33], helping to localize and stabilize signaling molecules such as SHH, FGF, and VEGF, which are essential for morphogenesis and wound healing [34]. For instance, SHH-driven hair follicle regeneration depends on its spatial presentation [35], which could be mimicked using GAG gradients. Techniques like 3D bioprinting or layer-by-layer assembly enable the fabrication of such gradients in the desired shape [36]. However, challenges include gradient stability, reproducibility, and added complexity in regulatory approval [37]. Despite these, spatially patterned scaffolds hold strong potential to improve regeneration and functional outcomes in skin substitutes.

Once these materials are integrated into porous scaffolds, mechanical characterization becomes essential. Properties such as tensile strength, stiffness, and elasticity are critical for clinical translation, as they influence integration and durability [38]. We examined how the inclusion of atelocollagen enriched with Col III impacts the mechanical stiffness of scaffolds in **Chapter 4**. While tensile testing is widely used, it was not feasible due to limited Col III availability and the large sample dimensions required. Techniques like atomic force microscopy and nano-indentation, though informative, are better suited for dense, flat samples and less reflective of the compliance in porous, hydrated scaffolds [39, 40]. Instead, compressive testing of small cylindrical samples was used to assess formulation differences. While such measurements provide important mechanical benchmarks, their clinical relevance also lies in predicting how scaffolds withstand manipulation, absorb exudate, and maintain structure *in vivo* [38]. Emerging techniques like Brillouin light spectroscopy could further link mechanical properties to biological outcomes [41].

Our focus was on collagen-based sponges for treating full-thickness wounds such as severe burns. These scaffolds are designed to provide structural support while also modulating the biological environment. However, other fabrication methods such as electrospinning and hydrogels are gaining traction. For instance, electrospinning yields ECM-like nanofibrous scaffolds that enhance cell adhesion [42], and hydrogels create moist, bioactive environments suitable for growth factor delivery [43]. Regardless of the technique, the selection of ECM-based raw materials remains central, as demonstrated in this thesis with Col III, HA, and OTR4120. Although materials like CACIPLIQ20® [44] and Hyalo4® [45] (topical format) are already used for chronic wounds, and Col III injections show promise in aesthetic applications [46], our approach aims to translate these bioactive cues into robust scaffold systems for complex wound environments. The integration of such cues into porous templates may extend their utility beyond current formats, offering new therapeutic avenues.

Creating a pro-regenerative ECM is only one of many steps towards engineering fully functional skin. Functional skin substitutes must replicate not just the skin's barrier role but also its full biological complexity, including vascularization, innervation, and appendages like hair follicles and sweat glands. Incorporation of proto-follicles, organoids, vascular cells, and neural elements has shown promise in recapitulating skin physiology [47-49]. Advances in skin organoid and tissue engineering technologies have enabled the generation of skin-like tissues containing multiple appendages that better replicate the natural state [50]. However, integrating vascular endothelial cells for rapid neovascularization remains a significant challenge due to issues like scaffold-host integration, cell survival, and the coordination of angiogenic signaling [51, 52]. Similarly, the inclusion of neural components to restore sensory function and modulate wound healing is in early stages, requiring precise spatial organization and functional synapse formation. Stem cell technologies, particularly the use of induced pluripotent stem cells (iPSCs), offer the potential for generating patient-specific constructs, but limitations related to extended culture time, genomic stability, and safety concerns must be addressed before clinical translation [53, 54]. Moving forward, combining pro-regenerative ECM design with vascular, neural, and appendageal integration may finally allow us to engineer full-thickness skin that not only closes wounds but also restores complete function.

Advancing wound healing models and non-invasive evaluation

In vitro modeling: strengths and limitations

Accurately modeling the biological response of cells to biomaterials is central to wound healing research. In this thesis, we prioritized *in vitro* testing using primary human cells to better mimic physiological conditions [55]. This included macrophages derived from monocytes and fibroblasts from different origins, including, adult and fetal dermis from healthy skin and eschar tissue from burn patients. While primary cells offer higher biological relevance, their use is challenged by donor variability due to sex, age, or other patient characteristics in addition to limited availability. Studies suggest that the application of cells from at least 4–10 donors improves reproducibility and reduces outlier bias, especially in transcriptomic and functional scaffold analyses [56-58].

Single-cell-type assays have provided insights into specific responses. For instance, adult fibroblasts cultured on our scaffolds did not transition into myofibroblasts, likely due to the scaffolds' lower stiffness and absence of TGF-β1 stimulation. In contrast, eschar-derived fibroblasts showed increased fibrotic sensitivity, making them a more representative model for burn wound response as observed in **Chapter 3** [58, 59]. To assess immune interaction, we measured macrophage polarization via flow cytometry, which revealed scaffold influence on the M1/M2 balance, a key differentiator between fetal, adult, and burn healing environments as described in **Chapter 1**. However, overlapping surface markers between macrophage subtypes posed evaluation challenges. T-cell suppression assays could complement these findings by offering functional insights, as they measure the ability of scaffold-conditioned macrophages to inhibit T-cell proliferation, a hallmark of M2-like, anti-inflammatory activity [60].

Given that wound healing involves intricate cell–cell communication, co-culture systems (e.g., fibroblasts with macrophages or keratinocytes) are promising for replicating intercellular dynamics, though media compatibility remains a hurdle. Recently, a study demonstrated that acute contact with macrophages can activate fibroblasts, which might lead to fibrosis [61]. Moreover, expanding to additional skin cell types such as dermal papilla cells may allow exploration of effector molecules such as SHH incorporation in scaffolds. For example, SHH activates early hair follicle markers such as Gli1 [62], which may stimulate hair growth, a vital aspect of complete skin repair. Lastly, *ex vivo* skin biopsy models serve as a valuable intermediate between *in vitro* and *in vivo*, maintaining native architecture and physiological relevance [63].

Pre-clinical testing and non-invasive tools

Preclinical models are essential for assessing the safety, efficacy, and biological behavior of skin substitutes before progressing to human clinical trials [64]. Traditional animal models, such as rodents and pigs, have long been used because of their ability to simulate key features of human wound healing, including inflammation, re-epithelialization, and scarring [65]. In this thesis we utilized a full-thickness Wistar rat wound model to evaluate scaffold performance in wound healing as observed in **Chapter 4 and 5**. While this model provides valuable insight into wound contraction and inflammation, rodents heal primarily through contraction due to the panniculus carnosus, a mechanism that differs significantly from the re-epithelialization process observed in humans [66]. Therefore, large animal models such as pigs, which closely mimic the human skin structure and healing dynamics, are more appropriate for advanced preclinical validation [67]. As ethical concerns and regulations evolve, including frameworks like the FDA Modernization Act 2.0, there is a growing push toward replacing or reducing animal testing through models such as organ-on-a-chip [68], which aligns with the 3Rs (Replacement, Reduction, and Refinement) principles.

Advancements in tissue engineering have led to the development of skin-on-a-chip systems, which aim to replicate the complex structure and function of human skin in a controlled microenvironment. These microfluidic devices incorporate multiple layers of skin cells, including epidermal, dermal, and vascular components, to simulate physiological conditions more accurately than traditional in vitro models [69]. In the context of this thesis, these models present exciting opportunities for future work, especially for testing immune responses, innervation, and advanced healing features like appendage regeneration, allowing for more accurate functional evaluation of scaffold components such as HA, Col III and OTR4120. Although still under development and not yet fully standardized, skin-on-a-chip systems offer a scalable, ethically favorable alternative to animal testing [70], and their utility will likely increase as regulatory acceptance grows.

Assessment of skin substitute performance relies on both invasive and non-invasive techniques. In this study, histological methods, including H&E and Masson's trichrome staining, were used to evaluate tissue integration, scaffold degradation, fibrotic response, and inflammation as presented in **Chapter 4 and 5**. At the molecular level, tools like RT-PCR and kinase activity assays (e.g. peptide-based signaling arrays) provide deeper insight into regenerative pathways [71]. Mass spectrometry offers precise identification of biomarkers involved in healing and fibrosis and, when properly configured, can also provide quantitative or semi-

quantitative data. However, its application is limited by high cost, complexity, and the need for invasive tissue sampling [72]. Non-invasive tools are increasingly valuable for real-time and longitudinal evaluation. Techniques such as optical coherence tomography (OCT), high-frequency ultrasound (including strain imaging and shear wave elastography), and laser Doppler imaging allow visualization of tissue architecture and perfusion without disturbing the wound site [73, 74]. For scar assessment, tools like POSAS, the Vancouver Scar Scale, cutometers (elasticity), mexameters (pigmentation), and 3D surface scanners provide objective, reproducible data to track healing progression without compromising the wound site [75, 76].

Translational medicine considerations and clinical outlook

The clinical translation of skin substitutes involves navigating complex regulatory, manufacturing, and therapeutic challenges. Medical devices indicated for use on wounds such as burns or chronic ulcers, must meet stringent safety and efficacy standards defined by agencies like the FDA and EMA [77, 78]. Skin scaffolds intended for deep dermal or full-thickness wounds are typically classified as Class II or III medical devices, depending on their material origin and level of host interaction [79]. The scaffolds developed in this thesis, based on bovine-derived Col I, fall under Class III, requiring rigorous validation for biocompatibility, sterility, and performance [80]. Accordingly, we developed standard operating procedures (SOPs) for scaffold fabrication and addressed batch-to-batch variability by producing multiple batches of scaffolds to ensure reproducibility. While our focus was on biological validation, regulatory compliance also extends to sourcing, traceability, and the incorporation of bioactive agents [81]. Molecules such as SHH, despite their regenerative potential, face regulatory barriers due to risks of tumorigenicity and challenges in dose control [82]. Alternatives like the clinically approved heparan sulfate mimetic compound OTR4120, used in this thesis, offer a safer approach by stabilizing endogenous factors without regulatory complications.

From a clinical perspective, personalized medicine is emerging as a transformative approach in regenerative therapies. Skin substitute strategies can be tailored based on wound characteristics, such as burn depth, infection status, and patient-specific immune responses [83]. In this thesis, we highlighted variability in cellular responses among primary dermal fibroblasts from different donors, underlining the necessity of including cells from multiple individual donors in *in vitro* studies. This variability has direct implications for clinical translation, as wound healing outcomes differ markedly between pediatric, adult, and burn patients as presented in **Chapter 1**. Personalized scaffolds, potentially incorporating patient-derived cells

or effector biomolecules (e.g., SHH, FGF2, IGF1), represent the next step in achieving more desirable outcomes. However, personalization increases complexity in manufacturing and clinical trial design, necessitating flexible clinical designs such as adaptive protocols—which allow for modifications based on interim results—and stratified trials, which group patients by biomarkers or wound type to better assess efficacy [84].

Future clinical translation of skin substitutes depends on multidisciplinary collaborations of researchers, clinicians, entrepreneurs, among others. While scaffold-based therapies are promising, their long-term outcomes, including fibrosis, vascularization, and scar quality, require thorough evaluation through high-resolution imaging, histological analysis, and validated patient-reported outcome measures [85]. Despite promising results in preclinical and early clinical settings, high cost of production, including biomaterial sourcing, process standardization, and scalability for scaffold-based therapies remains a major barrier for widespread implementation [86]. Although a detailed comparison is beyond this scope, many advanced skin substitutes fail to reach the market due to manufacturing complexity or lack of cost-effectiveness compared to existing treatments [1]. Therefore, engaging key stakeholders early, i.e., clinicians who apply these technologies, patients who receive them, and researchers who refine them, should be accompanied by early assessments of technical feasibility, manufacturing scalability, and economic viability to ensure the solutions meet real-world needs. Additionally, as regulatory frameworks gradually evolve to accommodate regenerative products, the integration of robust *in vitro* platforms, patient-specific data, and ethical, cost-effective preclinical models will be central to advancing the next generation of skin substitutes.

Concluding remarks

This thesis establishes a foundation for developing smarter, bioactive skin substitutes by integrating regenerative extracellular matrix components inspired by fetal healing and regenerative species. Building on these insights, future research should focus on optimizing scaffold design to better address key challenges such as immune modulation, vascularization, and appendage regeneration. By combining advanced biomaterials with emerging technologies, there is strong potential to create the next generation of customizable skin substitutes, ultimately moving closer to the goal of functional and scarless skin regeneration.

References

1. Dearman, B.L., S.T. Boyce, and J.E. Greenwood, *Advances in Skin Tissue Bioengineering and the Challenges of Clinical Translation.* Frontiers in Surgery, 2021. **Volume 8 - 2021**.
2. Schlottmann, F., et al., *A Short History of Skin Grafting in Burns: From the Gold Standard of Autologous Skin Grafting to the Possibilities of Allogeneic Skin Grafting with Immunomodulatory Approaches.* Medicina (Kaunas), 2021. **57**(3).
3. Shevchenko, R.V., S.L. James, and S.E. James, *A review of tissue-engineered skin bioconstructs available for skin reconstruction.* J R Soc Interface, 2010. **7**(43): p. 229-58.
4. Supp, D.M. and S.T. Boyce, *Engineered skin substitutes: practices and potentials.* Clin Dermatol, 2005. **23**(4): p. 403-12.
5. Clavet, H., et al., *Joint contracture following prolonged stay in the intensive care unit.* Cmaj, 2008. **178**(6): p. 691-7.
6. Galati, V., et al., *Split thickness skin graft versus application of the temporary skin substitute suprathel in the treatment of deep dermal hand burns: a retrospective cohort study of scar elasticity and perfusion.* Int J Burns Trauma, 2021. **11**(4): p. 312-320.
7. Burdick, J.A., et al., *Acellular biomaterials: an evolving alternative to cell-based therapies.* Sci Transl Med, 2013. **5**(176): p. 176ps4.
8. Avila-Martinez, N., et al., *Matrisomal components involved in regenerative wound healing in axolotl and Acomys: implications for biomaterial development.* Biomater Sci, 2023. **11**(18): p. 6060-6081.
9. Jacques, E. and E.J. Suuronen, *The Progression of Regenerative Medicine and its Impact on Therapy Translation.* Clin Transl Sci, 2020. **13**(3): p. 440-450.
10. Sheikholeslam, M., et al., *Biomaterials for Skin Substitutes.* Adv Healthc Mater, 2018. **7**(5).
11. Hynes, R.O. and A. Naba, *Overview of the Matrisome-An Inventory of Extracellular Matrix Constituents and Functions.* Cold Spring Harbor Perspectives in Biology, 2012. **4**(1).
12. Naba, A., et al., *The extracellular matrix: Tools and insights for the "omics" era.* Matrix Biol, 2016. **49**: p. 10-24.
13. Brosseau, J.P., et al., *Human cutaneous neurofibroma matrisome revealed by single-cell RNA sequencing.* Acta Neuropathol Commun, 2021. **9**(1): p. 11.
14. Smith, L.T., K.A. Holbrook, and J.A. Madri, *Collagen types I, III, and V in human embryonic and fetal skin.* Am J Anat, 1986. **175**(4): p. 507-21.
15. Ramelet, A.-A., et al., *Chronic wound healing by fetal cell therapy may be explained by differential gene profiling observed in fetal versus old skin cells.* Experimental Gerontology, 2009. **44**(3): p. 208-218.
16. Agarwal, P., et al., *Collagen XII and XIV, new partners of cartilage oligomeric matrix protein in the skin extracellular matrix suprastructure.* J Biol Chem, 2012. **287**(27): p. 22549-59.
17. Cheng, W., et al., *The content and ratio of type I and III collagen in skin differ with age and injury.* African Journal of Biotechnology, 2011. **10**(13): p. 2524-2529.
18. Stewart, D.C., et al., *Type III Collagen Regulates Matrix Architecture and Mechanosensing during Wound Healing.* Journal of Investigative Dermatology, 2024.
19. Longaker, M.T., et al., *Studies in fetal wound healing: III. Early deposition of fibronectin distinguishes fetal from adult wound healing.* Journal of Pediatric Surgery, 1989. **24**(8): p. 799-805.
20. Whitby, D.J. and M.W. Ferguson, *The extracellular matrix of lip wounds in fetal, neonatal and adult mice.* Development, 1991. **112**(2): p. 651-668.

21. Minamitani, T., et al., *Modulation of collagen fibrillogenesis by tenascin-X and type VI collagen.* Experimental cell research, 2004. **298**(1): p. 305-315.
22. Walraven, M., R. Beelen, and M. Ulrich, *Transforming growth factor-β (TGF-β) signaling in healthy human fetal skin: A descriptive study.* Journal of dermatological science, 2015. **78**(2): p. 117-124.
23. Lee, J.S., et al., *Influence of Transforming Growth Factors beta 1 and beta 3 in the Scar Formation Process.* J Craniofac Surg, 2023. **34**(3): p. 904-909.
24. Sun, T., et al., *Isoform-selective TGF-β3 inhibition for systemic sclerosis.* Med, 2024. **5**(2): p. 132-147. e7.
25. Shibuya, M., *Vascular Endothelial Growth Factor (VEGF) and Its Receptor (VEGFR) Signaling in Angiogenesis: A Crucial Target for Anti- and Pro-Angiogenic Therapies.* Genes Cancer, 2011. **2**(12): p. 1097-105.
26. Dang, C.M., et al., *Decreased expression of fibroblast and keratinocyte growth factor isoforms and receptors during scarless repair.* Plastic and reconstructive surgery, 2003. **111**(6): p. 1969-1979.
27. Takaya, K., et al., *Fibroblast Growth Factor 7 Suppresses Fibrosis and Promotes Epithelialization during Wound Healing in Mouse Fetuses.* Int J Mol Sci, 2022. **23**(13).
28. Uijtdewilligen, P.J.E., et al., *Towards embryonic-like scaffolds for skin tissue engineering: identification of effector molecules and construction of scaffolds.* Journal of Tissue Engineering and Regenerative Medicine, 2016. **10**(1): p. E34-E44.
29. Abe, Y. and N. Tanaka, *Roles of the Hedgehog Signaling Pathway in Epidermal and Hair Follicle Development, Homeostasis, and Cancer.* Journal of Developmental Biology, 2017. **5**(4).
30. Xiao, Y., et al., *Neural Hedgehog signaling maintains stem cell renewal in the sensory touch dome epithelium.* Proceedings of the National Academy of Sciences, 2015. **112**(23): p. 7195-7200.
31. Stamatas, G.N., et al., *Skin maturation from birth to 10 years of age: Structure, function, composition and microbiome.* Exp Dermatol, 2023. **32**(9): p. 1420-1429.
32. Ghatak, S., et al., *Roles of Proteoglycans and Glycosaminoglycans in Wound Healing and Fibrosis.* Int J Cell Biol, 2015. **2015**: p. 834893.
33. Horiguchi, Y., et al., *Distribution, ultrastructural localization, and ontogeny of the core protein of a heparan sulfate proteoglycan in human skin and other basement membranes.* J Histochem Cytochem, 1989. **37**(7): p. 961-70.
34. Sarrazin, S., W.C. Lamanna, and J.D. Esko, *Heparan sulfate proteoglycans.* Cold Spring Harb Perspect Biol, 2011. **3**(7).
35. Woo, W.M., H.H. Zhen, and A.E. Oro, *Shh maintains dermal papilla identity and hair morphogenesis via a Noggin-Shh regulatory loop.* Genes & Development, 2012. **26**(11): p. 1235-1246.
36. Do, A.V., et al., *3D Printing of Scaffolds for Tissue Regeneration Applications.* Adv Healthc Mater, 2015. **4**(12): p. 1742-62.
37. Niu, X., et al., *Integrated gradient tissue-engineered osteochondral scaffolds: Challenges, current efforts and future perspectives.* Bioact Mater, 2023. **20**: p. 574-597.
38. Sander, E.A., K.A. Lynch, and S.T. Boyce, *Development of the mechanical properties of engineered skin substitutes after grafting to full-thickness wounds.* J Biomech Eng, 2014. **136**(5): p. 051008.
39. Łabuś, W., et al., *Atomic force microscopy in the production of a biovital skin graft based on human acellular dermal matrix produced in-house and in vitro cultured human fibroblasts.* Journal of Biomedical Materials Research Part B: Applied Biomaterials, 2018. **106**(2): p. 726-733.

40. Wu, G., M. Gotthardt, and M. Gollasch, *Assessment of nanoindentation in stiffness measurement of soft biomaterials: kidney, liver, spleen and uterus.* Scientific Reports, 2020. **10**(1): p. 18784.
41. Rodríguez-López, R., et al., *Network Viscoelasticity from Brillouin Spectroscopy.* Biomacromolecules, 2024. **25**(2): p. 955-963.
42. Bhardwaj, N. and S.C. Kundu, *Electrospinning: A fascinating fiber fabrication technique.* Biotechnology Advances, 2010. **28**(3): p. 325-347.
43. Gaharwar, A.K., N.A. Peppas, and A. Khademhosseini, *Nanocomposite hydrogels for biomedical applications.* Biotechnol Bioeng, 2014. **111**(3): p. 441-53.
44. Roohi, S.A., Z. Keuylian, and D. Barritault, *ReGeneraTing Agents (rgta(R)) technology combined with antibiotics improves outcomes for infections in the upper limb.* Clinical Case Reports, 2021. **9**(3): p. 1083-1091.
45. Koutna, M. and L. Vasakova, *Hyaluronic Acid In Advanced Wound Care: A Case Series Using The Hyalo4 Line Products.* Journal of Medical Case Reports and Case Series, 2024. **5**(6).
46. Jia, Y., et al., *Efficacy and Safety of Type III Collagen Lyophilized Fibers Using Mid-to-Deep Dermal Facial Injections for the Correction of Dynamic Facial Wrinkles.* Aesthetic Plast Surg, 2024. **48**(13): p. 2500-2512.
47. Abaci, H.E., et al., *Human Skin Constructs with Spatially Controlled Vasculature Using Primary and iPSC-Derived Endothelial Cells.* Adv Healthc Mater, 2016. **5**(14): p. 1800-7.
48. Yang, X., et al., *Bioactive materials for in vivo sweat gland regeneration.* Bioactive Materials, 2024. **31**: p. 247-271.
49. Iqbal, M.Z., et al., *Breathing new life into tissue engineering: exploring cutting-edge vascularization strategies for skin substitutes.* Angiogenesis, 2024. **27**(4): p. 587-621.
50. Lee, J., et al., *Hair-bearing human skin generated entirely from pluripotent stem cells.* Nature, 2020. **582**(7812): p. 399-404.
51. Laschke, M.W. and M.D. Menger, *Vascularization in tissue engineering: angiogenesis versus inosculation.* Eur Surg Res, 2012. **48**(2): p. 85-92.
52. Chen, L., et al., *Pre-vascularization Enhances Therapeutic Effects of Human Mesenchymal Stem Cell Sheets in Full Thickness Skin Wound Repair.* Theranostics, 2017. **7**(1): p. 117-131.
53. Itoh, M., et al., *Generation of keratinocytes from normal and recessive dystrophic epidermolysis bullosa-induced pluripotent stem cells.* Proc Natl Acad Sci U S A, 2011. **108**(21): p. 8797-802.
54. Shi, Y., et al., *Induced pluripotent stem cell technology: a decade of progress.* Nat Rev Drug Discov, 2017. **16**(2): p. 115-130.
55. Sierra-Sánchez, Á., et al., *Comparison of Two Human Skin Cell Isolation Protocols and Their Influence on Keratinocyte and Fibroblast Culture.* Int J Mol Sci, 2023. **24**(19).
56. Kolliopoulos, V., et al., *DONOR VARIABILITY IN HUMAN MESENCHYMAL STEM CELL OSTEOGENIC RESPONSE AS A FUNCTION OF PASSAGE CONDITIONS AND DONOR SEX.* bioRxiv, 2023.
57. Koch, S.E., et al., *Donor Heterogeneity in the Human Macrophage Response to a Biomaterial Under Hyperglycemia In Vitro.* Tissue Eng Part C Methods, 2022. **28**(8): p. 440-456.
58. Kutluoğlu, G.C., et al., *Comparison of dermal and eschar fibroblasts in full skin equivalents.* Wound Repair Regen, 2025. **33**(1): p. e70001.
59. Avila-Martinez, N., et al., *Effect of Hyaluronan in Collagen Biomaterials on Human Macrophages and Fibroblasts In Vitro.* Journal of Functional Biomaterials, 2025. **16**(5): p. 167.
60. Kumar, S., et al., *Uncovering therapeutic targets for macrophage-mediated T cell suppression and PD-L1 therapy sensitization.* Cell Reports Medicine, 2024. **5**(9).
61. Ezzo, M., et al., *Acute contact with profibrotic macrophages mechanically activates fibroblasts via avβ3 integrin–mediated engagement of Piezo1.* Science Advances, 2024. **10**(43): p. eadp4726.

62. Lee, J., et al., *Gli1 is a target of Sonic hedgehog that induces ventral neural tube development.* Development, 1997. **124**(13): p. 2537-52.
63. Wurbs, A., et al., *A human ex vivo skin model breaking boundaries.* Scientific Reports, 2024. **14**(1): p. 24054.
64. Mukherjee, P., et al., *Role of animal models in biomedical research: a review.* Lab Anim Res, 2022. **38**(1): p. 18.
65. Masson-Meyers, D.S., et al., *Experimental models and methods for cutaneous wound healing assessment.* International Journal of Experimental Pathology, 2020. **101**(1-2): p. 21-37.
66. Naldaiz-Gastesi, N., et al., *The panniculus carnosus muscle: an evolutionary enigma at the intersection of distinct research fields.* Journal of anatomy, 2018. **233**(3): p. 275-288.
67. Ribitsch, I., et al., *Large Animal Models in Regenerative Medicine and Tissue Engineering: To Do or Not to Do.* Front Bioeng Biotechnol, 2020. **8**: p. 972.
68. Zushin, P.H., S. Mukherjee, and J.C. Wu, *FDA Modernization Act 2.0: transitioning beyond animal models with human cells, organoids, and AI/ML-based approaches.* J Clin Invest, 2023. **133**(21).
69. Risueño, I., et al., *Skin-on-a-chip models: General overview and future perspectives.* APL Bioeng, 2021. **5**(3): p. 030901.
70. Costa, S., et al., *Microfluidic-based skin-on-chip systems for safety assessment of nanomaterials.* Trends in Biotechnology, 2023. **41**(10): p. 1282-1298.
71. Vo, D.-K. and K.T.L. Trinh, *Polymerase Chain Reaction Chips for Biomarker Discovery and Validation in Drug Development.* Micromachines, 2025. **16**(3): p. 243.
72. Bastos, J.M., et al., *Innovations in heart failure management: The role of cutting-edge biomarkers and multi-omics integration.* Journal of Molecular and Cellular Cardiology Plus, 2025. **11**: p. 100290.
73. Schuetzenberger, K., et al., *Comparison of optical coherence tomography and high frequency ultrasound imaging in mice for the assessment of skin morphology and intradermal volumes.* Sci Rep, 2019. **9**(1): p. 13643.
74. Bray, R., et al., *Laser Doppler imaging of burn scars: a comparison of wavelength and scanning methods.* Burns, 2003. **29**(3): p. 199-206.
75. Rennekampff, H.O., et al., *Comparing the Vancouver Scar Scale with the cutometer in the assessment of donor site wounds treated with various dressings in a randomized trial.* J Burn Care Res, 2006. **27**(3): p. 345-51.
76. Baumann, M.E., et al., *Direct comparison of reproducibility and reliability in quantitative assessments of burn scar properties.* Burns, 2021. **47**(2): p. 466-478.
77. Belsky, K. and J. Smiell, *Navigating the Regulatory Pathways and Requirements for Tissue-Engineered Products in the Treatment of Burns in the United States.* J Burn Care Res, 2021. **42**(4): p. 774-784.
78. Chan, W.W., et al., *Commercialization of skin substitutes for third-degree burn wounds.* Trends in Biotechnology, 2024. **42**(4): p. 385-388.
79. Savoji, H., et al., *Skin Tissue Substitutes and Biomaterial Risk Assessment and Testing.* Front Bioeng Biotechnol, 2018. **6**: p. 86.
80. Aronson, J.K., C. Heneghan, and R.E. Ferner, *Medical devices: definition, classification, and regulatory implications.* Drug safety, 2020. **43**(2): p. 83-93.
81. Jurczak, K.M., et al., *Recent regulatory developments in EU Medical Device Regulation and their impact on biomaterials translation.* Bioeng Transl Med, 2025. **10**(2): p. e10721.
82. Ren, X., et al., *Growth Factor Engineering Strategies for Regenerative Medicine Applications.* Front Bioeng Biotechnol, 2019. **7**: p. 469.

83. Mahajan, N., S. Soker, and S.V. Murphy, *Regenerative Medicine Approaches for Skin Wound Healing: from Allografts to Engineered Skin Substitutes.* Current Transplantation Reports, 2024. **11**(4): p. 207-221.

84. Ho, D., et al., *Enabling Technologies for Personalized and Precision Medicine.* Trends Biotechnol, 2020. **38**(5): p. 497-518.

85. Šuca, H., et al., *Current Approaches to Wound Repair in Burns: How far Have we Come From Cover to Close? A Narrative Review.* Journal of Surgical Research, 2024. **296**: p. 383-403.

86. Wistner, S.C., L. Rashad, and G. Slaughter, *Advances in tissue engineering and biofabrication for in vitro skin modeling.* Bioprinting, 2023. **35**.

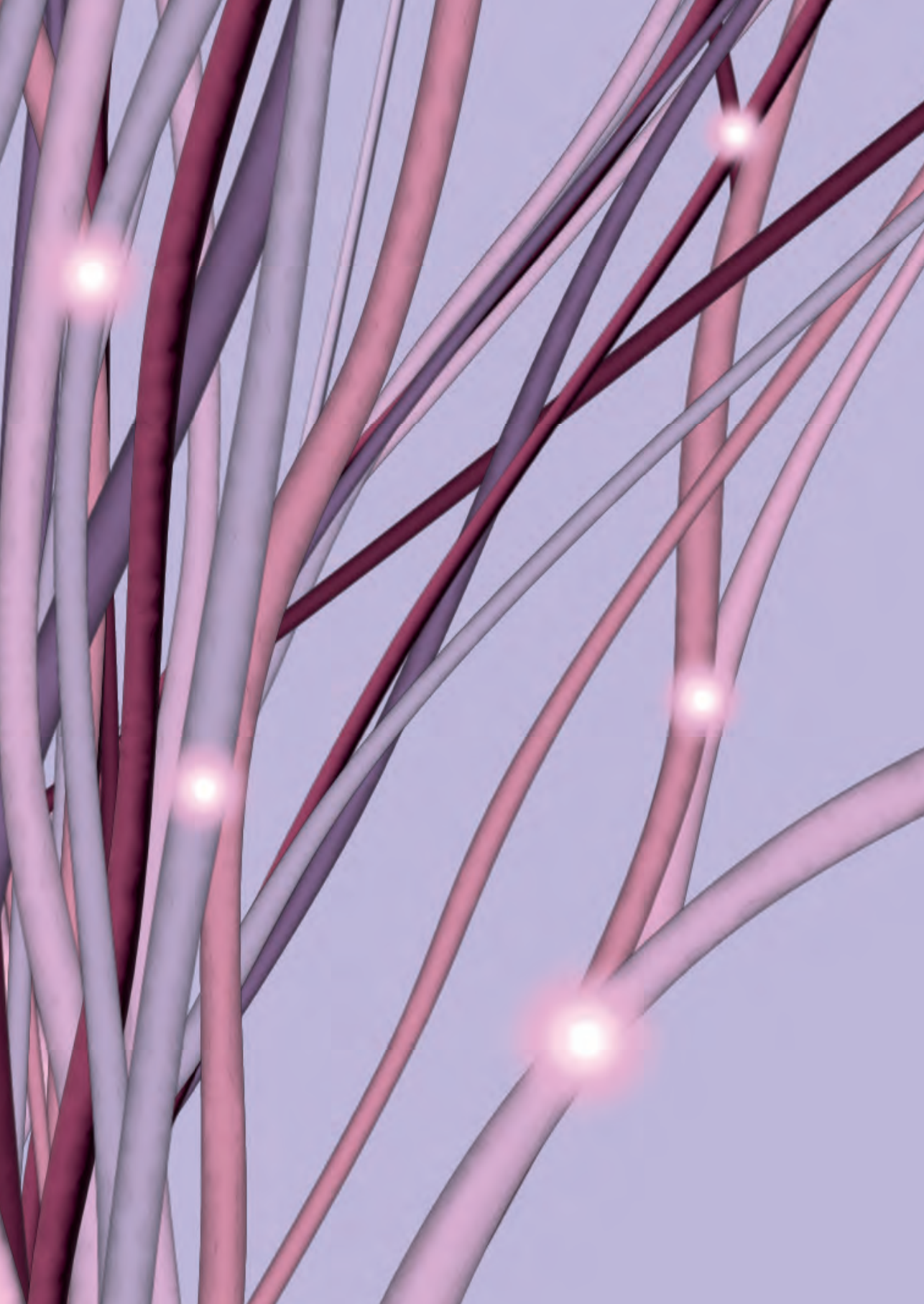

Chapter 7

English summary
Nederlandse samenvatting
Resumen en español

Summary

The development of skin substitutes capable of fully restoring the structure, function, and aesthetic qualities of human skin, especially after severe injuries such as burns, remains a significant challenge in regenerative medicine. One key insight from regenerative biology is that species capable of scarless healing often exhibit a distinct extracellular matrix (ECM) composition during wound repair, compared to non-regenerative species. This thesis focuses on the ECM not only as a structural scaffold but as a dynamic reservoir of biochemical cues that guide cellular behavior and tissue regeneration. Through the incorporation of regeneration-associated ECM components such as type III collagen (Col III), hyaluronan (HA), and sonic hedgehog (SHH) stabilized using the glycan mimetic OTR4120, a series of acellular bioactive dermal scaffolds were developed with the aim of promoting scarless skin regeneration.

In **Chapter 1**, a general introduction is given of the skin anatomy, the differences between fetal, adult and burn wound healing, and current therapeutic approaches for burn care. In addition, the overall outline and aim of this thesis is presented.

Chapter 2 explores the regenerative capabilities of two animal models: the axolotl, an amphibian capable of regrowing complex structures, and *Acomys*, a mammal that can regenerate full-thickness skin wounds without scarring. By comparing available transcriptomic and proteomics datasets from skin and blastema, we identified ECM components highly expressed during regeneration. These components were categorized within the matrisome, core matrisome (collagens, ECM glycoproteins, proteoglycans) and matrisome-associated framework (ECM regulators, secreted factors, and ECM-affiliated proteins). The findings generated a list of promising pro-regenerative ECM molecules to be integrated into future biomaterial design (peroxidasin homolog, tenascin C, and laminin, among others), emphasizing a rational and biologically informed approach.

In **Chapter 3**, we explored the regenerative role of HA, which is abundantly present in fetal skin and known for its ability to support cell migration and matrix hydration. We created porous type I collagen-based dermal scaffolds incorporating HA and evaluated their biological effect *in vitro* using primary human fibroblasts derived from fetal, adult, and eschar tissues, as well as macrophages. The inclusion of HA induced a pro-regenerative M2c-like macrophage phenotype and modulated fibrotic gene expression, particularly in eschar fibroblasts, where markers such as Col10a1 were significantly downregulated. These findings support HA's use

as a promising therapeutic component in regenerative scaffolds for treating severe wounds.

Different ratios of Col I/III in human skin as observed from fetal to newborn to adult stages were reproduced in scaffolds and studied in **Chapter 4**. Atelocollagen enriched with Col III was isolated from human placenta and incorporated into fibrillar Col I scaffolds. *In vitro,* these scaffolds decreased expression of fibrosis related genes ACTA2 and TGFB1 in fibroblasts and supported M2a macrophage polarization. *In vivo*, Col III-incorporated scaffolds improved wound healing compared to untreated wounds by promoting vascularization, reducing contraction, and guiding a more organized wound closure, effects consistent with a less fibrotic, more regenerative response.

In **Chapter 5**, we evaluated the use of OTR4120, a heparan sulfate mimetic marketed as a ReGeneraTing Agent (RGTA®), for its ability to improve wound healing when covalently bound to scaffolds. This OTR4120-containing scaffold was successfully functionalized with SHH, an effector molecule important for skin morphogenesis. *In vitro*, macrophages exposed to these scaffolds secreted higher levels of IL-10, indicating a shift toward a pro-healing response of M2c-like subtype. *In vivo*, OTR4120-containing scaffolds improved ECM remodeling, supported more organized wound closure, with an epidermal thickness closer to native skin, suggesting reduced fibrosis and improved healing dynamics.

Finally, **Chapter 6** places the findings of this thesis in a broader context, highlighting future directions for the development of acellular ECM-based scaffolds. It discusses strategies to integrate skin appendages, advancements in manufacturing techniques, the use of emerging wound healing models for preclinical testing, and the key challenges related to the clinical translation and regulatory approval of skin substitutes.

Overall, this thesis presents a biomaterial-based approach using rationally selected regenerative ECM components to design acellular dermal scaffolds that foster scarless wound healing. These strategies lay the groundwork for next-generation skin substitutes with potential for clinical impact in regenerative medicine.

Samenvatting

De ontwikkeling van huidsubstituten die in staat zijn de structuur, functie en esthetische eigenschappen van menselijke huid volledig te herstellen, met name na ernstige verwondingen zoals brandwonden, blijft een aanzienlijke uitdaging binnen de regeneratieve geneeskunde. Een belangrijk inzicht uit de regeneratieve biologie is dat organismen die in staat zijn tot littekenvrije genezing vaak een typische samenstelling van de extracellulaire matrix (ECM) vertonen tijdens wondherstel, vergeleken met niet-regeneratieve soorten. Dit proefschrift richt zich op de ECM, niet alleen als structurele scaffold, maar ook als een dynamisch reservoir van biochemische signalen die cellulair gedrag en weefselregeneratie kunnen sturen. Door componenten van de ECM die geassocieerd worden met regeneratie, zoals type III collageen (Col III), hyaluronan (HA) en sonic hedgehog (SHH) gestabiliseerd met behulp van het glycan-mimeticum OTR4120, te integreren in collageenscaffolds ontwikkelden we een reeks acellulaire, bioactieve dermale scaffolds met als doel littekenvrij huidherstel te bevorderen.

In **Hoofdstuk 1** wordt een algemene inleiding gegeven over de anatomie van de huid, de verschillen tussen foetaal en, volwassen herstel na brandwonden, en de huidige therapeutische benaderingen voor brandwondenzorg. Daarnaast wordt de algemene opzet en het doel van dit proefschrift gepresenteerd.

Hoofdstuk 2 onderzoekt de regeneratieve capaciteiten van twee diermodellen: de axolotl, een amfibie dat complexe structuren kan herstellen, en Acomys, een zoogdier dat een zoogdier dat diepe huidwonden volledig en zonder littekens kan regenereren. Door beschikbare datasets van transcriptomics en proteomics van huid en blastema's te vergelijken, identificeerden we ECM-componenten die sterk tot expressie komen tijdens regeneratie. Deze componenten werden gecategoriseerd binnen het kern-matrisoom (collagenen, ECM-glycoproteïnen, proteoglycanen) en het matrisoom-geassocieerd raamwerk (ECM-regulatoren, uitgescheiden factoren en ECM-verwante eiwitten). De bevindingen leverden een lijst op van veelbelovende pro-regeneratieve ECM-moleculen welke geïntegreerd kunnen worden in toekomstige biomateriaalontwerpen (zoals peroxidasine-homoloog, tenascine C, laminine), wat een rationele en biologisch onderbouwde benadering benadrukt.

In **Hoofdstuk 3** onderzochten we de regeneratieve rol van HA, dat overvloedig aanwezig is in foetale huid en bekend staat om zijn vermogen om celmigratie en matrixhydratatie te ondersteunen. We creëerden poreuze dermale scaffolds op basis

van collageen type I (Col I) met toevoeging van HA en evalueerden hun biologische effect *in vitro* met behulp van primaire menselijke fibroblasten afkomstig van foetale of volwassen huid, en van escharweefsel, evenals met macrofagen. De toevoeging van HA bevorderde een pro-regeneratief macrofaagfenotype (gelijkend op M2c) en moduleerde fibrotische genexpressie, met name in escharfibroblasten, waar expressie van markers zoals Col10a1 significant afnamen. Deze bevindingen ondersteunen het gebruik van HA als een veelbelovende therapeutische component in regeneratieve scaffolds voor de behandeling van ernstige wonden.

De verschillende verhoudingen van Col I/III tijdens de ontwikkeling van de menselijke huid, zoals waargenomen in foetale, neonatale en volwassen stadia, werden nagebootst in scaffolds en bestudeerd in **Hoofdstuk 4**. Atelocollageen verrijkt met Col III werd geïsoleerd uit menselijke placenta en geïncorporeerd in fibrillaire Col I-scaffolds. *In vitro* verminderden deze scaffolds de expressie van de fibrose-gerelateerde genen ACTA2 en TGFB1 in fibroblasten en ondersteunden ze polarisatie van macrofagen richting M2a. *In vivo* verbeterden met Col III verrijkte scaffolds de wondgenezing in vergelijking met onbehandelde wonden door het bevorderen van vascularisatie, het verminderen van contractie en het sturen van een meer georganiseerde wondsluiting, effecten die consistent zijn met een minder fibrotische en meer regeneratieve respons.

In **Hoofdstuk 5** evalueerden we het gebruik van OTR4120, een heparansulfaat variant dat op de markt wordt gebracht als ReGeneraTing Agent (RGTA®), vanwege het vermogen om wondgenezing te verbeteren, wanneer deze stof covalent gebonden is aan scaffolds. Deze OTR4120-bevattende scaffolds werden succesvol gefunctionaliseerd met SHH, een effectormolecuul dat belangrijk is voor huidmorfogenese. Macrofagen die *in vitro* aan deze scaffolds werden blootgesteld produceerden meer IL-10, wat wijst op een verschuiving naar een pro-helende M2c-achtige respons. *In vivo* verbeterden OTR4120-bevattende scaffolds de ECM-remodellering, ondersteunden een meer georganiseerde wondsluiting en zorgden voor een epidermale dikte die beter overeenkomt met die van de oorspronkelijke huid, hetgeen wijst op verminderde fibrose en verbeterde genezingsdynamiek.

Tot slot plaatst **Hoofdstuk 6** de bevindingen van dit proefschrift in een bredere context, waarbij toekomstige richtingen voor de ontwikkeling van acellulaire ECM-gebaseerde scaffolds worden belicht. Er werden strategieën besproken om huidadnexen te integreren, maar ook de vooruitgang in technieken voor fabricage,

het gebruik van nieuwe wondgenezingsmodellen voor preklinische testen, en de belangrijkste uitdagingen met betrekking tot de klinische vertaling en de regelgeving voor goedkeuring van huidsubstituten kwamen ter sprake.

Al met al presenteert dit proefschrift een op biomaterialen gebaseerde benadering om littekenvrije wondgenezing te bevorderen, waarbij rationeel geselecteerde regeneratieve ECM-componenten werden gebruikt om acellulaire dermale scaffolds te ontwerpen en te vervaardigen. Deze strategieën leggen de basis voor de nieuwe huidsubstituten van de toekomst met potentieel voor klinische toepassing in de regeneratieve geneeskunde.

Resumen

El desarrollo de sustitutos de piel capaces de restaurar completamente la estructura, función y cualidades estéticas de la piel humana, especialmente después de lesiones graves como las quemaduras, sigue siendo un desafío significativo en la medicina regenerativa. Un hallazgo clave de la biología regenerativa es que las especies capaces de curar sin formar cicatrices suelen presentar una composición distinta de la matriz extracelular (ECM por sus siglas en inglés) durante la reparación tisular, en comparación con las especies no regenerativas. Esta tesis se centra en la ECM no solo como un andamiaje estructural, sino como un reservorio dinámico de señales bioquímicas que guían el comportamiento celular y la regeneración del tejido. A través de la incorporación de componentes de la ECM asociados a la regeneración, como el colágeno tipo III (Col III), el hialuronano (HA) y el sonic hedgehog (SHH), estabilizados mediante el mimético de glicanos OTR4120, una serie de andamios dérmicos acelulares y bioactivos fueron desarrollados con el objetivo de promover una regeneración en la piel libre de cicatrices.

En el **Capítulo 1** se presenta una introducción general a la anatomía de la piel, las diferencias entre la curación de heridas fetal, adulta y en quemaduras, así como las estrategias terapéuticas actuales en el tratamiento de quemaduras. Además, se expone la estructura general y el objetivo de esta tesis.

El **Capítulo 2** explora las capacidades regenerativas de dos modelos animales: el ajolote, un anfibio capaz de regenerar estructuras complejas, y *Acomys,* un mamífero que puede regenerar heridas cutáneas de espesor completo sin formar cicatrices. Al comparar conjuntos de datos transcriptómicos y proteómicos disponibles de piel y de blastema, identificamos componentes de la ECM altamente expresados durante la regeneración. Estos componentes fueron clasificados dentro del matrisoma, el matrisoma central (colágenos, glicoproteínas de la ECM, proteoglicanos) y el marco asociado al matrisoma (reguladores de la ECM, factores secretados y proteínas asociadas a la ECM). Los resultados generaron una lista de moléculas pro-regenerativas prometedoras de la ECM para ser incorporadas en futuros diseños de biomateriales (por ejemplo, homólogo de peroxidasina, tenascina C, laminina, entre otras), destacando un enfoque racional e informado biológicamente.

En el **Capítulo 3** exploramos el papel regenerativo del HA, abundante en la piel fetal y conocido por su capacidad para favorecer la migración celular y la hidratación de la matriz. Se diseñaron andamios dérmicos porosos a base de colágeno tipo I (Col I) con incorporación de HA, y se evaluó su efecto biológico *in vitro* utilizando

fibroblastos humanos primarios derivados de tejidos fetales, adultos y de escara (costra necrótica profunda), así como macrófagos. La inclusión de HA indujo un fenotipo de macrófago tipo M2c pro-regenerativo y moduló la expresión de genes fibróticos, particularmente en fibroblastos provenientes de escara, donde marcadores como Col10a1 se vieron significativamente reducidos. Estos resultados respaldan el uso del HA como un componente terapéutico prometedor en andamios regenerativos para el tratamiento de heridas graves.

En el **Capítulo 4** se estudiaron diferentes proporciones de Col I/III en la piel humana, observadas desde etapas fetales hasta recién nacidos y adultos, reproduciéndolas en andamios. El atelocolágeno enriquecido con Col III fue aislado de placenta humana e incorporado en andamios de Col I fibrilar. *In vitro*, estos andamios redujeron la expresión de genes relacionados con la fibrosis como ACTA2 y TGFB1 en fibroblastos y promovieron la polarización de macrófagos M2a. *In vivo*, los andamios con Col III mejoraron la curación de heridas en comparación con heridas no tratadas, al favorecer la vascularización, reducir la contracción y guiar un cierre más organizado de la herida, efectos consistentes con una respuesta menos fibrótica y más regenerativa.

En el **Capítulo 5** se evaluó el uso de OTR4120, un mimético de heparán sulfato comercializado como ReGeneraTing Agent (RGTA®), por su capacidad para mejorar la cicatrización cuando se une covalentemente a andamios. Este andamio que contiene OTR4120 fue funcionalizado con SHH, una molécula efectora importante en la morfogénesis cutánea. *In vitro,* los macrófagos expuestos a estos andamios secretaron mayores niveles de IL-10, lo que indicando un cambio hacia un fenotipo M2c pro-regenerativo. *In vivo*, los andamios con OTR4120 mejoraron la remodelación de la ECM, promovieron un cierre más organizado de la herida y con un grosor epidérmico más similar al de la piel original/nativa, lo que sugiere una menor fibrosis y una mejor dinámica de curación.

Finalmente, el **Capítulo 6** contextualiza los hallazgos de esta tesis dentro de un marco más amplio, destacando futuras direcciones para el desarrollo de andamios acelulares basados en ECM. Se discuten estrategias para la integración de anexos cutáneos, avances en técnicas de fabricación, el uso de modelos emergentes de curación de heridas para ensayos preclínicos y los principales retos en la transferencia clínica y la aprobación regulatoria de sustitutos de piel.

En conjunto, esta tesis presenta un enfoque basado en biomateriales utilizando componentes regenerativos de la ECM seleccionados racionalmente para diseñar andamios dérmicos acelulares que fomenten una curación de heridas libre de cicatrices. Estas estrategias establecen las bases para la próxima generación de sustitutos de piel con potencial impacto clínico en medicina regenerativa.

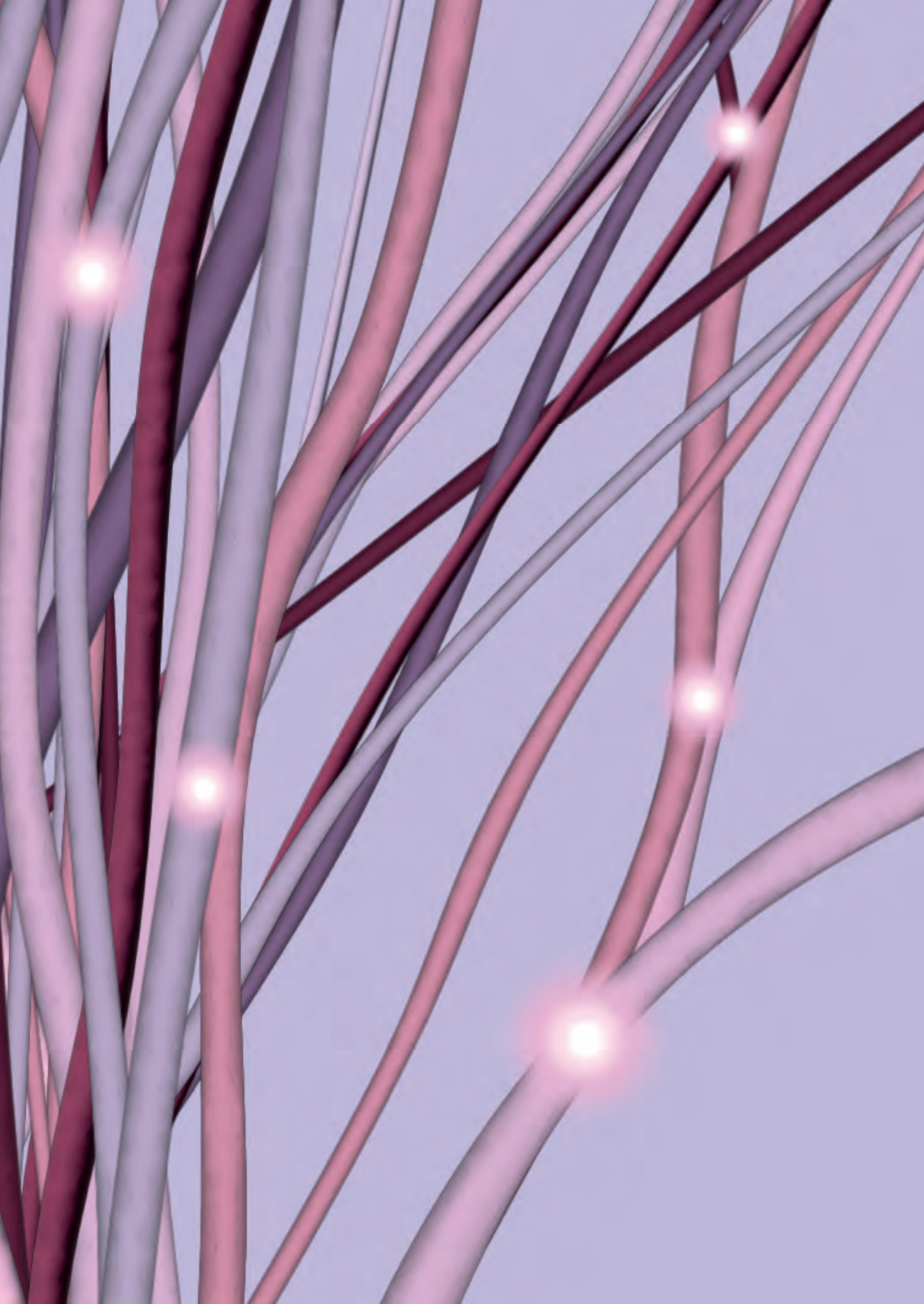

Chapter 8

Research Data Management Portfolio Curriculum Vitae List of publications and Awards Acknowledgements

Research Data Management

Ethics and privacy

All experiments were conducted in accordance with the Declaration of Helsinki. The use of human placenta was approved by the institutional medical ethics committee (CMO Arnhem/Nijmegen, File 2022-13523), and the study is registered at clinicaltrials.gov (NCT02438631, PIANO2 version 6). Research involving human primary fibroblasts was assessed by the Medical Ethics Review Committee and determined not to fall under the Medical Research Involving Human Subjects Act. Adult fibroblasts were isolated from skin samples of patients undergoing elective surgery at the Department of Plastic and Reconstructive Surgery, Red Cross Hospital (Beverwijk, NL). Eschar samples were collected during debridement procedures between post-burn days 13 and 19. Fetal fibroblasts were derived from skin tissue following pregnancy termination (gestational weeks 16–22), with informed consent obtained at the Center for Contraception, Abortion, and Sexuality (CASA, Leiden and The Hague, NL). The use of anonymized residual tissue followed the national ethical opt-out protocol (https://www.coreon.org/, accessed 23 November 2020) and institutional privacy regulations. Experiments involving blood-derived human cells were approved by the local ethics committee, with data protection following the Standard Operating Procedures of the Sanquin Blood Bank, compliant with national and international guidelines. Animal experiments were performed according to the Institute of Laboratory Animal Research guidelines and approved by the Radboud University Nijmegen Ethics Committee (DEC 2023-0016; license AVD10300202317189).

Data collection and storage

For Chapter 2, data generated from pre-existing datasets in literature was published Open Access (CC BY-NC license) and are available as Supplementary Information at DOI: 10.1039/d3bm00835e. For Chapters 3-5, raw and processed data were systematically recorded in laboratory notebooks, and digital platforms such as LabGuru and iVentionLES (Central Animal Facility). Data were securely stored on the department server (H:\ drive), with access restricted to authorized personnel. Data supporting these chapters originated from laboratory-based cell culture experiments (Chapter 3-5) and animal studies (Chapter 4-5). All processed datasets and explanatory documentation (e.g., readme files), were archived in the Data Sharing Collection (DSC)* of the Radboud Data Repository (RDR) with their respective chapter.

Data Sharing

Data generated and analyzed for this thesis are shared according to FAIR principles (Findable, Accessible, Interoperable, and Reusable) within the RDR for long-term access. Metadata, datasets, and sample processing descriptions are structured following RDR guidelines to ensure future reusability. After publication in open-access scientific journals the data will be published with open or restricted access. Data files are stored in standard formats (e.g., txt, docx, pdf, csv, xlsx, tif, png). The following table lists the DOIs where the datasets supporting each research chapter are available on the RDR.

**The table below details where the data and research documentation for each chapter can be found on the Radboud Data Repository (RDR). All data archived as a Data Sharing Collection remain available for at least 10 years after termination of the studies.*

Chapter	DSC	DSC access level	DSC license
3	10.34973/643p-rq10	Open	CC-BY-NC-4.0
4	10.34973/xmss-yd16	Restricted	*RUMC-RA-DUA-1.0*
5	10.34973/5trg-d996	Restricted	*RUMC-RA-DUA-1.0*

DSC = Data Sharing Collection

PhD portfolio of Nancy Avila-Martinez

Department: **Medical Biosciences**
PhD period: **01/05/2021 – 31/10/2024**
PhD Supervisor(s): **. Dr. ir. W.F. Daamen**
PhD Co-supervisor(s): **Dr. A.H.M.S.M. van Kuppevelt, Dr. ir. B.K.H.L. Boekema**

Training activities	Hours
Courses	
• SkinTERM Personal Development Plans (2021)	12.00
• SkinTERM Data management (FAIR principles) (2021)	10.00
• SkinTERM Workshop Biomaterials (2021)	28.00
• Radboudumc - Scientific integrity (2021)	20.00
• Radboudumc - Introduction day (2021)	6.00
• SkinTERM Intellectual Property Rights (2021)	9.00
• SkinTERM Writing a Scientific Paper (2021)	9.00
• SkinTERM Workshop Hair regeneration biology (2021)	18.20
• SkinTERM Scientific poster design (2021)	10.00
• SkinTERM Workshop Skin tissue engineering (2021)	18.20
• Radboudumc - Laboratory animal science (for Radboudumc researchers working with laboratory animals) (2021)	84.00
• RIMLS - Introduction course "In the lead of my PhD" (2021)	15.00
• Social Dutch I (2021)	67.50
• FIJI course 2022 (2022)	16.00
• SkinTERM Career perspectives after your PhD (2022)	10.00
• SkinTERM Communication and presentation skills (2022)	9.00
• SkinTERM Advance microscopy and image analysis (2022)	9.00
• SkinTERM Workshop Regeneration in Acomys sp (2022)	28.00
• Social Dutch II (2022)	67.50
• Social Dutch III (2022)	67.50
• RU - Statistics for PhD's by using SPSS (2022)	60.00
• SkinTERM Workshop Genetic lineage tracing and single cell clonal approaches (2022)	14.00
• SkinTERM Workshop Mass spectrometry and proteomics (2022)	14.00
• SkinTERM GCP standards (2023)	9.00
• SkinTERM Regulatory affairs (2023)	10.00
• SkinTERM Workshop Entrepeneurship and business planning (2023)	14.00
• SkinTERM GMP production (2023)	9.00
• SkinTERM Marketing in life sciences and healthcare (2024)	14.00
• SkinTERM Workshop From bench to clinic (2024)	14.00
• Communication course for pitching by DEBATRIX (2024)	14.00
• R basics for data preparation and presentation preparations (2024)	30.00
Seminars	
• Research Integrity Round 'Publication ethics: Promises, problems and perspectives' (2022)	1.50
• RIMLS Meet the expert 'Molecular imaging in mouse and rat models' (2022)	1.50
• Webinar - Global Scar Society (2023)	4.00
• RIMLS - Meet the expert 'Flow cytometry' (2023)	2.00
• RIMLS - Meet the expert 'Confocal Microscopy' (2023)	2.00

Conferences	
RIMLS PhD retreat (2021)	8.00
New Frontiers symposium Translational Glycoscience (2021)	12.50
30th Annual meeting NBTE (2022)	17.00
ESOF MSCA satellite event 2022 (2022)	8.00
RIMLS PhD retreat (2022) : Poster presentation	21.00
31st Annual meeting NBTE (2022) : Oral presentation	28.00
ETRS Annual meeting 2023 (2023) : Poster presentation	40.00
32nd Annual meeting NBTE (2023) : Poster presentation	28.00
MSCA conference 2024 (2024) : Oral presentation	22.00
EWMA conference 2024 (2024) : Oral presentation	16.00
2nd semana de Ingenieria de Bioprocesos de la UASLP (2024) : Oral presentation	5.00
7th TERMIS world congress 2024 (2024) : Poster presentation	55.00
ETRS Annual meeting 2024 (2024) : Oral presentation	65.00
Other	
Public Regenerative Medicine Day (2022)	8.00
PON PhD day (2022)	5.00
Radboud open science day (2022)	5.00
Teaching activities	
Lecturing	
MED-BMS34 - practical assistant (2023)	8.00
MED-MIN13 - Tutor for Med Biotechnology minor (2023)	14.00
MED-BMS34 - practical assistant (2024)	8.00
Supervision of internships / other	
Supervision internship master student (2022)	62.00
Supervision internship HBO student (2023)	62.00
Supervision research proposal master student (2023)	14.00
Supervision internship HBO student (2024)	62.00
Total	**1,300.40**

Curriculum Vitae

Nancy Margarita Avila Martinez was born in Soledad de Graciano Sánchez, México, on January 28th, 1994. In 2012, she began her Bachelor's degree in Bioprocess Engineering at the Autonomous University of San Luis Potosí, specializing in medical biotechnology. She later completed a research internship in cell therapy at the National Center for Research and Attention to Burn Patients (CENIAQ) in Mexico City. Her project, supervised by Dr. Sánchez Sánchez, received recognition at both state and national conferences and was awarded the 2017 Youth State Award in Science and Technology. She also collaborated with Rino-Q, supporting fundraising and outreach activities for pediatric burn survivors.

In 2018, Nancy was awarded the prestigious Chevening Scholarship by the UK government to pursue a Master's in Biomaterials and Regenerative Medicine at the University of Sheffield. During her studies, she completed an internship at the Kroto Research Institute, where she developed polycaprolactone-based biomaterials for skin repair under the supervision of Dr. Trikic. She presented her work at academic conferences and was selected to share her initiative on organ donation awareness at the Chevening Conference in Manchester. She graduated with Merit and was recognized as one of the 100 Leaders in Biotechnology in Latin America by Allbiotech.

Her academic path then led her to pursue a PhD as part of the SkinTERM project, funded by the Marie Skłodowska-Curie Actions, at Radboud University Medical Center in 2021. Her research, supervised by Dr.ir. Willeke Daamen, Dr. Toin van Kuppevelt, and Dr. Bouke Boekema, focused on developing collagen-based skin substitutes that mimic the skin in regenerative species to promote scarless healing in burn injuries. Her work included biomaterial design, *in vitro* and *in vivo* evaluation, and consideration of regulatory and translational aspects. She carried out secondments at institutions including the Alliance of Dutch Burn Centers, the University of Zurich, and the HARTMANN Group. Her research has been published in

several scientific journals and presented at national and international conferences. Notable recognitions include being a semifinalist in the Falling Walls Lab–MSCA chapter, receiving 2nd place in the Young Investigator Award from the European Tissue Repair Society, and the Dr. Suwelack Publication Award in Regenerative Technologies in Surgery.

List of Publications & Awards

Publications related to this thesis

- Avila-Martinez, N., Pfirrmann, M., Gomes, M. L. N. P., Krymchenko, R., Versteeg, E. M. M., Vlig, M., Verdoes, M., van Kuppevelt, T. H., Boekema, B. K. H. L., & Daamen, W. F. (2025). Effect of Hyaluronan in Collagen Biomaterials on Human Macrophages and Fibroblasts In Vitro. Journal of Functional Biomaterials, 16(5), 167. DOI: 10.3390/jfb16050167

- Avila-Martinez, N., Gansevoort, M., Verbakel, J., Jayaprakash, H., Araujo, I. M., Vitorino, M., Tiscornia, G., van Kuppevelt, T. H., & Daamen, W. F. (2023). Matrisomal components involved in regenerative wound healing in axolotl and Acomys: implications for biomaterial development. Biomaterials Science, 11(18), 6060-6081. DOI: 10.1039/D3BM00835E

Additional publications

- Krymchenko, R., Pfirrmann, M., van der Leeuw, S., Avila-Martinez, N., Versteeg, E. M. M., Meuwese, R. T. C., Vlig, M., Verdoes, M., Boekema, B. K. H. L., van Kuppevelt, T. H., & Daamen, W. F. (2025). Preparation, fractionation, and characterization of solubilized elastin and comparison of cellular response on fibroblasts and macrophages. International Journal of Biological Macromolecules, 315, 144548. DOI: 10.1016/j.ijbiomac.2025.144548

- Krymchenko, R., Avila-Martinez, N., Gansevoort, M., Bakker, G.-J., Gomes, M. L. N. P., Vlig, M., Versteeg, E. M. M., Boekema, B. K. H. L., van Kuppevelt, T. H., & Daamen, W. F. (2025). Collagen-elastin dermal scaffolds enhance tissue regeneration and reduce scarring in preclinical models. Materials today bio, 102239. DOI: 10.1016/j.mtbio.2025.102239

Awards

- Publication Award in Regenerative Technologies in Surgery (2025) – by Dr. Suwelack Foundation
- Young Investigator Award (2024)- 2nd place oral presentation by the European Tissue Repair Society
- Registration Bursary (2024) – To attend the ETRS-WHS-SKINTERM conference
- Falling Walls Lab (2024)– Semifinalist at the MSCA chapter

Acknowledgments

Crossing the ocean once more, I embarked on a new and transformative chapter of my life: my PhD journey. With its ups and downs, this experience allowed me to grow not only academically, but also personally and emotionally. Nijmegen became a second home, and along the way, I was fortunate to meet people whose guidance, kindness, and encouragement were essential in allowing me to complete and succeed in my doctorate. I would like to express my sincere gratitude to all of them, those mentioned here, and many others whose impact remains deeply appreciated from the bottom of my heart.

First of all, my promotor **Willeke**. I am deeply grateful for your unwavering guidance throughout this journey. As time passed, I came to know you not only as a supervisor but also as a person: approachable, supportive, and dedicated. When I shared with you how I felt, you responded with openness and empathy, which helped build trust. I admire how you consistently went above and beyond, working late hours and responding to emails even on weekends and holidays to ensure progress continues. Thank you for pushing me to grow, providing honest feedback, scientific insight, and constant encouragement.

Toin, although we did not have the pleasure to meet in person you were always present during my PhD and I truly appreciate that presence. I enjoyed our meeting and appreciate all the great ideas you brought to the table. Your expertise and knowledge were key to success in my PhD life. Moreover, you also cared beyond the scientific part and supported me on the personal side. **Bouke**, my heartfelt appreciation goes to you. It was comforting how you started as an advisor, listening as a mentor, giving me advice on how to endure and finish my PhD, and later becoming more involved, providing resources, helping design experiments, and even contributing to the writing of my thesis. Thank you for believing in me.

I want to thank my manuscript committee members **Frank, Alessandra,** and **Abdoel** for your time and dedication in carefully reviewing my thesis. Your effort in reading and evaluating my research is truly valued.

Two very important teams were crucial in my journey: **Radboudumc** and the SkinTERM consortium. I would like to start with someone who was part of both, my lab sibling **Roman**. There are not enough words to express my gratitude, but I will leave some here. We started almost at the same time, became colleagues, and finally friends. Working next to you was a joy. Even if our projects differed, your

support and suggestions in my experiments helped me achieve success. Thank you for your openness, your scientific advice, but most of all your friendship. Thanks for the conversations, for singing and dancing together, and for broadening my horizons. You are a great person, and it was an honour to walk this PhD journey alongside you, дякую. **Danique**, you went to the train station to pick me up on my first day, helped me settle in, and welcomed me with flowers and stroopwafels. Thanks for your listening to me and your advices in everything. You motivated me to try new experiences that I would not have the courage attempt myself.

Thanks **MXB group** for opened your doors to me, I miss our cookie's day and coffee breaks a lot. **Elly**, you keep the lab running on and I thank you for that. Your practical knowledge was very insightful to me and lead me to perform experiments independently. Thanks for accepting last-minute orders, your patience and thoughtful suggestions. **Rob**, anytime I had a question about how the lab works, you were the person I can rely on. Your kindness is unmatched, and I am grateful for your assistance in everything from sterilization to obtaining raw material (placenta). I admire your resilience and thanks for sharing nice and funny stories with me. **Merel**, I learnt so much from you, especially about structure and organization. I will always remember your fondness for pink. Working with you was nice, especially when we took care of our burrito boys, thanks for your commitment.

Lieke, we did not have the chance to work often together, but when we spent time together I got to know you more. I will remember our trip to Coimbra and wanted to let you know I respect your dedication and hard work. **Thierry**, thank you for always being my go-to person for GAGs and protein analysis questions and for your unique stories. **Lars** and **Tika**, thank you for helping me settle in the lab and for our pleasant talks, I wish we shared more time together. **Paola** and **Ahmed**, we shared little time, but it was a pleasure to work beside you. **Aarti**, meeting you at the start of my PhD and reconnecting at the end was wonderful. Thanks for helping me out with my first collagen isolation. I wish the three of you success in your PhD journey !. **Theo**, your guidance with histologies taught me so much, I could eventually perform them on my own thanks to you. You had the best tips.

Philipp, wir haben uns in der Kaffeepause kennengelernt. Wir hatten interessante Unterhaltungen, und du hast dir meine Sorgen angehört. Du hast mir sogar angeboten, mir bei meinem Projekt zu helfen. Das hat mir geholfen, weiterzukommen, als ich keine Lösung sah. Dafür werde ich dir immer dankbar

sein. **Maren**, vielen Dank, dass du meine Anfrage angenommen und mich bei der Immuntestung meiner Experimente unterstützt hast. Deine Expertise hat mir geholfen, meine Ziele zu erreichen. Du bist eine großartige Forscherin. **Martijn**, thanks for accepting collaborate with us, for your constructive suggestions, and for your kind and encouraging words throughout the process. **Dennis** and **Richard**, you opened your door and listened to my petition of performing compressing testing on my tiny scaffolds. Thanks for your generosity with time and effort. **Joris** and **Hedwig**, your assistance in obtaining and sharing the placenta was essential to producing the scaffolds for my project.

Team 1 and **CDL**, thanks for the training and assistance in caring for our burrito boys. I always felt welcome and happy in the CDL environment. I appreciate the effort and time you put in helping us finish our projects. **Maikel,** now I know how to hold scissors properly. Thanks for the great ideas and suggestions in our experiments, the nice life talks and kindness **Tim**, it was great to work with you, I am grateful for your commitment and interest in our project. You support in planning and organizing was crucial in our success. To the most patient biostatistician, **Steven**, thank you for your long-standing dedication to our calculations and analyses.

This work would have not be possible without the help of amazing students I had the privilege of supervise**: Sofia, Martin, Sjoerd** and **Marjolein**. I began with the goal of training you in order to get your help with my projects, yet your bright ideas and enthusiasm ended up enriching this thesis far beyond expectation. Thanks for your effort and wish all of you success in your career !

I had the privilege to also be part of the **SkinTERM** team. My thanks go to all those in the consortium, your collaborative effort made the completion of this thesis possible. **Denis, Franck** and **Agnes**, thank you for trusting me your valuable component and advices in the development of the project, as well as your support in regulatory tasks. **Hans**, I value your industry experience and wise words during my secondment, which helped me shape my career path. **Marcel**, thank you for your cell culture advices and encouragement from my time in Beverwijk to the very end.

My acknowledgements to my SkinTERM colleagues. **Madalena**, obrigada por los momentos compartidos, viajar contigo a congresos y secondments fue gratificante lo cual también ayudo al avance de esta tesis. **Gizem**, our time in the lab was comforting, we shared nice memories together and I miss dancing with you. **Zuzana**, I admire your diligence and calmness; eating out with you was always

delightful. **Masi**, your personality brought warmth to my days. Thank you for our talks about hair follicles and beyond. **George**, I was always impressed by your vast cultural knowledge and stories. I was delighted to hear them. **Prerna**, although we did not directly work together, you spared your time and answer all my question about proteomics. **Mahrukh** and **Zohaib**, I am grateful for your hospitality in Zurich and your help in the lab. **Haarshaa** and **Jiazheng**, I always enjoyed interacting with you on the meetings, thanks for your creativity and kindness.

I would like to thank my friends for cheering me up all the time when I needed the most. **Ileania**, nos conocimos sin planearlo y sin saber que estábamos conectadas desde antes. Gracias por ser un refugio constante, por los bubble teas, las pláticas de sobrevivimiento y confiarme a Miley. **Ely**, por nuestros encuentros en Mexico, Europa y todo el mundo, ser mi familia a la distancia y creer en mí, juntas hasta el fin del mundo. **Cynthia**, por tus consejos sabios y valiosos, escucharme, entenderme, las risas y tu dulzura. **Karen**, sin importar la hora o el lugar siempre respondiste mis mensajes, me ofreciste palabras de aliento y tu apoyo. **María**, mi médico de cabecera, mi rayito de sol, y por juntarnos cada Navidad como si el tiempo no pasara. **Claudia**, fue asombroso tenerte en casa y recordar nuestros tiempos de maestría, seguir compartiendo nuestro gusto por los mismo intereses y series. Thanks to all the Nimma friends I made along the way, you painted this journey with colours I will never forget.

To my first home in Nijmegen, the **116** gang, though I lived there just three months, I made great friendships and relationships that lasted during my whole journey. Thanks for the dinners, parties, laughs, and especially for presenting me someone that would stay longer than I imagined. **Takaya**, from being my roomie and dancing partner to offering me food, walks and your shoulder. You made this journey entertaining and delightful, our different personalities and tastes found out their way to complement each other. As you said when you left, thanks for being my family in Netherlands, 次の章に進みましょう. どうもありがとう.

This chapter of my life wouldn't have been possible without the unwavering encouragement my family gave me. To my parents, **Rosalba** and **Lupe**, que aun con incertidumbre, desde el principio abrazaron el hecho de tener una hija que adoraba la ciencia y quería ser investigadora. Les agradezco por el cariño, la fe y la paciencia que han tenido conmigo. Mis sueños se hicieron metas, y las metas, realidad. A mis hermanos **Ramiro, Jorge** y **Marcela**, por ser mis confidentes, por los memes que me alegraban, por alentarme y siempre incluirme en todos los planes, demostrarme lo que es la verdadera hermandad. A mis **cuñis** y **sobrinos**, por hacer todos los

momentos familiares más brillantes e inyectarme su energía. Mis queridas abuelitas **Marcelina** y **Maga**, con miedo de dejarme ir pero siempre pidiéndole a diosito que me protegiera, sé que desde el cielo siempre me cuidan. A toda mi familia **Ávila-Martínez**, por demostrarme que la familia siempre está, sin importar la distancia.

Finally, I wish to express my sincere gratitude to the institutions, organizations, and individuals whose contributions made this work possible: Radboudumc, especially the **Medical BioSciences** department and the CDL, the **Burn Research Lab** in Beverwijk, the **University of Zurich, OTR3, HARTMANN, CUTISS** and the whole SkinTERM consortium. This project received funding from the European Union's Horizon 2020 research and innovation programme under the Marie Skłodowska-Curie grant agreement No 955722.

And as I close this chapter, I find myself holding not just a thesis, but a mosaic of moments, each conversation, challenge, and kindness forming the fabric of these years. This journey was never mine alone, and for that, my heart will remain forever grateful.

ひつぜん.

9 789465 151564

Radboudumc university medical center

IN DEI NOMINE FELICITER

Radboud University